ISSN 1343-2230

CNS-REP-61
August, 2004

Annual Report 2003

Center for Nuclear Study,
Graduate School of Science, the University of Tokyo

Editors
T. Kawabata
N. Suzuki

Center for Nuclear Study

CNS Reports are available from:
Wako-Branch at RIKEN
Center for Nuclear Study,
Graduate School of Science, the University of Tokyo
2-1 Hirosawa, Wako
351-0198, Japan
Tel: +81-48-464-4191
Fax: +81-48-464-4554

Annual Report 2003

Center for Nuclear Study,
Graduate School of Science, the University of Tokyo

Preface

This is the annual report of the Center for Nuclear Study (CNS), Graduate School of Science, the University of Tokyo which includes activities during the fiscal year 2003 (April 2003 through March 2004).

In this year, the Ge-detector array GRAPE consisting of 18 position sensitive Ge detectors was completed as a system. The first experiment using the full set of the GRAPE was carried out successfully for the fusion reactions of neutron-rich nuclei for the study of high-spin states in nuclei around the ^{48}Ca region. In-beam γ-ray spectroscopy with direct reactions of unstable nuclei using a liquid-helium target is being planned. It is expected to provide new information on isoscalar responses as well as proton single-particle states in the unstable nuclei.

The polarized proton-target project has got into shape. The polarized solid proton-target developed at CNS can be operated under a high temperature of $\sim$ 100 K and a low magnetic field of $<$ 0.1 T while the conventional dynamic-nuclear-polarization target requires a low temperature of $<$ 1 K and a high magnetic field of $>$ 1 T. This polarized proton target was applied for the first time to the radioactive-ion beam experiment. The analyzing power for the p+^{6}He elastic scattering at 71 MeV/u was successfully measured. CNS and Joint Institute of Nuclear Physics, Russia concluded a treaty of the research collaboration agreement for the promotion of spin physics.

A Wien filter system was installed for the radioactive-ion beam separator CRIB. The radioactive-ion beam extracted from the CRIB is typically a mixture of the several kinds of ions with the same magnetic rigidity. The Wien filter system is cable to separate the ions by the mass-to-charge ratio A/q and consequently improves the purity of the radioactive-ion beam. Its performance as a velocity separator was tested by using the ^{14}O and ^{14}N ions, and it was confirmed that an ^{14}O beam with almost 100% purity was obtained.

The Hyper ECR ion source was improved to provide metal ions like $^{24}Mg^{7+}$ and $^{7}Li^{2+}$, which enabled experiments for nuclear astrophysics at CRIB. The beam-bunching system for the HiECR ion source, which was intensively used for the ion source research and R&D of new ion beam monitors, was introduced to increase the beam intensity. A cluster ion source was also improved to give an intense beam, and the first observations of Ti and Cu cluster-ion beams were made.

The PHENIX experiment at Relativistic Heavy Ion Collider (RHIC) at Brookhaven National Laboratory shows steady progress toward understanding of the collision process and finding of the evidence of Quark Gluon Plasma (QGP). Major contributions of the CNS group were the first observation of direct photons in heavy ion collisions and systematic study of J/ψ productions in various combination of colliding nuclear species. Several new types of detectors are being developed for future PHENIX upgrade in an in-house laboratory of CNS.

The theory group in CNS organized the 2nd CNS International Summer School (CISS03) in September 2003. There were 84 participants from 8 countries mainly from Asia. The 3rd summer school will be held in this August.

A lecturer Eiji IDEGUCHI joined CNS from RIKEN and started working on in-beam gamma-ray spectroscopy to study high-spin states of neutron-rich nuclei. A research associate Takashi TERANISHI left CNS to the Department of Physics at Kyushu University as an associate professor. As his successor, a research associate Hidetoshi YAMAGUCHI joined CNS from the Department of Physics at University of Tokyo.

Since we moved into the RIKEN Wako campus from the Tanashi campus of the University of Tokyo in 2000, we have made even greater efforts of collaboration with RIKEN and indeed made various scientific achievements. In April 2004, The University of Tokyo and RIKEN concluded the comprehensive collaboration agreements. This agreement will certainly reinforce the collaboration between CNS and RIKEN. We are currently planning to establish new organization, the international research center for the heavy-ion nuclear physics, which will be operated jointly by CNS and RIKEN.

The RIKEN RI beam facility (RIBF) which is under construction will deliver various exotic RI beams in 2007. Matching with construction, we have initiated two projects, an upgrade of the AVF injection cyclotron and a construction of the high resolution spectrometer SHARAQ. The upgrade plan is to provide high-energy ($K = 78$) and intense ion beam (for example, 10 pμA for $^{15}N^{5+}$). Presently available maximum beam energy is limited to $K = 70$ and 1 pμA for $^{14}N^{5+}$. The SHARAQ spectrometer is exclusively designed for the high resolution spectroscopic studies with RI beams of 200-400 MeV/nucleon. It will be installed in the new experimental hall of RIBF. The proposal of SHARAQ will be completed in this fall.

Hideyuki Sakai
Director of CNS

Table of Contents

1a. Experimental Nuclear Physics: Low and Intermediate Energies

1b. Experimental Nuclear Physics: PHENIX Experiment at BNL-RHIC

2. Accelerator and Instrumentation

Experimental Nuclear Physics: Low and Intermediate Energies

Excited States in ^{22}O with α Inelastic Scattering

M. Tamaki, S. Shimoura, H. Iwasaki[a], S. Michimasa[b], N. Aoi[b], H. Baba[c], N. Iwasa[d], S. Kanno[c], S. Kubono, K. Kurita[c], M. Kurokawa[b], T. Minemura[b], T. Motobayashi[b], M. Notani, H.J. Ong[a], S. Ota[e], A. Saito, H. Sakurai[a], S. Takeuchi[b], E. Takeshita[c], Y. Yanagisawa[b] and A. Yoshida[b]

Center for Nuclear Study, Graduate School of Science, University of Tokyo
[a]*Department of Physics, University of Tokyo*
[b]*RIKEN (The Institute of Physical and Chemical Research)*
[c]*Department of Physics, Rikkyo University*
[d]*Department of Physics, Tohoku University*
[e]*Department of Physics, Kyoto University*

1. Introduction

The spectroscopy of neutron-rich oxygen isotopes has attracted much attention, since information on nuclear structure such as single-particle nature and collectivities can be studied as a function of neutron numbers in proton-magic nuclei. In the previous experimental studies on ^{22}O nucleus, measurements of de-excitation γ rays from inelastic scattering with a Au target [1], and from a fragmentation reaction of both stable [2] and radioactive beams [3] have been performed. The excitation energy of the first 2^+ state and the $B(E2)$ value indicate a presence of sub shell closure at N = 14 [1].

In order to obtain more spectroscopic information on ^{22}O, we have performed an experiment with α inelastic scattering in inverse kinematics by measuring de-excitation γ rays coincident with the ^{22}O ejectile. Here the α inelastic scattering on a spin-0 nucleus can populate excited states having natural parities [4, 5]. The transferred angular momenta can be determined by the analysis of angular distributions of differential cross sections.

2. Experiment

The experiment was performed at the RIKEN Accelerator Research Facility. A ^{22}O beam was produced by fragmentation of a 63-MeV/nucleon ^{40}Ar primary beam incident on a beryllium target of 180 mg/cm^2 thickness. Fragments were separated by the RIPS separator. The ^{22}O beam particles were identified event-by-event using the TOF-ΔE method. the TOF was the flight time between two plastic scintillators at the second (F2) and third (F3) focal planes of the RIPS. The ΔE was measured with a 325-μm Si detector installed at F2. The average intensity of the ^{22}O beam was 2×10^3 pps, and its purity was 37%. The ^{22}O beam bombarded a liquid helium target of 100-mg/cm^2 thickness sealed by 6-μm havar foils with 30-mm diameter [6]. The energy of the ^{22}O beam was 35 MeV/nucleon at the center of the secondary target. The scattering angles of outgoing particles were determined by three PPACs. Two of them were installed upstream and the other was installed downstream of the secondary target. The particle identification of outgoing particles from the secondary target was performed using TOF, ΔE and E information measured using a telescope consisting of 9 SSD (3×3 matrix) of 0.5-mm thickness and a NaI(Tl) array (6×6 matrix) [7]. The telescope has an acceptance of 6 degrees in the laboratory system. The excited states in ^{22}O were identified by de-excitation γ rays which were detected by the DALI(II) system [8], which consists of 150 NaI(Tl) crystals surrounding the secondary target.

3. Analysis and Results

Figure 1 shows a Doppler-shift corrected energy spectrum of γ rays from the ^{4}He(^{22}O,^{22}Oγ) reaction. In Fig. 1, two peaks are clearly observed at 3.21 and 1.37 MeV. The 3.21-MeV γ ray corresponds to the known $2^+ \rightarrow 0^+$ transition. In order to identify a cascade transition, we examined a γ ray spectrum coincident with the 3.21-MeV γ ray as shown in Fig. 2. It is clear that the 1.37-MeV γ ray is a member of a cascade transition through the 2^+ state as reported in Ref. [3]. This fact indicates the existence of a 4.58-MeV state as well as the well-known 3.21-MeV state. Since an

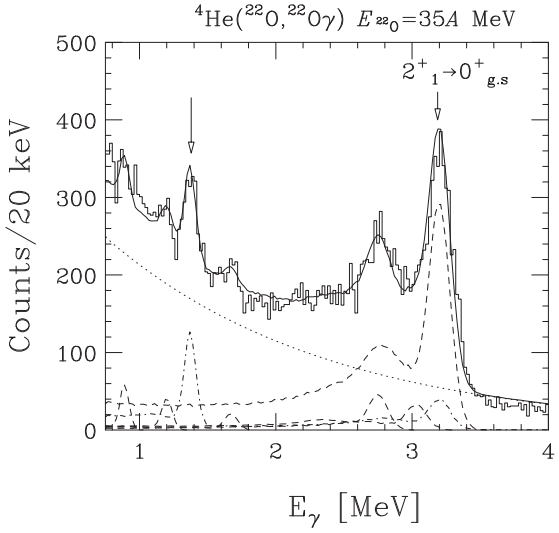

Figure 1. Doppler-shift corrected energy spectrum of γ rays from the ^{4}He(^{22}O,^{22}Oγ) reaction. The dashed line represents the 3.21-MeV transition, and the dash-dotted line denotes the cascade transition. Other dashed lines represents the contribution of ^{21}O. The solid curve represents the best fit.

α inelastic scattering excites natural parity states, we may exclude a speculation that the 4.58-MeV state has 3^+ [3].

The population yields of the two states were deduced by

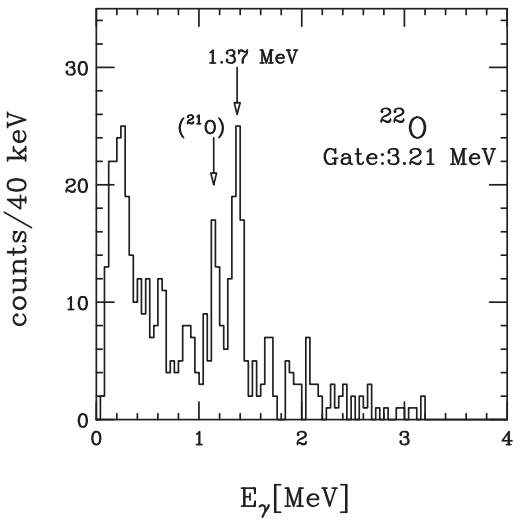

Figure 2. The γ ray energy spectrum coincident with 3.21-MeV γ ray. The γ ray of ^{21}O at 1.2MeV was seen together with the peaks of ^{22}O due to the limited resolution of particle identification.

fitting the observed γ ray spectrum with a sum of response functions for the de-excited γ rays , those from possible contaminants and the background as shown in the lines in Fig. 1. A response function for each state was calculated by a Monte Carlo simulation code GEANT3. The inelastic cross sections were deduced from the yields to be 13.3 $\pm$ 0.6 mb for the 3.21-MeV state and 2.3 $\pm$ 0.2 mb for the 4.58-MeV state, respectively.

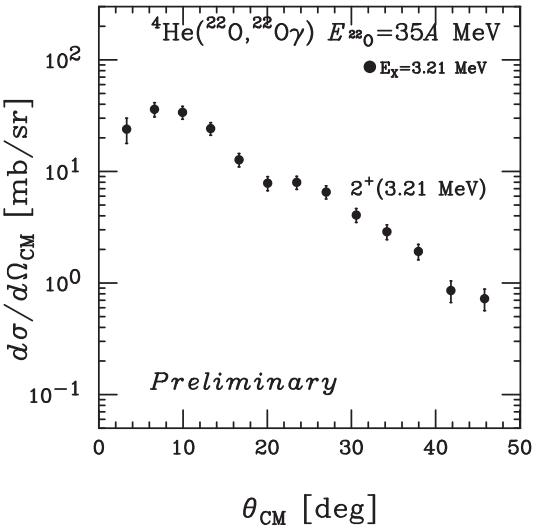

Figure 3. Angular distributions of differential cross sections for the 3.21-MeV state in ^{22}O is plotted versus center-of-mass angle.

The same fitting procedures were applied for the γ ray spectra under the conditions that the scattering angles of the ^{22}O ejectile were sliced in every 0.5 degrees step. Figure 3 shows a preliminary angular distribution for the 3.21-MeV state.

In order to determine the spin and the parity of the 4.58-MeV state, the angular distribution of the inelastic scattering and the angular distribution of the de-excited γ rays will be analyzed based on DWBA calculations.

References

[1] P.G. Thirolf *et al.*, Phys. Lett. B **485** (2000) 16.
[2] M. Belleguic *et al.*, Nucl. Phys. A **682** (2001) 136c.
[3] M. Stanoiu *et al.*, Phys. Rev. C **69** (2004) 034312.
[4] D.H. Youngblood *et al.*, Phys. Rev. C **57** (1998) 2748.
[5] H. Baba *et al.*, CNS Annual Report 2002 (2003) 17.
[6] H. Akiyoshi *et al.*, CNS Annual Report 2001 (2000) 73; H. Akiyoshi *et al.*, RIKEN Accel. Prog. Rep. **34** (2001) 193.
[7] M. Tamaki *et al.*, CNS Annual Report 2002 (2003) 76.
[8] S. Takeuchi *et al.*, RIKEN Accel. Prog. Rep. **36** (2003) 148.

In-beam Gamma-ray Spectroscopy of ^{23}F with Neutron-rich Secondary Beams

S. Michimasa, S. Shimoura[a], H. Iwasaki[b], M. Tamaki[a], N. Aoi, H. Baba[a], N. Iwasa[d], S. Kanno[c], S. Kubono[a], K. Kurita[c], M. Kurokawa, T. Minemura, T. Motobayashi, M. Notani[a], H.J. Ong[b], S. Ota[e], A. Saito[a], H. Sakurai[b] E. Takeshita[c], S. Takeuchi, Y. Yanagisawa and A. Yoshida

RIKEN (The Institute of Physical and Chemical Research)
[a]*Center for Nuclear Study, Graduate School of Science, University of Tokyo*
[b]*Department of Physics, University of Tokyo*
[c]*Department of Physics, Rikkyo University*
[d]*Department of Physics, Tohoku University*
[e]*Department of Physics, Kyoto University*

1. Introduction

The nuclear shell structure is mainly interpreted by single-particle motion in a mean-field including a spin-orbit potential. Recent findings of the disappearance of magic numbers and/or the new magic numbers in the neutron-rich nuclei may indicate that the mean-field changes as a function of neutron/proton numbers. In this respect, neutron-rich fluorine isotopes locate in a stimulating region connecting the exotic nuclear phenomena: the new magic number of $N = 16$ [1] and an island of inversion [2]. In the present work, we have studied excited states in ^{23}F by γ-ray spectroscopy with one-proton transfer reaction. A one-proton transfer reaction is a good probe for investigation on proton shell structure, because this reaction selectively populates single-particle states. Furthermore, we have measured α inelastic scattering and neutron knockout reaction, and compared population strengths by the transfer reaction with ones by these reactions to demonstrate single-particle nature of observed states. We are mainly interested in differences between energies of the proton single-particle states in ^{23}F and in ^{17}F. These differences are considered to reflect a change of mean-field, especially spin-orbit splitting, for protons due to the occupation number of neutrons in the $d_{5/2}$ shell; the $d_{5/2}$ shells in these nuclei are full and empty of neutrons, respectively.

2. Experiment

The experiment was performed at the secondary beam line in RIKEN Accelerator Research Facility. The secondary beams were produced by a projectile fragmentation reaction of 63-MeV/nucleon ^{40}Ar beam impinging on a ^{9}Be target of 180-mg/cm^2 thickness. Fragments were analyzed by the RIPS separator [3]. The secondary beam was a cocktail of ^{22}O,^{23}F and ^{24}F and these particles were identified event-by-event by ΔE-TOF method. Energy losses (ΔE) were measured by a silicon detector, and TOF was the time of flight between two plastic scintillators set 5 meters apart. The average intensities and the mean energies of the secondary beams are listed in Table 1. The secondary beams bombarded a liquid helium target [4] of 100 mg/cm^2, which was contained an aluminum cell with two windows of 6-μm havor foils. The window size was 30 mm in diameter. Reaction products were identified from a combination of time of flight (TOF), energy deposit (ΔE) and energy (E), which were measured by a telescope consisting of 9 SSDs of 0.5-mm thickness and 36 NaI(Tl) detectors [5]. The telescope has an acceptance of $0 - 6$ degrees in the laboratory system. TOF was the flight time between the secondary target and the NaI(Tl) scintillator, and ΔE and E were obtained from energy loss in the SSD and the NaI(Tl) scintillator, respectively. In the present experiment, resolutions of atomic and mass numbers for fluorine isotopes were 0.18 (σ) and 0.35 (σ), respectively. Scattering angles of reaction products were measured by three parallel-plate avalanche counters (PPACs). The two PPACs were placed before the secondary target to determine the direction and the hit point of the beam. The other PPAC was placed after the target to measure the direction of the reaction products. The resolution of scattering angle were was estimated to be 0.5 degrees (σ) in the laboratory flame. Excitation energies of reaction products were identified by de-excited γ rays from reaction products. For γ-ray detection, we used a NaI(Tl) detector array DALI (II) [6]. The array consisted of 150 NaI(Tl) scintillators and surrounded the secondary target in an angular range of $20 - 160$ degrees with respect to the beam axis. In the present experiment, the detection efficiency was 17.6% for 1.33-MeV γ rays, and the energy resolution after Doppler-shift corrections was 8.2% (σ) for the de-excited γ rays at 3.2 MeV from ^{22}O moving with $\beta \sim 0.27$.

Secondary Beam	^{22}O	^{23}F	^{24}F
Energy [AMeV]	35	41.5	36
Intensity [particles/s]	2×10^3	6×10^2	3×10^2

Table 1. Average intensities and mean energies of the secondary beams.

3. Results and Discussions

We have obtained γ-ray spectra in ^{23}F from the proton transfer reaction ^{4}He(^{22}O,^{23}Fγ), the inelastic scattering ^{4}He(^{23}F,^{23}Fγ) and the neutron knockout reaction ^{4}He(^{24}F,^{23}Fγ). Figures 3(a), (b) and (c) show Doppler-corrected γ-ray spectra measured by these three reactions. Population strengths of excited states are sensitive with compatibility between the nature of the states and the reaction mechanism. The proton transfer reaction mainly popu-

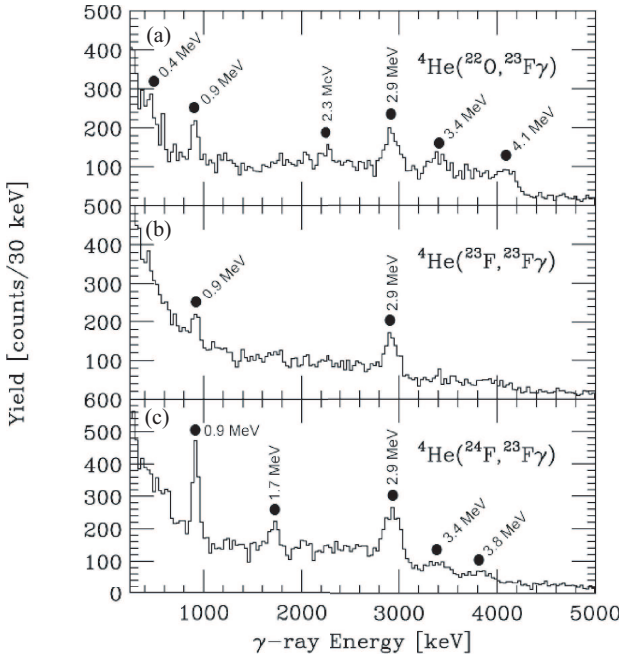

Figure 1. Gamma-ray spectra of three different reactions. Spectrum (a), (b) and (c) were of proton transfer reaction ^{4}He(^{22}O,^{23}Fγ), of inelastic scattering ^{4}He(^{23}F,^{23}Fγ), and of neutron knockout reaction ^{4}He(^{24}F,^{23}Fγ), respectively.

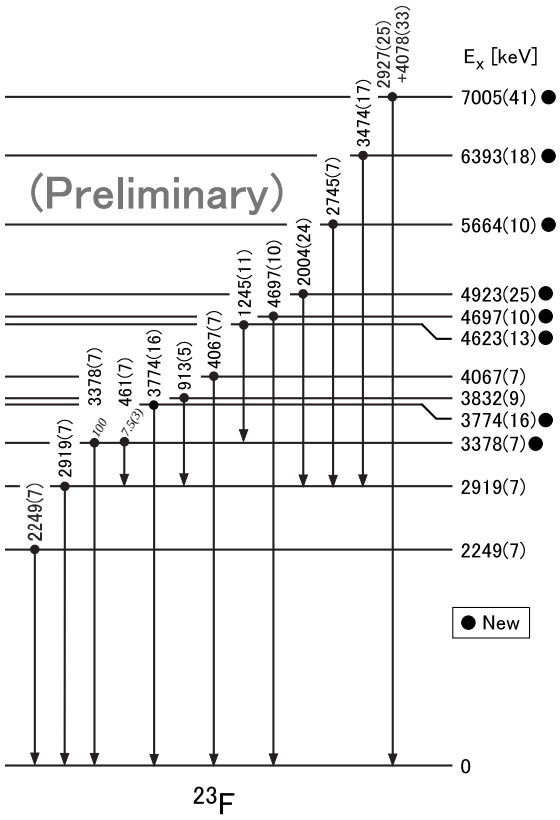

Figure 2. Level and γ-decay scheme in ^{23}F observed in the (^{22}O,^{23}Fγ) reaction. Closed circles in the figure show new excited levels deduced in the present experiment. Relative intensity of γ decay from the 3.378-MeV state is also shown in italics.

lates proton particle states. The α inelastic scattering makes core excitations and non-spin flip proton particle states, and the neutron knockout reaction populates neutron hole states. Taking these relations into account the 2.3-MeV and 4.1-MeV γ rays which were identified only in the transfer reaction are candidates for de-excitation γ rays from proton particle states.

In order to determine the energies of excited states in ^{23}F, existences of cascade γ decays were examined with multiple γ-detection events in the proton transfer reaction. Cross sections for excited states were determined by reproducing both the γ-ray spectrum and the γ-energy summed spectrum by response functions of DALI(II) for identified γ-ray cascades. The response functions were simulated by the code GEANT3. Figure 2 shows a reconstructed level scheme in ^{23}F and de-excited γ rays observed in the transfer reaction. We found new excited states at 3378, 3774, 4623, 4697, 4923, 5664, 6393 and 7005 keV, which are shown in the figure with closed circles, as well as the known states reported in Refs. [7, 8]. Errors shown in the figure are statistical errors estimated by an accuracy of maximum likelihood fitting. We identified that the 2.2-MeV and 4.1-MeV γ rays were produced by de-excitation from the 2.249-MeV state to the ground state and the 4.067-MeV state to ground state, respectively. We therefore consider the 2.249-MeV and 4.067-MeV states as the candidates for single particle states. Furthermore, we identified two paths for γ decay of the 3.378-MeV state, and determined its branching ratio. The one of the paths was a direct decay to the ground state, and the other was two-step γ decay *via* the 2.919-MeV state. We preliminarily deduced the ratio of the direct decay to the two-step decay was 100 to (7.5 ± 3) by the fitting for the reproduction of the γ-ray spectra.

In the next step of the analysis, we are to deduce the spectroscopic factors and the angular momenta of these candidates for single-particle states. In the near future, we will finish all the analysis to reveal the proton shell structure in ^{23}F.

References

[1] A. Ozawa *et al.*, Phys. Rev. Lett. **84** (2000) 5493.
[2] E.K. Warburton *et al.*, Phys. Rev. C **41** (1990) 1147.
[3] T. Kubo *et al.*, Nucl. Instrum. Methods. B **70** (1992) 322.
[4] H. Akiyoshi *et al.*, RIKEN Accel. Prog. Rep. **34** (2001) 193.
[5] M. Tamaki *et al.*, CNS Annual Report 2002 (2003) 76.
[6] S. Takeuchi *et al.*, RIKEN Accel. Prog. Rep. **36** (2003) 148.
[7] N.A. Orr *et al.*, Nucl. Phys. A **491** (1989) 457.
[8] D. Guillemaud-Mueller, Eur. Phys. J. A **13** (2002) 63.

Isoscalar Electric Excitation in ^{14}O

H. Baba, S. Shimoura, T. Minemura[a], Y. U. Matsuyama[b], A. Saito, H. Akiyoshi[a], N. Aoi[a], T. Gomi[a], Y. Higurashi[a], K. Ieki[b], N. Imai[a], N. Iwasa[d], H. Iwasaki[c], S. Kanno[b], S. Kubono, M. Kunibu[b], S. Michimasa[a], T. Motobayashi[a], T. Nakamura[e], H. Sakurai[c], M. Serata[b], E. Takeshita[b], S. Takeuchi[a], T. Teranishi[f], K. Ue[c], K. Yamada[a] and Y. Yanagisawa[a]

Center for Nuclear Study, University of Tokyo
[a]*The Institute of Physical and Chemical Research (RIKEN)*
[b]*Department of Physics, Rikkyo University*
[c]*Department of Physics, University of Tokyo*
[d]*Department of Physics, Tohoku University*
[e]*Department of Applied Physics, Tokyo Institute of Technology*
[f]*Department of Physics, Kyushu University*

1. Introduction

Intermediate energy radioactive isotope (RI) beams enable us to investigate the excited unstable nuclei by using inverse kinematics and by measuring decaying particles. Coulomb dissociation and (p, p') reactions for unstable nuclei have been successfully investigated for the $E1$ and $E2$ excitation in these decades. As another probe for excitation, the inelastic α scattering is useful for isoscalar electric excitation. Recently, isoscalar electric multipole strength for light stable nuclei of ^{12}C [1] and ^{16}O [2] have been obtained via the inelastic scattering of 60 A MeV α particle.

In order to measure the inelastic α scattering reactions in inverse kinematics, we developed a liquid helium target [3]. Here, we report a measurement of inelastic α scattering on the unstable nuclei ^{14}O. The present experiment aimed at measuring the excitation energy spectrum and the isoscalar multipole strength in wide energy range by using the invariant-mass method for various particle decay channels and the multipole decomposition (MD) analysis [4].

2. Experimental Procedure

The experiment was performed at the RIKEN projectile fragment separator (RIPS). A beam of 60 A MeV ^{14}O was produced by the fragmentation of a 135 A MeV ^{16}O beam in a ^{9}Be target with a 1.3-g/cm^2 thickness. The ^{14}O particles were identified event-by-event by the time-of-flight (TOF) measured by two 0.5-mm thick plastic scintillators placed 5.3 m apart. An ^{14}O beam bombarded a 120-mg/cm^2 thick liquid-helium secondary target. The incoming angle and position on the target were measured using two sets of Parallel Plate Avalanche Counters (PPAC's) installed upstream of the target.

Outgoing particles were identified using a ΔE-E1-E2 plastic hodoscope [5] located at 4-m downstream from the target. The hodoscope consisted of three layers (ΔE, E1 and E2 walls) of 5-, 60- and 60-mm thickness, respectively. The ΔE wall was divided horizontally into 13 plastic scintillators. The E1 and E2 walls were divided vertically into 16 and 13 plastic scintillators, respectively. The momenta of outgoing particles were determined by measuring TOF between the target and the hodoscope. The scattering angles were detected by hit positions in the hodoscope.

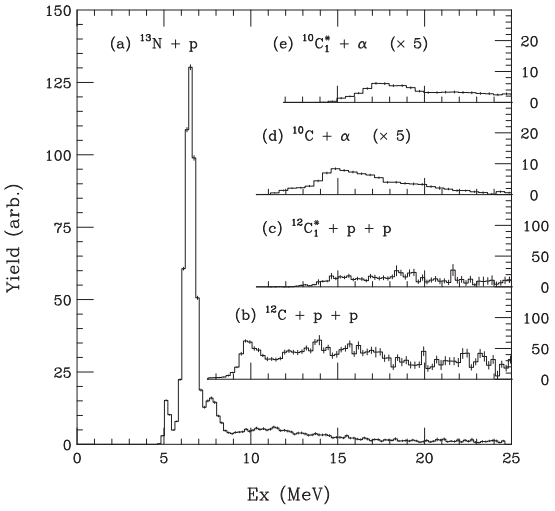

Figure 1. Excitation energy spectra of the ^{14}O (E_x = 4.6 – 25.0 MeV) that constructed by every decay channel via the invariant-mass method.

To obtain de-excitation γ-rays from the outgoing particles, an array of sixty-eight NaI(Tl) scintillators were set around the secondary target. The segmentation of the array allowed us to correct for any Doppler shifts from moving reaction products.

3. Analysis and Results

The excitation energy were constructed from the momentum vectors of decay products with invariant-mass method. We have measured decay channels of ^{14}O$^* \rightarrow {}^{13}$N + p, ^{12}C + p + p, ^{10}C + α, ^{12}C$^*_1$ + p + p, ^{10}C$^*_1$ + α and ^{11}C + ^{3}He. In case of ^{12}C* and ^{10}C* particles, they emit de-excitation γ-rays of 4.4389 [6] and 3.354 MeV [7], respectively.

Excitation energy spectra of the ^{14}O* (E_x = 4.6 – 25.0 MeV) are shown in Fig. 1.

In order to obtain the multipole strength distributions, the MD analysis with the distorted wave Born approximation (DWBA) method has been extensively used. In this analysis, the DWBA calculations for inelastic α scattering were performed using the computer code ECIS97 [8] with exter-

nal optical and transition potentials. We employed a single-folding model with a nucleon-α interaction of the density-dependent Gaussian [9] in the DWBA calculations. Within the folding model approach, the optical potential $U(r)$ is given by:

$$U(r) = \int d\mathbf{r}' V\left(|\mathbf{r} - \mathbf{r}'|, \rho_0(r')\right) \rho_0(r'), \qquad (1)$$

where $V(|\mathbf{r} - \mathbf{r}'|, \rho_0(r'))$ is the nucleon-α interaction, and $\rho_0(r')$ is the ground-state density. The ground-state density was obtained by TIMORA [10] which provided the proton and neutron densities with the relativistic mean field calculations. The transition potential $\delta U(r, E)$ is given by:

$$\delta U(r, E) = \int d\mathbf{r}' \delta\rho_L(\mathbf{r}', E) \left[V\left(|\mathbf{r} - \mathbf{r}'|, \rho_0(r')\right) + \rho_0(r') \frac{\partial V\left(|\mathbf{r} - \mathbf{r}'|, \rho_0(r')\right)}{\partial \rho_0(r')} \right], \qquad (2)$$

where $\delta\rho_L(\mathbf{r}, E)$ and E are transition density and the excitation energy, respectively. The details of the transition densities were described in Refs. [11, 12]

Figure 2 shows the multipole strength distributions of L = 0–4 obtained from the MD analysis. The sum of each strength were identified corresponding to 45.1±8.5, 61.2±8.2, 19.5±1.9, 9.7±2.2, and 20.8±4.6% of the isoscalar $E0$, $E1$, $E2$, $E3$ and $E4$ energy weighted sum rule (EWSR) in E_x = 4.6–25.0 MeV, respectively. The obtained isoscalar electric multipole strength distributions were fragmented in the wide excitation energy range, and the sum of strength were not exhausted 100% of EWSR in $E_x < 25.0$ MeV. Same aspect has been observed in light stable nuclei in Refs. [1, 2]. The details of discussion are in progress.

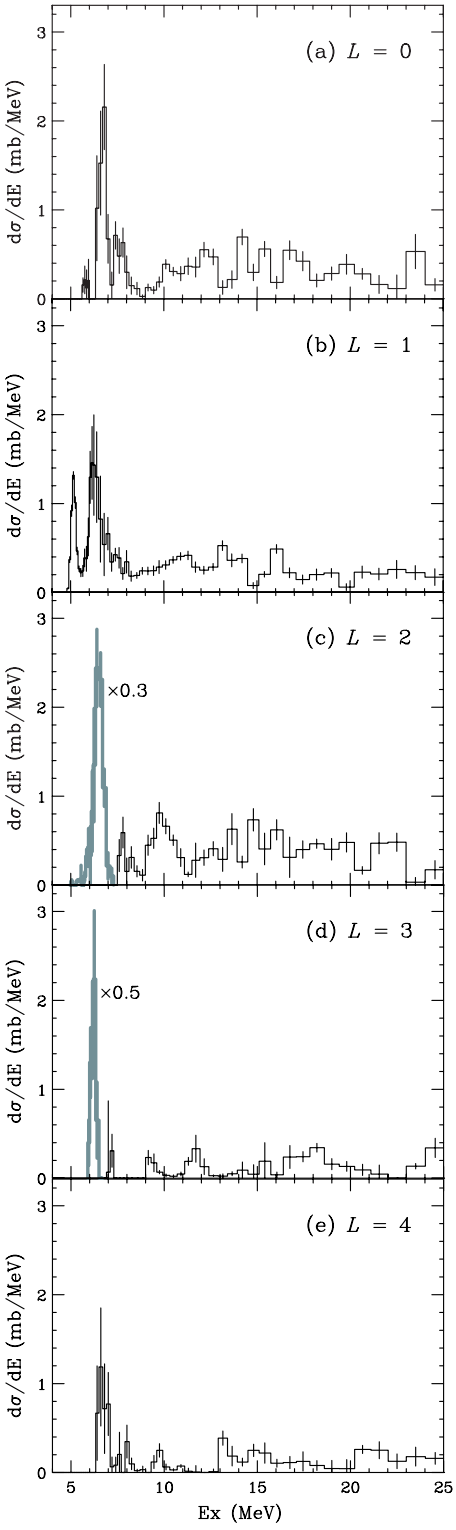

Figure 2. Multipole strength distributions of (a) $L = 0$, (b) $L = 1$, (c) $L = 2$, (d) $L = 3$ and (e) $L = 4$ obtained from the MD analysis.

References

[1] B. John *et al.*, Phys. Rev. C **68** (2003) 014305.
[2] Y.-W. Lui *et al.*, Phys. Rev. C **64** (2001) 064308.
[3] H. Akiyoshi *et al.*, CNS Annual Report 2001 (2002) 73; *ibid.* RIKEN Accel. Prog. Rep. **34** (2001) 193.
[4] M. Itoh *et al.*, Phys. Lett. B **549** (2002) 58.
[5] I. Hisanaga *et al.*, RIKEN Accel. Prog. Rep. **31** (1998) 162.
[6] F. Ajzenberg-Selove, Nucl. Phys. A **506** (1990) 1.
[7] F. Ajzenberg-Selove, Nucl. Phys. A **490** (1988) 1.
[8] J. Raynal, ECIS97 (unpublished).
[9] A. Kolomiets *et al.*, Phys. Rev. C **61** (2000) 34312.
[10] C.J. Horowitz *et al.*, Comp. Nucl. Phys. **1** (1991) 129.
[11] G.R. Satchler, Nucl. Phys. A **472** (1987) 215.
[12] M.N. Harakeh and A.E.L. Dieperink, Phys. Rev. C **23** (1981) 2329.

Production of Low-Energy Secondary Beams for Secondary Fusion Reactions

E. Ideguchi, H. Baba, T. Fukuchi, N. Hokoiwa[a], C. Ishida[b], H. Iwasaki[c] , T. Koike[d], T. Komatsubara[e], T. Kubo[f], M. Kurokawa[f], S. Michimasa[f], K. Miyakawa[e], K. Morimoto[f], M. Niikura, T. Ohnishi[f], S. Ota[g], A. Ozawa[e], S. Shimoura, T. Suda[f], M. Tamaki, I. Tanihata[h], Y. Wakabayashi[a], K. Yoshida [f] and B. Cederwall[b]

Center for Nuclear Study, Graduate School of Science, the University of Tokyo
[a] Department of Physics, Kyushu University
[b]Department of Physics, Royal Institute of Technology, Sweden
[c] Department of Physics, Graduate School of Science, the University of Tokyo
[d] Physics and Astronomy, SUNY Stony Brook, USA
[e] Department of Physics, Tsukuba University
[f] RIKEN (The Institute of Physical and Chemical Research)
[g] Department of Physics, Kyoto University
[h] Argonne National Laboratory, USA

1. Introduction

Studies of high-spin states in atomic nuclei by in-beam gamma-ray spectroscopy have provided detailed information on the nuclear structure. In such studies, high-spin states are achieved mostly through a fusion reaction using a combination of a stable-isotope beam and a stable-isotope target, since large angular momentum can be brought to the nucleus of interest in the reaction. However, nuclei produced in the fusion reaction are limited, in many cases, to the proton-rich side relative to the β-stability line. By utilizing a neutron-rich beam in the fusion reaction, neutron-rich nuclei will be produced and the region available for high-spin studies will be largely expanded.

2. Experimental procedures and results

In order to actualize the method, experiments to produce low-energy secondary beams ($\sim$5MeV/nucleon), which are indispensable for inducing the fusion reaction, were performed at the RIKEN accelerator research facility. Two experiments were carried out. In the first experiment, a low-energy ^{37}P beam was produced for the feasibility study of lowering the energy of secondary beam using Al degraders. In the second experiment, a low-energy ^{46}Ar beam was produced in order to investigate high-spin states of ^{50}Ti via secondary fusion reaction.

2.1. Production of ^{37}P beam

A neutron-rich secondary-beam, ^{37}P, was produced at the RIPS Facility [1] in RIKEN by the fragmentation reaction. The primary ^{40}Ar beam with an energy of 63 MeV/nucleon was provided by the RIKEN Ring cyclotron with a typical intensity of 60 pnA, and it was impinged on a ^{9}Be target of 1.5 mm thick. An aluminum wedge with a mean thickness of 221 mg/cm^2 placed at the momentum-dispersive focal plane (F1) was used to achieve a clear isotope separation and to lower the energy of the fragment to 26 MeV/nucleon. The energy of the ^{37}P beam was further lowered to $\sim$6 MeV/nucleon by placing an aluminum rotatable degrader of 0.425 mm thick at the achromatic focal plane (F2). The energy of the beam was optimized by adjusting the rotation angle of the degrader relative to the beam direction. By operating RIPS at the maximum values of momentum acceptance and solid angle, a typical intensity of 2.0×10^5 counts per second for the ^{37}P beam was obtained at F2. Particle identification of the secondary beam was carried out by the time-of-flight (TOF)-ΔE method, and it was found that an almost pure ^{37}P beam was obtained as shown in Fig. 1. The TOF and ΔE information was obtained from the timing of the plastic scintillator relative to the RF signal of the cyclotron and from the energy loss in the 0.5-mm-thick silicon detector placed at F2, respectively.

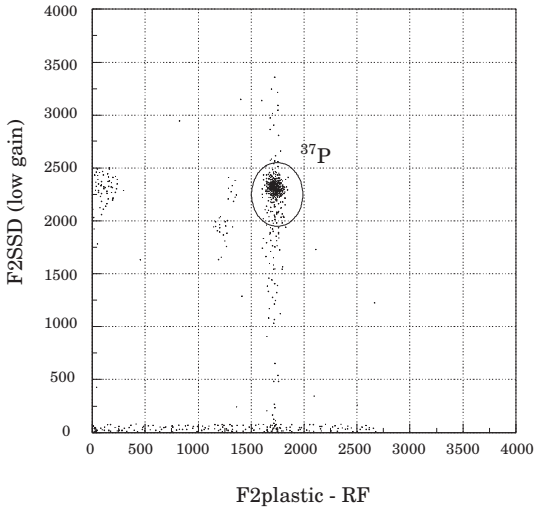

Figure 1. TOF-ΔE plot of ^{37}P at F2.

The ^{37}P beam was transported to the final focal plane (F3) and irradiated on the secondary ^{9}Be target of 10 μm thick in order to induce the secondary fusion reaction, ^{9}Be(^{37}P, xn)$^{46-x}$K. The intensity of the ^{37}P beam at F3 was about 1.0×10^5 counts per second. Two PPAC counters [2] were placed up stream of the secondary target in order to profile the image and the incident angle of the beam on the target, as well as to determine energy from TOF information

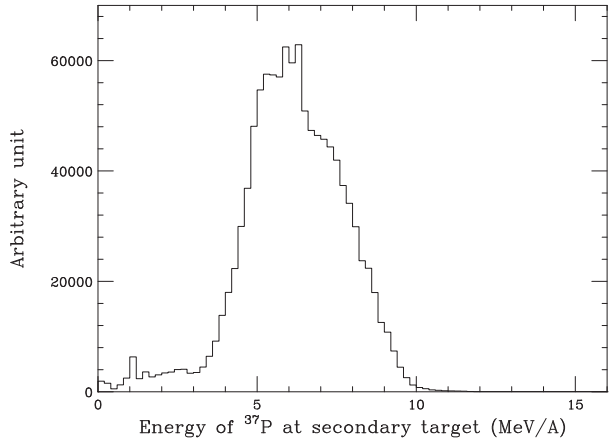

Figure 2. Energy spectrum of the ^{37}P beam at secondary target position deduced from TOF information.

relative to the plastic timing at F2, event by event. Beam spot size on the secondary target extrapolated by using positions in two PPACs was 18 mm and 7.6 mm for horizontal and vertical direction, respectively. Another PPAC counter was also placed downstream of the target to detect recoil nuclei produced in the secondary reaction and to measure the TOF. Figure 2 shows the energy spectrum of the ^{37}P beam at the secondary target position. Details of the gamma-ray analysis is reported elsewhere in this CNS report [3].

2.2. Production of ^{46}Ar beam

Low-energy ^{46}Ar beam was produced in a similar procedure as ^{37}P case. A primary ^{48}Ca beam with a maximum intensity of 100 pnA and the energy of 64 MeV/A was used. It was impinged on the 1.0 mm ^{9}Be target to produce ^{46}Ar beam by the fragmentation reaction. In the ^{46}Ar case, thicknesses of the wedge at F1 and rotatable degrader at F2 were 221 mg/cm^2 and 0.5 mm, respectively. Purity of the ^{46}Ar beam was found to be 90% by TOF-ΔE method as shown in Fig. 3.

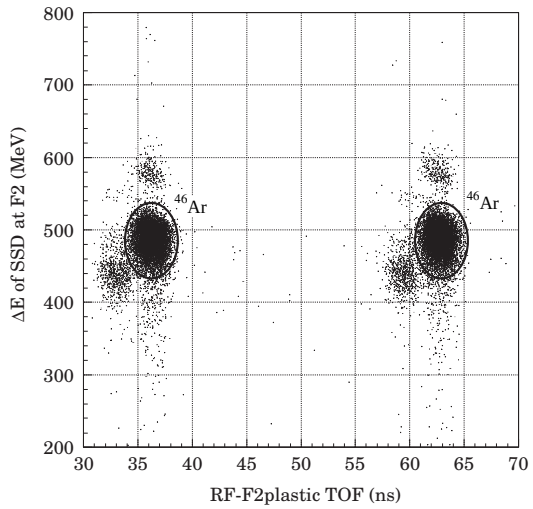

Figure 3. TOF-ΔE plot of ^{46}Ar at F2.

After passing through the rotatable degrader at F2, energy of the ^{46}Ar beam was lowered to 4.3±1.3 MeV/A which was optimum to produce ^{50}Ti via secondary fusion reaction, ^{9}Be(^{46}Ar,$5n$)^{50}Ti. Beam spot size of the ^{46}Ar beam on the secondary target was measured to be 16.5 mm and 8.0 mm in horizontal and vertical direction, respectively. The beam intensity of 3.2×10^5 cps was obtained at the secondary target. Details of the analysis of high-spin study in ^{50}Ti are shown elsewhere in this CNS report [4].

3. Summary

Productions of the low-energy secondary secondary beams, ^{37}P and ^{46}Ar, were demonstrated. Beam energies were lowered by Al degrader to 6±2 MeV/A and 4.3±1.2 MeV/A and the intensities were 1.0×10^5 cps and 3.2×10^5 cps for ^{37}P and ^{46}Ar, respectively, at the secondary target. These low-energy secondary beams were irradiated to the secondary target ^{9}Be and the γ-rays due to the secondary fusion reactions were successfully observed [3, 4]. This method will provide new regions of high-spin studies which were not accessible so far.

References

[1] T. Kubo *et al.*, Nucl. Instrum. Methods. B **461** (1992) 309.
[2] H. Kumagai *et al.*, Nucl. Instrum. Methods. A **470** (2001) 562.
[3] C. Ishida *et al.*, CNS Annual Report 2003 (2004) 9.
[4] M. Niikura *et al.*, CNS Annual Report 2003 (2004) 11.

Gamma-ray Measurement Using Position Sensitive Germanium Detectors in the Secondary Fusion Reaction ^{37}P + ^{9}Be

C. Ishida, E. Ideguchi[a], H. Baba[a], T. Fukuchi[a], N. Hokoiwa[b] N. Iwasaki[c], T. Koike[d], T. Komatsubara[e], T. Kubo[f], M. Kurokawa[f], S. Michimasa[f], K. Morimoto[f], K. Miyakawa[e], M. Niikura[a], T. Ohnishi[f], S. Ota[g], A. Ozawa[e], S. Shimoura[a], T. Suda[f], M. Tamaki[a], I. Tanihata[h], Y. Wakabayashi[b], K. Yoshida[f] and B. Cederwall

Department of Physics, Royal Institute of Technology
[a]*Center for Nuclear Study, Graduate School of Science, University of Tokyo*
[b]*Department of Physics, Kyushu University*
[c]*Department of Physics, Graduate School of Science, University of Tokyo*
[d]*Department of Physics and Astronomy, SUNY Stony Brook, USA*
[e]*Department of Physics, Tsukuba University*
[f]*RIKEN(The Institute of Physical and Chemical Research)*
[g]*Department of Physics, Kyoto University*
[h]*Argonne National Laboratory, USA*

1. Introduction

A secondary ^{37}P beam was produced using RIPS [1] at RIKEN in the fragmentation reaction of a primary beam of ^{40}Ar impinging on a ^{9}Be target [2]. The secondary beam of ^{37}P was used to initiate fusion reactions at the secondary ^{9}Be target according to ^{9}Be(^{37}P, xn)$^{46-x}$K. The recoil velocity of the reaction products in experiments using inverse kinematics is large. These large recoil velocities will induce large Doppler shifts of the emitted gamma rays. For good Doppler correction it is important to know the direction of the emitted gamma rays. The CNS Ge detector array was used in the experiment and the segmentation of the detectors in the array enables good Doppler correction. By using pulse shape analysis the interaction depth of individual gamma rays in the Ge crystals was deduced and the resulting improvement of the Doppler broadening was investigated.

2. CNS Ge Detector Array (GRAPE)

The CNS Ge detector array was surrounding the secondary target [3]. In this experiment the array consisted of 14 segmented Ge detectors. Each detector comprises two planar crystals that share a common anode. The cathode sides are divided electrically into nine segments (Fig. 1). The detectors are aligned so that their side surfaces face the target.

3. Analysis

The segmentation of the detectors make it possible to use pulse shape analysis to obtain information on the interaction points of gamma rays. The rise time of the signal from different segments contains information on the interaction point. In this experiment the net charge signal and the total signal were used for pulse shape analysis. The net charge signal is the signal from the segment containing the interaction point and the total signal is the sum of the signals from the nine segments. The total signal is obtained by using a sum amplifier which gives the analogue sum of the segment signals. The rise time of the pulses is extracted using their zero cross timings after a (CR)^2-(RC)^4 shaping. The zero cross timings of the net charge signal and of the total signal have previously been calculated in 1 mm steps from z=0 mm to z=20 mm for different interaction locations in the crystal (Fig. 2) [4]. In this way the zero cross timings can be related to the interaction depth. To relate the experimental zero cross timings to the interaction depth the signals have to be identified in pairs. This means that there has to be one net charge signal and one total signal from the same crystal in the same event in order to enable comparison with the calculated data. If the photon is Compton scattered between the segments in the same crystal so that one event contains several hits in the same crystal, these signals can not be used for interaction depth determination in this way. This is because the calculated data assumes that the photon only interacts once in the same crystal. By taking this into account, zero-cross timing of the total signal was plotted against that of the net-charge signal minus zero-cross timing of the total signal for a corner-, side- and central segment in Fig. 3. Data shows very good agreement with the simulations as can be seen in the figure.

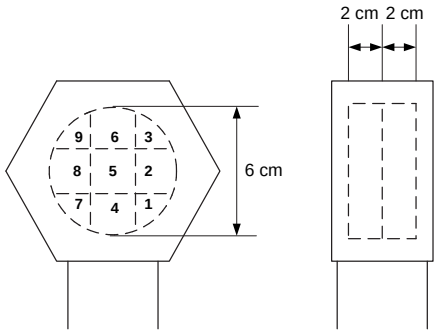

Figure 1. Schematic overview of the detector from the front and the side. The cathode is divided into nine segments. Two crystals are put in the same cryostat and share the anode.

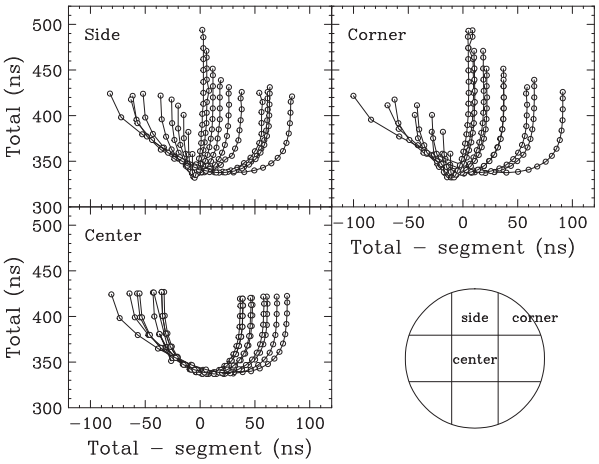

Figure 2. Simulation result for side, center, and corner segment of the zero cross timings for different interaction points. Points connected with the same line correspond to the same r and ϕ location in the segment. The timings were calculated in 1 mm steps from $z = 0$ mm to $z = 20$ mm. The upper left points in the graph correspond to $z = 0$ mm and the upper right points correspond to $z = 20$ mm.

Table 1. Width of the 570 keV peak.

Doppler correction using:	Peak width	Error
center of the detector	20.88 keV	0.88 keV
center of the segment	16.40 keV	0.64 keV
interaction depth	13.16 keV	0.48 keV

4. Analysis Results

The spectrum in Fig 4 shows that ^{42}K [5] was produced in the secondary fusion reaction. Only single-hit events in the detector were used to increment this spectrum. The 106.8-keV peak should have a high relative intensity but can not be seen in the spectrum. The reason for this is the rather high discriminator thresholds used to reduce noise triggering in the present experiment. The peak at 570 keV most probably originates from the transition between the energy levels at 1948 keV and 1376 keV in ^{42}K [5]. In order to evaluate the improvement of the Doppler broadening the width of the peak at 570 keV is examined using three different Doppler corrections (table 1). The Doppler broadening is improved by 21% in case the central position of the segment is used instead of the central position of the detector. When using the interaction depth information for the Doppler correction, the broadening is improved by 20% compared to the case using the central position of the segment.

5. Summary

Gamma rays from the decay of ^{42}K were observed using the CNS Ge detector array in the secondary fusion reaction ^{9}Be(^{37}P, $4n$)^{42}K. The data analysis shows that our pulse shape analysis using analogue electronics improves the Doppler broadening by 20% compared to the case using the central position of the hit segment. However, in the analysis only single hits in the detectors were included

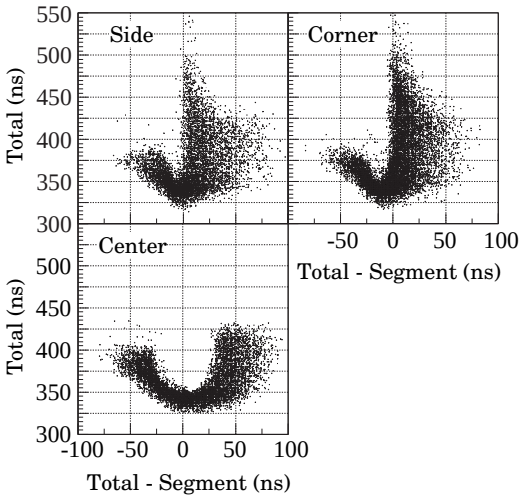

Figure 3. Zero cross timing of the total signal plotted against the zero cross timing of the net charge signal minus the zero cross timing of the total signal for a corner-, side- and center segment.

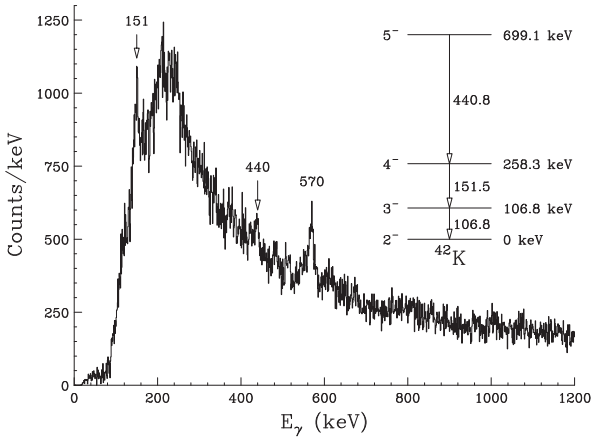

Figure 4. Peaks originating from ^{42}K can be seen in the spectrum.

and much data were therefore lost since the photon is often Compton-scattered between different segments. Further developments are in progress, aiming at including in the Doppler correction procedure also gamma rays that Compton scatter between crystal segments.

References

[1] T. Kubo *et al.,* Nucl. Instrum. Methods. B **461**, 309 (1992).
[2] E. Ideguchi *et al.,* RIKEN Accel. Prog. Rep. **37** (2004)
[3] S. Shimoura *et al.,* CNS Annual Report 2000 (2001) 15.
[4] M. Kurokawa *et al.,* IEEE Trans. Nucl. Sci. **50** (2003) 1309.
[5] M. Moralles *et al.,* Phys. Rev. C **58** (1998) 739.

Study of High-Spin States in ^{50}Ti via the Secondary Fusion Reaction

M. Niikura, E. Ideguchi, T. Fukuchi, H. Baba, N. Hokoiwa[a], C. Ishida[b], H. Iwasaki[c], T. Koike[d], T. Komatsubara[e], T. Kubo[f], M. Kurokawa[f], S. Michimasa[f], K. Miyakawa[e], K. Morimoto[f], T. Ohnishi[f], S. Ota[g], A. Ozawa[f], S. Shimoura, T. Suda[f], M. Tamaki, I. Tanihata[h] Y. Wakabayashi[a] and K. Yoshida[f]

Center for Nuclear Study, Graduate School of Science, University of Tokyo
[a]*Department of Physics, Kyushu University*
[b]*Department of Physics, Royal Institute of Technology*
[c]*Department of Physics, Graduate School of Science, University of Tokyo*
[d]*Department of Physics and Astronomy, State University of New York at Stony Brook*
[e]*Institute of Physics, University of Tsukuba*
[f]*RIKEN (The Institute of Physical and Chemical Research)*
[g]*Department of Physics, Faculty of Science, Kyoto University*
[h]*Argonne National Laboratory*

1. Introduction

Since the discovery of superdeformed bands in ^{40}Ca [1] and ^{36}Ar [2], high-spin studies in this mass region have attracted much attention. These observations support a presence of superdeformed shell gaps in $N, Z = 18$ and 20. Because similar deformed shell gaps were predicted at $N = 28$ and $Z = 22$, an onset of collective rotational bands due to the large deformation is expected in high-spin states of ^{50}Ti. Excited states in ^{50}Ti were previously studied using the $^{48}\mathrm{Ca}\,(\alpha, 2n)\,^{50}\mathrm{Ti}$ reaction, and high-spin levels up to 11^+ state at 8.8 MeV have been reported in Refs. [3, 4]. No rotational bands were, however, observed. In order to search for the rotational bands in ^{50}Ti, it is necessary to investigate higher spin states using heavy ion fusion reaction, but the lack of beam and target combinations with stable isotopes have prevented the experimental studies thus far. A usage of neutron-rich radioactive-isotope (RI) beams can relax this experimental constraint and allowed investigation of high-spin states in ^{50}Ti with the secondary fusion reaction, $^{9}\mathrm{Be}\left(^{46}\mathrm{Ar}, 5n\right)^{50}\mathrm{Ti}$.

2. Experiment and Result

The experiment was performed at RIKEN Accelerator Research Facility. A secondary ^{46}Ar beam was produced by the fragmentation using a ^{48}Ca primary beam accelerated up to an energy of 63.36 MeV/u by the RIKEN Ring Cyclotron (RRC) incident upon a ^{9}Be production target of 1.0-mm thickness. The maximum intensity of the primary ^{48}Ca beam was 100 pnA.

The ^{46}Ar was separated by a RIKEN Projectile-fragments Separator (RIPS) [5] using an aluminum wedge degrader with mean thickness of 221 mg/cm^2 at the momentum dispersive focal plane (F1). A particle identification of the fragments was performed by measuring time-of-flight (TOF) and energy loss (ΔE) information, enabling a selection of almost uniquely ^{46}Ar.

For the fusion reaction, the energy of the secondary ^{46}Ar beam was lowered to 4.3 ± 1.3 MeV/u using a rotatable degrader with a thickness of 0.5 mm placed at the achromatic focal plane (F2). The beam energy was optimized to produce ^{50}Ti with the maximum cross section which was predicted by CASCADE code [6]. The low-energy secondary beam was transported to the final focal plane (F3), where a thin 10-μm ^{9}Be secondary target was placed for the fusion reaction, $^{9}\mathrm{Be}\left(^{46}\mathrm{Ar}, 5n\right)^{50}\mathrm{Ti}$.

Two parallel plate avalanche counters (PPAC's) [7] were placed upstream of the secondary target to monitor the profile and incident angle of the beam on the target. The PPAC's were also used to measure the incident beam energy from the TOF information relative to the timing of the plastic scintillator placed at F2 event by event. The other PPAC was put downstream of the target to detect outgoing particles produced in the secondary reaction and measure the TOF information.

Gamma rays from the high-spin states in ^{50}Ti were detected by GRAPE (Gamma-Ray detector Array with Position and Energy sensitivity) system [8]. In this experiment the GRAPE system was composed of 17 detectors, each of which contains two planar germanium crystals and each germanium crystal is electrically segmented to nine pieces. These γ-ray detectors were placed around the secondary target to cover at the angle between 60 degrees and 120 degrees. With a trigger condition of two or more Ge detectors firing in coincidence, a total of 1.2×10^7 events was collected.

In order to correct the energy of Doppler-shifted γ rays emitted from moving nuclei, it is necessary to obtain the hitting position of the beam on the target, direction of the recoil out of the target, energies of the beam and reaction products, and the polar angle of the γ-ray hit position in the GRAPE detector with respect to the direction of the reaction products. Energies, positions, and directions of the beam and the reaction products were extracted from the TOF and the deduced position information using the PPAC's. In the current analysis, we took the center of each segment for the information on the interaction points of the incident γ rays.

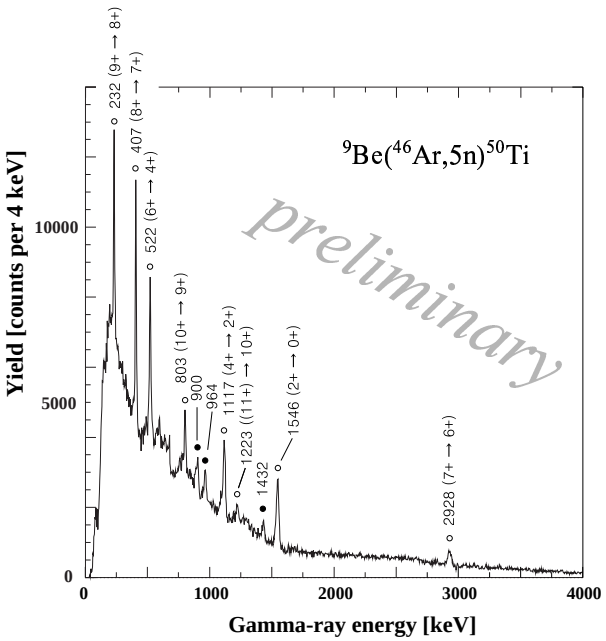

Figure 1. Doppler-corrected γ-ray energy spectra. The known γ rays reported in Refs. [3,4] were marked by open circles. New γ rays observed in this work were marked by closed circles.

Advanced analysis to extract the position information from the pulse shape analysis, reported in Ref. [9, 10], is now in progress.

Figure 1 shows a Doppler-corrected γ-ray energy spectrum. Previously reported γ rays from ^{50}Ti of 232, 407, 522, 803, 1117, 1223, 1546, and 2928 keV, were confirmed in the present study. By gating on these γ rays to check the coincidence relations between them, cascade sequences for known γ rays were also confirmed. Intensity distributions of the individual transition was consistent with the ordering of the gamma transitions in the level scheme of Refs. [3, 4]. By gating on the fold of γ-ray coincidence, the γ-ray yields from the higher spin states were indeed enhanced in the high multiplicity spectrum (Fig. 2). This fact also supports the reported level scheme.

We have identified three new transitions with 900-, 964-, and 1432-keV γ rays, which were in coincidence with known γ rays of ^{50}Ti. Gamma rays originating from other evaporation channels were not observed. This result was in accordance with the optimal secondary beam energy predicted by the CASCADE calculations.

Further analysis to extend the level scheme based on the observed γ-ray coincidence relations are now in progress.

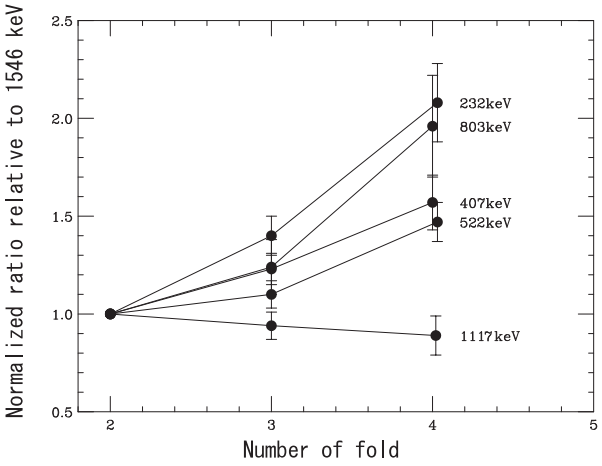

Figure 2. Relative γ-ray yields as a function of the detected γ-ray multiplicities. The gamma-ray yields are normalized to the intensity of the lowest transition at 1546 keV.

References

[1] E. Ideguchi *et al.*, Phys. Rev. Lett. **87** (2001) 222501.
[2] C. E. Svensson *et al.*, Phys. Rev. Lett. **85** (2000) 2693.
[3] J. Styczen *et al.*, Nucl.Phys. A **327** (1979) 295.
[4] B. Haas *et al.*, Phys. Rev. Lett. **40** (1978) 1313.
[5] T. Kubo *et al.*, Nucl. Instrum. Methods. B **461** (1992) 309.
[6] F. Pühlhofer, Nucl. Phys. A **280** (1977) 267.
[7] H. Kumagai *et al.*, Nucl. Instrum. Methods. A **470** (2001) 562.
[8] S. Shimoura *et al.*, CNS Annual Report 2003 (2004) 87.
[9] C. Ishida *et al.*, CNS Annual Report 2003 (2004) 9.
[10] M. Kurokawa *et al.*, IEEE Trans. Nucl. Sci. **50** (2003) 1309.

Spectroscopy of ^{13}B via ^{4}He(^{12}Be,^{13}Bγ) Reaction

S. Ota, S. Shimoura[a], H. Iwasaki[b], M. Kurokawa[c], S. Michimasa[c], S. Kubono[a], T. Teranishi[a], M. Notani[a], M. Tamaki[a], T. Murakami, N. Iwasa[d], T. Motobayashi[c], Y. Yanagisawa[c], T. Minemura[c], S. Takeuchi[c], T. Gomi[e], K. Yamada[e], A. Saito[a], H. Baba[a], Y. U. Matsuyama[e], S. Kanno[e], E. Takeshita[e], K. Demichi[e], K. Hasegawa[e], K. Kurita[e], N. Aoi[c], H. Sakurai[b], E. Ideguchi[a], A. Odahara[f], T. Fukuchi[a], K. Miller[g], Z. Elekes[c] and M. Ishihara[c]

Department of Physics, Kyoto University
[a]*Center for Nuclear Study, Graduate School of Science, University of Tokyo*
[b]*Department of Physics, University of Tokyo*
[c]*RIKEN (The Institute of Physical and Chemical Research)*
[d]*Department of Physics, Tohoku University*
[e]*Department of Physics, Rikkyo University*
[f]*Nishinippon Institute of Technology*
[g]*Michigan State University, USA*

1. Introduction

Recently, the ^{12}Be nuclei has been found to lose the regular neutron magic number [1, 2, 3, 4]. The magicity loss may be caused by the unbalance between the number of protons and neutrons. The neutron shell structure is affected by the proton number so that the shell gap disappear. On the other hand, the proton shell structure may also be affected by the neutron number or shell structure. In order to investigate the relationship between the proton shell structure and the neutron magicity loss, we have studied the excited states in the ^{13}B by using proton transfer to the ^{12}Be. A differential cross section of the reaction may provide the information on the angular momentum of the excited state. So far ^{13}B is studied via several reactions, where the energies and parities of the excited states are determined [5, 6, 7, 8] but their spins have not been assigned except for a few suggestions [6, 8] .

Since the (^{4}He,t) reaction has relatively large cross section in the energy ragion of a few tens *A*MeV, we chose the proton transfer reaction ^{4}He(^{12}Be,^{13}Bγ). We measured de-excitation γ rays in coincidence with the scattered particles ^{13}B produced via the proton transfer reaction. An angular distribution of the ^{13}B was extracted from the observed γ ray yields for each scattering angle of ^{13}B.

2. Experiment

The experiment was performed at RIKEN Accelerator Research Facility. A ^{12}Be secondary beam of 50 *A*MeV was produced by a projectile-fragmentation of ^{18}O primary beam of 100 *A*MeV. The secondary beam bombarded a secondary target of liquid helium, in which the excited ^{13}B nucleus was produced and de-excitation γ ray was emitted from the moving ^{13}B nucleus. De-excitation γ rays were detected with an array of six Germanium detectors (one third of GRAPE [9]) at 140 degrees with respect to the beam direction. The outgoing ^{13}B was detected with a ΔE-E plastic scintillator hodoscope located at 4.3-m downstream of the secondary target.

Detail of experimental setup is written in Ref [10].

3. Result

An excited state in ^{13}B is identified by the energy of de-excitation γ ray. A Doppler-shift corrected energy spectrum of γ rays measured in coincidence with scattered ^{13}B is shown in Fig. 1. There are peaks corresponding to the known excited states. The intensities of these states are obtained by fitting simulated γ-ray energy spectra to the experimental one described as follows.

A response function [$f_i(x)$] of the detector array for each de-excitation γ ray of i-th excited state is simulated with a Monte Carlo simulation code, GEANT4 [11], taking into account the energy resolution and the angular resolution of each detector. The simulated energy spectrum [$Y_{sim}(x)$] is represented as the linear combination of $f_i(x)$ and an exponential background,

$$Y_{sim}(x) = \sum_i A_i f_i(x) + B\exp(-Cx). \qquad (1)$$

The fitting parameters are the normalization factor (A_i) for each response function and height (*B*) and slope (*C*) of the background term. The energy of each γ ray is fixed to be the known one. By fitting $Y_{sim}(x)$ to the experimental spectrum, we obtain the intensities.

The obtained relative intensities are listed in Table 1. The 3.71-MeV and 4.83-MeV excited states are more strongly populated than the other states. In the other reactions, where neutron states or proton-particle neutron-hole states are more populated, these states are not strongly populated. So, these two states may be of a single particle nature.

We extract the angular distribution of ^{13}B by decomposing Eq. (1) with the scattering angle θ as below,

$$Y_{sim}(x) = 2\pi \int \Big[\sum_i a_i(\theta) f_i(x) + b(\theta)\exp(-cx) \Big] d\cos\theta. \qquad (2)$$

The intensities is obtained by fitting $Y_{sim}(x)$ to the spectrum of γ ray measured in coincidence with the ^{13}B scattered in the ($\theta \pm \Delta\theta/2$) angular region. Assuming the

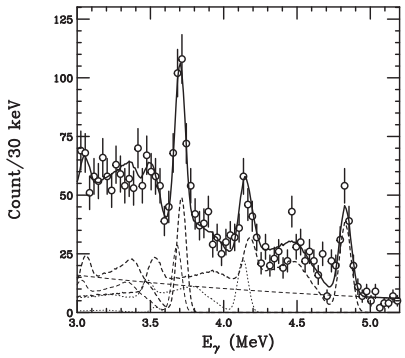

Figure 1. A Doppler-shift corrected gamma-ray energy spectrum obtained in coincidence with ^{13}B. Solid curve shows the simulated spectrum including exponential background.

Ex (MeV)	Present ^{4}He (^{12}Be,^{13}Bγ)	a	b	c
3.48	0.00 ± 0.16	0.06	0.6	
3.53	0.03 ± 0.08	0.19		1
3.68	0.43 ± 0.15	0.38	1	
3.71	0.76 ± 0.16	0.25		
4.13	0.42 ± 0.10	1	0.04	
4.83	1	0.03		

Table 1. Excitation energies of the known states in ^{13}B and relative intensities of those states measured via four reactions. The error is only statistical one.
a: ^{11}B(t,p)^{13}B, b: ^{9}Be(^{14}B,^{13}B)X, c: ^{14}Be(βn)

isotropic distribution of the γ ray for each scattering angle, the angular distribution $\frac{d\sigma}{d\Omega}(\theta)$ of ^{13}B is deduced from $a_i(\theta)$.

The experimental angular distribution obtained for the highest excited state with $\Delta\theta_{lab} = 0.5^\circ$ is shown in Fig. 2 by closed circles. A forward peaking distribution may indicate that the transfered angular momentum (l) is zero. In order to confirm that, we performed DWBA calculations assuming $l = 0$, 1 and 2 with DWUCK5 code. The optical potentials used for entrance and exit channels are listed in Table 2 (see the caption for detail). The experimental angular distribution is well reproduced by the DWBA calculation with l=0. Small variation of optical potential parameters does not change the tendency.

We assign J^π=1/2$^+$ to the 4.8-MeV excited state, considering J^π of ^{12}Be(g.s.) is 0^+ and the isotropic distribution of the γ ray from J^π=1/2$^+$ state.

4. Summary

We measured the proton transfer reaction ^{4}He(^{12}Be,^{13}Bγ) at 50 MeV per nucleon. From the analysis on the angular distribution of the ^{13}B for the 4.83-MeV excited state, we assigned J^π=1/2$^+$ to the excited state for the first time. Analyses on the other states are in progress.

The present study shows that the (^{4}He,t) reaction in the inverse kinematics at intermediate energy becomes one of the powerful tools for the spectroscopy of neutron-rich nuclei.

		V_0 (MeV)	r_V (fm)	a_V (fm)	W_0 (MeV)	r_W (fm)	a_W (fm)
I	^{4}He+^{12}C	75.680	1.277	0.728	13.880	1.885	0.425
II	^{3}He+^{12}C	108.47	1.020	0.828	18.483	1.171	0.594
III	^{3}He+^{12}C	85.580	1.253	0.760	18.354	1.714	0.674

Table 2. Optical potentials used in DWBA calculations. Potential I [12] is for entrance channel. Potential II and III [13] are for exit channel.

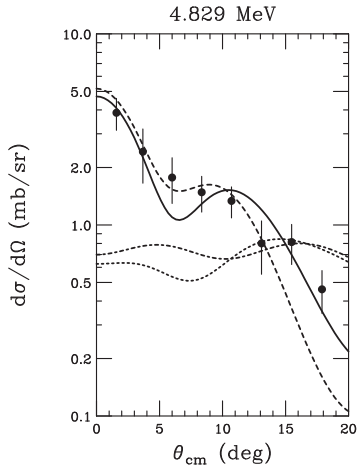

Figure 2. An angular distribution of ^{13}B with DWBA calculation. Solid and dashed curves are for $l = 0$ with potential I-II and I-III, respectively. Dotted and dash-dotted curves are for $l = 2$ and 3 with potential I-II, respectively.

References

[1] A. Navin *et al.*, Phys. Rev. Lett. **85** (2000) 266.
[2] H. Iwasaki *et al.*, Phys. Lett. B **481** (2000) 7.
[3] H. Iwasaki *et al.*, Phys. Lett. B **491** (2000) 8.
[4] S. Shimoura *et al.*, Phys. Lett. B **560** (2003) 31.
[5] F. Ajzenberg-Selove *et al.*, Phys. Rev. C **17** (1978) 1283.
[6] V. Guimarães *et al.*, Phys. Rev. C **61** (2000) 064609.
[7] N. Aoi *et al.*, Phys. Rev. C **66** (2002) 014301.
[8] R. Kalpakchieva *et al.*, Eur. Phys. J. A **7** (2000) 451.
[9] S. Shimoura *et al.*, CNS Annual Report 2003 (2004) 87
[10] S. Ota *et al.*, CNS Annual Report 2002 (2003) 14.
[11] GEANT4 (http://wwwasd.web.cern.ch/wwwasd/geant4/geant4.html).
[12] A. Ingemarson *et al.*, Nucl. Phys. A **676** (2000) 3.
[13] A. Ingemarson *et al.*, Nucl. Phys. A **696** (2001) 3.

Molecular States in Neutron-Rich Beryllium Isotopes

A. Saito, S. Shimoura[a], S. Takeuchi, T. Motobayashi, T. Minemura[b], Y. U. Matsuyama, H. Baba, H. Akiyoshi[b], Y. Ando, N. Aoi[c], Zs. Fülöp[d], T. Gomi, Y. Higurashi, M. Hirai[e], K. Ieki, N. Imai[b], N. Iwasa[f], H. Iwasaki[a], Y. Iwata[e], S. Kanno, H. Kobayashi, S. Kubono[a], M. Kunibu, M. Kurokawa[a], Z. Liu[g], S. Michimasa[a], T. Nakamura[h], S. Ozawa[b], H. Sakurai[c], M. Serata, E. Takeshita, T. Teranishi[a], K. Ue[c], K. Yamada, Y. Yanagisawa[b] and M. Ishihara[b]

Department of Physics, Rikkyo University
[a]*Center for Nuclear Study, Graduate School of Science, University of Tokyo*
[b]*RIKEN (The Institute of Physical and Chemical Research)*
[c]*Department of Physics, University of Tokyo*
[d]*ATOMKI, Debrecen, Hungary*
[e]*National Institute of Radiological Science*
[f]*Department of Physics, Tohoku University*
[g]*Institute of Modern Physics, Lanzhou, China*
[h]*Department of Physics, Tokyo Institute of Technology*

1. Introduction

Structure of the neutron-rich beryllium isotopes is an interesting subject in the studies of unstable nuclei. Especially the cluster structure of ^{12}Be is one of the most important phenomena. The recent experimental study by Freer *et al.* [1] stimulated researches on highly excited states in ^{12}Be. They measured inelastic scattering of ^{12}Be on proton and carbon targets at 378 MeV. Several peaks were observed in the excitation-energy spectrum obtained for the invariant mass of two ^{6}He's. The angular correlations for some of these peaks were analyzed to determine their spins. The excited states with spin-parities in the range of 4^+ to 8^+ were identified. By the energy-spin systematics, the new excited states were expected to form a rotational band of a ^{6}He-^{6}He cluster structure. A multi-nucleon transfer reaction of ^{9}Be(^{15}N,^{12}N)^{12}Be at 240 MeV was performed by Bohlen *et al.* [2]. The observed levels in the missing-mass spectrum were classified as members of the other rotational band by assuming their spins. Several theoretical calculations reasonably reproduced these excited states in ^{12}Be, *e. g.* the Antisymmetrized Molecular Dynamics (AMD) [3], the microscopic coupled channel calculation [4], and the microscopic cluster model calculation [5]. The AMD calculation predicted existence of 0^+ and 2^+ states above the ^{6}He+^{6}He threshold.

We performed two experiments to search for excited states with low spins, such as 0^+ and 2^+, which may lie above the ^{6}He+^{6}He decay threshold. The first experiment was for a two-neutron removal reaction with a ^{14}Be beam on a carbon target [6]. Some peaks were observed in the decay-energy spectrum of two ^{6}He's. The second experiment was for inelastic scattering of ^{12}Be on a liquid helium target. The inelastic-alpha scattering reaction has the advantage of well-known reaction mechanism, and here it is possible to determine spins by angular distributions of the inelastic scattering compared with DWBA calculations.

2. Experimental Procedure

The experiment was carried out in RIKEN Accelerator Research Facility. A primary beam of ^{18}O at 100 MeV/nucleon was supplied by RIKEN Ring Cyclotron accelerator. The intensity of the primary beam was 150 pnA. A radioactive ^{12}Be beam was produced using a projectile-fragmentation reaction of the ^{18}O beam on a ^{9}Be target. The ^{12}Be beam was separated from the other fragments using RIKEN Projectile-fragment Separator (RIPS) [7]. Remaining contaminants were rejected using the time-of-flight (TOF) and energy losses measured by two plastic scintillators separated by 5.3 m each other. A typical intensity of the secondary beam was 3×10^4 particles per second. The ^{12}Be beam bombarded a liquid helium target, which was confined in a cell with a 6-μm-thick Havar window of 24-mm diameter. The direction and the hit position of each beam particle at the secondary target were measured by two sets of Parallel Plate Avalanche Counters (PPAC's) installed upstream of the secondary target. The energy of the ^{12}Be secondary beam was 60 MeV/nucleon in the middle of the secondary target.

The reaction products of two helium isotopes were measured and identified using a hodoscope of a plastic scintillator array with an active area of 1×1 m^2 located 3.9 m downstream of the target. the thicknesses of the ΔE, $E1$, and $E2$ layers were 5 mm, 60 mm, and 60 mm, respectively. The resolutions (in sigma) of the TOF, horizontal, and vertical positions were 0.15 ns, 0.9 cm, and 1.3 cm, respectively. The decay energies for ^{12}Be$\rightarrow^{6}$He+^{6}He and α+^{8}He were extracted by the invariant-mass method. The resolution of the decay energy was estimated using Monte Carlo simulations including the resolutions of the detectors and the multiple scattering of the beam and the reaction products. The energy resolution was proportional to a square root of the decay energy ($\sqrt{E_{\rm d}}$) as $\Delta E_{\rm FWHM} = 0.34 \times \sqrt{E_{\rm d}}$ MeV.

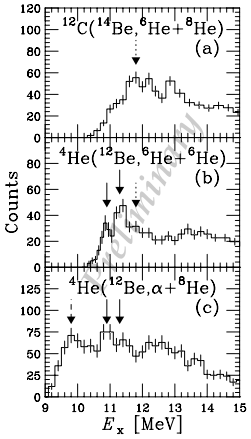

Figure 1. Excitation energy spectra of ^{12}Be obtained in (a) ^{12}C(^{14}Be,^{6}He+^{6}He)X, (b) ^{4}He(^{12}Be,^{6}He+^{6}He), and (c) ^{4}He(^{12}Be,α+^{8}He) reactions.

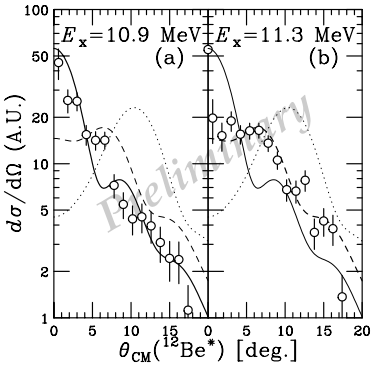

Figure 2. Angular distributions for the peaks at (a) 10.9 MeV and (b) 11.3 MeV. The solid, dashed, and dotted curves denote the predictions of DWBA calculations with Δl=0, 2, and 4, respectively.

3. Results and Discussions

The excitation-energy spectra of ^{12}Be were obtained for three different reactions. Figure 1 (a) shows a spectrum obtained in the ^{12}C(^{14}Be,^{6}He^{6}He)X reaction [6]. Figure 1 (b) and (c) are the results for the ^{4}He(^{12}Be,^{6}He^{6}He) and ^{4}He(^{12}Be,^{8}Heα) reactions, respectively. In the present experiment, new peaks were observed at 10.9 MeV and 11.3 MeV in the spectrum of ^{6}He+^{6}He decay channel (indicated by solid arrows in Fig. 1 (b)). These peaks are also seen in the α+^{8}He spectrum (Fig. 1 (c)). The bump around 11.8 MeV in Fig. 1 (b) indicated by dotted arrow may correspond to the peak in the previous data of the two-neutron removal reaction (Fig. 1 (a)). The peak at around 10 MeV observed in the α+^{8}He decay channel (indicated by a dashed arrow in Fig. 1 (c)) may correspond to the excited state observed in the inelastic-proton scattering of ^{12}Be by Korsheninnikov *et al.* [8].

The angular distributions of the excited ^{12}Be for the peaks at (a) 10.9 MeV and (b) 11.3 MeV are shown in Fig. 2. The distribution for the 10.9-MeV peak has a forward peak, then the spin-parity of this peak is expected to be 0^+. The one for the 11.3 MeV peak has a flat distribution at forward angles, then this peak is expected to have a larger spin. The solid, dashed, and dotted curves denote the predictions of the DWBA calculations by ECIS97 [9] with $\Delta l = 0$, 2 and 4, respectively, which is folded with the angular resolution. By comparing the angular distributions with the DWBA calculations, the spin-parities of the 10.9-MeV and 11.3-MeV states were determined to be 0^+ and 2^+, respectively.

Figure 3 shows the energy-spin systematics of excited states in ^{12}Be. The dotted line is the ground state band. The open squares are the excited states measured by Bohlen *et al.*, using the multi-nucleon transfer reaction, which may

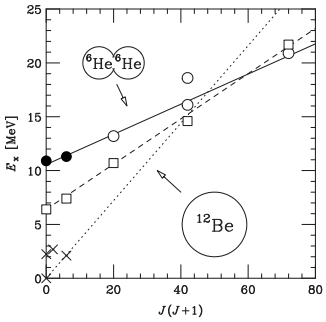

Figure 3. Energy-spin systematics of excited states in ^{12}Be.

form a possible rotational band starting from around 6 MeV. The open circles are the data of Freer *et al.* using the inelastic scattering. The closed circles are the new excited states observed in the present study. The solid line is the rotational band excluding the 6^+ state at 18.6 MeV, which has a large moment of inertia corresponding to $\hbar^2/2\mathcal{I}$=140 keV. The rotational band is good agreement with the assumption of the ^{6}He-^{6}He cluster structure in ^{12}Be

4. Summary

Inelastic-alpha scattering reaction of ^{12}Be was measured using the liquid helium target. New excited states at 10.9 MeV (0^+) and 11.3 MeV (2^+) were observed in the decay-energy spectrum of ^{6}He+^{6}He decay channel. These spins were determined by the angular distributions of the inelastic scattering compared with the DWBA calculations. These excited states may be members of the rotational band with the developed ^{6}He-^{6}He cluster structure in ^{12}Be.

References

[1] M. Freer *et al.*, Phys. Rev. Lett. **82** (1999) 1383.
[2] H. G. Bohlen *et al.*, Proc. Intr. Symp. on Exotic Nuclei (2002) 453 .
[3] Y. Kanada-En'yo and H. Horiuchi, Phys. Rev. C **68** (2003) 014319.
[4] M. Ito and Y. Sakuragi, Phys. Rev. C **62** (2000) 064310.
[5] P. Descouvemont and D. Baye, Phys. Lett. B **505** (2001) 71.
[6] A. Saito *et al.*, Suppl. Prog. Theor. Phys. **146** (2002) 557.
[7] T. Kubo *et al.*, Nucl. Instrum. Methods. B **70** (1992) 309.
[8] A. A. Korsheninnikov *et al.*, Phys. Lett. B **343** (1995) 53.
[9] J. Raynal, coupled-channel code ECIS97 (unpublished).

Measurement of Vector Analyzing Power in the $\vec{p} + {}^6\mathrm{He}$ Elastic Scattering at 71 MeV/u

T. Uesaka, M. Hatano[a], T. Wakui, H. Sakai, A. Tamii[b], T. Kawabata, K. Itoh[c], T. Ikeda[c], K. Yako[a], Y. Maeda[a], T. Saito[a], H. Kuboki[a], M. Sasano[a], K. Sekiguchi[d], T. Ohnishi[d], N. Aoi[d], Y. Yanagisawa[d], H. Iwasaki[a], T. K. Onishi[a], Y. Ichikawa[a], Y. Satou[e] and N. Matsui[c]

Center for Nuclear Study, Graduate School of Science, University of Tokyo
[a]*Department of Physics, University of Tokyo*
[b]*Reserach Center for Nuclear Physics, Osaka University*
[c]*Department of Physics, Saitama University*
[d]*RIKEN (the Institute of Physical and Chemical Research)*
[e]*Department of Physics, Tokyo Institute of Technology*

1. Introduction

For the purpose to investigate polarization phenomena in nuclei far from the stability line, a polarized proton solid target has been constructed at the Center for Nuclear Study [1]. In the design of the target system, special attentions have been paid to facilitate detection of recoiled protons. Since, under the inverse kinematics condition, the recoiled protons have low energies of $\sim$10 MeV at forward angles in the center-of-mass system, they can be easily blocked by materials or magnetic field around the target. Complicated cryogenic apparatus and high magnetic field of $>$ 1 T, therefore, have to be excluded from the target region. Our polarized target which works under a high temperature of $\sim$ 100 K and a low magnetic field of $<$ 0.1 T can suffice the requirements, exhibiting a good contrast to conventional dynamic-nuclear-polarization targets which necessarily requires a low temperature of $<$ 1 K and a high magnetic field of $>$ several Tesla.

In 2003, the polarized proton solid target was applied to the radioactive isotope beam experiment for the first time [3]. In the experiment, the vector analyzing power for the $p + {}^6\mathrm{He}$ elastic scattering was measured at 71 MeV/u in the angular range of 40°–78° in the center of mass system.

2. RI Beam Experiment

The experiment was carried out at RIKEN Accelerator Research Facility. A ${}^6\mathrm{He}$ beam was produced by bombarding a 92-MeV/u ${}^{12}\mathrm{C}$ primary beam on a ${}^9\mathrm{Be}$ target of 1.39 g/cm^2. The intensity of the primary beam was 600 pnA throughout the experiment. ${}^6\mathrm{He}$ ions with an energy of $\sim$ 72 MeV/u were selected with RIKEN Projectile Fragment Separator, RIPS. To achieve a small beam-spot size of $<$ 14 mmϕ, an aluminum wedge-degrader as thin as 316 mg/cm^2 was used for the charge selection. Beam emittance was limitted by the rhombic slit at the final focal position (F3) of RIPS. The polarized target was placed $\sim$ 1 m downstream from the F3. The beam-spot size on the target position was 10 mmϕ (FWHM). The angular spread of the ${}^6\mathrm{He}$ beam was 18 mr (FWHM). The measured position and angular profiles of the ${}^6\mathrm{He}$ beam in the horizontal plane are shown in Figs. 1 and 2. The purity and the intensity of the ${}^6\mathrm{He}$ target at the target position were 95% and 1.7×10^5 s^{-1}, respectively.

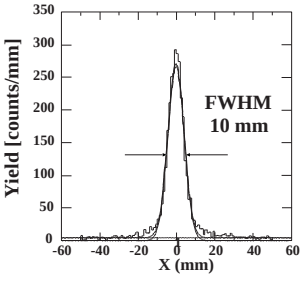

Figure 1. Position profile of the ${}^6\mathrm{He}$ beam in the horizontal plane. The width was found to be 10 mm (FWHM).

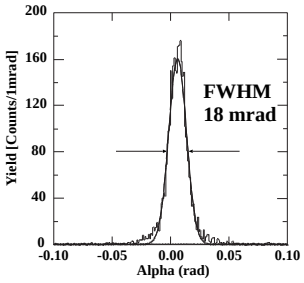

Figure 2. Angular profile of the ${}^6\mathrm{He}$ beam in the horizontal plane. The width was found to be 18 mrad (FWHM).

The target was a single crystal of naphthalne doped with a small amount of pentacene. The cross section and the thickness of the target were 14 mmϕ and 1 mm, respectively. An Ar-ion laser is used for the optical pumping [5, 6]. Details of the target system are described in Refs. [2] and [7].

Scattered ${}^6\mathrm{He}$ particles were detected with multiwire drift chambers and three-layers of plastic scintillation detectors. The first layer consisting of 5-mm thick plastic scintillation detecters provides ΔE information. The following 30-mm$\times$2 thick layers give E information. From the ΔE-E correlation, ${}^6\mathrm{He}$ particles were reasonablly discriminated from the other nuclides. Scattering angle of ${}^6\mathrm{He}$ and the vertex position on the target were determined by the data of drift chambers with an angular resolution of 0.18° and a position resolution of 1.3 mm in FWHM, respectively.

Recoiled protons were detected with counter telescopes located left and right sides of the beam axis. Each telescope consists of two layers of position sensitive silicon detectors (PSD) and plastic scintillation detectors. The PSD has a 50×50 mm^2 active area devided into 10 strips on the front face. Two PSDs with orthogonal strip directions located 120 mm and 140 mm from the target provided scattering angles of the recoiled protons in vertical and horizontal directions, respectively. The strip width of 5 mm corresponds to the angular span of 2.4° (2.0°) in the vertical (horizontal) direction.

3. Results

Figure 3 shows the correlation between the scattering angle of ^{6}He and the PSD channel. The PSD strip ID 1–10 corresponds to the proton scattering angle of 51°–70° (78°–40°) in the laboratory system (the center-of-mass system). The position of prominent peaks in the figure are consistent with the kinematics of the $p + {}^6\mathrm{He}$ elastic scattering at 71 MeV/u. Small background events at small $\theta_{^6\mathrm{He}}$ are observed for PSD strips of 9 and 10. These are attributed to a leak of ${}^1\mathrm{H}({}^6\mathrm{He}, {}^4\mathrm{He}p)nn$ events due to the imperfection of the particle identification. Since the background peaks are well isolated from the peaks of interest, these background events have negligible effects on the cross section and the vector analyzing power.

The cross section are obtained with a statistical uncertainty of $\left(\Delta\frac{d\sigma}{d\Omega}\right)/\frac{d\sigma}{d\Omega}$ = 1.5%–7.5% depending on the angle [3]. The data are found to be consistent with the previously measured data at the same energy [8] within the statistical uncertainty, in the overlapping angular range of $\theta_{\mathrm{cm}} = 40°$–$50°$. In the angular range, the energies of recoiled protons are 12–38 MeV. This results clearly demonstrate that the detection of recoiled protons with energies of $\sim$ 10 MeV is possible in the CNS polarized target system. Data analysis to obtain the vector analyzing power is now in progress.

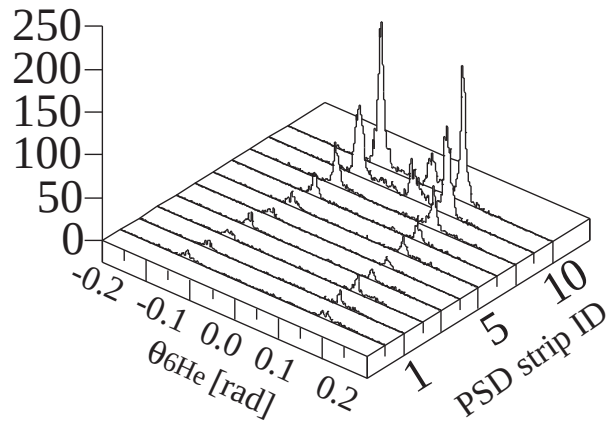

Figure 3. The correlation between the scattering angle of ^{6}He and the PSD channel. The PSD strip ID 1–10 corresponds to the proton scattering angle of 50°–70° in the laboratory system.

4. Summary

The first measurement of the elastic scattering between a polarized proton and a radioactive ^{6}He isotope has been carried out with the CNS polarized proton solid target. The $p+{}^6\mathrm{He}$ elastic scattering events are clearly identified by the angular correlation between ^{6}He and a recoiled proton. The cross section data at forward angles are consistent with the previously measured ones, which clearly demonstrates the capability of the target system to facilitate the detection of recoiled protons.

References

[1] T. Wakui *et al.*, AIP Conf. Proc. **675** (2003) 911.

[2] T. Uesaka *et al.*, Nucl. Instrum. Methods A **526** (2004) 186.

[3] M. Hatano, Ph. D Thesis, University of Tokyo (2004).

[4] H. W. van Kesteren, W. T. Wenckebach, J. Schmidt, Phys. Rev. Lett. **55** (1985) 1642.

[5] T. Wakui *et al.*, Nucl. Instrum. Methods A **526** (2004) 182.

[6] T. Wakui *et al.*, CNS Annual Report 2003 (2004) 84.

[7] M. Hatano *et al.*, CNS Annual Report 2002 (2003) 72.

[8] A. A. Korsheninnikov *et al.*, Nucl. Phys. A **616** (1997) 45.

Experimental Test of Bell's Inequality via the $(d,^2\mathrm{He})$ Reaction II

T. Saito[a], H. Sakai[a,b], T. Ikeda[c], K. Itoh[c], T. Uesaka[b], T. Kawabata[b], H. Kuboki[a], M. Sasano[a], Y. Satou[d], K. Suda[b], K. Sekiguchi[e], A. Tamii[f], Y. Maeda[b], N. Matsui[d] and K. Yako[a]

[a]*Department of Physics, University of Tokyo*
[b]*Center for Nuclear Study, Graduate School of Science, University of Tokyo*
[c]*Department of Physics, Saitama University*
[d]*Department of Physics, Tokyo Institute of Technology*
[e]*RIKEN (The Institute of Physical and Chemical Research)*
[f]*Research Center for Nuclear Physics, Osaka University*

1. Introduction

It is well known that Einstein, Podolsky and Rosen (EPR) presented a paradox by which they concluded that quantum mechanical description of nature is incomplete [1]. To reach the conclusion, EPR used some classical assumptions such that objects should have definite properties whether they are measured or not, and that there is no action-at-a-distance in nature. Some attempts were made to explain quantum mechanical nature from classical assumptions by introducing 'hidden variables' outside the scope of quantum mechanics. Bell showed, however, if two particles are in an *entangled* state, the correlation of the two particles can be stronger than that allowed by any hidden variable models [2]. Since Bell's proof was given by an inequality which can be tested experimentally, many experiments have been performed and have given consistent results with quantum mechanics [3].

It should be noted that Bell's inequality (BI) was originally derived from a consideration on a two spin-$\frac{1}{2}$ particle system in the spin singlet state $|^1S_0>= \frac{1}{\sqrt{2}}(|\uparrow>|\downarrow> -|\downarrow>|\uparrow>)$. However, most of the experiments performed so far have used two photon systems. It is of considerable interest to show that such two-particle correlations arising from entanglement are not limited to photons, but also to hadoronic systems.

There is only one experiment that tested BI by measuring correlations of two hadrons. Lamehi-Rachti and Mittig (LRM) measured spin-correlations of proton pairs produced by 13.5-MeV *pp*-elastic scattering [4]. Although their results agree with quantum mechanics and violated the classical limits of BI, there are some problems in their estimation of systematic errors [6, 5].

We are interested in testing BI by measuring spin-correlation of proton pairs produced by the $(d,\,^2\mathrm{He})$ reaction. Here we define a $^2\mathrm{He}$ as a pair of protons coupled to the $^1S_0$ state by the final state interaction. Use of $(d,^2\mathrm{He})$ reaction has following advantages: (1) In the case of LRM's experiment, the relative energy of the two protons was fixed kinematically, while the $(d,\,^2\mathrm{He})$ reaction enables us to select as small relative energy as possible. Hence we can produce high purity of $^1S_0$-state proton pairs. (2) Since the kinetic energy of the protons in the laboratory frame is high, the proton polarizations can be measured easily.

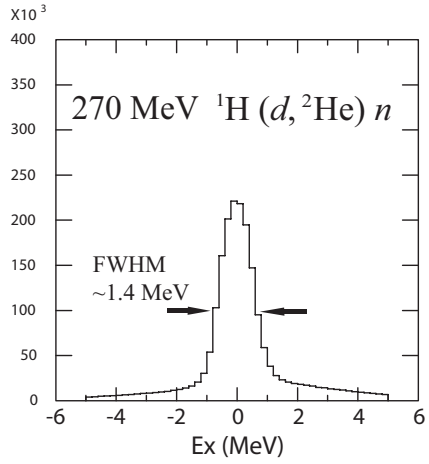

Figure 1. Excitation energy spectrum of $^1\mathrm{H}(d,\,^2\mathrm{He})n$ reaction at E_d =270 MeV.

2. Experiment

We measured the $^1\mathrm{H}(d,\,^2\mathrm{He})n$ reaction at RIKEN in 2003. The beam of 270 MeV was injected into a liquid hydrogen target [7] of 100-mg/cm^2 thick. The proton pairs scattered at 0° were momentum analyzed by a spectrometer SMART [8] and detected with a proton polarimeter EPOL placed at the second focal plane of SMART. Typical beam intensity was 0.3 nA and we detected $^2\mathrm{He}$ at the rate of 1 - 1.5 kcps. An example of the energy spectrum is shown in Fig. 1. The distribution of the relative energy E_{rel} of the two protons is presented in Fig. 2. A simulation study has shown that selecting the events of $E_{rel} < 1$ MeV enables us to increase the purity of the $^1S_0$ state more than 98%.

A schematic view of EPOL is presented in Fig. 3. EPOL consists of three multi-wire drift chambers (MWDCs), two sets of plastic scintillator hodoscopes and an analyzer target (5.0-cm thick carbon block). The incident pairs of protons are simultaneously scattered from the analyzer target.

3. Spin-correlation function

The strength of the correlation of the two protons in the $^1S_0$ state can be expressed by a spin-correlation function $C(\phi) =< \vec{\sigma}_1 \cdot \vec{a}\ \vec{\sigma}_2 \cdot \vec{b} >$, where $\vec{a}$ and $\vec{b}$ are the directions of measuring axes of each proton spin, and ϕ is the angle between $\vec{a}$ and $\vec{b}$. $C(\phi)$ corresponds to the expecta-

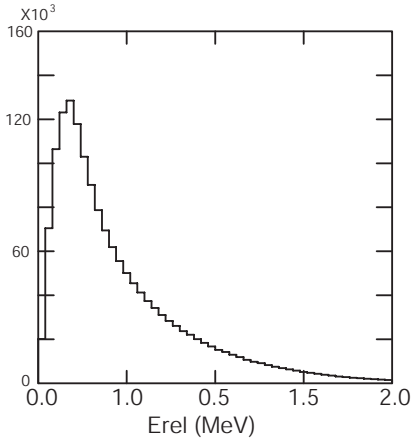

Figure 2. Distribution of the relative energy of two protons.

tion value of the product of the signs of each spin. If the classical assumptions are correct, BI gives following limits: $|C\left(\frac{\pi}{6}\right)| \leq \frac{2}{3}$, $|C\left(\frac{\pi}{4}\right)| \leq \frac{1}{2}$, and $|C\left(\frac{\pi}{3}\right)| \leq \frac{1}{3}$. Note that these limits are on a line $|C_{\rm Bell}(\phi)| = |\frac{2}{\pi}\phi - 1|$. These inequalities are violated by quantum mechanical prediction $C_{\rm QM}(\phi) = -\cos\phi$.

To derive $C(\phi)$ experimentally, we define two pairs of virtual sectors (L_1, R_1) and (L_2, R_2) on the $\alpha\beta$-plane (see Fig 4). Here, α and β are the scattering angles at the analyzer target in the horizontal and vertical planes, respectively. Then we calculate

$$C_{\rm exp}(\phi) = \frac{1}{{A_y}^2}\frac{LL + RR - LR - RL}{LL + RR + LR + RL},$$

where LR is the number of coincidence events such that proton 1 entered the sector L_1 and proton 2 entered the sector R_2 and so on. A_y is the effective analyzing power of EPOL.

4. Preliminary results

Figure 5 shows preliminary results of $C(\phi)$, which were deduced by a brief analysis of 5% of the total data. Although the statistical accuracy is poor, we can clearly see spin-correlations of the two protons. If we analyze all the data, statistical errors of $C(\phi)$ will reduce to 0.05, by which

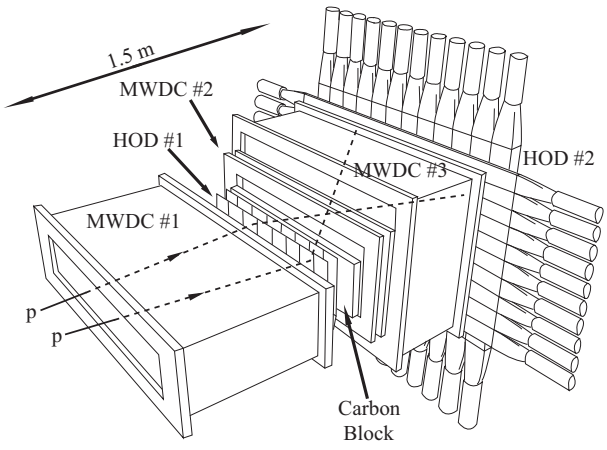

Figure 3. Schematic view of the proton polarimeter EPOL.

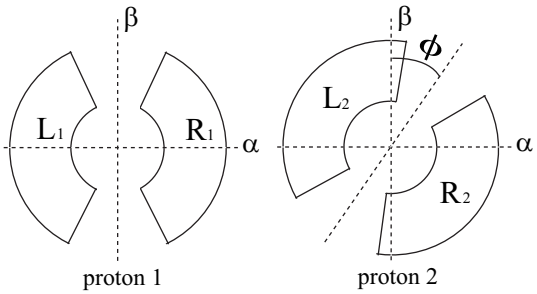

Figure 4. Virtual sectors for the derivation of $C(\phi)$.

we can verify the violation of BI by an accuracy of 4σ at $\phi = 45°$. Data analysis is now in progress.

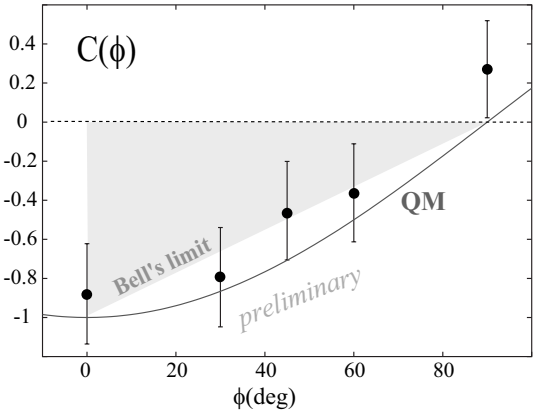

Figure 5. Preliminary results of the spin-correlation function.

References

[1] A. Einstein, B. Podolsky and N. Rosen, Phys. Rev. **47** (1935) 777.
[2] J.S. Bell, Physics **1** (1964) 195.
[3] F. Laloë, Am. J. Phys. **69** (2001) 655, and the references therein.
[4] Lamehi-Rachti and W. Mittig, Phys. Rev. D **14** (1976) 2543.
[5] T. Saito *et al.*, CNS Annual Report 2002 (2003) 23.
[6] H. Sakai *et al.*, J. Phys. Soc. Jpn. **72** Suppl. C (2003) 193.
[7] T. Ikeda *et al.*, CNS Annual Report 2003 (2004) 86.
[8] T. Ichihara *et al.*, Nucl. Phys. A 569 (1994) 287c.

Tensor Analyzing Power for the $\vec{d} + \alpha$ Backward Scattering

T. Uesaka, T. Ikeda[a], T. Kawabata, H. Okamura[a], K. Itoh[a], H. Sakai[b], K. Yako[b], T. Saito[b], H. Kuboki[b], M. Sasano[b] and K. Sekiguchi[c]

Center for Nuclear Study, Graduate School of Science, University of Tokyo
[a]*Department of Physics, Saitama University*
[b]*Department of Physics, University of Tokyo*
[c]*RIKEN (the Institute of Physical and Chemical Research)*

1. Introduction

Short-range structure of nuclei has a close connection to the high-momentum behavior of nuclear interactions which can not be fully described, for the moment, neither by meson exchange theories nor by non-perturbed quantum chromodynamics. Information on the short-range structure, especially spin-dependent one, is crucial to establish a better understanding of nuclear interactions.

^{4}He nucleus, which has a large binding energy of 28.3 MeV and a small root mean square radius of $\langle r \rangle_{\rm rms}/A^{1/3} \sim 1$ fm , is considered to be an object appropriate for the study. Spin-dependence of the short-range structure of s-shell nuclei can be characterized by its D-state admixture to the wave function [1]. The D-state admixture in ^{4}He was studied via the radiative capture reaction $\vec{d}d \rightarrow \gamma^4$He and the $(\vec{d}, \alpha)$ pick-up reactions on medium-mass targets at low energies [3]. These studies, however, have been made only in the asymptotic region, that is, in the region where low momentum components of ^{4}He concern.

The extension to the higher momentum region was attempted by using a radiative capture induced by an intermediate-energy polarized deuteron beam [2]. However, it was found to be difficult to extract the information on ^{4}He structure from the radiative capture data. This is because E1 transition is forbidden for the $^4\mathrm{He}(\gamma, dd)$ reaction due to the isospin selection rule. Thus the d-d partition in ^{4}He is diffcult to access with electro-magnetic probes.

Measurement of the $d + \alpha$ backward scattering, which is the $d + \alpha$ elastic scattering at $\theta \sim 180^\circ$, at intermediate energies can be an alternative candidate as a probe to the D-state admixture in ^{4}He. Since the reaction is considered to be dominated by two-nucleon transfer processes in the backward region, the polarization observables as well as the cross sections are expected to be sensitive to the ^{4}He form factor of d-d or d-pn partition. In particular, tensor analyzing powers, A_{yy} and A_{xx}, can provide an information on the D-state admixture.

We have recently measured the cross section and analyzing powers, A_y, A_{yy}, and A_{xx}, for the $d + \alpha$ backward scattering at E_d =140 and 270 MeV. In addition, data for the $^4\mathrm{He}(d, ^3\mathrm{He})^3\mathrm{H}$ reaction was measured in the same experimental conditions. The latter data is used to estimate the contribution from the sequential transfer of two nucleons, $d + \alpha \rightarrow {}^3\mathrm{He} + {}^3\mathrm{H} \rightarrow \alpha + d$.

2. Experiment

The experiment was carried out at the E4 experimental area of RIKEN Accelerator Research Facility. A cryogenic ^{4}He gas target [4] placed in the scattering chamber was cooled down to $\sim$ 6 K. The target density and thickness were 8.1 mg/cm^3 and 4.3 mg/cm^2, respectively. Polarized deuteron beams with energies of 140 and 270 MeV were used to bombard the target. α particles emitted at forward angles in the laboratory system were analyzed in the magnetic spectrograph SMART [5] and detected with multiwire drift chambers and three-layers of plastic scintillation counters located in the focal plane. Timing and pulse height information of the plastic scintillation counters was used to identify the particle. Momentum and scattering angle of the particle were reconstructed from the particle trajctory determined from the timing data of drift chambers with a help of ion-optical parameters of SMART. The energy resolution was obtained to be 800 keV (FWHM), which is high enough to resolve the $d + \alpha$ backward events from $pn - \alpha$ events.

3. Results

Figure 1 shows the preliminary results of the differential cross sections for the d+α backward scattering at 270 MeV. The statistical uncertainty of each data point is 1%–5% de-

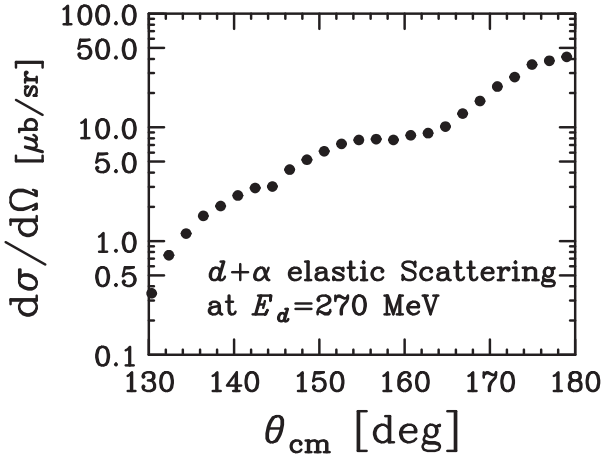

Figure 1. Differntial cross section for the $d + \alpha$ elastic scattering at backward angles.

pending on the angle and is smaller than the symbol in the figure. The data obviously exhibits a 180°-peak distribution which is typical for the nucleon transfer processes.

Tensor analyzing powers, A_{yy} and A_{xx} are shown in

Fig. 2. Both A_{yy} and A_{xx} take large values of $A_{yy} = +0.2$–+0.7 and $A_{xx} = -0.7$–+0.2, respectively. These are, at least partly, due to the D-state admixture in the ^{4}He nucleus. Contributions from the D-state of deuteron and the reaction mechanism, for example, effects due to couplings to continuum states, will be evaluated through theoretical analysis of the $d + \alpha$ elastic scattering and the $^4\mathrm{He}(d, ^3\mathrm{He})^3\mathrm{H}$ reactions.

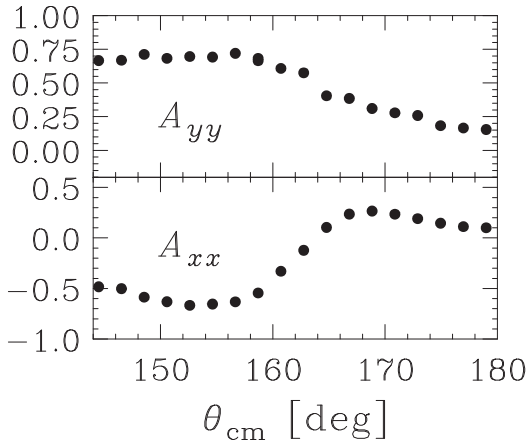

Figure 2. Tensor analyzing powers for the $d + \alpha$ elastic scattering at backward angles.

4. Summary

In summary, we have measured the cross sections and analyzing powers, A_y, A_{yy}, and A_{xx}, for the $d + \alpha$ backward scattering and the $^4\mathrm{He}(d, ^3\mathrm{He})^3\mathrm{H}$ reaction at 140 and 270 MeV. The $d + \alpha$ backward scattering data at 270 MeV exhibit a 180°-peak angular distribution which is typical for the nucleon transfer processes. Measured tensor analyzing powers are a clear manifestation of D-state admixture in ^{4}He at finite momenta.

References

[1] T. E. O. Ericson and M. Rosa-Clot, Ann. Rev. Nucl. Part. Sci. **35** (1985) 271; H. R. Weller and D. R. Lehman, Ann. Rev. Nucl. Part.Sci. **38** (1988) 563; A. M. Eiro and F. D. Santos, J. Phys. G **16** (1990) 1139.

[2] W. K. Pitts *et al.*, Phys. Rev. C **39** (1989) 1679.

[3] B. C. Karp *et al.*, Phys. Rev. Lett. **53** (1984) 1619.

[4] T. Ikeda *et al.*, CNS Annual Report 2003 (2004) 86.

[5] T. Ichihara *et al.*, Nucl. Phys. A **569** (1994) 287c.

Tensor Analyzing Power of the ^{16}O(d, ^{2}He) Reaction at 0 Degrees and Structure of the Spin-Dipole Resonances

K. Suda[a], H. Okamura[b], T. Uesaka[a], R. Suzuki[c], H. Kumasaka[c], T. Ikeda[c], K. Itoh[c], H. Sakai[a,d], A. Tamii[e], K. Sekiguchi[f], K. Yako[d], Y. Maeda[a], M. Hatano[d], T. Saito[d], H. Kuboki[d], N. Sakamoto[f] and Y. Satou[g]

[a] *Center for Nuclear Study, Graduate School of Science, University of Tokyo*
[b] *Cyclotron and Radioisotope Center, Tohoku University*
[c] *Department of Physics, Saitama University*
[d] *Department of Physics, University of Tokyo*
[e] *Research Center for Nuclear Physics, Osaka University*
[f] *RIKEN (The Institute of Physical and Chemical Research)*
[g] *Department of Physics, Tokyo Institute of Technology*

1. Introduction

The spin-dipole resonance (SDR) is a spin-coupled analog state of the well-known giant dipole resonance. The spin-dipole states have spin-parity $J^\pi = 2^-, 1^-$ and 0^-, when excited from the ground states of even-even nuclei. The understanding of SDR is still limited partly due to the difficulty of identifying three different spin-parity states. The (d, ^{2}He) reaction is one of the most effective tools to study SDR states [1]. Recently, a model-independent spin-parity determination method using the tensor analyzing power A_{zz} at 0° was proposed [2]. For reactions having a spin-parity structure of $1^+ + 0^+ \rightarrow 0^+ + J^\pi$, the tensor analyzing power A_{zz} shows extreme values at $\theta = 0^\circ$ and 180° for some J^π residual states solely by the requirement of parity-conservation [2, 3]:

$$A_{zz}(0^\circ, 180^\circ) = \begin{cases} -2, & \text{if} \quad J^\pi = 0^- , \\ +1, & \text{if} \quad \pi = (-)^J . \end{cases} \qquad (1)$$

This is the case for the (d, ^{2}He) reaction on even-even targets. By using Eq. (1), we can determine two of three spin-dipole states unambiguously. This method was successfully applied to ^{12}C target, where a 0^- state in ^{12}B residual states was identified at $E_x = 9.3$ MeV [2].

The ^{16}O nucleus is particularly interesting since the spin-dipole states are predominantly excited by the (d, ^{2}He) reaction. In this double-magic nucleus with $N = Z = 8$, the excitation involves primarily $\Delta L = 1$ transition since a particle crosses the shell-gap in $1p$-$1h$ configuration. Consequently, Gamow-Teller transition ($\Delta L = 0$) is suppressed to the first order, and the spin-dipole states are mainly excited. In addition to this interesting feature, the spin-dipole states in ^{16}O recently receives attention as a possible detector material for the supernovae neutrino [4]. A detailed study of the ^{16}O nucleus is desired for this purpose.

2. Experiment

The experiment was performed at the RIKEN Accelerator Research Facility. The ^{16}O(d, ^{2}He)^{16}N reaction was measured at $E_d = 270$ MeV by using the magnetic spectrograph SMART [5]. The solid oxygen with a thickness of 5–40 mg/cm^2 was used as a target [6, 7]. Scattered protons were momentum analyzed by the spectrograph and detected at the large acceptance ($\Delta\Omega = 13.1$ msr) focal plane with two multi-wire drift chambers and trigger scintillator hodoscope [8]. The momenta and scattering angles of two protons were deduced from reconstructed trajectories and the optical property of the spectrograph.

3. Results and Discussion

Figure 1 shows the energy spectra and the tensor analyzing power A_{zz} for the ^{16}O(d, ^{2}He)^{16}N reaction at $\theta_{\rm c.m.} = 0^\circ$–$1^\circ$. In the upper panel, the energy spectra for two polarization modes of the deuteron beam ($P_{zz} = -0.35$ and $+0.56$) are shown. The lowest four states with the spin parity of 2^- (0.0 MeV), 0^- (0.12), 3^- (0.30) and 1^- (0.40) [9]

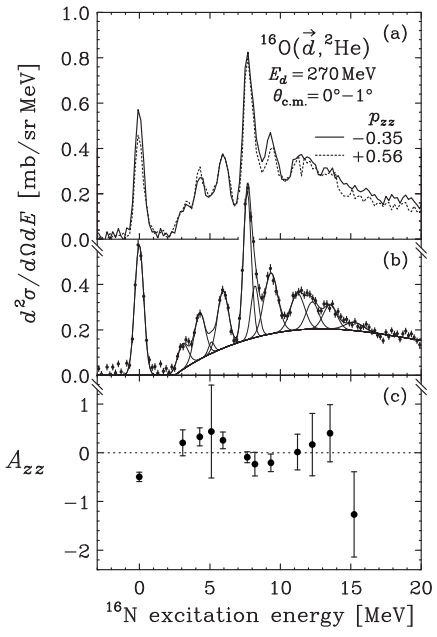

Figure 1. Energy spectra of the ^{16}O(d, ^{2}He)^{16}N reaction at $\theta_{\rm c.m.} = 0^\circ$–$1^\circ$ for two tensor polarized beams (a), the peak fitting result of the spectrum with $P_{zz} = -0.35$ (b), and the corresponding values of A_{zz} for each peak (c).

are not resolved. The energy resolution are estimated to be about 700 keV at FWHM. A prominent peak is observed at $E_x = 7.7$ MeV. In order to extract the tensor analyzing power A_{zz}, a Gaussian peak fitting is performed. The non-resonant continuum background caused by the quasi-free scattering is subtracted by using the semi-phenomenological function [10]. In the middle panel, the fitting result of the energy spectrum for one of the polarization modes ($P_{zz} = -0.35$) is shown. In the lower panel, the deduced tensor analyzing power A_{zz} corresponding to each peak is shown.

At $E_x = 7.7$ MeV, the A_{zz} value is nearly equal to zero, and is significantly different from -2 and $+1$ which correspond to $J^\pi = 0^-$ and 1^-, respectively [see Eq. (1)]. Thus, the A_{zz} result suggests that 2^- states are dominant at $E_x = 7.7$ MeV. In order to confirm this 2^- dominance, we performed the adiabatic coupled-channels Born approximation calculation [11] and compared the angular distributions of the cross sections and A_{zz} at very forward angles. In the calculation, the one-body transition densities were obtained from the wave functions of Millener and Kurath [14] for negative-parity states by using the shell model code OXBASH [15]. The shell model calculation was performed within $1\,\hbar\omega$ configuration space.

Figure 2 shows the angular distribution of the cross section and A_{zz} for the spin-dipole states at $E_x = 7.7$ MeV (right panel) as well as at $E_x = 0$ MeV (left panel). The calculated cross sections are normalized by factors of 0.5 and 0.4 for $E_x = 0$ and 7.7 MeV, respectively. At both excitation energies, the A_{zz} data are systematically smaller than the calculation for 2^- states by $0.2 \sim 0.5$. However, a monotonous distribution of the A_{zz} data at $E_x = 7.7$ MeV is well reproduced by assuming the 2^-_3 state rather than the 1^-_2 state. Thus, we confirmed the above suggestion.

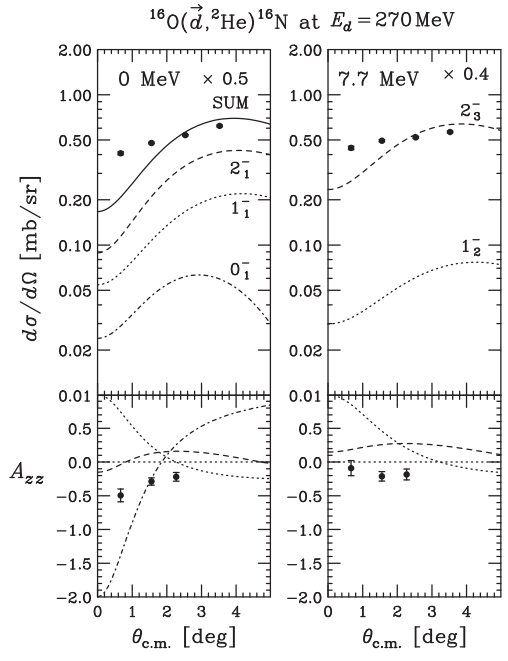

Figure 2. Cross sections and tensor analyzing power A_{zz} for the spin-dipole states at $E_x = 0$ MeV (left panel) and 7.7 MeV (right panel). The data are plotted as closed circles. The theoretical predictions for the 2^-, 1^- and 0^- states are shown as dashed, dotted, and dot-dashed curves, respectively. For $E_x = 0$ MeV, the sum of the cross sections for the three states is also shown as solid curve (upper-left panel).

Figure 3 compares the energy spectrum with the calculated strength at $\theta_{\rm c.m.} = 3.5°$. The calculated strengths are smeared by Gaussian function with the width of the experimental resolution. The overall strength is well reproduced normalized by a factor of 0.45. The observed peak at $E_x = 7.7$ MeV corresponds to the calculated one at $E_x = 5.7$ MeV. In contrast, at $E_x \sim 12.6$ MeV, no concentration of the strength of a 1^- state are observed. This missing strength of the 1^- state may be attributed to the higher-order effects such as the mixing of $3p$-$3h$ configuration or the tensor correlation [16].

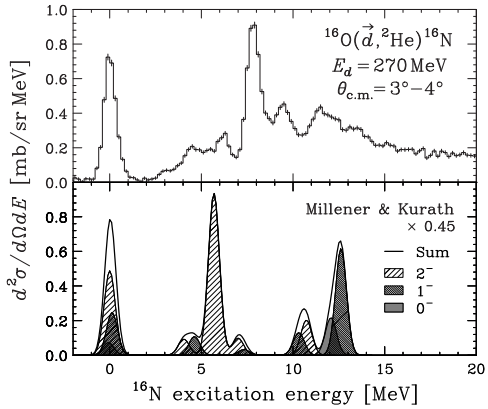

Figure 3. Comparison of the energy spectrum and the calculated strength of the spin-dipole states at $\theta_{\rm c.m.} = 3.5°$. The upper panel shows the experimental result. The lower panel shows the calculated spectra for 2^-, 1^- and 0^- states as well as a sum of them. The calculated strengths are smeared by Gaussian function with the width of the experimental resolution. The overall strength is normalized by a factor of 0.45.

4. Summary

We have measured the tensor analyzing power A_{zz} for the ^{16}O(d,^{2}He)^{16}N reaction at 0° and $E_d = 270$ MeV for the first time. The prominent peak was observed at $E_x = 7.7$ MeV, and was found to be dominated by 2^- states rather than 1^- states. The shell-model calculation reasonably reproduced the energy and strength. In contrast, the predicted 1^- state at $E_x = 12.6$ MeV was not observed. This missing strength of the 1^- state may be attributed to the higher-order effects such as the mixing of $3p$-$3h$ configuration or the tensor correlation [16].

References

[1] H. Okamura *et al.*, Phys. Lett. B **345** (1995) 1.
[2] H. Okamura *et al.*, Phys. Rev. C **66** (2002) 054602.
[3] J. A. Kuehner *et al.*, Phys. Rev. Lett. **35** (1975) 423.
[4] K. Langanke *et al.*, Phys. Rev. Lett. **76** (1996) 2629.
[5] T. Ichihara *et al.*, Nucl. Phys. A **569** (1994) 287c.

[6] R. Suzuki *et al.,* RIKEN Accel. Prog. Rep. **36** (2003) 188.
[7] T. Uesaka *et al.,* CNS Annual Report 2002 (2003) 56.
[8] H. Okamura *et al.*, Nucl. Instrum. Methods. **406** (1998) 78.
[9] D. R. Tilley *et al.*, Nucl. Phys. A **564** (1993) 1.
[10] K.J. Raywood *et al.*, Phys. Rev. C **41** (1990) 2836.
[11] H. Okamura, Phys. Rev. C **60** (1999) 064602.
[12] M.A. Franey *et al.*, Phys. Rev. C **31** (1985) 488.
[13] M. Golin *et al.*, Phys. Lett. B **64** (1976) 253.
[14] D.J. Millener *et al.*, Nucl. Phys. A **255** (1975) 315.
[15] B.A. Brown *et al.,* The Oxford-Buenos-Aires-MSU Shell-Model Code, Michigan State University Cyclotron Laboratory Report 524 (1986).
[16] H. Sagawa *et al.*, in *International Symposium on New Facet of Spin Giant Resonances in Nuclei*, edited by H. Sakai et al. (World Scientific, Singapore, 1998) 191.

Isoscalar and Isovector Spin-M1 Strengths in ^{11}B

T. Kawabata, H. Akimune[a], H. Fujimura[b], H. Fujita[b], Y. Fujita[c], M. Fujiwara[b], K. Hara[b], K. Y. Hara[a], K. Hatanaka[b], T. Ishikawa[d], M. Itoh[b], J. Kamiya[b], S. Kishi[d], M. Nakamura[d], K. Nakanishi[b], T. Noro[e], H. Sakaguchi[d], Y. Shimbara[b], H. Takeda[d], A. Tamii[b], S. Terashima[d], H. Toyokawa[f], M. Uchida[b], H. Ueno[c], T. Wakasa[e], Y. Yasuda[d], H. P. Yoshida[b] and M. Yosoi[d]

Center for Nuclear Study, Graduate School of Science, University of Tokyo
[a]*Department of Physics, Konan University*
[b]*Research Center for Nuclear Physics, Osaka University*
[c]*Department of Physics, Osaka University*
[d]*Department of Physics, Kyoto University*
[e]*Department of Physics, Kyushu University*
[f]*Japan Synchrotron Radiation Research Institute*

The M1 transition strengths provide important information on the nuclear structure because they could be a good measure to test theoretical nuclear models. Recently, the M1 transition strengths are of interest from a view of not only the nuclear physics but also neutrino astrophysics because the spin part of the M1 operator is identical with the relevant operators mediate neutrino induced reactions.

Raghavan *et al.* pointed out that the ^{11}B nucleus can be used as a possible neutrino detector to investigate stellar processes [1]. High-energy neutrinos from the stellar processes like the proton-proton fusion chain in the sun and the supernova explosions excite low-lying states in ^{11}B and ^{11}C by M1 and Gamow-Teller (GT) transitions via the neutral-current (NC) and charged-current (CC) processes, respectively. Such neutrinos can be detected by measuring emitted electrons from the CC reaction and γ rays from the de-excitations of the low-lying states. Since there is an isospin symmetrical relation between the ^{11}B and ^{11}C and both the NC and CC reactions can be measured simultaneously in one experimental setup, the systematic uncertainty in measuring a ratio of the electron-neutrino flux to the entire neutrino flux is expected to be small. Since the isospin of the ground state of ^{11}B is $T = 1/2$, low-lying states in ^{11}B are excited by both the isovector and isoscalar transitions. Therefore, both the isoscalar and isovector spin-M1 strengths are needed for estimating the CC and NC cross sections.

The cross sections of hadronic reactions provide a good measure for the weak interaction response since the relevant operators in the hadronic reactions are identical with those in β-decay and neutrino capture processes. Thus, we recently measured cross sections for the ^{11}B(^{3}He,t) and ^{11}B(d,d') reactions to determine the isovector and isoscalar spin-M1 strengths in ^{11}B.

The experiment was performed at Research Center for Nuclear Physics, Osaka University using 450-MeV ^{3}He and 200-MeV deuteron beams. The measured cross sections were shown in Figs. 1 and 2. Since the ground state of ^{11}B has non-zero spin, the cross sections for the ^{11}B(^{3}He,t) and ^{11}B(d,d') reactions are described by an incoherent sum over the cross section of the different multipole contributions,

$$\frac{d\sigma}{d\Omega} = \sum_{\Delta J} \frac{d\sigma}{d\Omega}(\Delta J).$$

In order to determine the spin-M1 strengths, the cross section for each ΔJ transition must be given to extract the $\Delta J = 1$ contribution.

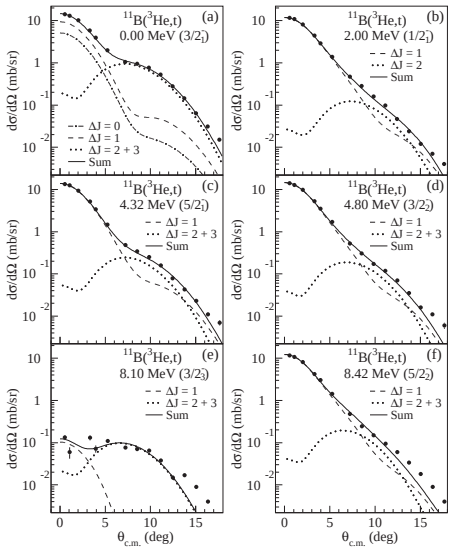

Figure 1. Cross sections for the ^{11}B(^{3}He,t) reactions compared with the DWIA calculation. The dash-dotted, dashed, and dotted curves show $\Delta J = 0$, $\Delta J = 1$ and $\Delta J \geq 2$ contributions, respectively. The solid curves are sums of the all multipole contributions.

For the ^{11}B(^{3}He,t) analysis, the cross section for the each ΔJ transition was calculated by the distorted wave impulse approximation (DWIA) as seen in Fig. 1. Since the GT strength $B(\mathrm{GT})$ for the ground-state transition is known to be 0.345 ± 0.008 from the β-decay strength, the cross sections for the $\Delta J = 1$ transitions to the excited states in ^{11}C can be related to the $B(\mathrm{GT})$ values by assuming the linear proportional relation. The obtained $B(\mathrm{GT})$ values are compared with the previous (p,n) result [2] in Table 1. The present results are consistent with the (p,n) result al-

E_x (MeV)	J^π	$B(\mathrm{GT})$ Present	$B(\mathrm{GT})$ (p,n)
0.00	$3/2^-$	0.345 ± 0.008	
2.00	$1/2^-$	0.402 ± 0.031	0.399 ± 0.032
4.32	$5/2^-$	0.454 ± 0.026	0.961 ± 0.060
4.80	$3/2^-$	0.480 ± 0.031	
8.10	$3/2^-$	≤ 0.003	0.444 ± 0.010
8.42	$5/2^-$	0.406 ± 0.038	

Table 1. Measured $B(\mathrm{GT})$ values compared with the (p,n) result [2].

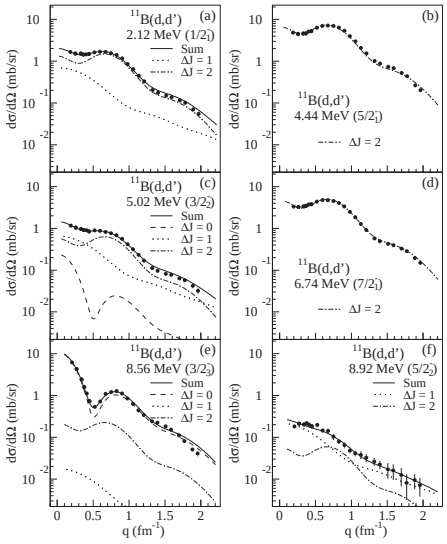

Figure 2. Cross sections for the ^{11}B(d,d') reactions. The dashed, dotted, and dash-dotted curves show $\Delta J = 0$, 1 and 2 contributions, respectively. The solid curves are sums of the all multipole contributions.

though several states are not separately resolved due to the poor energy resolution in the (p,n) measurement. Assuming isospin symmetry is conserved, the GT strengths are easily related to the isovector spin-M1 strength $B(\sigma\tau_z)$,

$$\frac{B(\mathrm{GT})}{B(\sigma\tau_z)} = \frac{8\pi}{3}\frac{\langle T_i, T_{iz}, 1, \pm 1 | T_f, T_{fz}\rangle^2}{\langle T_i, T_{iz}, 1, 0 | T_f, T_{fz}\rangle^2}.$$

Although the isospin-symmetry breaking changes this ratio, the variation is usually small. Therefore, the GT strengths obtained from the charge exchange reaction are still useful to study the isovector spin-M1 strengths.

For the ^{11}B(d,d') analysis, the cross section for each ΔJ transition was determined from the ^{12}C(d,d') reaction. Since the ground state of ^{12}C has a zero spin, transitions to the discrete states in ^{12}C are expected to be good references for the angular dependence of the cross sections for certain ΔJ transitions. As shown in Fig. 2, the cross section for the ^{11}B(d,d') reaction was successfully decomposed into the each ΔJ contributions. Although the 4.44-MeV ($5/2_1^-$) state can be excited by both the $\Delta J^\pi = 1^+$ and 2^+ transitions, the main part of the transition is due to $\Delta J^\pi = 2^+$. This result is explained by the fact that the strong coupling between the ground and 4.44-MeV states is expected since the 4.44-MeV state is considered to be a

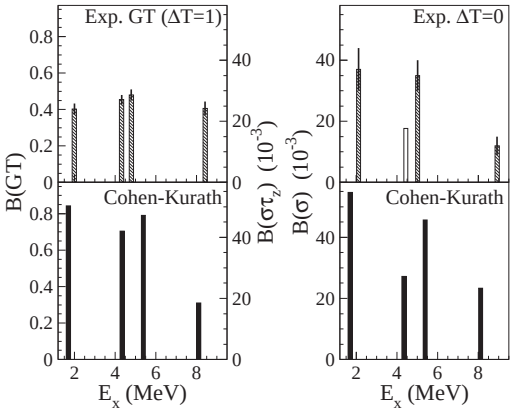

Figure 3. Measured $B(\mathrm{GT})$ ($B(\sigma\tau_z)$) and $B(\sigma)$ values are compared with the shell model predictions using the Cohen-Kurath wave functions [4]. The open bar in the right-upper panel shows the $B(\sigma)$ value for the 4.44-MeV state estimated from $B(\mathrm{GT})$ (see text).

member of the ground-state rotational band. Since the observed $\Delta J^\pi = 2^+$ transition strength is much larger than the expected $\Delta J^\pi = 1^+$ strength, the $\Delta J^\pi = 1^+$ component of the transition strength can not be reliably extracted for the 4.44-MeV state. The transition strength for the 6.74-MeV ($7/2_1^-$) state is also dominated by the $\Delta J^\pi = 2^+$ component, but the $\Delta J^\pi = 1$ transition to this state is not allowed. The isoscalar spin-M1 strength $B(\sigma)$ for the transition to the 2.12-MeV ($1/2_1^-$) state is deduced to be 0.037 ± 0.008 from the γ-decay widths of the mirror states and the $B(\mathrm{GT})$ value [3]. Using this value, the cross section for the $\Delta J = 1$ transitions to the other excited states can be related to the $B(\sigma)$ values. Since the $\Delta J = 1$ cross section for the 4.44-MeV state was not reliably obtained in the (d,d') analysis, the isoscalar spin-M1 strength was determined from the measured $B(\mathrm{GT})$ value and the relative strength of the isoscalar transition to the isovector transition calculated by using the Cohen-Kurath wave functions (CKWF) [4].

The obtained $B(\mathrm{GT})$ ($B(\sigma\tau_z)$) and $B(\sigma)$ values are compared with the shell model predictions using the CKWFs in Fig. 3. The CKWFs reasonably explain the experimental result except the quenching by a factor of 0.5-0.7. The present result will be useful in the measurement of the stellar neutrinos using the NC and CC reactions on ^{11}B.

References

[1] R.S. Raghavan, Sandip Pakvasa and B.A. Brown, Phys. Rev. Lett. **57** (1986) 1801.

[2] T.N. Taddeucci *et al.*, Phys. Rev. C **42** (1990) 935.

[3] J. Bernabéu, T. E. O. Ericson, E. Hernández and J. Ros Nucl. Phys. B **378** (1992) 131.

[4] S. Cohen and D. Kurath, Nucl. Phys. **73** (1965) 1.

Study of Dispersion Matching of the Magnetic Spectrograph PA

N. Iwasa, S. Kubono[a], Y. Fuchi[b], H. Fujikawa[a], N. Fukunishi[c], J.J. He[a], S. Kato[d], J. Moon[a], M. Notani[a], A. Saito[a], T. Teranishi[a], M.H. Tanaka[b], N. Yamazaki[a], and Y. Wakabayashi[a]

Department of Physics, Tohoku University.
[a] *Center for Nuclear Study, Graduate School of Science, University of Tokyo.*
[b] *Institute of Particle and Nuclear Studies (IPNS), High Energy Accelerator Research Organization (KEK).*
[c] *RIKEN (The Institute of Physical and Chemical Research).*
[d] *Department of Physics, Yamagata University.*

1. Introduction

The high resolution magnetic spectrograph (PA) [1] had been installed at the E2 experimental hall of the RIKEN accelerator research facility. The first beam test experiment was performed in 2002 using an α beam from the ring cyclotron impinged on gold and CH_2 targets [2]. The momentum resolution for the scattered helium nuclei was measured to be 0.1% in FWHM, although the intrinsic momentum resolution of PA is 0.01% calculated by the code TRANSPORT. This poor resolution was considered to be caused by the energy spread and finite spot size of the α beam from the ring cyclotron. To achieve the excitation energy resolution of 100 keV in FWHM in the (^{4}He,^{8}He) reactions with a 135 MeV α beam, the dispersion matching operation is necessary. In this article, the result of a study of the dispersion matching of PA is reported.

2. Experimental Setup

A helium beam at 104 MeV accelerated by the ring cyclotron was transported to PA.

The beam was achromatically focused on the target. The PA setup was checked using α particles elastically scattered at 10° from a gold target with a thickness of 1 μm. The solid angle was set to 0.1 msr. Momenta of scattered α particles were measured by a position-sensitive gas proportional counter (GPC) [3] with an active area of 400 × 35 mm^2 placed at the focal plane of PA. The energy and time of flight (TOF) were measured by a plastic scintillator with a thickness of 2 mm placed behind GPC. Momenta were calibrated using the α particles with four different magnetic field settings of PA, $\Delta B/B_0$ = −0.746%, 0%, 0.898% and 1.804%. The momentum resolution was measured to be 0.1% in FWHM which is the same as the previous experiment.

Dispersion matching was studied with a hole target with 1mmϕ, a faint beam, and PA setting at 0°. The position of the hole in the target can be selected to be −5, 0, and +5 mm in the horizontal direction from the optical axis. The target hole at 0 mm was used during this experiment. The momentum spread of α particles on GPC in dispersion matching transportation (DMT) was compared to that in achromatic beam transportation (ABT). Several parameters for the beam transport line for DMT were tested.

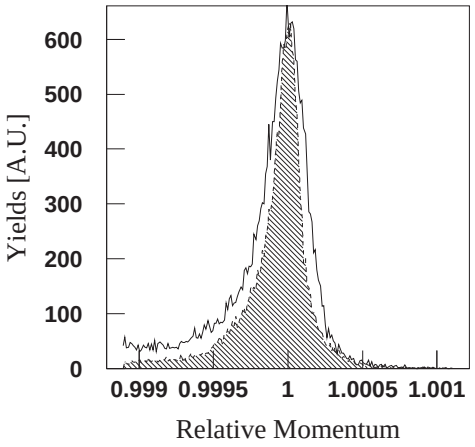

Figure 1. Relative momentum spectra. The solid curve and the dashed curve with the hatch denote momentum distributions in achromatic beam transportation and in dispersion matching transportation, respectively. Note that in dispersion matching transportation, the momentum was selected to be 0.01% using a dispersive focus in the beam transport and 1mmϕ hole.

3. Results

The solid curve in Fig. 1 shows relative momentum spectra in ABT. The momentum resolution in ABT was measured to be 0.03% in FWHM which is better than the resolution of 0.1% measured at 10° with the 1-μm thick gold target. The momentum spread caused by the energy straggling in the gold target was measured to be 0.03% which agrees with the energy straggling of 0.054 MeV calculated by the energy loss code ATIMA developed at GSI. This momentum spread can be reduced using a thinner target. The remaining momentum spread of 0.08% caused by PA setting at 10° and using a higher-intensity beam is not understood. Since the 0.1-msr slit was used in PA, the momentum spread caused by the kinematics is neglected. It is probably due to the higher order effect which could be corrected by further analysis.

The dashed curve with the hatch in Fig. 1 shows relative momentum spectra when the beam was focused dispersively at the target. The momentum resolution was measured to be 0.02% in FWHM. Note that the momenta of the beam was selected to be 0.01% (full width) by a dispersive focused beam on the target and a 1-mmϕ hole. This measured momentum resolution is slightly larger than the calculated intrinsic momentum resolution 0.01% of PA.

In the case of DMT, the shape of the momentum spectra should not be changed although the position of the hole was changed. However no beam was observed at the target hole of +5 mm. Further investigation will be made without the target to confirm DMT.

4. Summary

A possible parameter for beam transfer line in the dispersion matching transportation was tested. The momentum resolution was measured to be 0.02% in FWHM when the momenta of the beam were selected to be 0.01% by the dispersive focused beam and the hole target. However, this momentum resolution 0.02% is the best resolution measured in the RIKEN accelerator research facility. The fact encouraged us to study the dispersion matching of the spectrograph PA.

Further checks for dispersion matching are necessary before studying the (^{4}He,^{8}He) reactions, because their cross sections are so small. However, the present test results indicate that the spectrograph PA can be used for measurement of reactions that have relatively large cross section, for example (^{4}He,^{6}He) reactions, with a limited target size.

References

[1] S. Kato, M.H. Tanaka, and T. Hasegawa, Nucl. Instrum. Methods. **154** (1978) 19.

[2] N. Yamazaki, *et al.*, CNS Annual Report 2000 (2001) 14.

[3] M.H. Tanaka, S. Kubono and S. Kato, Nucl. Instrum. Methods. **195** (1982) 509.

Development of a ^{17}N Secondary Beam II

Y. Wakabayashi, A. Odahara[a], Y. Gono, T. Fukuchi[b], N. Hokoiwa,
M. Kibe, T. Teranishi, S. Kubono[b], M. Notani[b], Y. Yanagisawa[c],
S. Michimasa[c], J.J. He[b], H. Iwasaki[d], S. Shimoura[b], H. Watanabe[c], T. Kishida[c],
E. Ideguchi[b], H. Baba[b], S. Nishimura[c], M. Nishimura[c], J.Y. Moon[e] and S. Kato[f]

Department of Physics, Kyushu University
[a] *Nishinippon Institute of Technology*
[b] *Center for Nuclear Study, Graduate School of Science, University of Tokyo*
[c] *RIKEN (The Institute of Physical and Chemical Research)*
[d] *Department of Physics, Graduate School of Science, University of Tokyo*
[e] *Chung-Ang University, Korea*
[f] *Yamagata University*

1. Introduction

High spin isomers are known in $N = 83$ isotones systematically [1]. These isomers are of stretch coupled configurations of valence nucleons excited by the breaking of neutron magic 82 and proton semi-magic 64 cores. They are considered to be shape isomers caused by sudden shape changes from near spherical to oblate shapes. In order to search for high-spin isomers in other mass regions, we selected $N = 51$ isotones which have one neutron outside a magic 50 core and proton numbers close to semi-magic 40 core.

High spin isomers of $N = 51$ isotones stem from stretch coupled configurations similar to those of $N = 83$ isotones [1]. Configurations of these anticipated isomers in $N = 51$ isotones are expected to be $[\nu(d_{5/2}g_{7/2}h_{11/2})\pi g^2_{9/2}]_{39/2^-}$ for odd nuclei and $[\nu(d_{5/2}g_{7/2}h_{11/2})\pi(p_{1/2}g^2_{9/2})]_{20^+}$ for odd-odd nuclei.

2. Experimental procedure and results

We developed a ^{17}N secondary beam using the low-energy radioisotope beam separator (CRIB) [2] of the Center for Nuclear Study (CNS), Graduate School of Science,University of Tokyo, in order to search for high-spin isomers in $N = 51$ isotones. Since the nuclei with $Z < 40$ of $N = 51$ isotones are close to the stability line, it is difficult to produce high-spin states of these nuclei using reactions by combinations of stable beams and targets. Therefore, it is very effective to use the radioisotope beam. By means of the γ spectroscopy method, high-spin isomers can be searched for the nuclei ^{90}Y, ^{89}Sr, ^{88}Rb produced by the $\alpha 5n$, $\alpha p5n$, $2\alpha 3n$ channels of the ^{82}Se+^{17}N reaction, respectively.

A ^{17}N secondary beam was produced by using CRIB [2] which consists of two dipole (D1 and D2), three quadrupole (Q1, Q2 and Q3) and small correction magnets (M1 and M2). A ^{9}Be primary target of 2.3 mg/cm^2 was bombarded by a $^{18}O^{8+}$ primary beam of 126.4 MeV to obtain a ^{17}N beam. The beam intensity was 0.4 pμA at the primary target position.

A parallel plate avalanche counter (PPAC) was set at a dispersive focal plane (F1) for beam monitoring. In order to identify reaction products, a PPAC and a Si detector of 1.5-mm thick were installed at an achromatic focal plane (F2). These detectors were located at 681 and 731 mm downstream of Q3, respectively. A ^{82}Se secondary target of 4.9 mg/cm^2 was placed at 1251 mm downstream of Q3, which was closer to a focal plane than that position in the previous experiment, 1921 mm, to get the smaller spot size of a ^{17}N secondary beam within 20 mmϕ. Two clover Ge detectors were set at 40 mm apart from the secondary target to measure γ-rays emitted from nuclei produced by the secondary fusion reaction. Plastic scintillator was placed at 597mm down stream from the secondary target position in order to detect the secondary beam.

Particle identification was achieved by using energies of reaction products and time differences between RF and F2-PPAC signals. Energy of $^{17}N^{7+}$ was deduced to be 104 ± 2 MeV. As the Si detector was moved out during the γ-ray measurement, $^{17}N^{7+}$ + $^{17}O^{7+}$ could not be separated. The intensity and fraction of $^{17}N^{7+}$ in the cocktail beam were 1.1×10^5 particles/s and 24%, respectively.

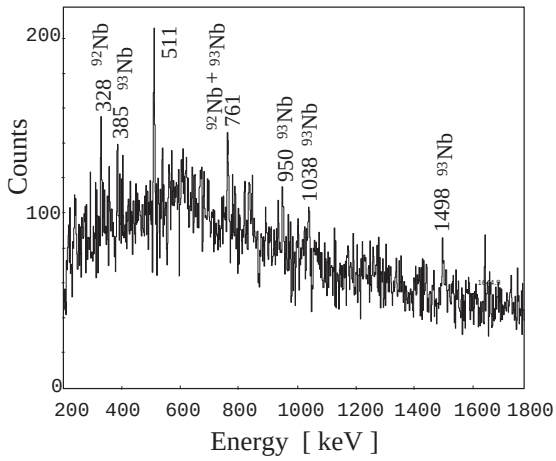

Figure 1. Projection spectrum of $\gamma\gamma$ coincidence

The total events of 2.1×10^8 were stored in the measurement during 2.4 days. Data acquisition was started when F2-PPAC and one Ge detector were hit. A plastic scintillator signal was used to veto the secondary beams reached

without making a secondary reaction. Only data with signal of cocktail beam of ^{17}N and ^{17}O at F2 position was accumulated. Although the background level originated from the thermal neutron capture γ-rays was 200 times higher than counts of peaks coming from secondary fusion reaction, seven γ-rays from ^{92}Nb and ^{93}Nb produced by the $7n$ and $6n$ channels of the ^{82}Se+^{17}N reaction, respectively, were observed, as shown in Fig.1.

3. Summary

A ^{17}N secondary beam was produced by using CRIB [2] in order to search for high-spin isomers in $N = 51$ isotones. By means of the γ spectroscopic method, we measured γ-rays emitted from nuclei produced by the secondary fusion reaction.

As a result, de-excited γ-rays of ^{92}Nb and ^{93}Nb from secondary fusion reactions were observed.

References

[1] Y. Gono *et al.*, Eur. Phys. J. A **13** (2002) 5, and reference therein.

[2] Y. Yanagisawa *et al.*, RIKEN Accel. Prog. Rep. **34** (2001) 183.

Development of a ^{7}Be RI Beam with CRIB

J. J. He, S. Kubono, T. Teranishi, M. Nishimura[a], S. Nishimura[a], M. Notani, S. Michimasa and H. Baba

Center for Nuclear Study, Graduate School of Science, University of Tokyo
[a]RIKEN(The Institute of Physical and Chemical Research)

1. Introduction

It is well-known that the stellar ^{7}Be$(p,\gamma)^8$B reaction plays an important role in the "solar neutrino puzzle" [1, 2, 3]. Many experimental and theoretical works had been performed to investigate this reaction [4, 5, 6, 7, 8, 9, 10, 11, 12, 13]. In order to calculate the solar neutrino flux the cross section σ_{17}(E) of the ^{7}Be$(p,\gamma)^8$B reaction should be deduced better than 5% [1, 13]. Thus astrophysis, nuclear physics, and particle physics meet in addressing the solar neutrino problem.

So far, the derived astrophysical factors $S_{17} = \lim_{E\to 0} Ee^{2\pi\eta(E)}\sigma_{17}(E)$ are not converging well, although they mostly agree within the uncertainties [14] which are not small enough to discuss precisely the solar model. The traditional direct measurements to date suffered from systematic uncertainties from the radioactivity of a ^{7}Be target, and the indirect methods (*e.g.*, Coulomb dissociation and ANC method) have many physical limitations as well. With the advent of radioactive beam facilities extensive investigations of reactions between radioactive and stable nuclei have become possible. At Naples, a direct measurement with a ^{7}Be radioactive ion (RI) beam bombarding a hydrogen target, followed by a separator to detect the ^{8}B recoils was attempted [4, 5, 6, 7]. However, low beam intensity limited the statistical precision of the cross section (about 25%). So far it was the first attempt to study this reaction by using the inverse kinematics method. The advantage of this method is that the detectors do not face the radioactive target, and it is much easier to detect the recoiled ^{8}B particles at the forward angle as well.

Recently, a low-energy and high-purity ^{7}Be RI beam has been developed with CRIB. In this report, the beam production and the beam properties are presented.

2. Experiment

The ^{7}Be radioactive ion beam has been developed by using the CNS RI beam separator (CRIB) [15]. A ^{7}Li^{2+} primary beam was accelerated up to 3.42 MeV/nucleon by the RIKEN AVF cyclotron. A full intensity of 100 pnA was attenuated by a factor of 2×10^4 during the experiment. By bombarding a CH_4 gas target (1.3 mg/cm^2) the ^{7}Be secondary beam was produced by the ^{1}H(^{7}Li,^{7}Be)n reaction in the inverse kinematics. After the F0 gas target, the mean energy of the ^{7}Be particles was 2.31 MeV/nucleon.

At the momentum-dispersive focal plane (F1), a 6-μm-thick Mylar foil was used to eliminate the light-ion background from the secondary beam. In addition, an aperture was set to $\pm$ 10 mm corresponding to a momentum spread of $(\Delta p/p) = \pm$ 0.63%, to select the aimed particles.

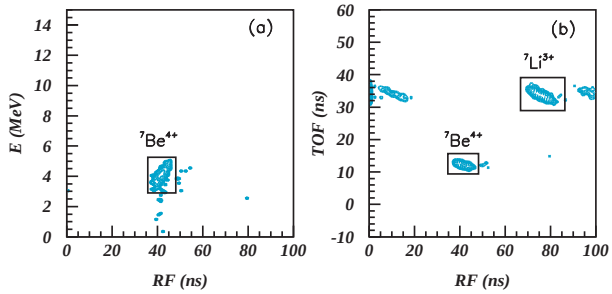

Figure 1. Plots of particle identification without using the degrader at F1. RF is related to the particle time-of-flight (TOF) between F0 gas target and the second PPAC at F2. (a) RF vs Energy measured by the Si detector, (b) RF vs TOF between the two PPACs.

At the achromatic focal plane (F2), two delay-line type PPACs and one Si detector (1.5-mm thick) were installed. The beam profile was monitored by the position information of the PPACs. The ^{7}Be particles were identified in an event-by-event mode by using the TOF information obtained from the PPACs, the RF signal provided by the AVF cyclotron and the energy signal in the Si detector.

A particle identification plot is shown in Fig. 1. In the case without the degrader at F1 [see Fig. 1(b)], the main contaminants were ^{7}Li^{3+} particles which however were stopped in the second PPAC, and therefore only the ^{7}Be particles were detected in the Si detector with a purity of about 100% [Fig. 1(a)]. In the case of using a 6-μm Mylar degrader at F1, all particles had very low energies after two PPAC's, so one of the PPACs was moved out. In this case, the purity of ^{7}Be^{4+} beam was about 90%, with the contaminant of ^{7}Li^{3+} particles at very low energies.

The properties of the ^{7}Be^{4+} RI beam produced under three different experimental conditions are presented in Table 1. The extrapolate intensities were calculated by a 100-pnA intensity of primary beam. The ^{7}Be^{4+} beam spot sizes at the second PPAC position are listed in Table 2. The 4.1-MeV ^{7}Be^{4+} beam had a very large beam spot size because of the low-energy particles having the larger energy straggling in the materials.

3. Summary

A low-energy, high-purity ^{7}Be secondary beam has been developed with CRIB. An intensity on the order of 10^5 particles/s was achieved by a 100-pnA primary beam intensity. It would provide a chance to investigate the stellar ^{7}Be$(p,\gamma)^8$B reaction with CRIB if we improve the experimental conditions. According to the previous experiments, the very small reaction cross-sections were deduced at low

Table 1. Properties of the $^{7}Be^{4+}$ RI beam. The intensities are in units of aps. (The condition of "w/o deg.; 2 PPACs" means that the degrader was not used at F1, and two PPACs were used at F2.)

E (MeV)	Purity	Intensity	Conditions
4.1	100 %	4.5×10^{5}	w/o deg.; 2 PPACs
10.9	50 %	4.7×10^{5}	w/o deg; 1 PPAC
8.6	90 %	7.2×10^{5}	with deg.; 1 PPAC

Table 2. Typical beam spot size for the $^{7}Be^{4+}$ RI beam (@2nd PPAC).

E (MeV)	X (FWHM)	Y (FWHM)
4.1	26 mm	22 mm
10.9	11 mm	7 mm
8.6	16 mm	13 mm

energies, for example, only about 0.5 μb and 0.25 μb at $E_{\rm c.m.}$ = 1.0 and 0.5 MeV, respectively. Therefore, a lot of preparation work is needed to investigate this reaction. Recently the experimental conditions are being considered and prepared.

References

[1] J.N. Bahcall and M.H. Pinsonneault, Rev. Mod. Phys. **64** (1992) 885.
[2] J.N. Bahcall, *Solar Neutrinos, in Unsolved Problems in Astrophysics*, (Bahcall and Ostriker eds, Princeton University Press, 1997).
[3] S. Turck-Chieze *et al.*, Phys. Rep. 230 (1993) 57.
[4] L. Gialanella *et al.*, Nucl. Instrum. Methods. A **376** (1996) 174.
[5] L. Campajola *et al.*, Z. Phys. A **356** (1996) 107.
[6] L. Gialanella *et al.*, Eur. Phys. J. A **7** (2000) 303.
[7] F. Terrasi *et al.*, Nucl. Phys. A **688** (2001) 539c.
[8] W. Liu *et al.*, Phys. Rev. Lett. **77** (1996) 611.
[9] F. Strieder *et al.*, Eur. Phys. J. A **3** (1998) 1.
[10]B. Davids *et al.*, Phys. Rev. C **63** (2001) 065806.
[11]T. Motobayashi *et al.*, Eur. Phys. J. A **13** (2002) 207.
[12]H.M. Xu *et al.*, Phys. Rev. Lett. **73** (1994) 2027.
[13]J.N. Bahcall *et al.*, Phys. Lett. B **433** (1998) 1.
[14]S. Kubono, Nucl. Phys. A **230** (2001) 221.
[15]S. Kubono *et al.*, Eur. Phys. J. A **13** (2002) 217.

Study of Proton Resonant States of Astrophysical Interest in ^{23}Al and ^{22}Mg using RI Beams from CRIB

J. J. He, S. Kubono, T. Teranishi, M. Notani, H. Baba, S. Nishimura[a], J. Y. Moon[b], M. Nishimura[a], S. Michimasa, H. Iwasaki[c], Y. Yanagisawa[a], N. Hokoiwa[d], M. Kibe[d], J. H. Lee[b], S. Kato[e], Y. Gono[d] and C. S. Lee[b]

Center for Nuclear Study, Graduate School of Science, University of Tokyo
[b]*The Institute of Physical and Chemical Research (RIKEN)*
[c]*Department of Physics, Chung-Ang University, Korea*
[d]*Department of Physics, University of Tokyo*
[e]*Department of Physics, Kyushu University*
[f]*Department of Physics, Yamagata University*

1. Introduction

The stellar ^{22}Mg$(p,\gamma)^{23}$Al and ^{21}Na$(p,\gamma)^{22}$Mg reactions play an important role in the hot Ne-Na cycle during the early stage of the rp process and possibly influence the production of a γ emitter ^{22}Na in Ne-rich novae [1,2,3,4]. The reaction rate of the capture process is determined by the contributions of direct capture and resonance capture [5]. The resonant capture rate is related to the properties of the relavant resonant states, such as resonant energy E_r, resonant widths, Γ_p and Γ_γ, and spin-parity J^π. The research status of the excited states in ^{23}Al and ^{22}Mg nuclei was described in the previous report [6].

In the present work, the proton resonant states in ^{23}Al and ^{22}Mg were investigated by using resonant elastic scattering of the ^{22}Mg and ^{21}Na radioactive beams on a thick hydrogen target. As described in reference [7], the excitation functions of ^{22}Mg+p and ^{21}Na+p can be obtained by measuring the energies of recoiled protons by a thick target method for a certain energy range simultaneously. If a resonant state exists with a sufficiently large width, it can be identified as an interference pattern of potential and resonance scattering in the excitation function. The resonance energies, widths and the spin-parity information can be deduced from the R-matrix analysis.

2. Experimental method

The experiment was carried out with the CNS radioactive ion beam separator (CRIB) [8, 9]. The experimental procedure and setup (Fig. 1) were described in the previous report [6] in detail. The new results are presented in the following parts.

On the secondary target [$(CH_2)_n$], the beam spot sizes (FWHM) were 15 mm horizontally and 11 mm vertically; the mean energies of ^{22}Mg and ^{21}Na beams were 4.37 MeV/nucleon and 3.92 MeV/nucleon respectively, with an energy spread of 0.20 MeV/nucleon (FWHM).

To facilitate the following description, the ΔE-E telescopes at angles of $\theta_{\rm lab} = 0^\circ$, 16° and -23° are referred to as SET1, SET2 and SET3, respectively (Fig. 1). In SET1, a double-sided-strip (16×16 strips) ΔE was used to determine the two-dimensional positions, while for ΔE in SET2 and SET3 only horizontal strips were used. The resolution

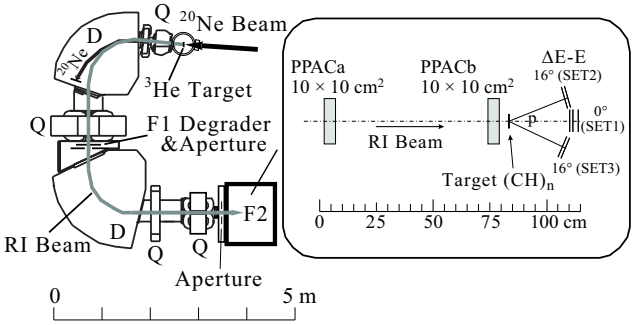

Figure 1. Experiment setup in the scattering measurement.

of the scattering angle (FWHM) was 1.0°, 1.4° and 1.3° at three cases, respectively.

In order to identify the proton resonant states in the ^{23}Al and ^{22}Mg nuclei, the center-of-mass energy ($E_{\rm c.m.}$) was reconstructed by taking into account the kinematics of ^{22}Mg+p (or ^{21}Na+p) and the energy loss of particles in the target. The overall energy resolution of $E_{\rm c.m.}$ was determined by the energy resolution of the ΔE-E detector system, the angular resolution of the scattering angle, the energy width of the secondary beam and the particle straggling in the target material. The energy resolution of the detector system was the main source in all three SETs. The overall energy resolution (FWHM) of $E_{\rm c.m.}$ in SET1 was about 20 keV (at 0.5 MeV) to 45 keV (at 3.5 MeV). While those in SET2 and SET3 were about 20 to 70 keV because of the larger scattering angles resulted in the larger kinetics shifts.

Experimental data with a C target (9.3 mg/cm^2) was also acquired in a separate run to evaluate the background contribution from the reactions of ^{22}Mg and ^{21}Na with C atoms in the $(CH_2)_n$ target. The proton spectrum with the C target had a wide bump shape but no sharp structure. The yield ratio of these two proton spectra (with $(CH_2)_n$ and C targets) was normalized by the number of beam particles and by the target thickness per unit beam energy loss in the corresponding target. Finally, the spectrum of a pure proton target was obtained by subtracting the spectrum of normalized C-target from that of $(CH_2)_n$-target accordingly.

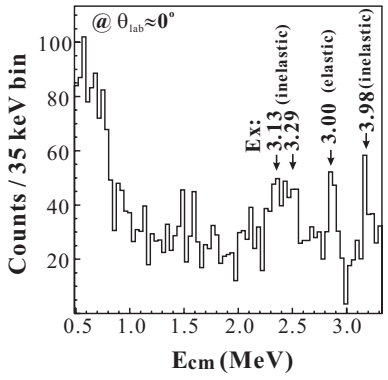

Figure 2. Experimental proton spectrum for the ^{22}Mg+p scattering (elastic and inelastic) at $\theta_{\rm lab}$ = 0° (SET1).

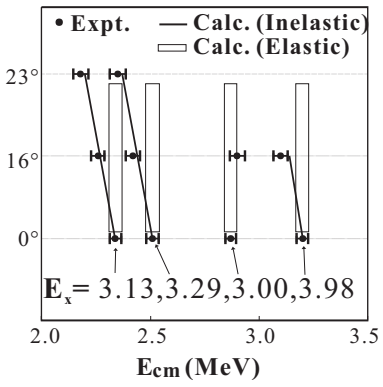

Figure 3. Identification of excited states induced by elastic and inelastic scattering.

3. Results and Discussion

Figure 2 shows an experimental proton spectrum for the ^{22}Mg+p scattering at $\theta_{\rm lab}$ = 0° ($\theta_{\rm c.m.}$ = 180°). After corrected by the number of ^{22}Mg beam particles, and the stopping cross sections (dE/dx) of the beam particles in the target material, the excitation functions $d\sigma/d\Omega$ of differential elastic scattering for ^{22}Mg+p can be deduced [7]. The proton threshold in ^{23}Al is known to be 0.123 MeV [10]. Therefore, the excitation energy in ^{23}Al can be calculated by $E_x = E_{\rm c.m.} + 0.123$ MeV. The arrows in the figure indicate the energies of excited states in ^{23}Al. It should be pointed out that the figure was obtained by assuming an elastic scattering case. Therefore, in an inelastic scattering case, the $E_{\rm c.m.}$ energy in the figure needs to be corrected. Comparing the experimental scattering data at three different SETs, inelastic scattering contributions were evaluated. As shown in Fig. 3, the $E_{\rm c.m.}$ energies for the excited states at 3.13, 3.29 and 3.98 MeV were shifted in SET2 ($\sim$70 keV) and SET3 ($\sim$130 keV), but that of the state at 3.00 MeV was only shifted within the error. This fact indicates that three peaks are due to inelastic scattering. In Fig. 3, the bold line indicates the kinematics calculation for the inelastic scattering case, where the excited state in ^{23}Al de-excites into the excited ^{22}Mg nucleus (the first excited state at 1.25 MeV) by a proton emission. The black dot indicates the experimental $E_{\rm c.m.}$ energy, together with the systematic error bar. The rectangular box indicates the $E_{\rm c.m.}$ energy range of the elastic scattering case, and its width equals to the systematic error of the deduced $E_{\rm c.m.}$ energy. It can be seen that the theoretical calculations are in good agreement with the experimental results within the errors. A conclusion is drawn that the excited state at 3.00 MeV decays to the ground state of ^{22}Mg by a proton emission, while the excited states at 3.13, 3.29 and 3.98 MeV all decay to the first excited state in ^{22}Mg by a proton emission. According to the preliminary analysis, the 3.00-MeV state is a new proton resonant state in ^{23}Al, which was not observed in the previous experiments.

A preliminary R-matrix fit was performed for the resonant state at $E_x = 3.00$ MeV, and a d-wave fitting reproduces the experimental data very well. Therefore, we assign this state with the spin-parity of (3/2$^+$, 5/2$^+$) tentatively. Detailed studies of resonant energies, spin-parities and widths for these excited states are being made with an R-matrix code SAMMY-M6-BETA [11].

References

[1] I. Iyudin *et. al.*, Astron. Astrophys. **300** (1995) 422.
[2] L. VanWormer *et. al.*, Astrophys. J. **432** (1994) 326.
[3] H. Herndl *et. al.*, Phys. Rev. C **52** (1995) 1078.
[4] H. Schatz *et. al.*, Phys. Rev. Lett. **79** (1997) 3845.
[5] C.E. Rolfs and S. Rodney, *Cauldrons in the Cosmos*, the University of Chicago Press (1988).
[6] J.J. He *et al.*, CNS Annual Report 2002 (2003) 51.
[7] S. Kubono, Nucl. Phys. A **230** (2001) 221.
[8] S. Kubono *et al.*, Eur. Phys. J. A **A13** (2002) 217.
[9] T. Teranishi *et al.*, Phys. Lett. B **556** (2003) 27.
[10] J.A. Caggiano *et. al.*, Phys. Rev. C **64** (2001) 025802.
[11] N.M. Larson, *A Code System for Multilevel R-Matrix Fits to Neutron Data Using Bayes' Equations*, ORNL/TM-9179/R5 (Oct. 2000).

Study of Proton Resonances in ^{26}Si and ^{27}P by the Elastic Scattering of ^{1}H(^{25}Al, p)^{25}Al and ^{1}H(^{26}Si, p)^{26}Si

J. Y. Moon, C. S. Lee, J. H. Lee, C. C. Yun, J. C. Kim[a], M. Youn[a], S. Kubono[b], T. Teranishi[b], J. J. He[b], M. Notani[b], S. Nishimura[c], M. Nishimura[c], V. Guimarães[d], R. F. Lihitenthaler[d] and S. Kato[e]

Department of Physics, Chung-Ang University, Korea
[a]*Department of Physics, Seoul National University, Korea*
[b]*Center for Nuclear Study, Graduate School of Science, University of Tokyo*
[c]*RIKEN (The Institute of Physical and Chemical Research)*
[d]*Instituto de Física, Universidade de São Paulo, Brazil*
[e]*Department of Physics, Yamagata University*

1. Introduction

Gamma rays from the sky can be observed by gamma-ray telescopes, like COMPTEL aboard CGRO (Compton Gamma-Ray Observatory). Recently, the nine-year survey of COMPTEL has updated the all-sky map of the 1.809-MeV gamma ray, which is produced by the decay of ^{26}Al to the first excited state of ^{26}Mg, followed by de-excitation to its own ground state. Knowledge of its sources is not yet clear though massive stars, novae, and X-ray busters are assumed to be its sources. Therefore, spectroscopic information on resonance states, such as energy, spin, and parity, is very crucial to the reaction rate for each reaction contributing to the production of the gamma-ray emitter, ^{26}Al(g.s.) at the stellar condition. In a thermonuclear runaway under the explosive hydrogen burning, the ^{25}Al$(p,\gamma)^{26}$Si reaction hinders production of ^{26}Al(g.s.). In spite of previous measurements on resonance states in ^{26}Si, some states could not be clearly identified. Especially, the astrophysically important 3^+ state with $E_R = 0.427$ MeV above the proton threshold could be neither seen [1] nor definitely identified [2]. On the other hand, the ^{26}Si$(p,\gamma)^{27}$P reaction prevents ^{26m}Al from being produced. It has been suggested that higher temperature novae (T $\geq$ 0.4 GK) may be hot enough to establish an equilibrium between ^{26}Al(g.s.) and ^{26m}Al [3]. Thus, study on resonance states in ^{27}P should be needed to determine the reaction rate of proton capture on ^{26}Si. Until now, only one state at 1.199 MeV above the proton threshold has been reported [4]. In this experiment, we investigated the resonance states in ^{26}Si and ^{27}P using the inverse elastic scattering of ^{1}H(^{25}Al,p)^{25}Al and ^{1}H(^{26}Si,p)^{26}Si together with the thick target method.

2. Experimental procedure

The radioactive beams used in this experiment were obtained by the CNS radioactive ion beam separator (CRIB). A ^{24}Mg^{8+} primary beam, accelerated by the RIKEN AVF cyclotron ($K = 70$), bombarded a ^{3}He gas target at 7.434 A MeV. The thickness of the ^{3}He gas target was 0.32 mg/cm^2. With two primary reactions of ^{3}He(^{24}Mg,n)^{26}Si*$(p)^{25}$Al and ^{3}He(^{24}Mg,n)^{26}Si, two different kinds of secondary beam, ^{25}Al and ^{26}Si, were produced and used for measurement of the elastic scattering of ^{1}H(^{25}Al,p)^{25}Al and ^{1}H(^{26}Si,p)^{26}Si, respectively. The secondary beams were identified by using TOF (Time of Flight) between the two PPAC's (Parallel Plate Avalanche Counters) on the achromatic focal plane (F2), the beam energy, and TOF between the production target and a PPACb on the F2 plane. With the slit on the momentum-dispersive focal plane (F1), the purities of secondary beams were enhanced. Additionally, an energy degrader made of 2.6 μm mylar was used to provide another particle separation. Figure 1 and Table 1 show the secondary-beam identification using the two TOF signals and the specification of each beam, respectively.

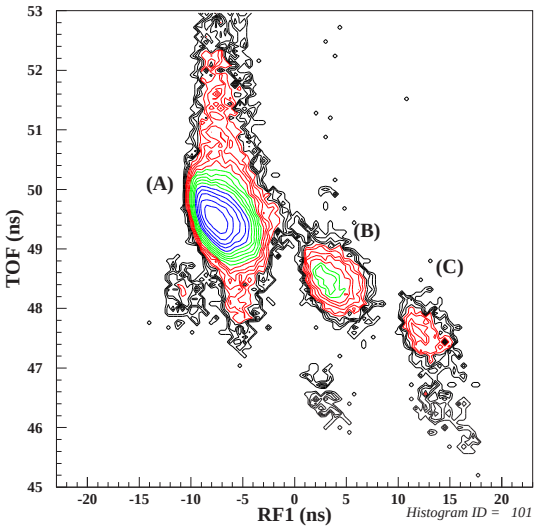

Figure 1. Secondary beams are shown. (A) ^{24}Mg; (B) ^{25}Al; (C) ^{26}Si

Table 1. Specifications of secondary beams (averaged)

Beam	Energy (A MeV)	Intensity (kcps)	Purity (%)
^{25}Al	3.44	9.325	4.72
^{26}Si	3.95	1.573	0.7

The secondary beams were bombarded on a polyethylene (CH_2) target of 8.24 mg/cm^2, and fully stopped in the target. To detect the recoiled protons, two sets of the silicon counter telescope which consists of PSD (Position-sensitive

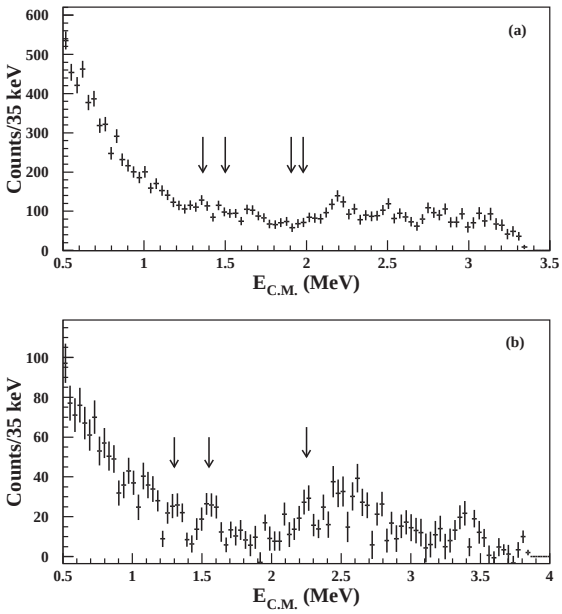

Figure 2. Excitation functions are shown for (a) ^{25}Al + p and (b) ^{26}Si + p, where the arrows indicate the ^{26}Si states with uncertain spin-parity in (a) and the ^{27}P candidate states unknown so far in (b), respectively.

Silicon Detector with the thickness of 75 μm) and SSD (Surface-barrier Silicon Detector with the thickness of 1500 μm) were installed at 0° and 17°. They were also used as a ΔE-E telescope to identify protons from other recoiled particles such as α and heavy ions. In the second set at 17°, an additional SSD was added to reject high-energy protons. In this experiment, we used the thick target method to examine a wide range of excitation energy in ^{26}Si and ^{27}P, where the incident beam can have different energies in the target and interact with the target until its energy is fully absorbed. The secondary beams had energies of 3.4407 A MeV for ^{25}Al beam and 3.9575 A MeV for ^{26}Si beam on the target, respectively. With these energies, we could scan up to E_x = 8.8243 MeV for ^{26}Si and E_x = 4.7109 MeV for ^{27}P, respectively above the proton threshold. A carbon target was used for subtraction of a contribution by carbons in the CH_2 target from the proton spectrum of CH_2 target. The energy calibration of the detectors was done with protons whose energies were determined by the CRIB magnetic setting.

3. Preliminary results

As shown in Fig. 2(a), we observed some resonance states in the ^{25}Al + p spectrum. In this experiment, we could not identify the 3^+ unnatural parity state with E_R = 0.427 MeV because the target was too thick for the recoiled protons to escape. Determination of their spin-parities and energies is underway by using the R-matrix analysis. For the ^{26}Si + p spectrum shown in Fig. 2(b), we have also seen several peaks though with low counting statistics. These peaks are unknown so far and probably belong to ^{27}P. Further analysis is in progress.

References

[1] D.W. Bardayan *et al.*, Phys. Rev. C **65** (2002) 032801(R).
[2] J.A. Caggiano *et al.*, Phys. Rev. C **65** (2002) 055801.
[3] A. Coc, M.-G. Porquet and F. Nowacki, Phys. Rev. C **61** (1999) 015801.
[4] J.A. Caggiano *et al.*, Phys. Rev. C **64** (2001) 025802.

Elastic Resonance Scattering of ^{23}Mg+p

T. Teranishi, S. Kubono, J.J. He, M. Notani, T. Fukuchi, S. Shimoura, S. Nishimura[a], M. Nishimura[a], S. Michimasa[a], Y. Gono[b], Y. Wakabayashi[b], N. Hokoiwa[b], A. Odahara[c], H. Baba[d], J.Y. Moon[e], J.H. Lee[e], C.S. Lee[e], J.C. Kim[e], H. Ishiyama[f], Y.X. Watanabe[f], T. Hashimoto[g], T. Ishikawa[g], M. H. Tanaka[f], H. Miyatake[f], V. Guimarães[h], R. F. Lihitenthaler[h], K. Sato[i], T. Kawamura[i] and S. Kato[i]

Center for Nuclear Study, Graduate School of Science, University of Tokyo
[a]*The Institute of Physical and Chemical Research (RIKEN), Japan*
[b]*Department of Physics, Kyushu University, Japan*
[c]*Nishinippon Institute of Technology, Japan*
[d]*Department of Physics, Rikkyo University, Japan*
[e]*Chung-Ang University, Korea*
[f]*Institute of Particle and Nuclear Studies, KEK, Japan*
[g]*Department of Physics, Tokyo University of Science, Japan*
[h]*Department of Physics, University of São Paulo, Brazil*
[i]*Department of Physics, Yamagata University, Japan*

1. Introduction

Levels in ^{24}Al above the proton threshold of $E_x = 1.871$ MeV may play important roles in the astrophysical reaction of ^{23}Mg$(p,\gamma)^{24}$Al, which is one of the breakout paths from the Ne-Na cycle [1]. Values of J^π are not precisely determined yet for many of these levels. There are almost no experimental data of Γ for resonance levels in ^{24}Al [2]. We performed an experiment of the ^{23}Mg+p elastic resonance scattering, aiming at deducing new information on J^π and Γ for the ^{24}Al levels.

2. Experiment

The ^{23}Mg+p experiment was performed in inverse kinematics with a secondary ^{23}Mg beam and a proton target. The ^{23}Mg beam was produced by the ^{24}Mg$(d,t)^{23}$Mg reaction in inverse kinematics. The primary beam of ^{24}Mg was accelerated by an AVF cyclotron up to 7.5 MeV/nucleon with an intensity of 60 pnA. The deuterium gas target had a thickness of 0.33 mg/cm^2 confined in a cell by two Havar window foils of 2.2 μm. After the CRIB separator [3,4], the ^{23}Mg secondary beam had an energy of 4.0 MeV/nucleon and an intensity of 3.2×10^4 particles/sec, which was 12% of the total intensity. A major contaminant in the beam was ^{24}Mg with an energy of 3.5 MeV/nucleon originated from scattering of the primary beam at beam pipes and inner walls of the separator magnets. This ^{24}Mg contaminant was utilized to measure a spectrum of known resonance levels in the ^{24}Mg+p (^{25}Al) system simultaneously with the ^{23}Mg+p data of interest.

The setup for the elastic scattering measurement consisted of two parallel-plate avalanche counters (PPACs) [5] as beam counters, a polyethylene ($(CH_2)_n$) sheet as a proton target, and two sets of silicon detectors for recoil protons. The PPACs were set upstream of the proton target and used to tag beam particles on an event-by-event basis. The beam incident angle and reaction position on the target were determined by the hit positions at the two PPACs. The beam nuclides of ^{23}Mg and ^{24}Mg were identified by the time-of-flight between the two PPACs to make the spectra of ^{23}Mg+p and ^{24}Mg+p, respectively.

A thick-target technique [6, 7] was used to measure the excitation function efficiently. The thickness of the polyethylene target was chosen to be 8.2 mg/cm^2, which was a little thicker than the stopping range for the beam particles. Utilizing energy-loss process of the beam in the target, a wide range of center-of-mass energy ($E_{\rm c.m.}$) was scanned without changing the beam energy before the target. While the beam particles were completely stopped in the target, most of the recoil protons went out from the target with small energy losses.

The recoil protons were detected by the two sets of silicon detectors at laboratory angles of $\theta_{\rm lab}$ = 0° and 17°. Each set consisted of ΔE and E layers with thicknesses of 75 and 1500 μm, respectively. Protons were identified with the information of ΔE, E, and timing. The $E_{\rm c.m.}$ and center-of-mass angle ($\theta_{\rm c.m.}$) were determined by measuring the energy and angle of proton. At $\theta_{\rm lab} = 0°$, the proton energy is roughly four times of $E_{\rm c.m.}$. An $E_{\rm c.m.}$ resolution of 30 keV (FWHM) was achieved because of this kinematic factor and a silicon detector resolution of about 100 keV (FWHM).

A carbon target was also used to measure the background contribution to the proton spectrum from C atoms in the $(CH_2)_n$ target. The proton spectrum with the C target was subtracted from that with the $(CH_2)_n$ target to deduce the excitation function of proton elastic scattering.

In the excitation function, a resonance level can be identified as an interference pattern of potential scattering and resonance scattering. The energy, Γ, and J^π of the level may be deduced from an R-matrix analysis for the interference pattern. The angle of $\theta_{\rm lab} = 0°$ corresponds to $\theta_{\rm c.m.} = 180°$, where the Coulomb-potential scattering am-

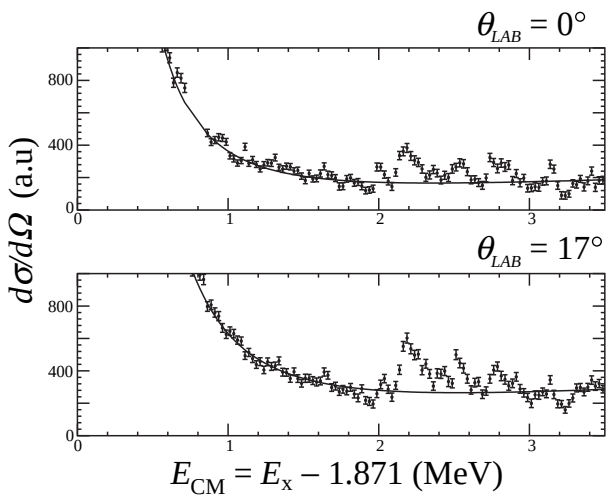

Figure 1. Preliminary excitation functions for ^{23}Mg+p at $\theta_{\rm lab} = 0^\circ$ and 17°. The solid curves represent cross sections deduced by the Coulomb and hard-sphere scattering amplitudes.

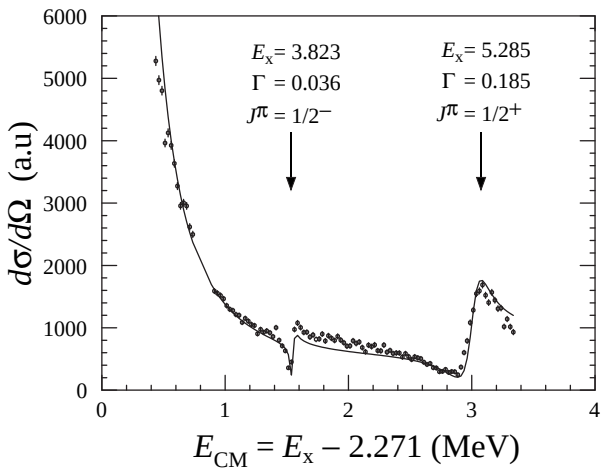

Figure 2. Excitation function for ^{24}Mg+p at $\theta_{\rm lab}$=0°. The solid curve represents a tentative result of R-matrix analysis.

plitude is minimum. Therefore, angles around $\theta_{\rm lab} = 0^\circ$ are suitable for observing resonance contributions.

3. Results

Preliminary spectra of ^{23}Mg+p at $\theta_{\rm lab} = 0^\circ$ and 17° are shown in Fig. 1. The solid line represents cross sections deduced from the Coulomb and hard-sphere scattering amplitudes. Deviation of the experimental cross sections from the solid line is seen in a region of $E_{\rm c.m.} > 1.6$ MeV both at 0° and 17°. Those deviation patterns at 0° and 17° are similar to each other and indicating presence of several resonance levels. A small bump at $E_{\rm c.m.}$ = 1.6 MeV and two peaks at 2.0 and 2.2 MeV may be attributed to three levels. The spectral pattern above $E_{\rm c.m.}$ = 2.4 MeV is possibly due to three or more resonance levels. Some of the peaks seem to be consistent with the latest compilation of ^{24}Al levels [2]. Quantitative analysis of these patterns is in progress. Some J^π values will be newly determined by an R-matrix analysis. The Γ for these levels will be also evaluated for the first time.

The ^{24}Mg+p data, taken simultaneously with the ^{23}Mg+p data, is useful to check the energy calibration of the silicon detectors and analysis procedures. Figure 2 shows the result of ^{24}Mg+p excitation function, covering $E_x = 2.7$–5.6 MeV in ^{25}Al. The spectrum clearly shows resonance shapes due to two known levels in ^{25}Al at E_x = 3.823 and 5.285 MeV with Γ = 0.036 and 0.185 MeV, respectively [2]. The solid curve in Fig. 2 represents a tentative result of R-matrix analysis and agrees with the experimental data.

4. Summary

The excitation function of the ^{23}Mg+p elastic scattering was measured by using a low-energy ^{23}Mg beam and a thick proton target. The resonance patterns seen in the excitation function are under analysis and will provide new information on J^π and Γ of the resonance levels in ^{24}Al. To extract the resonance contribution to the ^{23}Mg$(p,\gamma)^{24}$Mg reaction rates, one has to know the gamma widths, which are unable to be deduced from the present experiment. However, the information from the present experiment will help further study on this stellar reaction. The validity of the ^{23}Mg+p data was proven by the calibration spectrum of ^{24}Mg+p, which was measured simultaneously with the same experimental setup. Measurement and analysis of other resonance-scattering experiments on proton-rich unstable nuclei are in progress or being planned with interests in nuclear astrophysics and nuclear structure.

References

[1] S. Kubono *et al.*, Nucl. Phys. **588** (1995) 521, and references therein.
[2] P.M. Endt, Nucl. Phys. A **633** (1998) 1.
[3] T. Teranishi *et al.*, Nucl. Phys. A **718** (2003) 207c.
[4] S. Kubono *et al.*, Eur. Phys. J. A **13** (2002) 217.
[5] H. Kumagai *et al.*, Nucl. Instrum. Methods **A470** (2001) 562.
[6] K.P. Artemov *et al.*, Sov. J. Nucl. Phys. **52** (1990) 408.
[7] S. Kubono, Nucl. Phys. A **693** (2001) 221, and references therein.

Study of ^{14}O(α, p)^{17}F Reaction using a Radioactive Ion Beam of ^{14}O

M. Notani, T. Teranishi, Y. Yanagisawa[a], S. Michimasa, K. Ue[b], J.J. He, S. Kubono, H. Iwasaki[b], H. Baba[c], M. Tamaki, T. Minemura[a], S. Shimoura, N. Hokoiwa[d], Y. Wakabayashi[d], T. Sasaki[d], T. Fukuchi[d], A. Odahara[e], Y. Gono[d], Zs. Fülöp[f], E.K. Lee[g], K.I. Hahn[g], J.Y. Moon[h], C.C. Yun[h], J.H. Lee[h], C.S. Lee[h] and S. Kato[i]

Center for Nuclear Study, Graduate School of Science, University of Tokyo
[a]*RIKEN (The Institute of Physical and Chemical Research)*
[b]*Department of Physics, University of Tokyo*
[c]*Department of Physics, Rikkyo University*
[d]*Department of Physics, Kyushu University*
[e]*Nishinippon Institute of Technology*
[f]*Institute of Nuclear Research (ATOMKI), Hungary*
[g]*Ewha Woman's University, Korea*
[h]*Chung-Ang University, Korea*
[i]*Department of Physics, Yamagata University*

1. Introduction

Explosive hydrogen burning may be the main source of energy generation in novae and X-ray bursts, and provides an important route for nucleosynthesis up to the mass 100 region via the rapid proton-capture (rp-) process. The rp-process is considered to start with nuclear reactions of the breakout process from the hot-CNO cycle [1]. One of the breakout reactions is the ^{14}O(α, p)^{17}F reaction, because hydrogen burning of ^{14}O is inhibited since ^{15}F is proton unbound. Significant amount of ^{14}O may be accumulated due to the relatively long half-life of the beta decay ($t_{1/2}$ = 71 sec) in the hot-CNO cycle. The rate of the ^{14}O(α, p)^{17}F reaction determines the ignition process of the astrophysical events. Thus the ^{14}O(α, p)^{17}F reaction is essential for understanding the breakout process.

However, this reaction was studied only via indirect methods and time-reverse reactions so far. The ^{14}O(α, p)^{17}F reaction rate at low temperatures is believed to be dominated by a resonance corresponding to a 1^- state at $E_x = 6.15$ MeV in ^{18}Ne. Several states at $E_x = 7.0$–7.5 MeV may also contribute to the reaction rate at higher temperatures up to 3×10^9 K, and this topic motivated a novel research via the time-reverse ^{17}F(p, α)^{14}O reaction with a radioactive ^{17}F beam [2, 3]. This reaction, however, only provides the partial widths for proton decay to the ground states of ^{17}F. Since the proton decay to the first-excited $1/2^+$ state in ^{17}F at $E_x = 0.495$ MeV would also contribute to the astrophysical yield, these proton widths have to be determined experimentally.

A direct measurement of the cross section for the ^{14}O(α, p)^{17}F reaction has been carried out by the combination of a newly-developed low-energy in-flight RI beam separator and a helium gas target cooled to 30 K. We report the first measurement of a direct measurement of the nuclear reaction ^{4}He(^{14}O, p)^{17}F with the thick target method [4, 5].

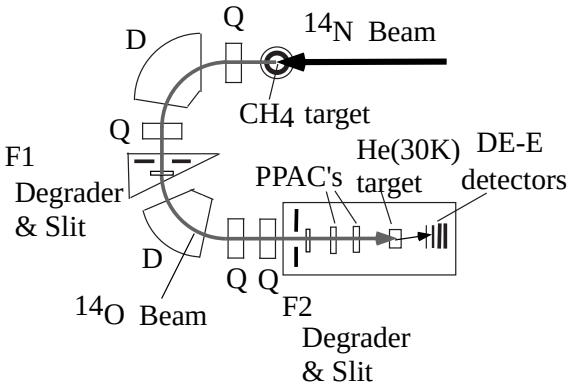

Figure 1. Schematic view of the experimental setup used for the measurement of the ^{14}O(α, p)^{17}F reaction cross section.

2. Experiment

The experiment was performed using the CNS radioactive ion beam separator (CRIB) [6], which was recently installed by CNS, in the RIKEN accelerator research facility. Figure 1 shows the experimental setup of the measurement. A primary beam of ^{14}N was accelerated up to an energy of 8.4 A MeV in the RIKEN AVF cyclotron with K = 70. The maximum intensity of the beam was 300 pnA. The primary beam bombarded a CH_4 gas target with a thickness of 1.3 mg/cm^2. The target gas was confined in a small chamber with entrance and exit windows. The gas pressure was one atmosphere and Havar foils of thickness of 2.2 μm were used for the windows. A secondary beam of ^{14}O was produced by the ^{1}H(^{14}N,^{14}O)n reaction.

The secondary ^{14}O particles were separated in the CRIB. An energy degrader of 10-μm thick Mylar foil was installed at the momentum dispersive focal plane (F1) to remove background light ions from the secondary beam. A holizontal slit was set to select the ^{14}O particles at a mean energy of 6.40 A MeV after the degrader with the momentum acceptance of 1%.

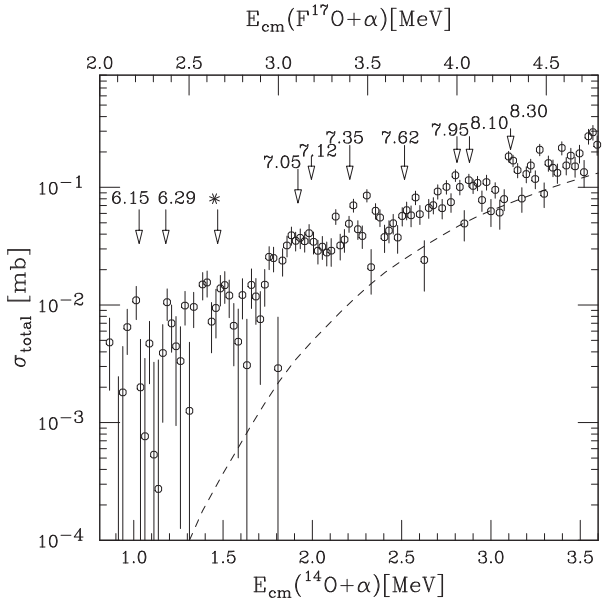

Figure 2. Spectrum of measured cross sections for the ^{14}O$(\alpha,p)^{17}$F reaction. The asterisk mark is the new peak.

At the achromatic focal plane (F2), a series of detectors and a secondary target were installed in a vacuum chamber. The setup consisted of two parallel-plate avalanche counters (PPAC's) [7], a cold helium gas target, and a silicon-detector stuck with thicknesses of 0.02, 0.07, 1.5 and 1.5 mm. The secondary beam was monitored with two PPAC's during the data taking. Particle identification was performed for each event on the basis of time of flight (TOF) between the two PPAC's. The purity of the ^{14}O beam was 85% at F2.

The cold helium gas target was bombarded by the ^{14}O beam. The He gas was confined in a 50-mm thick cell with two windows of 2.2-μm thick Havar foils. It was kept at a pressure of 0.6 atm and was cooled to 30 K. The effective thickness of ^{4}He was about 3.1 mg/cm^2. The target thickness was chosen as thin as possible, being thick enough to stop the ^{14}O nuclei in it. The reaction products emitted from the helium target were identified by the ΔE-E method, using a telescope of four silicon detectors located at 0°. The energy deposit in each detector was measured, where the energy calibration of each detector was carried out using proton beams produced through the CRIB facility.

3. Experimental Results and Discussion

The ^{4}He(^{14}O,p)^{17}F reaction was measured with a ^{14}O beam at an incident beam energy of 43 MeV on the helium gas target. The reaction cross sections were deduced from the energy spectrum of protons emitted from the target. Assuming the final state of ^{17}F is ground state, the cross sections were obtained in the energy region of $E_{\rm c.m.}(^{14}{\rm O}{+}\alpha) = 0.8$–$3.8$ MeV. The measured cross sections are presented in Fig. 2 as a function of the center-of-mass energy. Eight resonances are evident in the data which correspond to previously observed states in ^{18}Ne at 6.15, 6.29, 7.05, 7.12, 7.35, 7.62, 7.95 and 8.30 MeV [8,9]. The eight arrows with the labels of excitation energy in Fig. 2 indicate the location of these resonances. The rate for the breakout reactions is dominated by the resonance parameters for the 1^- state at 6.15 MeV at around the temperature $T_9 = 1$, while the contributions from the three higher-lying resonances at 7.05, 7.37 and 7.60 MeV start to dominate the reaction rate in the temperature range $T_9 \geq 3$ [10]. Compared with the previous experiments using time-reversed reaction, we observed these astrophysically important resonances with good statistics.

In addition, we newly observed a resonance at around 1.5 MeV of the ^{14}O-α center-of-mass energy, where no states in ^{18}Ne were expected. The ^{18}Ne states in the energy region have been investigated by nmeans of indirect method, however, no resonances between 6.15 and 7.05 MeV were reported. This resonance would be a transition to the excited state in ^{17}F. The first excited state of ^{17}F is located at excitation energy of 0.495 MeV from the ground state. The newly observed resonance was located at the excitation energy to be 0.5-MeV lower than the 7.10-MeV level. Thus one could understand it to be the ^{14}O$(\alpha,p)^{17}$F* reaction leading to the $1/2^+$ first-excited state in ^{17}F, which goes through resonances at 7.05 and 7.12 MeV.

4. Summary

The astrophysical ^{14}O$(\alpha,p)^{17}$F reaction, which is important in various hot and dense stellar environments, has been measured directly for the first time, by using a low-energy radioactive ^{14}O beam. We observed these astrophysically important resonances with better statistics, compared with the results of previous experiments using time-reversed reaction. Furthermore, we newly observed a decay from the ^{18}Ne levels at E_x = 7.05 and 7.12 MeV to the first-excited state in ^{17}F. These results would suggest an increase for ^{14}O$(\alpha,p)^{17}$F reaction rate and might affect the scenario of ignition phase of X-ray burst.

References

[1] R. K. Wallace and S. E. Woosley, Astrophys. J., Suppl. Ser. **45** (1981) 389.
[2] B. Harss *et al.*, Phys. Rev. Lett **82** (1999) 3964.
[3] J.C. Blackmon *et al.*, Nucl. Phys. A **688** (2001) 142.
[4] K. P. Artemov *et al.*, Sov. J. Nucl. Phys. **52** (1990) 408.
[5] S. Kubono *et al.*, Nucl. Phys. A **693** (2001) 221.
[6] Y. Yanagisawa *et al.*, RIKEN Accel. Prog. Rep. **34** (2001) 183.
[7] H. Kumagai *et al.*, Nucl. Instrum. Methods. A **470** (2001) 562.
[8] K.I. Hahn *et al.*, Phys. Rev. C **54** (1996) 1999.
[9] S. H. Park *et al.*, Phys. Rev. **C 59** (1999) 1182.
[10] B. Harss *et al.*, Phys. Rev. C **65** (2002) 035803.

Feasibility Study for Measurement of ^{8}Li(α, n)^{11}B Reaction Cross Section with Low-Energy ^{8}Li Beam at CRIB

M. Kurata-Nishimura, S. Nishimura, T. Teranishi[a], S. Kubono[a], M. Notani[a], J. He[a], S. Michimasa[a] and H. Baba[b]

RIKEN (The Institute of Physical and Chemical Research)
[a]*Center for Nuclear Study, Graduate School of Science, University of Tokyo*
[b]*Department of Physics, Rikkyo University*

1. Introduction

The standard big bang model [1, 2] is known to predict observed abundances of light elements up-to 7 amu with fairly good agreement, but to predict small abundances of heavier elements. In contrast to this model, the inhomogeneous big bang model (IM) has succeeded making reasonable accurate prediction of heavy element abundances [3, 4]. In the IM, a path ^{4}He$(t,\gamma)^7$Li(n,γ) ^{8}Li$(\alpha,n)^{11}$B$(n,\gamma)^{12}$B$(\beta,\nu)^{12}$C is considered to be a dominant flow path to explain the synthesis of ^{12}C and heavy elements in the very early universe. Recently, it has also been discovered by the full network calculation [5] that this path plays an important role in r-process nucleosynthesis occurring in supernova explosions. In both environments, it is claimed that the reaction cross section should be determined in a direct reaction with the center of mass energy less than 1 MeV. In that sequence, the ^{8}Li$(\alpha,n)^{11}$B is recognized as a particularly important reaction and the reaction cross section should be measured experimentally at the low-energy region below 1 MeV in the center of mass. Some previous experiments were conducted to determine this reaction cross section [6, 7, 8, 9]; however, the results of these experiments were not in qualitative agreement with each other. Moreover, measurements of the low-energy cross section below 1 MeV, which is the most important energy region, have not been conducted yet due to difficulty of detecting low-energy ions.

An in-flight low-energy radioisotope beam separator (CRIB) [10, 11, 12] constructed at CNS is suitable for studies of unstable nuclear structures and nuclear reactions for astrophysics. A thick degrader is, however, still needed to be inserted in the beam line to reduce the secondary beam energy down to 1 MeV/nucleon. Due to thick materials of the energy degrader, an energy straggling and beam profile degeneration will be a crucial problem for the measurement. In this article, we will report results of an experiment to develop a low-energy ^{8}Li beam in CRIB.

In addition, we propose an new experimental method for the measurement of ^{8}Li$(\alpha,n)^{11}$B cross section with less than 1 MeV in $E_{\rm c.m.}$ using a monolithic silicon telescope (MST) [13]. The feasibility study of this system is also reported.

2. ^{8}Li Beam Production Experiment

An unstable ^{8}Li beam was created by a reaction of ^{7}Li$(d,p)^8$Li. The primary beam of ^{7}Li^{2+} was accelerated to an energy of 3.14 MeV/nucleon by the RIKEN AVF cyclotron with the beam current of 100 pnA. The primary beam was focused at F0 where a deuteron gas target of 0.39 mg/cm^2 was located. A removable aluminum foil with a thickness of 40 μm was placed upstream of the gas target cell in order to reduce the beam energy. The produced ^{8}Li beams were separated from ^{7}Li in the D1 magnetic field, traveling to a momentum-dispersive focal plane (F1). The ions passing through a F1 slit were transported to the second focal plane (F2) where two delayed-line PPACs and SSD were installed to identify ions and to measure the energy spread and beam profile. Mylar foil degraders with thickness of 0, 10, 29 and 50 μm were changed by a stepping motor in front of the PPACs. For the purpose of estimating the neutron background level, four liquid scintillation counters were prepared; three were placed near the F2 chamber and the other was placed 6 m downstream from the F2 chamber.

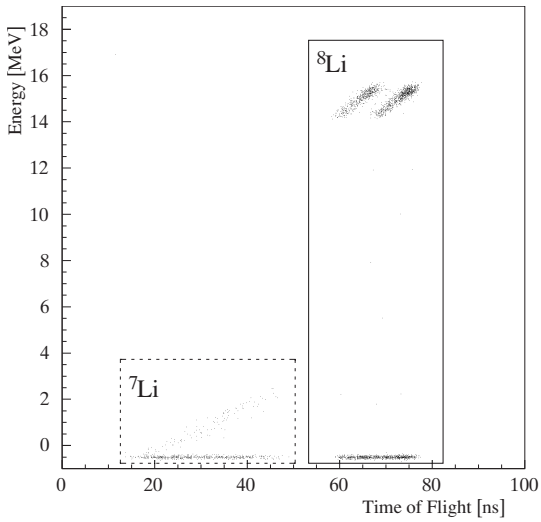

Figure 1. Particle identification of ^{8}Li. Horizontal axis and vertical axis indicate time of flight between two PPACs and the energy deposit in the SSD, respectively. Two clusters in the ^{8}Li region are known to be caused by the problem of double timing triggers. Some ions shows zero energy deposit on SSD due the relatively small acceptance of SSD.

The particle identification without any degrader is shown in Fig. 1. The ^{8}Li ions are clearly separated from ^{7}Li ions. The maximum ^{8}Li beam intensity of 5.1 $\times$ 10^5 counts per second (cps) was obtained for a 100 pnA ^{7}Li beam. The contamination of low energy ^{7}Li was removed completely by the energy degrader placed in the F2 chamber. At the ^{8}Li

energy of 1.57 MeV corresponding to 0.52 MeV in $E_{\mathrm{c.m.}}$ for the ^{8}Li$(\alpha, n)^{11}$B reaction, the ^{8}Li beam purity of 99.5% and the intensity of 4×10^{4} cps is obtained. The energy straggling and beam profile could be improved by adapting a degrader at F1 and adjusting the slit size at F1 and F2. The beam property for each energy degrader configuration is summarized in the reference [14].

3. Detector Study with Simulation

We have performed a feasibility study of the MST for the measurement of ^{8}Li$(\alpha, n)^{11}$B reaction cross section using GEANT4 simulation code [15]. We adopt an experimental approach to detect ^{8}Li as well as ^{11}B with precise particle identification. The ^{11}B identification is necessary to reduce a systematic error caused by a contamination of ^{8}Li scattered elastically. An ordinary means of identifying low-energy ions is the ΔE-E method. A ΔE detector, however, must be as thin as possible so as not to stop ions in this detector. A gas detector is conventionally used for such a thin detector. Recently, the MST has been developed in collaboration between STMicroelectronics and INFN(the Italian institute for nuclear physics). This detector consists of 1 μm pad SSD and 508 μm thick SSD. Signals from the first and second layers could be used to measure ΔE and a total energy deposit, respectively. Such a thin SSD has been produced only recently.

In the GEANT4 simulation code, a gas target is filled with helium gas at a pressure of 100 Torr, at 3 cm in length. The 8 MSTs are placed at the end cap of the gas target. A ^{8}Li beam with an energy of 0.2 MeV/nucleon reacts with helium nuclei along the beam axis and ^{11}B is emitted.

The result of this simulation is shown in Fig. 2. In the upper part of the figure, the ^{11}B detected by the MST is shown. In the GEANT4 simulation code, the same amount of ^{11}B in the ground state and from the first, second and third excited states are generated. ^{11}B in the ground and the first excited states are clearly separated, while those in the second and third excited states are impossible to be distinguished. At the same time, elastic scattering is also simulated in the code as is seen in the lower part of the figure. The ^{8}Li and α nuclei are also clearly identified in this plot. This simulation result indicates that MST is can be used in inclusive measurement in a low-energy reaction.

4. Detector Study with an Alpha Source

The performance of the MST has been experimentally studied using a calibration alpha source. Signals from both layers were amplified using AMPTEK 250 placed in a vacuum chamber. These signals were re-shaped by a shaping amplifier of Seiko-EG&G 671. A trigger for data taking was generated by a signal from the second pad. A scatter plot of energy deposits in two layers are shown in Fig. 3. Three clusters corresponding to alphas from ^{237}Np, ^{241}Am and ^{244}Cm are identified clearly. The excellent energy resolutions was obtained for the first and the second pad of about 26 keV and 46 keV in FWHM, respectively.

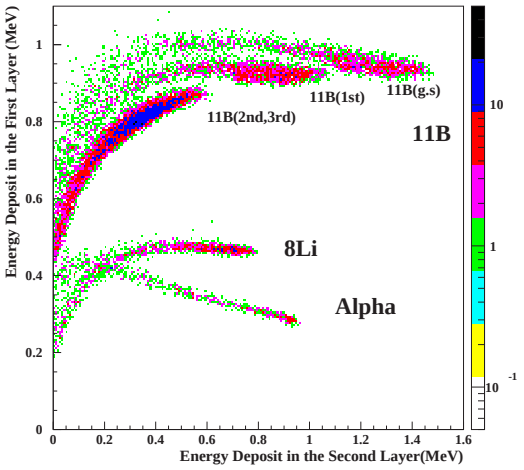

Figure 2. ΔE and E detected by monolithic silicon telescope simulated for ^{8}Li$(\alpha, n)^{11}$B reaction

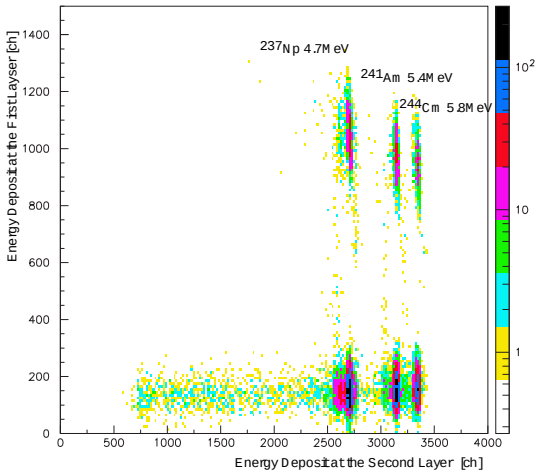

Figure 3. The scatter plot of energy deposits at two layers. The calibration alpha source is used.

5. Summary

We have succeeded in producing ^{8}Li beam at CRIB for the first time. The results show that the purity and intensity of this beam satisfy our requirements. We proposed a new method using the MST for the determination of ^{8}Li$(\alpha, n)^{11}$B cross section at the low-energy. It is concluded that the MST effectively work even at 0.5 MeV in $E_{\mathrm{c.m.}}$, according to the results of the GEANT4 simulation and the alpha source calibration.

References

[1] R.V. Wagoner *et al.*, Astro. J. **148** (1967) 3.
[2] D.N. Schramm *et al.*, Ann. Rev. Nucl. Part. Sci. **27** (1977) 37.
[3] M. J. Balbes *et al.*, Phys. Rev. Lett. **71** (1994) 3931.
[4] N. Hata *et al.*, Phys. Rev. Lett. **75** (1995) 3977.
[5] M. Terasawa *et al.*, Astro. J. **562** (2001) 470.
[6] X. Gu *et al.*, Phys. Lett. B **343** (1995) 31.
[7] R. N. Boyd *et al.*, Phys. Rev. Lett. **68** (1992) 1283.

[8] Y. Mizoi *et al.*, Phys. Rev. C **6206** (2000) 5801.
[9] S. Cherubini *et al.*, Eur. Phys. J. A **20** (2004) 355.
[10]S. Kubono *et al.*, Eur. Phys. J. A **13** (2002) 217.
[11]T. Teranishi *et al.*, CNS-REP-39 (2001).
[12]S. Watanabe *et al.*, CNS-REP-48 (2002).
[13]A. Musumarra *et al.*, Nucl. Instrum. Methods. A **409** (1998) 414.
[14]M. K-Nishimura *et al.*, RIKEN Accel. Prog. Rep. **36** (2003), in press.
[15]Geant4 collaborations (http://geant4.web.cern.ch).

Experimental Nuclear Physics: PHENIX Experiment at RHIC-BNL

Progress of the PHENIX Experiment in the Year 2003

H. Hamagaki, K. Ozawa, T. Sakaguchi, M. Inuzuka, T. Matsumoto, S. Kametani, F. Kajihara, T. Gunji, T. Isobe, N. Kurihara, S. Oda, J. Kikuchi[a], Y. Yamaguchi[a] and Y. Tanaka[b], for the PHENIX Collaboration

Center for Nuclear Study, Graduate School of Science, University of Tokyo
[a] Advanced Research Institute for Science and Engineering, Waseda University
[b] Nagasaki Institute of Advanced Science

1. Introduction

Since the first successful collisions between ultra-relativistic Au ions in June 2000, Relativistic Heavy Ion Collider (RHIC) of Brookhaven National Laboratory, USA, has been the central place for the study of hot QCD matter.

The CNS group has been participating in the PHENIX experiment, which is one of the major experiments at RHIC. The goal of the PHENIX experiment is to find evidence of the QCD phase transition from normal nuclear matter to deconfined quark matter, called quark-gluon plasma (QGP), and to study the properties of the hot QCD matter.

A schematic view of the the PHENIX experimental setup is shown in Fig. 1. It consists of two central arms (East and West), two muon arms (North and South) and inner detectors for enent trigger and event characterization. The PHENIX has a very unique capability of being able to measure photons, electrons and muons as well as hadrons. With this capability, the PHENIX experiment aims to address as many signatures as possible for QGP formation.

In this article, progress of the PHENIX experiment and the activities of the CNS group in the Japanese fiscal year (JFY) 2003 are briefly summarized.

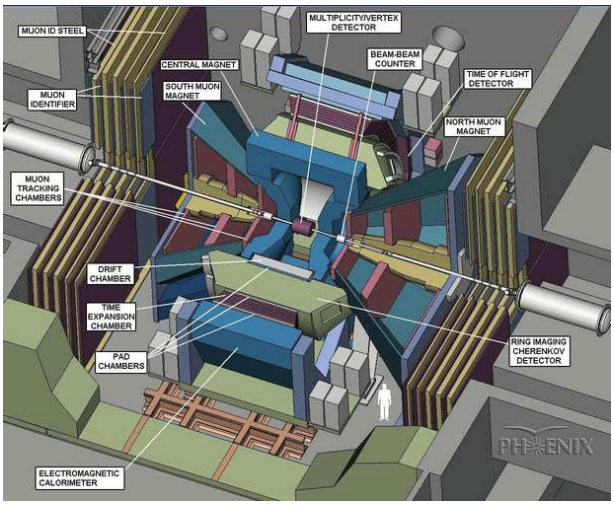

Figure 1. Layout of the PHENIX experiment.

2. Year-4 RUN at RHIC

In the JFY 2003, the fourth physics run, RHIC Year-4 RUN, was performed, where mainly Au + Au collisions at $\sqrt{s_{NN}} = 200$ GeV were employed. The experimental run began in the beginning of January 2004, and ended in the end of March. In total, ~ 1.6 billion of min-biased Au + Au collisions events were accumulated, which is about 30 times larger than those from the Year-2 run.

After Au + Au run at $\sqrt{s_{NN}} = 200$ GeV, a short Au + Au run at lower energy, $\sqrt{s_{NN}} = 63$ GeV, was performed. After these successful runs, beam study of polarized protons were performed for several weeks, and the RHIC Year-4 run was completed in May 14, 2004.

3. Activities of the CNS group

There were several distinct activities in the CNS group in the JFY 2003. Only brief introduction is provided in this article, and detailed descriptions will be provided in the following separate articles.

3.1. RICH operation

The RICH (Ring Imaging CHerenkov) subsystem is a main device for electron identification. The CNS group has been responsible for its maintenance, operation and calibration. The RICH subsystem worked without serious problems throughout the Year-4 run.

3.2. Development of AEROGEL Cherenkov Counter

PHENIX has been unique to have capability of identifying charged hadrons in a wide momentum region, with the high-resolution TOF and RICH. With increase of interest to the hadron production in the medium to high momentum region, extension of particle identification (PID) was planned. Idea was to install AEROGEL Cherenkov counter with refractive index $n \sim 1.01$. PID capability of identifying π, K and p up to ~ 7 GeV/c can be achieved, when operated together with TOF and RICH.

The AEROGEL project was carried out by the collaboration of Tsukuba, BNL, Russia and CNS. The CNS group took responsibility of constructing readout electronics.

The first half of the AEROGEL counters were installed in the West central arm before the Year-4 run, and was successfully commissioned during the run. The rest will be assembled and installed in the summer of 2004. Performance of the AEROGEL counter is described in Ref. [1].

3.3. Data analysis and results

Eleven physics papers as well as a set of PHENIX detector papers were published from the PHENIX collaboration in JFY 2003, as listed in the publication list of this annual report.

Major efforts of the CNS group has been on the physics with photons and leptons, and various achievements were made as described below.

Single photon is considered to be a sensitive probe on

the early hot stage of the collisions, and efforts have been continued to deduce single photon yield from the EMCAL data. The PHENIX succeeded in measuring direct photons from hard process in Au + Au collisions, as described in Ref. [2]. This is the first observation in high-energy heavy-ion collisions.

Investigation on single electron production in d + Au collisions has been initiated. Majority of single electrons comes from 'photonic' background sources, such as Dalitz decay of neutral mesons and external conversion of photons. Leptonic decay of charm and bottom mesons are currently considered to be the main 'non-photonic' sources, which are obtained after subtracting major 'photonic' sources. Charm and bottom quarks are considered to be a good reference probe of hard processes. The first step of the investigation is to study performance of 1st-level electron trigger, used for measuring electrons in d + Au collisions [3]. Current status of single electron measurements is presented in Ref. [4].

The J/ψ production has been thought to be a key probe of QGP formation. Suppression of J/ψ yield has been considered to be a direct evidence of deconfinement, and possible enhancement of the yield is proposed by theorists which is due to coalescence production of J/ψ from charm and anti-charm quarks in QGP phase or in the hadronization stage. The CNS group has been taking leading roles in the analysis of J/ψ productions. The yield in Au + Au collisions has been investigated for the Year-2 run [5], and recently for the Year-4 run [6]. The J/ψ production in d + Au collisions from the Year-3 run is also under way, whose result should serve as a reference to the heavy ion collisions [7].

3.4. R & D efforts for PHENIX upgrade

R & D efforts have been made to develop detectors which enhance capability of electron measurements at PHENIX. Focus is on the detectors which sits inside the current tracking system, and identifies and rejects effectively electron-pairs from π^0 Dalitz decay and external conversion of photons over large solid angle [8]. Huge combinatorial background of these sources makes it impossible to have clean signals from light-mass vector mesons for study of Chiral symmetry restoration.

HBD (Hadron Blind Detector), which is the gaseous Cherenkov counter with a UV-photon detector, is the most promising yet ambitious detector for such purpose. A key R & D issue of HBD is how to make insensitive to charged particles, while keeping good efficiency for UV photons. Development of new detectors is thought to be indispensable. A candidate is GEM (Gas Electron Multiplier), which have drawn strong attention because of its structural simplicity and expected high performance. GEM may have a wide variety of applications, and basic performance study have been performed. Development of GEM is under way, and current status is described in Ref. [9].

Another candidate is the micro-TPC (Time Projection Chamber) which uses CF4 gas. CF4 is chosen as a candidate because of small diffusion and high drift velocity. A conventional TPC with an anode wire plane and cathode readout pads was constructed firstly, and performance was studied [10]. Last year, TPC with GEM chamber readout was devised, and performance study is in progress [11].

3.5. R & D of ALICE TRD

The CNS group has being involved in the R & D effort for the development of TRD (transition radiation detector) in the ALICE experiment at CERN-LHC, which is planned to start operation in 2007. The TRD, when installed, will provide unique capability of electron identification to the ALICE experiment.

The CNS group participated in the test of TRD prototypes using secondary beams from CERN-PS in the fall of 2002. A new analysis method based on neural network was developed for identifying electrons, and TRD performance was studied [12].

4. Summary and Outlook

In the year 2003, the PHENIX experiment had an extremely fruitful Year-4 run with Au + Au collisions at $\sqrt{s_{NN}} = 200$ GeV and $\sqrt{s_{NN}} = 63$ GeV.

The major activities of the CNS groups are presented, which includes development of AEROGEL, data analysis efforts, R & D efforts for PHENIX upgrade and for ALICE TRD.

The Year-5 RUN is planned to start in the fall of 2004, and various plans are currently under consideration.

References

[1] N. Kurihara *et al.*, CNS Annual Report 2003 (2004) 61.
[2] T. Sakaguchi *et al.*, CNS Annual Report 2003 (2004) 53.
[3] F. Kajihara *et al.*, CNS Annual Report 2003 (2004) 49.
[4] F. Kajihara *et al.*, CNS Annual Report 2003 (2004) 51.
[5] T. Matsumoto *et al.*, CNS Annual Report 2003 (2004) 57.
[6] T. Gunji *et al.*, CNS Annual Report 2003 (2004) 59.
[7] S. Kametani *et al.*, CNS Annual Report 2003 (2004) 55.
[8] K. Ozawa *et al.*, CNS Annual Report 2003 (2004) 47.
[9] M. Inuzuka *et al.*, CNS Annual Report 2003 (2004) 67.
[10] T. Isobe *et al.*, CNS Annual Report 2003 (2004) 63.
[11] S. Oda *et al.*, CNS Annual Report 2003 (2004) 69.
[12] T. Gunji *et al.*, CNS Annual Report 2003 (2004) 65.

Next Steps of the PHENIX Experiment

K. Ozawa, H. Hamagaki, M. Inuzuka, C.L. Woody[a], C. Aidala[b] and I. Tserruya[c]

Center for Nuclear Study, Graduate School of Science, University of Tokyo
[a]*Brookhaven National Laboratory, N.Y., U.S.A.*
[b]*Columbia University, N.Y., U.S.A.*
[c]*Weizmann Institute, Rehovot, Israel*

1. Introduction

Since the first Au+Au collisions were observed at the Relativistic Heavy Ion Collider (RHIC) in the Brookhaven National Laboratory (BNL), many new phenomena of hot and dense nuclear matter are discovered. Especially the PHENIX experiment produces many results for a very comprehensive physics subjects, including charged and neutral hadron production, single electron production, jet quenching, event isotropy, and so forth [1].

In spite of these fruitful results in the first three years of the RHIC operation, there are still remaining physics questions to be answered to further characterize the state of matter formed at RHIC. In particular, direct information for deconfinement of quarks and gluons and chiral properties of the matter should be provided by the study of penetrating probes. Penetrating probes here contain hard probes and electro-magnetic probes. Hard probes are created at the very early stage of the collisions which propagate through the medium. The main observable are high transverse momentum particles [2] and open and hidden charm (J/ψ) production [3]. Electro-magnetic probes are created by the medium and leave the medium without final state interaction. Thus, they can carry direct information about conditions and properties of the medium. The main observable are low-mass e^+e^- pairs and the thermal radiation of the medium [4]. The PHENIX experiment is specifically designed to address these probes with current and upgraded capabilities.

Measurements of J/ψ production and identified particle spectra in the high transverse momentum region will be done using the improved statistics in run 2003. To extend the capability of the particle identification in the high transverse momentum region, an Aerogel counter is installed in 2003.

Some measurements are beyond the scope of the present PHENIX detector. To extend the capability of the measurement of lepton pairs and open charms, upgrade projects of the detector are underway.

2. Charm Production

Open charm production is an interesting subject to investigate production mechanism itself and nuclear shadowing effect. Moreover, charm enhancement might be expected, since charm can be produced thermally in hot and dense matter.

For tagging of decays of charm mesons, the precise determination of displaced vertex points of charm decays is needed. The vertex determination with high precision is realized with silicon detectors with large acceptance. The vertex resolution is estimated to be less than 50 μm and the acceptance of the detector is $\Delta\phi = 2\pi$ and $\Delta\eta = \pm 1$. A detector system which consists of silicon strip detectors and two inner layers of pixel detector is being proposed.

3. Low-mass Dileptons

The measurements of lepton pairs is a key measurement in the study of chiral symmetry restoration. The difficulty of this measurement is from the large combinatorial background which is mainly caused by π^0 Dalitz decays and external conversions of photons.

The calculated invariant mass spectrum of electron-positron pairs is shown in Fig. 1. In this figure, invariant

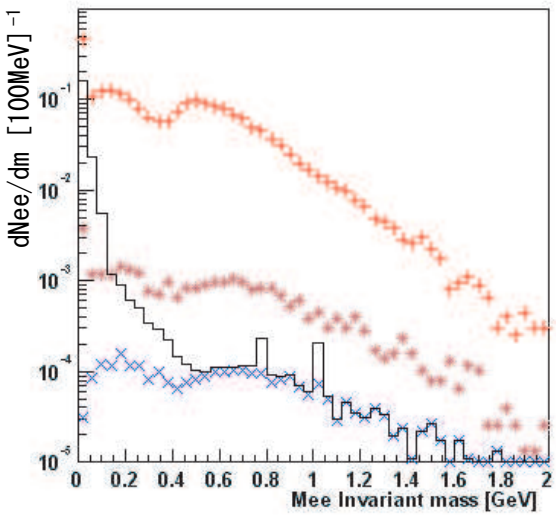

Figure 1. Invariant mass spectrum of electron-positron pairs is shown. The solid line represents the summation of all correlated signals. Plus symbols represent the all combinatorial background, which include gamma conversions, charm decays, and meson decays. Star symbols represent the combinatorial background which comes from charm decays. Cross symbols represent the correlated charm signals.

mass is calculated with all combination all opposite sign electrons in one event. Electrons from Dalitz decays of π^0, η, and $\eta\prime$, decays of vector mesons and open charm decays, gamma conversion, and miss-identified π's are took account into the calculation. In Fig. 1, the solid line represents the summation of all correlated signals. It means this

line will appear after the subtraction of the combinatorial background. Plus symbols represent the all combinatorial background. After applying Dalitz rejection, background is suppressed by two order of magnitude. The remaining background is the combinatorial background from charm decays. It is represented by the star symbols in Fig. 1.

The Dalitz rejector is composed of two essential elements; zero magnetic field, and electron identification. Electron positron pairs from Dalitz decays and gamma conversion has a very small angle. Thus, these pairs produce very close hits in the electron identification detector under zero field condition. The zero magnetic field is realized by adding the second coil, which is installed in 2002.

There are two ideas to realize electron identification near the vertex region. One idea is to use a hadron blind detector (HBD), which is a threshold-type Čerenkov counter using CF_4 gas as a radiator [5]. Another idea is dE/dx measurements by using Time Projection Chamber (TPC). The details of TPC will be described in the another manuscript in this report [6].

The conceptual design of HBD is shown in Fig. 2. The

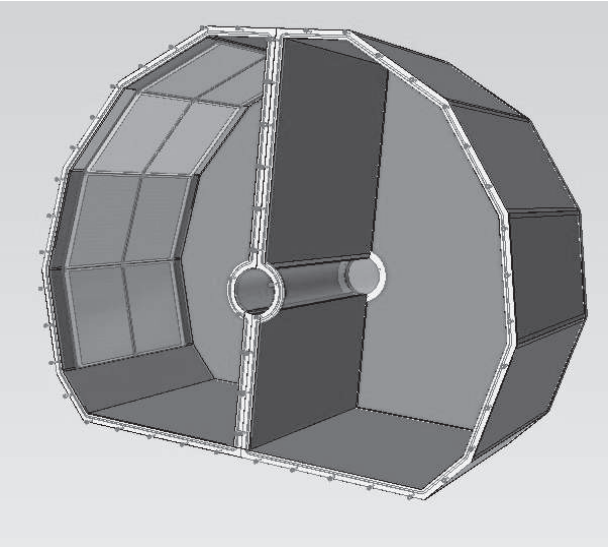

Figure 2. Conceptual design of hadron blind detector

detector, operated in pure CF_4, consists of a 50 cm long radiator directly coupled, in a windowless configuration, to a triple GEM detector which has CsI photo cathode evaporated on the top face of the first GEM foils and pad read out at the bottom of the GEM stack [7]. Eight pieces of GEM stacks are shown in Fig. 2.

The R&D phase to demonstrate the validity of the concept is nearing completion. The final test of the detector prototype is performed at KEK using electron and charged π meson beam. The very preliminary result of tests shows that electron produces about 20 photo-electrons with the prototype. The detector construction will start soon and the detector will be installed before run 2006.

4. Summary

The PHENIX data set from RHIC Runs from 2000 to 2002 provides an extensive set of measurement to understand properties of hot and dense matters. In spite of these results, much remains to be done to further characterize the state of matter formed at RHIC. Study of the collisions using hard probes and electro-magnetic probes is important. Among these probes, measurements of (J/ψ) production and identified particle spectra in the high transverse momentum region will be done using the improved statistics in run 2003.

The upgrade aims of the PHENIX experiment address prime physics questions beyond the scope of the present PHENIX detector. To measure open charm production, vertex silicon detector is proposed. To measure low-mass electron-positron pairs for the study of the chiral symmetry, large combinatorial background from π^0 Dalitz decays and external conversions of photons cause a problem. As a Dalitz rejector, Hadron Blind Detector (HBD) and Time Projection Chamber (TPC) are proposed. After applying the Dalitz rejection, the background is suppressed by two orders of magnitude. The R&D phase to demonstrate the validity of the HBD concept is nearing completion. The HBD construction will start soon and the detector will be installed before run 2006.

References

[1] H. Hamagaki *et al.*, CNS Annual Report 2003 (2004) 45.
[2] N. Kurihara *et al.*, CNS Annual Report 2003 (2004) 61.
[3] T. Gunji *et al.*, CNS Annual Report 2003 (2004) 59.
[4] T. Sakaguchi *et al.*, CNS Annual Report 2003 (2004) 53.
[5] Z. Fraenkel, *et al.*, Proposal for a Hadron Blind detector for PHENIX, PHENIX Technical Note 391 (2001).
[6] T. Isobe, *et al.*, CNS Annual Report 2003 (2004) 63.
[7] A. Kozlof, *et al.*, Nucl. Instrum. Methods. A **523** (2004) 345.

Electron Trigger Performance in the PHENIX Run3 Experiment

F. Kajihara, F. Bauer[a], T. Gunji, H. Hamagaki, M. Inuzuka, T. Isobe, S. Kametani, K. Kato[b], N. Kurihara, T. Matsumoto[c], K. Okada[d], K. Ozawa, T. Sakaguchi and X. Wei[a,d], for the PHENIX Collaboration

Center for Nuclear Study, Graduate School of Science, University of Tokyo
[a]*University of California, Riverside*
[b]*Advanced Research Institute for Science and Engineering, Waseda University*
[c]*Nagasaki Institute of Applied Science*
[d]*RIKEN, BNL Research Center, Brookhaven National Laboratory*

1. Introduction

The PHENIX is a unique experiment that can identify individual electrons (the word "electron" represents both of e^+ and e^- in this report) produced in the gold-gold (Au-Au), deuteron-gold (d-Au) and (polarized) proton-proton (p-p) collisions which are provided by the Relativistic Heavy Ion Collider (RHIC) in the Brookhaven National Laboratory (BNL), U.S.A. The measurement of electrons from leptonic decay of heavy flavor quarks (charm and bottom), thermal di-electrons, and electron pairs from decays of light vector mesons are very powerful tools to investigate the properties of hot and dense matter, and to verify the realization of the Quark Gluon Plasma (QGP) in the RHIC-PHENIX Au-Au experiment. Their measurements in p-p and d-Au collisions are crucial to understand the basic production mechanism and nuclear effects. In the polarized p-p experiment, the measurement of electrons from heavy flavored particles is expected to provide the polarized gluon distribution function for the elucidation of spin structure of nucleons.

For the above measurements, the special trigger has been developed in the PHENIX experiment. The Ring-Imaging Čerenkov counter (RICH) and Electro-Magnetic Calorimeter (EMC) are the main devices for electron identification [1] and were used to construct the EMC-RICH Trigger (ERT). The requirement of trigger performance is summarized in Ref. [2]. CNS group has developed the RICH part of the trigger system since 1998. This report presents the performance of the ERT electron trigger in d-Au and p-p collisions at the RHIC Year-3 run (Run3), which were performed from January to May in 2003.

2. The EMC-RICH Trigger (ERT) System

The ERT performs a coincidence between trigger information of the EMC and RICH, which is produced in each Front End Module (FEM) of them. The EMC FEM is capable to trigger an electron when the measured deposit energy is over a threshold in each trigger tile. The non-overlapping tile consists of 36 units of 2×2 = 4 Photomultipliers (PMT) (the trigger tile is called a "super-module", and the unit of 2×2 PMTs is called a "tower" in the PHENIX). The FEM collects signals from a super-module and has six daughter cards (ASIC cards) which hold six MONDO chips [7]. The chip performs energy summation for 4 PMTs of a tower. The total number of super-modules is 172 at present. The programmable threshold can be set at 63 different value (DAC) for each tile separately. If the trigger tile produces noisy signal and the trigger rejection factor becomes low, it is possible to mask off the tile. The RICH FEM is capable to trigger an electron when the measured number of photoelectrons from the Čerenkov ring is over a threshold in each trigger tile. The RICH has 5120 PMTs which form non-overlapping 256 trigger tiles (4×5 = 20 PMTs). The RICH part is described in Refs. [3, 4, 5, 6]. The electron trigger is constructed by requiring geometrical coincidences between the EMC and RICH tiles so as to confirm that the tracks penetrate through the same geometrical region.

3. The ERT Operation Status in the Run3

During the Run3, some noisy trigger tiles were found for both of RICH 4×5 and EMC 2×2 by on-line monitoring. They were all masked (RICH; 11.7 %, EMC; 5.20% of each total). The trigger tile status in Run3 is summarized in Ref. [6]. Table 1 gives an overview of the EMC and RICH thresholds used during d-Au and p-p runs. The EMC 2×2 DAC was set to 24 (∼400 MeV), 29 (∼600 MeV) and 34 (∼800 MeV). RICH 4×5 ADC was set to 920 (∼ 3.0 photoelectrons).

Run Number	EMC2×2	RICH4×5
66304 (d-Au)	34(34)	920
67219 (d-Au)	29(29)	920
78312 (d-Au)	34(34)	920
86768 (p-p)	34(34)	920
87618 (p-p)	24(24)	920
89463 (p-p)	34(34)	920

Table 1. The EMC and RICH trigger thresholds in Run3 d-Au and p-p experiment. The DAC for the PbSc (PbGl) and the ADC for RICH threshold are shown.

Two types of triggers were used for electron trigger in the Run3. The first one is named "ERT_Electron&BBCLL1" trigger in which ERT is combined with the PHENIX Minimum Bias (MB) trigger. The MB trigger is constructed by the PHENIX Beam-Beam Counter (BBC) [1]. The second one is called the "ERT_Electron" trigger without the MB trigger coincidence. Table 2 shows the total number of events which were recorded by each trigger in the Run3.

Trigger Name	Run3 d-Au	Run3 p-p
BBCLL1	110,874,637	41,282,805
ERT_Electron&BBCLL1	67,789,443	16,338,345
ERT_Electron	Disabled	16,443,788

Table 2. The number of recorded trigger events in the Run3 d-Au and p-p experiment.

4. The PHENIX Electron Trigger Performance

There are two factors which characterize trigger performances; the rejection factor and trigger efficiency of electrons. The rejection factor is given by the MB raw trigger rate divided by the raw electron trigger rate. Figure 1 shows the run dependence of rejection factor on the ERT_Electron&BBCLL1 in d-Au runs and Figure 2 shows it on the ERT_Electron trigger in p-p runs. Tables 3 and 4

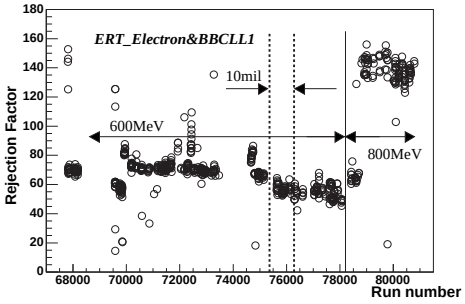

Figure 1. The run dependence of rejection factor in d-Au runs. Only ERT_Electron&BBCLL1 trigger (circle) was used. A 0.25 mm thick photon converter was installed for the indicated runs.

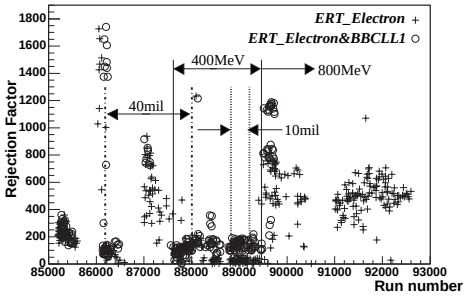

Figure 2. The run dependence of rejection factor in p-p runs. The ERT_Electron&BBCLL1 (circle) and ERT_Electron (squire) trigger were used. 0.25 and 1.00 mm photon converters were installed for the indicated runs.

show the average of rejection factors. The simulation study estimates the ideal rejection factor is $\sim$700 at the EMC 800 MeV threshold in p-p runs. The actual value got smaller because of appearance of noisy trigger tiles. According to the simulation study [8], the rejection factor is considerably sensitive to changing of the trigger thresholds, especially, the EMC deposit energy threshold. In the Run3, brass photon converters were installed around the Multiplicity Vertex Detector (MVD) [1] (a 0.254 mm thick converter of 1.70% radiation length was installed in d-Au runs. 0.254 mm and 1.00 mm thick converters were installed in p-p runs). Figures 1 and 2 show that the effect of conversion electron enhancement is much smaller than tuning of the EMC threshold. It agrees with the simulation result.

The trigger efficiency is defined by the number of triggered events divided by the number of MB events including electrons. Figure 3 shows the example for the ERT_Electron&BBCLL1 trigger in a particular region (East Sector 2, one-eighth of the PHENIX central detector's acceptance). Each data point in the figure is fitted with the integrated Gaussian function multiplied by a factor which is determined by the fit. The factor can be regarded as the flat efficiency in the high P_T region (> 1.8 GeV/c). The errors indicated by bars are statistical only. Table 3 includes the factor's average of all the eight sectors at each EMC threshold in d-Au runs. Table 4 shows it for the ERT_Electron trigger in the case of p-p runs. It is found by the off-line analysis that the main source of loss of these efficiencies is attributed to appearance of noisy trigger tiles of the RICH or EMC.

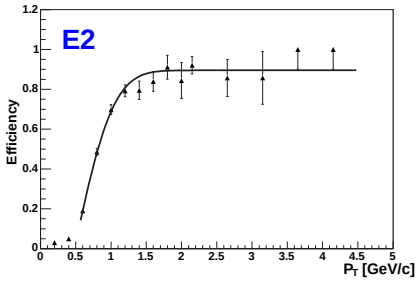

Figure 3. The example of P_T distribution of the ERT_Electron&BBCLL1 trigger efficiency in d-Au runs with the EMC 600 MeV threshold (at the East Sector 2).

Run Type (EMC Threshold)	Rejection	Efficiency
Run3 d-Au (600 MeV)	64.48	73.5 %
Run3 d-Au (800 MeV)	148.1	76.4 %

Table 3. The rejection factor and flat efficiency of the ERT_Electron&BBCLL1 trigger in d-Au runs.

Run Type (EMC Threshold)	Rejection	Efficiency
Run3 p-p (400 MeV)	66.20	73.1 %
Run3 p-p (800 MeV)	504.1	78.5 %

Table 4. The rejection factor and flat efficiency of the ERT_Electron trigger in p-$p$runs.

References

[1] K. Adcox et AL., Nucl. Instrum. Methods. A **499** (2003) 469.

[2] T. Matsumoto *et al.*, CNS Annual Report 1999 (2000) 23.

[3] T. Matsumoto *et al.*, CNS Annual Report 2000 (2001) 43.

[4] M. Tamai *et al.*, CNS Annual Report 2000 (2001) 45.

[5] F. Kajihara *et al.*, CNS Annual Report 2001 (2002) 37.

[6] F. Kajihara *et al.*, CNS Annual Report 2002 (2003) 41.

[7] http://www.ornl.gov/sci/engineering_science_technology/msd/Personal/cbritton/clb_papers/S30.pdf

[8] https://www.phenix.bnl.gov/WWW/p/draft/xiewei/EMCal-RICH-Trigger/dAu/eff_ana.html

Single Electron Measurement in the PHENIX Run3 d+Au Experiment

F. Kajihara, Y. Akiba[a], F. Bauer[b], T. Gunji, H. Hamagaki, M. Inuzuka, T. Isobe, S. Kametani, K. Kato[c], N. Kurihara, T. Matsumoto[d], K. Okada[e], K. Ozawa, T. Sakaguchi, T. Tabaru[a], M. Togawa[f] and X. Wei[b,e], for the PHENIX Collaboration

Center for Nuclear Study, Graduate School of Science, University of Tokyo
[a]*RIKEN (The Institute of Physical and Chemical Research)*
[b]*University of California, Riverside*
[c]*Advanced Research Institute for Science and Engineering, Waseda University*
[d]*Nagasaki Institute of Applied Science*
[e]*RIKEN, BNL Research Center, Brookhaven National Laboratory*
[f]*Kyoto University*

1. Introduction

Heavy flavor quarks (charm or bottom) are notable probes to investigate the mechanism and characteristics of deconfined quark-gluon system in extremely hot and dense matter, created by the relativistic heavy ion collisions. Their production yields will provide better understanding of the initial gluon density. The charm and bottom are mainly produced through gluon-gluon fusion in the initial stage of the heavy ion collisions, therefore the yields are sensitive to such a gluon density. Recently, strong modification of high p_T light quark meson was observed [1]. Energy loss of heavy flavor quarks, which propagate through hot and dense medium, is also predicted and the measurement will extend our knowledge of energy loss dependence on flavors. Besides, especially charm measurements provide an important base of J/ψ measurement.

The heavy quark production can be determined from measurement of single leptons which are produced via the semi-leptonic decay of charm or bottom mesons. So far, single electrons were measured in the PHENIX experiment for $\sqrt{s_{NN}} = 200$ GeV Au-Au collisions with the Relativistic Heavy Ion Collider (RHIC) in the Brookhaven National Laboratory (BNL), U.S.A. [2] (In this report, the word "electron" expresses both of e^+ and e^-, *e.g.*, the number is always counted as $\frac{N(e^-)+N(e^+)}{2}$). Not only heavy ion collisions, but also basic p-p and p-A collisions are needed to study the modification due to nuclear matter effects. The RHIC can provide very high luminosity in proton-proton (p-p) and deuteron-nucleus (d-A) collisions. The RHIC-PHENIX has performed the d-Au experiment at $\sqrt{s_{NN}} = 200$ GeV since Jan. to Mar. in 2003 (the period is called Year-3 or Run3) and collected $2.73\ \mathrm{nb}^{-1}$ integrated luminosity. This report provides the current status of single electron measurement and analysis in the d-Au collisions.

2. Electron Measurement in the PHENIX

In the PHENIX, electron measurement is performed by two central arm spectrometers. Each arm is composed of subsystems; the Drift Chamber (DC), the Pad Chamber (PC), the Ring-Imaging Čerenkov counter (RICH) and the Electro-Magnetic Calorimeter (EMCal), and covers $|\eta| < 0.35$ and $\pi/2$ in azimuth (ϕ). The PHENIX Minimum Bias (MB) trigger information is produced with two Beam-Beam Counters (BBC) which are placed at ± 145 cm from the center of the PHENIX along beam axis (z) (acceptance: $3.1 < |\eta| < 4.0$ and 2π in azimuth). The BBC provides measurement of centrality and vertex position, too. The DC measures charged particles trajectories in $r-\phi$ direction to determine p_T of the particles. The PC provides 3-D spatial point measurement for tracking charged particles and longitudinal momentum reconstruction in combination with the DC hit information. The RICH is a threshold gas Čerenkov detector and detects the Čerenkov light which only electrons produce in its CO_2 radiator (1 atm) below 4.9 GeV/c (Čerenkov threshold momentum of pion). The EMCal is composed of lead scintillator calorimeter and lead glass Čerenkov calorimeter, and measures the deposited energy and spacial position of the electromagnetic shower. Information obtained from the RICH and EMCal are used for electron identification (eID) in the off-line analysis. They also compose the PHENIX electron event trigger system, the EMCal-RICH Trigger (ERT) which is described in Refs [3, 4, 5, 6, 7]. The trigger efficiency was about 70 % in Run3 d-Au experiment [8]. The hit information of each ERT unit tile is also utilized to provide a tag for eID in the off-line analysis.

Figure 1. The brass photon converter which was installed in Run3 d-Au experiment (1.7 % radiation length).

3. Converter Subtraction Method

To extract inclusive yield for single electrons, the so-called "converter subtraction" method described below is applied. At first, the detected electrons are categorized into two groups in this method. The first component is named "photonic electrons" whose productions have a relation

with photons. The electrons derived from (1) Dalitz decay of π^0, η, η', ω and ϕ, and (2) photon conversions. They are considered to be main background. The second one is called "non-photonic electrons". The decays of charm and bottom quarks are dominant source of the non-photonic component, with small background from (3) kaon decays (K_{e3}), (4) di-electron decays of light vector mesons, and (5) thermal di-leptons.

The basic idea of this method is that the yield of photonic component will linearly increase by the additional radiation length of photon converter since the items (1) and (2) described above are the main source of photonic electrons and have a similar p_T distribution. In the Run3 experiment, a brass sheet (10.0 mil thick (0.254 mm) and 1.70% radiation length) was installed as a photon converter (see Figure 1) and covered around the PHENIX Multiplicity Vertex Detector (MVD) at the interaction point. While the converter was installed (called "converter run"), $\sim 312 \times 10^9$ MB events were recorded. The PHENIX detector simulation estimates that the photonic component increase by approximately 80%. Here, we define the yield of photonic component in the non-converter runs as $P(p_T)$, the yield of non-photonic component in the non-converter runs as $N(p_T)$, the total inclusive electron yield in the no converter runs as $A(p_T)$, the total inclusive electron yield in the converter runs as $C(p_T)$, and the ratio of the photonic electron yield in the converter run to non-converter run as $R(p_T)$ ($\sim$ 1.8). $C(p_T)$ and $A(p_T)$ can be expressed with only $P(p_T), N(p_T)$ and $R(p_T)$.

$$C(p_T) = R(p_T)P(p_T) + N(p_T). \quad (1)$$
$$A(p_T) = P(p_T) + N(p_T). \quad (2)$$

Then, $P(p_T)$ and $N(p_T)$ are determined as the following relations;

$$P(p_T) = \frac{C(p_T) - A(p_T)}{R(p_T) - 1}. \quad (3)$$
$$N(p_T) = \frac{R(p_T)A(p_T) - C(p_T)}{R(p_T) - 1}. \quad (4)$$

The runs immediately following the converter runs were used to deduce inclusive electron yields for the non-converter run (the data includes $\sim 844 \times 10^9$ MB events).

4. Photonic and Non-Photonic Electron yield

Figure 2 shows photonic electron yield. The MB and ERT electron triggered data [8] are used. They are consistent with each other in the range of $0.8 < p_T < 2.8$ GeV/c. These results are compared with a calculation of the PHENIX photonic source simulation [9]. The solid curve shows the total of simulated photonic components. The real photonic component is well consistent with simulated one. The errors indicated by bars in the Fig. 2 are statistical only. The MB data in $p_T > 1.2$ GeV/c has too small statistics compared with the ERT data. On the other hand, the ERT data is estimated to have larger systematic error than the MB data in $p_T < 1.2$ GeV/c. Therefore, the MB data is used in $p_T \leq 1.2$ GeV/c, and the ERT data is used in $p_T > 1.2$ GeV/c in the calculation of non-photonic components. Figure 3 shows non-photonic electron yield. The error bars in the figure indicate only statistic error for each data point.

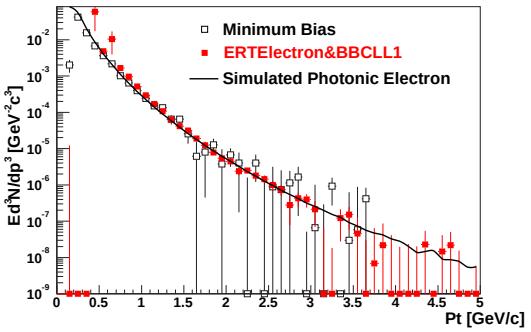

Figure 2. The transverse momentum distribution of photonic electron invariant yield.

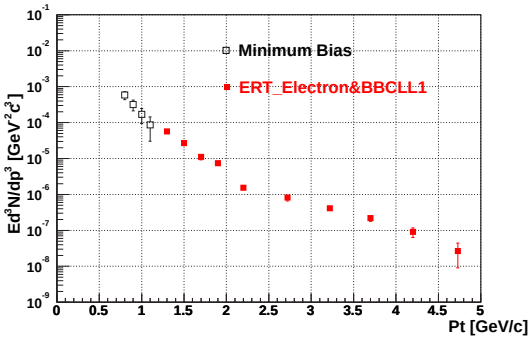

Figure 3. The transverse momentum distribution of non-photonic electron invariant yield.

5. Summary and Outlook

The photonic and non-photonic electron spectra were obtained for d-Au collisions at $\sqrt{s_{NN}} = 200$ GeV, taken in the RHIC Year-3 run. Currently, the parameter tunings of Run3 d-Au simulation are in progress, then more precise simulation study will be performed to calculate $R(p_T)$, acceptance and systematic errors. There are two methods of the photonic component subtraction (light hadron simulation and $\gamma - e^{\pm}$ tagging to estimate yield of electrons from Dalitz decays). They will be used to cross-check the photonic component subtraction.

References

[1] S.S. Adler *et al.*, Phys. Rev. Lett. **91** (2003) 072301.
[2] K. Adcox *et al.*, Phys. Rev. Lett. **88** (2002) 192303.
[3] T. Matsumoto *et al.*, CNS Annual Report 1999 (2000) 23.
[4] T. Matsumoto *et al.*, CNS Annual Report 2000 (2001) 43.
[5] M. Tamai *et al.*, CNS Annual Report 2000 (2001) 45.
[6] F. Kajihara *et al.*, CNS Annual Report 2001 (2002) 37.
[7] F. Kajihara *et al.*, CNS Annual Report 2002 (2003) 41.
[8] F. Kajihara *et al.*, CNS Annual Report 2003 (2004) 49.
[9] R. Averbeck, PHENIX Analysis Note AN254 (unpublished).

Direct Photon Search in Au-Au Collisions at RHIC-PHENIX

T. Sakaguchi, H. Hamagaki, T. Isobe, G. David[a], S. Mioduszewski[a], D. d'Enterria[b], J. Frantz[b], C. Klein-Bösing[c], K. Reygers[c] and T. Awes[d], for the PHENIX Collaboration

Center for Nuclear Study, Graduate School of Science, University of Tokyo
[a]*Brookhaven National Laboratory, New York, U.S.A.*
[b]*Columbia University, New York, U.S.A.*
[c]*Institut für Kernphysik, University of Münster, Münster, Germany*
[d]*Oak Ridge National Laboratory, Tennessee, U.S.A.*

1. Introduction

It is predicted from lattice QCD calculation that at high energy density, a phase transition from hadronic matter to a plasma of deconfined quarks and gluons (QGP) may occur, which is believed to have existed in a few microseconds after the Big Bang. Relativistic heavy ion collisions at the Relativistic Heavy Ion Collider (RHIC) at Brookhaven National Laboratory (BNL) are expected to produce such a phase transition.

Direct photon has long been considered to be an excellent probe of the early stages of the collisions because it has a long mean free path compared to the size of the nuclear volume involved in the collisions. Figure 1 shows a prediction for the yield of direct photons from various stages of the collisions [1]. The spectrum can roughly be decomposed into three regimes: at low energies (p_T ($\equiv$ q_t) $<$1 GeV), the spectrum is dominated by the contribution from thermal hadron gas via non-strange ($\pi\rho \rightarrow \pi\gamma$) and strange ($\pi K^* \rightarrow K\gamma$, etc.) meson interactions as shown in long-dashed line, whereas at high energies (p_T>3 GeV), prompt pQCD photons dominate the spectrum (short-dashed line). The intermediate region of 1< p_T <3 (dot-dashed line) is a promising window that is sensitive to thermal QGP radiation. However, since the $\gamma_{meas}/(\pi^0 \rightarrow \gamma\gamma)$ ratio is estimated to be $\sim$ 10% in the region, we need to measure the yield with the systematic uncertainty better than 10%.

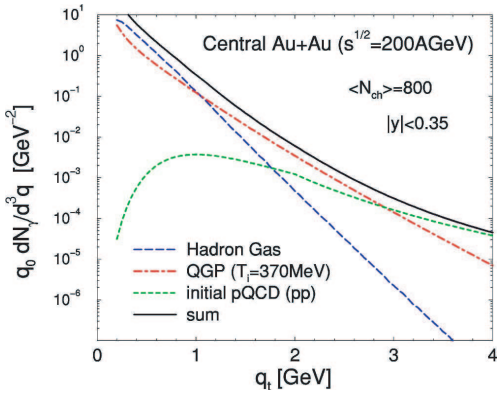

Figure 1. Prediction on the yield of direct photons from various stages after collisions [1].

To extract direct emissions from the various stages, photons from known hadronic sources must be precisely subtracted, and the efficiency and purity of identified inclusive photons must be correctly evaluated. The hadronic sources are listed in Table 1. Of those listed, π^0 and η are the major contributors. The sum of the other sources is $\sim$ 4% to the total for p_T >2 GeV/c. Thus, the evaluation of π^0 and η contributions are primarily important. In this report, the latest result on a direct photon search is presented.

Table 1. Hadrons from which photons are emitted.

State	Mass (MeV/c^2)	$R_{X/\pi^0}(p_{T\infty})$	Decay Br.	Br. Ratio
π^0	134.98		$\gamma\gamma$	98.798
			$e^+e^-\gamma$	1.198%
η	547.3	0.55	$\gamma\gamma$	39.21%
			$\pi^+\pi^-\gamma$	4.77 %
			$e^+e^-\gamma$	4.9×10^{-3}
			$\pi^0\gamma\gamma$	7.1×10^{-4}
			$\mu^+\mu^-\gamma$	3.1×10^{-4}
ρ^0	770.0	1.0	$\pi^+\pi^-\gamma$	9.9×10^{-3}
			$\pi^0\gamma$	7.9×10^{-4}
ω	781.9	1.0	$\pi^0\gamma$	8.5%
			$\eta\gamma$	6.5×10^{-4}
η'	957.8	0.25	$\rho\gamma$	30.2%
			$\omega\gamma$	3.01%
			$\gamma\gamma$	2.11%
K^0_S	497.7	0.4	($\pi^0\pi^0$)	(31.39%)
Σ^0	1192.6	1.0	$\Lambda\gamma$	100.0%

2. Analysis

Events are classified in accordance with the impact parameters of two colliding gold nucleuses. 0% corresponds to an impact parameter of 0, and 100% to that of the diameter of a gold ion. In this analysis, 55M events obtained with a high p_T trigger that had 100% efficiency for $p_T \geq 5$ GeV/c, was combined with the 30M minimum bias events used in the previous analysis [2].

In order to obtain the inclusive single photon spectrum, all the clusters detected with EMCal [3] are counted in each p_T bin, with shower shape and timing cuts, or combined variable cuts applied to reduce the hadronic shower contributions as shown in Fig 2. The spectra are corrected for the remaining charged track contamination estimated by the amount of clusters having corresponding hits in Pad Chamber [3], and also by the full PHENIX detector simulation. The spectra of $n/\overline{n}$ is estimated from the PHENIX measurements of $p/\overline{p}$, and the contamination to the photon spectra is evaluated by feeding the spectra into the detector simulation. The total hadron contamination to the photon spectra is 18-25% for p_T<$\sim$3 GeV/c, and 5-15% above $\sim$6 GeV/c. The spectra were finally corrected for acceptance and energy smearing. The systematic uncertainty of hadron contamination is $\sim$ 10%, and that of photon identification effi-

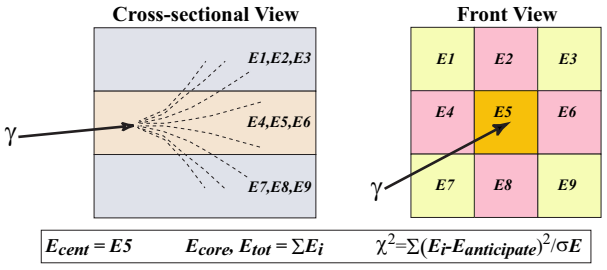

Figure 2. Photon identification cut conditions.

ciency is $\sim$ 12%, respectively.

The expected background photons are estimated from the measured transverse momentum spectra of π^0 at $\sqrt{s_{NN}} =$ 200 GeV [2]. The spectra are fitted with a function of $f(p_T)$=$A(1 + p_T/p_0)^{-n_1} g(p_T) + Bp_T^{-n_2}(1 - g(p_T))$, where A, p_0, n_1, B and n_2 are the fitting parameters, and $g(p_T)$=[1+exp{(p_T-3.75)/0.1}]$^{-1}$. The uncertainty due to fitting was estimated by moving data points up and/or down within systematic errors of the points, and re-fitting. The systematic error on the π^0 fit is estimated to be $\sim$ 15%. Since the η measurement has a large uncertainty, the η spectra are estimated by substituting p_T with $(p_T^2 - m_{\pi^0}^2 + m_\eta^2)^{1/2}$ in the above function, where m_{π^0} is the mass of π^0, and m_η is that of η. The spectra are compared with the data, and the normalization factor of 0.55$\pm$0.17 is obtained. The systematic error on the sum of the yield of π^0 and η is estimated to be $\sim$ 16%. In order to cancel certain systematic errors, we divide by the final π^0 spectrum both the photon measurement (using π^0 data points) and the background expectation (using a π^0 fit). The systematic uncertainty on the ratio of measured to expected background photons is $\sim$ 21% in total.

3. Results and Summary

Figure 3 shows the ratio of measured to expected background photons for 0-10% central Au-Au collisions, with systematic error bands in gray and statistical errors in error bars. The solid line is a pQCD photon prediction [4] scaled by number of binary collisions (N_{coll}) that describes the initial hard scattering process, with taking the expected background photons into account. The dashed lines show uncertainty of the prediction. There is no siginificant excess seen in the intermediate region (1 GeV $< p_T <$ 3 GeV). However, a significant photon excess is seen at $p_T >$ 4 GeV/c, the size of which is consistent with the prediction. The excess is largely enhanced because of the suppression of π^0 yield at high p_T in the central Au-Au collisions [2]. The centrality dependence of the ratio is shown in Fig. 4. In peripheral events, due to less suppression of high p_T π^0's, the excess photons become undetectable within the current uncertainties, which is still consistent with the predictions. This is the first observation of direct photons that come from initial hard scattering process in relativistic heavy ion collisions.

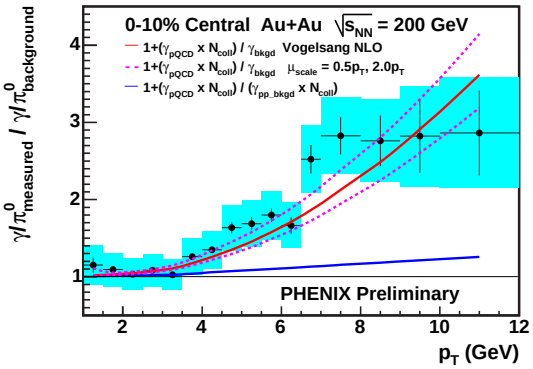

Figure 3. Ratio of measured to expected background photons in 0-10% central Au-Au collisions at $\sqrt{s_{NN}} =$ 200 GeV. pQCD direct photon predictions [4] is shown in solid line with its uncertainty in dashed lines.

The observation suggests that the yield of photons produced in the initial hard scattering process is not suppressed, while that of the hard scattered partons are suppressed. It is the evidence of that the initial hard scattering probability is not suppressed in Au-Au collisions, and the suppression of high p_T hadrons are due to the final state interaction (energy loss) of hard scattered partons with possibly formed hot dense medium.

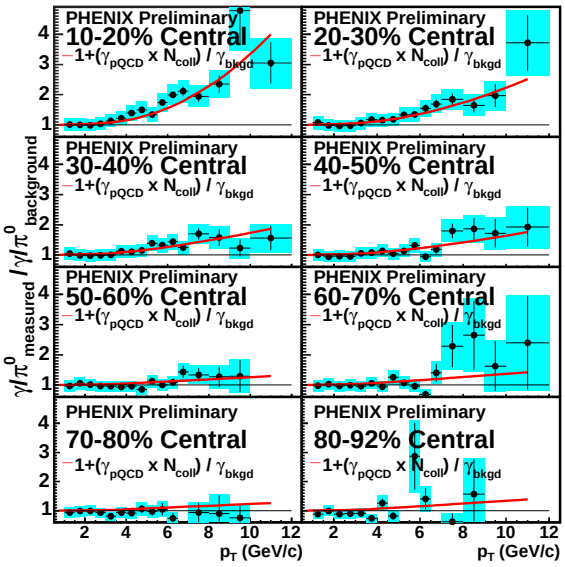

Figure 4. Same as Fig. 3 for other centralities.

References

[1] S. Turbide, R. Rapp and C. Gale, Phys. Rev. C **69** (2004) 014903.

[2] S.S. Adler *et al.* (PHENIX Collaboration), Phys. Rev. Lett. **91** (2004) 072301.

[3] K. Adcox *et al.* (PHENIX Collaboration), Nucl. Instrum. Methods. A **499** (2003) 469.

[4] S. Catani *et al.*, JHEP **9903** (1999) 025; Private Communication.

Measurement of $J/\psi \rightarrow e^+e^-$ Yield in d+Au Collision

S. Kametani, H. Hamagaki, F. Kajihara, K. Ozawa, Y. Akiba[a], A. Lebedev[b] and X. Wei[c], for the PHENIX Collaboration

Center for Nuclear Study, Graduate School of Science, University of Tokyo
[a] *RIKEN*
[b] *Department of Physics and Astronomy, Iowa State University*
[c] *RIKEN-BNL Research Center*

1. Introduction

The PHENIX experiment had a very successful electron-pair measurement for d+Au collisions at $\sqrt{s}_{NN}$ = 200 GeV in the RHIC Year-3 run from January 13th to March 23rd, 2003. With the d+Au collisions, basic studies on the production mechanism of J/ψ and the nuclear effect in the normal nucleus matter are planned.

Assuming J/ψ particles are produced in hard processes, the J/ψ production is proportional to the number of binary nucleon-nucleon collisions ($N_{\rm coll}$) to the first order. A produced J/ψ will undergo strong interactions with the surrounding nucleons of Au nucleus (spectator) [1]. The number of survived J/ψs after traveling distance x can be expressed as,

$$N_{J/\psi} \propto e^{-x/\lambda_{abs}},$$

where λ_{abs} denotes the absorption length.

Meanwhile, "nuclear shadowing", that is, the depletion of parton component in the small x_F region in a nucleus compared to those in a nucleon, is considered to reduce the production rate of J/ψ.

As the path length of the produced J/ψ in the spectator is related to the impact parameter, the nuclear effect on the J/ψ yield described above appears as a function of collision centrality [2]. The centrality can be determined as a function of multiplicity, because the number of binary nucleon-nucleon collisions each of which is inelastic scattering increases as the collision is more central.

These nuclear effects must be studied carefully in order to understand the modification of the J/ψ yield in the normal nuclear matter, which should be a reference to understand the J/ψ production in nucleus-nucleus collisions, where a suppression [3] or an enhancement [4] has been predicted due to the formation of the Quark Gluon Plasma.

In this report, a measurement of J/ψ in its di-electron decay channel in the PHENIX experiment is described, and a preliminary result is shown.

2. Detector Setup

Figure 1 shows the PHENIX experimental setup [5]. The centrality, collision vertex and collision time were measured using a pair of Beam-Beam counters (BBC), which were placed along the beam line at ± 144 cm from the center of collision point. The electron measurement was performed using with the PHENIX central arms. The PHENIX Central Arm achieves momentum measurement and tracking by a Drift Chamber (DC) and three layers of Pad Chambers (PC). Electron identification is performed by a Ring Imaging Cherenkov Counter placed just outside of the most inner PC. An Electro-Magnetic Calorimeter (EMC) is placed outside of the most outer PC and measures the energy of tracks. The PHENIX Central Arm covers an acceptance region of $|\eta| < 0.35$ for polar angles and $22.5^\circ < |\phi| < 112.5^\circ$ for azimuthal angles.

Two kinds of triggers were used for data taking. One is Z vertex trigger using BBC. For electron and electron-pair measurements in the d+Au collisions, the first-level electron trigger, called ERT trigger, was used. The ERT is the mix of EMC and RICH local trigger.

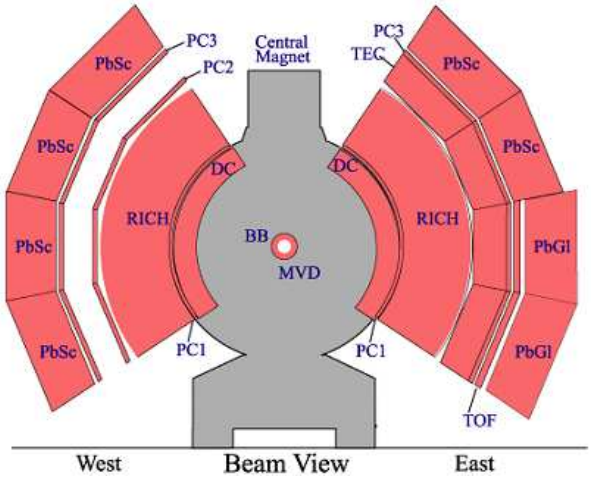

Figure 1. PHENIX Run-3 detector setup

3. Analysis

Totally, 3.5×10^6 ERT triggered events were analyzed. As RICH can not separate electron and pion at momentum region more than 5 GeV/c, only the track which has momentum less than 5 GeV/c were picked up. For electron identification in the analysis level, only the tracks with associated RICH hits were selected as electron candidates. However, hadrons from the collision can be accidentally associated to RICH hits. To reject these backgrounds, we required also that the ratio of energy measured by EMC to the momentum of the track to be ~ 1. The parameters were well selected to reject backgrounds so that the efficiency of electron was about 90%.

Invariant masses were calculated for all the combinations of electron candidates for each event. Figure 2 shows invari-

ant mass spectra for unlike-sign electron pair (e^+e^-) and like-sign electron pair (e^+e^+ or e^-e^-). The combinatorial background in unlike-sign pair spectra caused by a wrong combination was estimated from like-sign pair spectra. After subtracting the invariant mass spectrum of like-sign pair from that of unlike-sign pair, the count around J/ψ mass region was about 400. The resolution of J/ψ was about 100 MeV/c^2.

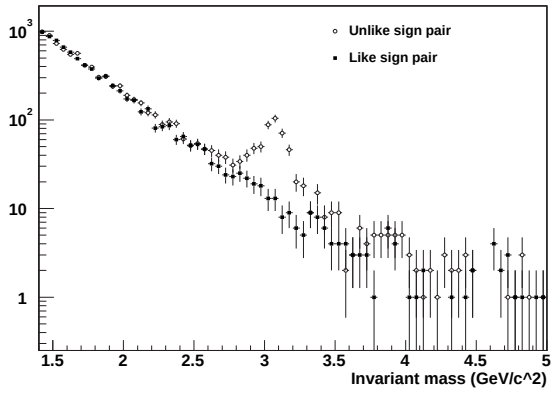

Figure 2. Invariant mass spectrum of unlike-sign electron pair (open circle) and like-sign pair (square). Statistical errors are also shown.

Collision centrality is determined from the BBC multiplicity and the number of J/ψ was counted for each centrality. Careful studies for acceptance, triggering efficiency and periodical fluctuation of efficiency for J/ψ were performed [6, 7]. The simulation was well tuned to reproduce the experimental data and the total systematic error is well minimized. After correction by these efficiency studies, the J/ψ yield for each centrality was estimated.

4. Result

Figure 3 shows a preliminary result of $R_{\rm cp}$ (Ratio of yield per binary collision of each centrality divided by that of the most peripheral collision) as a function of $N_{\rm coll}$ instead of centrality is shown. The yield is normalized by $N_{\rm coll}$ to understand nuclear effect clearly. The mean of $N_{\rm coll}$ value at each centrality is estimated using the simulation based on the Glauber model [8]. The shaded area shows the scale error for the most peripheral collisions which include the statistical error as well as the systematic error mainly from the $N_{\rm coll}$ determination. The error on the data point is the quadratic sum of statistical and systematic errors. The $R_{\rm cp}$ ratio decreases with increase of centrality.

5. Summary

To understand nuclear effects on the J/ψ production in high energy heavy ion collisions, a J/ψ measurement was performed for the d+Au collisions.

The measurement of the J/ψ yield from di-electron detection in the d+Au collisions is described. About 400 $J/\psi \rightarrow e^+e^-$ events were reconstructed from RHIC-PHENIX Year-3 data. The J/ψ yield was shown as a function of the number of binary nucleon-nucleon collisions.

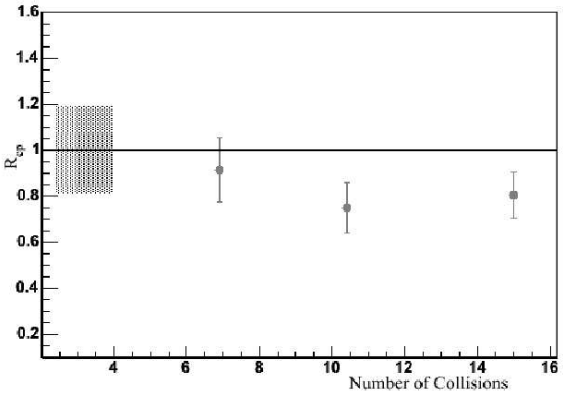

Figure 3. PHENIX Run-3 preliminary result for R_{cp} (Ratio of yield per binary collision of each centrality divided by that of most peripheral collision) as a function of $N_{\rm coll}$.

The result shown in this report is still preliminary one. More elaborate studies are to be made to reduce the systematic errors.

References

[1] R. Vogt, Phys. Rep. **310** (1999) 197.

[2] S. Kametani *et al.*, CNS Annual Report 2002 (2003) 47.

[3] T. Matsui and H. Sats, Phys. Lett. B **178** (1986) 416.

[4] M. Gazdzichki and M. I. Gorenstein, Phys. Rev. Lett. **83** (1999) 4009.

[5] K. Adcox *et al.* (PHENIX Collaboration), Nucl. Instrum. Methods. A **499** (2003) 469.

[6] F. Kajihara *et al.*, CNS Annual Report 2003 (2004) 49.

[7] S. Kametani *et al.*, CNS Annual Report 2001 (2002) 33.

[8] R. J. Glauber, in Lectures in Theoretical Physics, edited by W. E. Brittin and L. G. Dunham (Interscience, N.Y., 1959), Vol. 1, p. 315.

$J/\psi \rightarrow e^+e^-$ Measurement in Au+Au Collisions at $\sqrt{s_{NN}} = 200$ GeV at PHENIX Run2

T. Matsumoto, T. Gunji, H. Hamagaki, S. Kametani and K. Ozawa, for the PHENIX Collaboration

Center for Nuclear Study, Graduate School of Science, University of Tokyo

1. Introduction

The goal of PHENIX experiment at RHIC is to search for a possible phase transition of ordinary matter to Quark Gluon Plasma (QGP) and to understand its property. The suppression of J/ψ yield has been proposed as one of the most promising probe of QGP formation [1].

This article describes the updated results of J/ψ measurement in Au+Au and p+p collisions at PHENIX Run2. The major update was the correction of the colliding position in $x-y$ plane. It affects to the momentum determination and the mass resolution of the J/ψ peak. The procedure and result were described below.

2. Variation of Colliding Position

Since PHENIX tracking algorithm assumes that all tracks come from $(x, y) = (0, 0)$, shift of colliding position from (0,0) introduces the error in the momentum determination.

In the ideal case, bending angle $\Delta\alpha$ of the tracks in no field should distribute around zero ($\Delta\alpha = 0$). However if the colliding position is off centered, $\Delta\alpha$ becomes finite.

Correction of x and y position of colliding position. was performed by the PMT hit information in Beam Beam Counter (BBC) using the relation;

$$x_{offset} = \frac{\sum(X_{PMT} \times Q_{PMT})}{\sum Q_{PMT}}, \quad (1)$$

$$y_{offset} = \frac{\sum(Y_{PMT} \times Q_{PMT})}{\sum Q_{PMT}}, \quad (2)$$

where X_{PMT} and Y_{PMT} show x and y position of a PMT, Q_{PMT} shows the amount of charge in a PMT. Figure 1 shows the beam position offset in $x-y$ plane relative to no field run (run 29236).

The detector was aligned to run 29236 in Au+Au so that the relative differences of the position (Δx, Δy) were converted to α angle offset, $\Delta\alpha$, using the relation:

$$\Delta\alpha \sim \tan^{-1}\frac{\Delta y - R\sin\phi}{\Delta x - R\cos\phi} - \phi, \quad (3)$$

where R=220 cm is the Drift Chamber (DC) reference radius, ϕ is the azimuthal angle. After calculating $\Delta\alpha$ in each run, p_T was corrected using the relation:

$$p_T(\mathrm{Corr}) = p_T(\mathrm{No\ Corr}) \times \frac{\alpha}{\alpha + \Delta\alpha} \quad (4)$$

3. e^+e^- Invariant Mass Distribution

After the correction of colliding position, e^+e^- invariant mass was reconstructed. Figure 2 shows the invariant mass distribution of electron pair in Au+Au data. Simultaneous

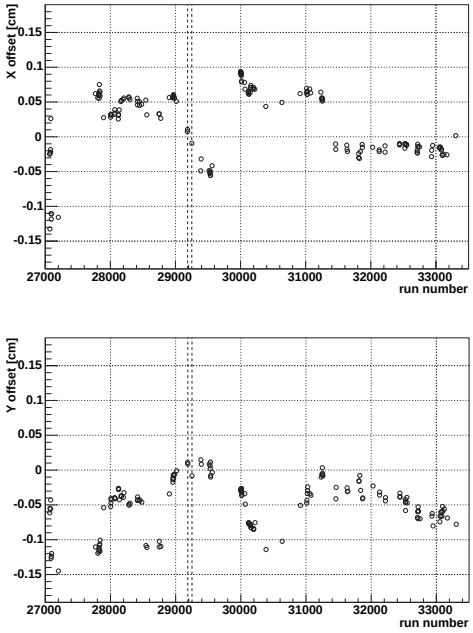

Figure 1. Beam position offset in $x-y$ plane during Au+Au data taking period.

fit with a Gaussian and an exponential functional form was performed. Dashed curve shows the estimation of combinatorial background with following functional form:

$$F_{\mathrm{back}}(m) = A \times \exp(-Bm), \quad (5)$$

where m, A and B are invariant mass of pairs, the normalization factor and the exponential slope factor, respectively. The exponential slope factor was evaluated by fitting the spectrum of unlike sign pairs derived from mixed events in the mass range from 2.5 GeV/c^2 to 3.5 GeV/c^2.

Table 1 is the summary of fitting results of invariant mass distribution in Au+Au collisions. The number of J/ψ signals was determined by the integral of Gaussian curve with $\pm 2\sigma$ range:

$$\mathrm{Counting\ Range\ [GeV}/c^2\mathrm{]} = 3.015 < M < 3.147. \quad (6)$$

Correction of colliding position variation was also applied in p+p data analysis. Figure 3 shows the invariant mass distribution of electron pairs in p+p. Left figure was derived using same cut parameters as used in Au+Au analysis. Due to the large dead area of DC in p+p run period, reconstructed track was limited. However peak position and width were consistent with Au+Au data. Right figure was

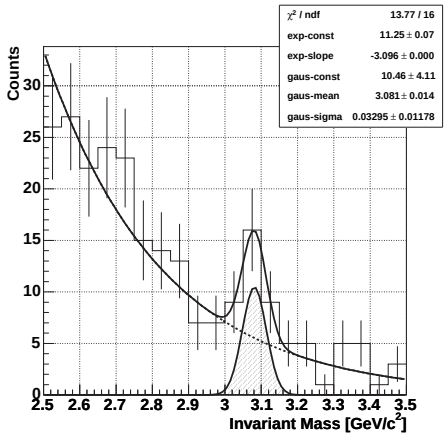

Figure 2. The invariant mass distribution of electron pairs in Au+Au data. Fitting curve of exponential and Gaussian is also shown.

	fit result
Peak Position [GeV/c^2]	3.081 ± 0.014
Width [GeV/c^2]	0.033 ± 0.012
Number of signals	16.48 ± 4.06

Table 1. Fitting results of Au+Au invariant mass distribution. The number of signal shows the integral of Gaussian with $\pm 2\sigma$ range.

derived using relaxed cuts and tracks reconstructed from Pad Chamber and EMCal hit position (PC-EMCal tracking) in addition to DC tracking. This track reconstruction method enhances the statistics but the peak becomes broader. Since p+p data was used as a reference for Au+Au data analysis, J/ψ counts from PC-EMCal tracking were used in order to have high statistics and reduce statistical uncertainty.

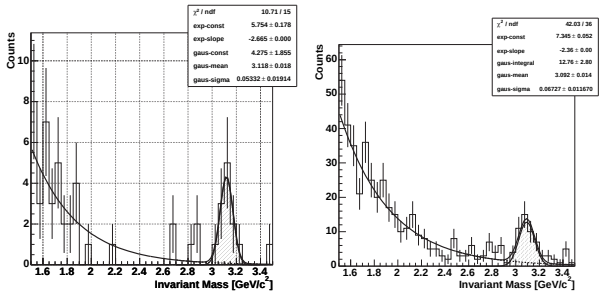

Figure 3. The invariant mass distribution in p+p data. Left: cut parameters were same as used in Au+Au analysis. Right: cut was relaxed and PC-EMCal tracking was used. The fits was performed by exponential and Gaussian. Gaussian fit was performed in the range from 2.8 GeV/c^2 to 3.4 GeV/c^2. Shaded area shows the Gaussian curve derived from the fitting.

4. Centrality Dependence of J/ψ Yield

Au+Au data set was subdivided into three centrality classes. The number of J/ψ was counted in each centrality. The procedure of the confidence level calculation, efficiency evaluation, and invariant yield ($BdNdy$) calculation were same as described in the reference [2, 3]. Figure 4 shows the distribution of $BdN/dy|_{y=0}$ per binary collision as a function of number of participants (N_{part}). $N_{part} = 2$ data point is the p+p result. Open circle shows the minimum bias data point derived using the J/ψ counts in Table 1. Peripheral and mid-central data was shown as 90 % confidence level.

	Au +Au Cuts	Relaxed Cuts
Peak Position [GeV/c^2]	3.118 ± 0.018	3.092 ± 0.014
Width [GeV/c^2]	0.053 ± 0.019	0.067 ± 0.012
Number of signals	10.91 ± 3.91	39.36 ± 6.27

Table 2. The summary of fitting results of p+p invariant mass. The numbers are derived using both Au+Au cuts and relaxed.

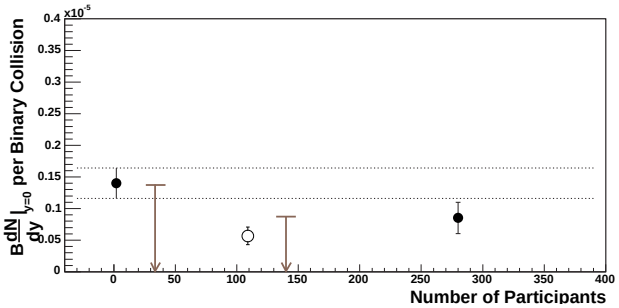

Figure 4. The $BdN/dy|_{y=0}$ per binary collision as a function of number of participants.

The Au+Au data points show that J/ψ yield is suprressed relative to binary collision scaling (dashed line). The central data point is higher relative to minimum bias data point. This effect suggest that the mechanism of enhancement needs to be taken into account with the increase of centrality. It is consistent with the previous results.

5. Summary

The analysis of J/ψ yield extraction using PHENIX Run2 data was updated. The correction of colliding position variation was applied and clear J/ψ peak was reconstructed. The statistical uncertainty was reduced compared with previous results, especially in minimum bias and central data point in Au+Au data.

References

[1] T. Matsui and H. Satz, Phys. Lett. B **178** (1986) 416.
[2] T. Matsumoto *et al.*, CNS Annual Report 2002 (2003) 29 .
[3] T. Matsumoto *et al.*, CNS Annual Report 2002 (2003) 31 .

$J/\psi \rightarrow e^+e^-$ Measurements in Au+Au Collisions at $\sqrt{s_{NN}}$ = 200 GeV at RHIC-PHENIX

T. Gunji, H. Hamagaki, K. Ozawa, T. Matsumoto, S. Kametani, T. Sakaguchi and F. Kajihara, for the PHENIX Collaboration

Center for Nuclear Study, Graduate School of Science, University of Tokyo

1. Introduction

Lattice QCD calculations predict that there is a phase transition from ordinary hadronic matter to plasma of de-confined quarks and gluons, called Quark-Gluon-Plasma (QGP), at extremely high temperature $T_c \sim 160$ MeV. The condition for such a phase transition can be realized with high energy heavy ion collisions. The PHENIX experiment at the Relativistic Heavy Ion Collider (RHIC) in the Brookhaven National Laboratory (BNL) searches for evidences of such a phase transition via Au+Au collisions at $\sqrt{s_{NN}} = 200$ GeV.

Heavy quarkonia have been proposed as a promising probe to inspect the QGP formation. In the de-confined environment, long-range confining potential of heavy quarkonium vanishes due to the Debye type color screening. This leads to the suppression of heavy quarkonium yields, which was predicted by Matsui and Satz [1]. Beside this senario, the absorption of J/ψ by surrounding nucleon (spectators) and hadronic secondaries also lead to the suppression of J/ψ yield.

Recently, it is predicted that J/ψ yield will be enhanced due to $c\bar{c}$ coalescence in QGP [2] and at hadronization stage [2,3] at RHIC energies, where abundant c and $\bar{c}$ quarks are produced,

At RHIC, p+p, d+Au and Au+Au collisions were performed and those data has been analyzed to investigate the contributions of these competing effects to the J/ψ yield [4, 5].

2. Au+Au collisions at Year-4

The Au+Au collisions were performed in the RHIC Year-4 Run from the beginning of January to the end of March in 2004. During the period, 1.6 billion events, which corresponds to the integrated luminosity of $\sim 240\ \mu\mathrm{b}^{-1}$, were recorded. This is $\sim$ 30 times larger than the number of events which were used in the Year-2 J/ψ analysis.

3. Identification of electron pairs in PHENIX

The electron and positron measurements were performed with the central detectors of the PHENIX experiment [6], each of which has the coverage of $|\eta| < 0.35$ and $\Delta\phi = 90^\circ$. Drift Chamber (DC) is the device for the momentum measurement of charged particles and gives the information on particle trajectory. Pad Chamber (PC) is the tracking device and determines the particle trajectory in conjunction with DC. Ring Imaging Cherenkov Counter (RICH) and Electromagnetic Calorimeter (EMCal) are the main devices for electron identification.

Electrons are identified by requiring the following criteria. The charged tracks were associated with a RICH ring ($\geq$ 2 hit PMT's in a ring) and with a EMCal ($\pm 4\sigma$ position association) and satisfied $(E/p - 1)/\sigma(p) > -2$, where E is the EMC cluster energy and p is the reconstructed track momentum.

4. Analysis

Analysis was performed for $\sim$ 95 million events, which corresponds to $\sim$ 6% of all the data. In this analysis, the events which contained more than one electron pair (e^-e^-, e^+e^+ or e^-e^+) whose invariant mass was larger than 2.4 GeV/c^2 were selected to enrich a fraction of J/ψ to the number of selected events.

Figure 1 shows the invariant mass distributions of electrons and positrons for centrality of 0-90% (upper left), 0-20% (upper right), 20-40% (lower left) and 40-90% (lower right).

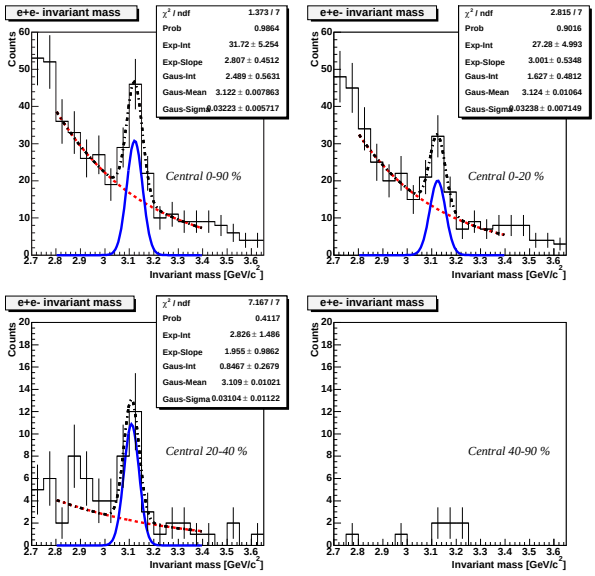

Figure 1. e^+e^- Invariant mass distribution for centrality of 0-90%(upper left),0-20% (upper right), 20-40% (lower left) and 40-90% (lower right). The fitting result with exponential (dashed-line) and gaussian (solid-line) are shown for centrality of 0-90%, 0-20%, 20-40%. The dash-dotted line is the convolution of fitted exponential function and gaussian.

Centrality corresponds to measured fraction of total inelastic cross section of Au+Au collisions. Centrality of 0-20% and 40-90% corresponds to the most central collisions and the peripheral collisions, respectively. To extracted the J/ψ signals for centrality of 0-90%, 0-20% and

20-40%, the invariant mass distributions were fitted with a linear combination of an exponential function (dashed-line) and a gaussian (solid-line). The exponential and gaussian correspond to continuum and the J/ψ peak, respectively. The fitting results of mass centroid, mass width and number of J/ψ counts are summarized in Table 1. The mass centroid is slightly different from 3.097 GeV/c^2

Table 1. The fitting results of mass centroid, mass width and number of J/ψ counts for centrality of 0-90%, 0-20% and 20-40%. The mass centroid and width are in units of GeV/c^2 and MeV/c^2, respectively.

centrality	centroid	width	J/ψ counts
0-90%	3.12 ± 0.01	32.2 ± 5.73	49.7 ± 11.3
0-20%	3.12 ± 0.01	32.4 ± 7.20	32.5 ± 9.67
20-40%	3.11 ± 0.01	31.0 ± 11.2	16.9 ± 5.30

from PDG value [7], becuase the response of each detector and the momentum scale factor haven't been fully tuned. The J/ψ width is mostly due to the momentum resolution of DC. The momentum resolution in Year-2 was $1.0 \times p$ (GeV/c) $\bigoplus$ 0.7 [8], and the expected J/ψ mass width was $\sim$ 36 MeV for stationary J/ψ. Since the strength of magnetic field was $\sim$1.3 times larger in Year-4, the momentum resolution should be improved and J/ψ mass width will be narrower. Further study concerning momentum resolution is underway.

5. J/ψ yield calculation

J/ψ invariant yield is expressed as follows:

$$B\frac{dN}{dy} = \frac{N_{J/\psi}}{N_{evt}} \frac{1}{\Delta y \epsilon_{acc} \epsilon_{eff}}, \quad (1)$$

where $N_{J/\psi}$ and N_{evt} stand for the number of J/ψ counts and number of analyzed event, respectively. Δy in Eq. (1) is the rapidity coverage. The correction factor, ϵ_{acc}, is the acceptance of electrons and positrons from J/ψ, where run-by-run fluctuation of acceptance is taken into account. The correction factor, ϵ_{eff}, is the multiplication factor of tracking, electron identification and embedding efficiency. B is the branching ratio (5.93% from PDG [7]). Since the PHENIX detector system is composed of two arm spectrometers, a fraction of electrons and positrons from J/ψ falls into the detector acceptance. Moreover the acceptance of J/ψ depends on the p_T of J/ψ. The J/ψ p_T dependence of the acceptance has been evaluated with the single J/ψ Monte Carlo simulation, where the run-by-run acceptance fluctuation due to the dead channels of each subsystem will be taken into account. Now this study is underway.

Tracking efficiency, which is the probability that electrons and positrons from J/ψ are reconstructed by offline tracking code, has been studied with the same Monte Carlo simulation.

Electron identification efficiency, which is the probability that the electrons and positrons satisfy the criteria used in this analysis, has been also evaluated from Monte Carlo simulation and from conversion photons in real data.

The embedding efficiency depends on the centrality. In a high multiplicity environment, the miss association of tracks to EMCal or PC causes the inefficiency of reconstructed tracks. To evaluate this effect, embedding efficiency will be studied by embedding the simulated single J/ψ into the real events and by extracting the probability that the embedded J/ψ are reconstructed after that.

After these correction factors are evaluated, the centrality dependence of J/ψ invariant yield will be studied.

6. Summary and Outlook

J/ψ analysis was started and was performed for $\sim$ 6% of all the Year-4 data. Invariant mass spectra of electron pairs show clear peak around J/ψ mass region and $\sim$ 50 J/ψ counts were obtained for $\sim$ 6% statistics.

To extract the invariant yield, correction factors such as electron pair acceptance, tracking efficiency, electron identification efficiency and embedding efficiency have been studied in detail.

References

[1] T. Matsui and H. Satz, Phys. Lett. B **178** (1986) 416.
[2] Robert. L. Thews, *et al.*, Phys. Rev. C **63** (2001) 054905.
[3] A. Andronic, *et al.*, Phys. Lett. B **571** (2003) 36.
[4] T. Matsumoto, *et al.*, CNS Annual Report 2003 (2004) 57.
[5] S. Kametani, *et al.*, CNS Annual Report 2003 (2004) 55.
[6] K. Adcox, *et al.*, Nucl. Instrum. Methods. A **499** (2003) 489.
[7] K. Hagiwara *et al.*, Phys. Rev. D **66** (2002) 010001.
[8] S.S. Adler *et al.* (PHENIX collaboration), Phys. Rev. C **69** (2004) 014901.

Performance of the Aerogel Cherenkov Counter at RHIC-PHENIX

N. Kurihara, H. Hamagaki, K. Ozawa, T. Sakaguchi, S. Kametani
E. Kistenev[a], Y. Miake[b], S. Esumi[b], H. Masui[b], M. Konno[b] and S. Takagi[b],
for the PHENIX Collaboration

Center for Nuclear Study, Graduate School of Science, University of Tokyo
[a]Brookhaven National Laboratory, N.Y., U.S.A.
[b]High Energy Nuclear Physics Group,University of Tsukuba

1. Introduction

A phase transition from hadronic matter to deconfined quark and gluon matter, called as quark gluon plasma (QGP), is predicted under a condition realized with the head-on collisions of heavy nuclei at ultra-relativistic energies. To study this very dense partonic matter at high temperature is the main subject of the PHENIX experiment at RHIC. RHIC can provide gold-gold (Au-Au) collision at the center of mass energy $\sqrt{s_{NN}}$ = 200 GeV.

The recent experimental studies at RHIC, a new phenomena called Jet Quenching [1, 2] was discovered, and its extensive studies has started. Particle creation is reduced in the Au-Au collision compared with the binary scaling. This is seen as if jets are quenched in high dense matter. The observed phenomena are consistent with the picture that a parton, origin of jet, radiates gluons and loses its energy while penetrating through very dense and high temperature matter. It is one of the most promising signatures of QGP.

High p_T particles should be a unique probe to study such dense matter, since they are mainly originated from jets. Strong interaction is dominant in very dense and high temperature matter, thus jets inherit a state of the matter. The jet profiles are strongly affected by the condition of hot and dense matter because partons interact with that medium. Jet quenching is explained as energy loss of partons, however very interesting but yet unexplored possibility is that the energy loss could be different depending on the species of partons. Compared with quark jet, gluon jet tends to lose energy larger in a prediction of QCD. If this is the case, the yield of particles originated from gluon jets should be more suppressed than the particles from quark jet at QGP. The effect could be revealed in the change of particle ratio as a function of transverse momentum. Baryon conservation lead to create more proton than anti-proton at heavy ion collision. If gluon jets are more suppressed, the fragmentation from u, d jets are emphasized and the ratio of $\bar{p}/p$ is expected to be small [3]. It is also believed that strange quark is affected less by bremsstrahlung effect because the s quark is heavier than u and d quarks. Therefore the ratio of pion/kaon is expected to be reduced [4].

2. PHENIX detector

One of the features of the PHENIX detector is the capability of measuring charged hadrons with particle identification in the wide momentum range at mid-rapidity region. For that purpose, the PHENIX has a pair of central arms. Momenta of charged particles are measured by Drift Chamber (DC), and particle identification (PID) is performed mainly using Time-of-flight (TOF). The particle identification by TOF is limited because of its poor time resolution. In order to enhance PID capability, Aerogel Cherenkov Counter was constructed and installed before RUN4. The capability of PID for previous and RUN4 are listed in Table 1. This advancement of PID lets observe high p_T particles from hard collision.

PHENIX PID	$\pi^{\pm}$	$K^{\pm}$	$p, \bar{p}$
Past PID (GeV/c)	$0.2 \sim 2.5$	$0.5 \sim 2.5$	$1.0 \sim 4.0$
RUN4 PID (GeV/c)	$1.0 \sim 3.7$	$5.5 \sim 7.0$	$3.7 \sim 7.0$

Table 1. Momentum range which can identify each particle.

3. Aerogel Cherenkov Counter at PHENIX

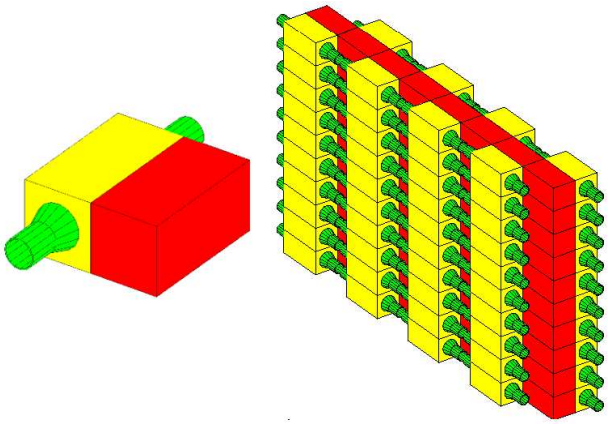

Figure 1. Schematic drawing of Aerogel Cherenkov Counter.

Aerogel Cherenkov Counter is located in West central arm, and it covers 1/8 of acceptance of the West arm. One counter cell is categorized three parts; aerogel, diffusion box, PMTs. One Aerogel cell is shown in the left side of Fig. 1. Ten layered Aerogel tiles (shown in darkened part) are placed inside of reflector. Generated Cherenkov light are integrated at diffusion box (shown in light part) and counted by two PMTs which face to diffusion box. 80 Aerogel cells are assembled as shown in right side of Fig. 1. All of Aerogels are placed in the same plane in order to reduce dead space.

Aerogel index of refraction is $n = 1.012$. Cherenkov thresholds for pion, kaon and proton are 0.8 GeV/c,

3.2 GeV/c and 6.0 GeV/c respectively. These difference of the threshold can be used for PID. However at a region upper than 3.0 GeV/c, particle separation between pion and kaon is difficult by using only Aerogel Counter. In the region kaon starts to emit Cherenkov photons as well as pions. To separate pion and kaon, Ring Imagine Cherenkov detector (RICH), with CO_2 as a radiator gas is used. The refractive index of CO_2 is $n = 1.00042$ and the Cherenkov threshold of pion is 5 GeV/c. This makes it possible to do PID at the range from 5.5 GeV/c to 7.0 GeV/c. Details of the Aerogel Counter are written in Ref. [5].

4. Performance of Aerogel Counter

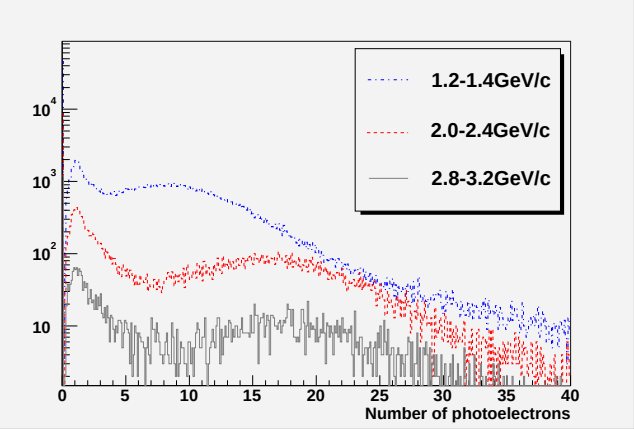

Figure 2. Number of photoelectron distributions, dot-dash line is a distribution at the range of 1.2-1.4 GeV/c, dashed line is 2.0-2.4 GeV/c and solid line is 2.8-3.2 GeV/c.

Figure 2 shows distribution of number of photoelectrons at the momentum range of 1.2 - 1.4 GeV/c, 2.0 - 2.4 GeV/c and 2.8 - 3.2 GeV/c. Peaks at one photoelectron are primarily due to background hits. Another broad peaks are caused by cherenkov light from charged pions. The central position of the broad peaks shifts upward with increase of momentum. Peak values are fitted to empirical equation

$$N_{p.e.} \propto \left[1 - (1/\beta n)^2\right]. \quad (1)$$

In the equation, n denotes reflective index of Aerogel.

Figure 3 shows scatter plots of associated tracks, whose axis are momentum and number of photoelectrons. Lines in Fig. 3 are expected peak value of number of photoelectrons for pions, kaons and protons, respectively. Locus corresponding to pions can be seen at momentum from 0.9 GeV/c to 3.0 GeV/c. These tracks are able to be separated from kaons and protons. This pion separation in the momentum range between 2.0 GeV/c and 3.0 GeV/c is what became possible only with AEROGEL. Kaons emit Cherenkov light at the momentum range over 3.0 GeV/c, however there are no clear indication of kaons, primarily because of low statistics. Total amounts of analyzed data are about 3% of all PHENIX RUN4 data. These data are under processing now, it is expected that capability of identifying protons and kaons can be evaluated with larger event samples as data production progresses.

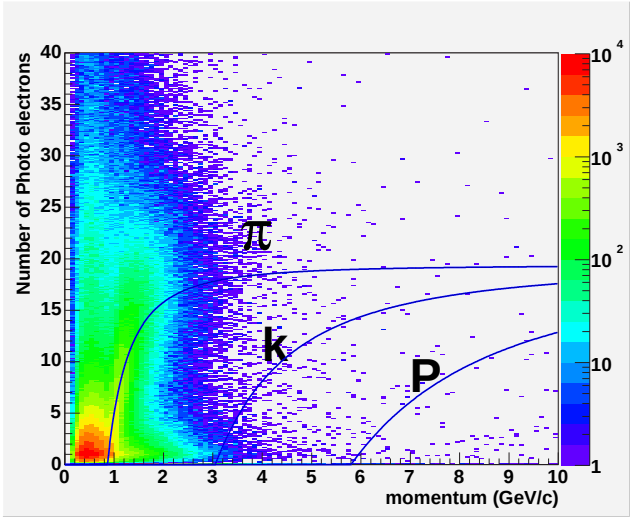

Figure 3. Number of photo-electrons according to momentum.

5. Summary

Aerogel Cherenkov Counter was installed to PHENIX in order to enhance particle identification capability of PHNEIX experiment. PHENIX RUN4 was operated from Februaly 2004 to May 2004. The performance of Aerogel Counter has been studied. The correlation of number of photoelectrons and momentums are checked. Charged pions were clearly identified in the momentum range from 0.8 GeV/c to 3.0 GeV/c. This pion separation in the momentum range between 2.0 GeV/c and 3.0 GeV/c is what became possible only with AEROGEL. It is expected that capability of identifying protons and kaons can be evaluated with larger event samples as data production progresses.

References

[1] K. Adocx *et.al.* (PHENIX collaboration), Phys. Rev. Lett. **88** (2002) 022301.

[2] K. Adocx *et.al.* (PHENIX collaboration), Phys. Rev. Focus. **88** (2002) story 34.

[3] Xin-Nian Wang, Phys. Rev. lett. **81** (1998) 2655; hep-ph/9701227 v2.

[4] P.Levai, G.Papp, G.Fai and M.Gyulassy, nucl-th/0012017; nucl-th/01120062.

[5] PHENIX high p_T upgrade team, Conceptual Design Report for High p_T Upgrade (2003).

Development of Time Projection Chamber using CF_4 for PHENIX-Upgrade

T. Isobe, H. Hamagaki, K. Ozawa, M. Inuzuka, T. Sakaguchi, F. Kajihara, T. Gunji, S.X. Oda, S. Sawada[a] and S. Yokkaichi[b]

Center for Nuclear Study, Graduate School of Science, University of Tokyo
[a]KEK, High Energy Accelerator Research Organization
[b]RIKEN (The Institute of Physical and Chemical Research)

1. Introduction

The PHENIX experiment [1] has been carried out at the Relativistic Heavy Ion Collider (RHIC) at Brookhaven National Laboratory (BNL) in order to find evidences of phase transition from normal nuclear matter to Quark Gluon Plasma (QGP), which is a new phase of matter consisting of de-confined quarks and gluons.

It is predicted that the chiral symmetry will be restored as a consequence of QGP formation and the mass of vector mesons (ρ, ω and ϕ) will be modified [2]. Measurement of the vector mesons in the electron decay channel is considered to be one of the promising ways to study the chiral symmetry restoration.

2. Motivations for PHENIX-TPC

For the identification of electrons, a Ring Imaging CHerenkov (RICH) detector has been used at the PHENIX setup. However, it is difficult to detect the low momentum electrons of $p_T < 200$ MeV/c in PHENIX magnetic field condition because of the small acceptance. Electron pairs coming from γ conversions or π^0 Dalitz decays lead to a huge combinatorial background. The present PHENIX setup does not allow an efficient measurement of low-mass electron pairs. Actually, the first results of PHENIX experiment show that the signal to background ratio was as small as 1/20 for ϕ mesons mass region [3].

It is important to identify the low momentum electrons with large acceptance detector for the rejection of the background. The installation of the Time Projection Chamber (TPC) is proposed as an upgrade option of the PHENIX experiment. TPC can identify the low momentum electrons from *dE/dx* measurements with a coverage of large acceptance. The proposed PHENIX-TPC has 35 cm drift length with full coverage in azimuthal angle and pseudo-rapidity coverage $|\eta| \leq 0.50$.

The PHENIX-TPC is expected to be mounted near the collision point. In Au+Au most central collisions at $\sqrt{s_{NN}}$ = 200 GeV, the charged particle density, dN_{rmch}/dy, is $\sim$ 600. Then, it is required to be capable of separating two hits which are as close as a few millimeters as well as good position resolution. In order to satisfy the requirement, pure CF_4 gas is chosen [4] as a chamber gas. From a simulation study, CF_4 is estimated to have small diffusion of ~ 100 μm for 1 cm drift at the electric field of 1 kV/cm.

3. Development of Prototype TPC using CF_4

A prototype TPC was developed to investigate the basic characteristics of CF_4 and the TPC performance. In order to use CF_4 as a chamber gas, the drift cage was designed to be able to sustain the field of more than 900 V/cm in order to achieve saturation of drift velocity. Basic properties of CF_4 were measured with laser and X-ray source [5]. As a result of the laser test, the longitudinal diffusion of CF_4 is 60 μm for 1 cm drift at the electric field of 900 V/cm.

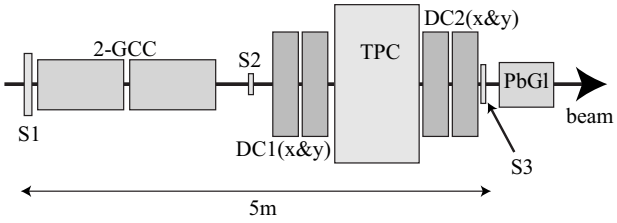

Figure 1. A schematic view of the beam test setup. TPC, three plastic scintillators (S1, S2 and S3), drift chambers (DC1 and DC2), a lead glass calorimeter (PbGl) and gas Cherenkov detector s(GCC) were used at the beam test.

4. Evaluation of the TPC Performance

For the evaluation of the prototype TPC performance, the beam test was carried out at T1 beam line of the Proton Synchrotron (PS) at High Energy Accelerator Research Organization (KEK). It was carried out with electron, pion, proton and deuteron beams in the momentum range from 0.5 GeV/c to 2 GeV/c.

Figure 1 shows a schematic view of detector setup. Drift chambers were used as a reference tracker. Gas Cherenkov detectors, scintillation counters and a lead glass calorimeter were used for particle identification.

Basic performances of the TPC such as a tracking resolution, a two hits resolution and a particle-identification capability from *dE/dx* measurements were evaluated.

4.1. Position resolution

The position resolution was measured for three type of pads: 2.5 mm, 6.0 mm and 9.5 mm square. The position resolution was calculated using the each positions, which were obtained with charge ratio method, of three adjacent layers. The resolution is defined by the difference between the position obtained at second layer and the position using the trajectory obtained from first and third layers.

Figure 2 shows the position resolution as a function of incident angle between beam and anode wires. A position resolution of 100 μm along the anode wire was achieved with 2.5 mm square pad. The resolution along the anode wire becomes worse as the input angle gets smaller. This is because induced charge distributes more broadly at small input angle.

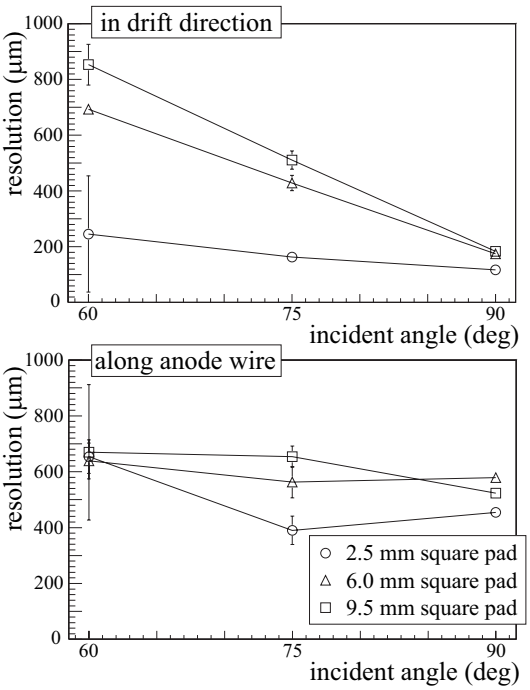

Figure 2. Position resolution as a function of the incident angle. The upper figure and the lower figure show the resolution along the anode wire and in the drift direction, respectively.

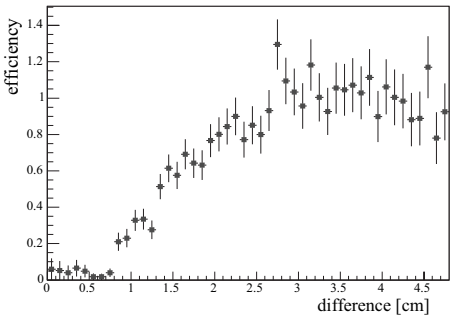

Figure 3. Efficiency of the two tracks identification as a function of difference in distance between two tracks.

4.2. Two hits resolution

In order to evaluate the two hits resolution, multiple tracks were generated by converting electron beams using a lead plate placed in front of the TPC.

The two hits resolution was evaluated as identification efficiency as shown in Fig. 3. The horizontal axis is the distance between the two tracks in the drift direction and the vertical axis is efficiency, which is obtained as the ratio of number of tracks identified in measurements over number of tracks estimated from GEANT simulation. Two hits can be completely resolved when they are separated in the drift direction by $>$ 2.8 cm. In Au+Au most central collisions at $\sqrt{s_{NN}}$ = 200 GeV, the average charged particle density is $\sim$ 0.4 cm^{-2} at the radial distance of 20 cm from the beam line. If the two hits resolution along the anode wire is less than 0.9 cm, charged particles are measured separately at the above condition.

4.3. Particle identification

The particle-identification capability was evaluated with electrons, pions, protons and deuterons. Incident particle

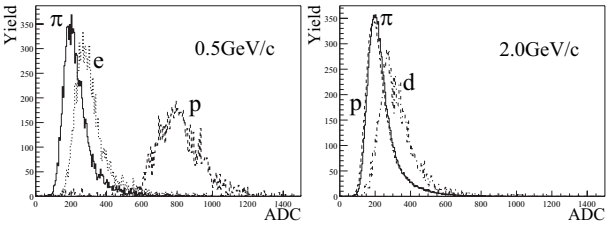

Figure 4. ADC sum distribution of each particle, electron, pion, proton and deuteron.

was identified by TOF measurements mainly. Figure 4 shows the ADC distributions for each momentum. The energy loss of the 5 cm track was obtained as the summation of the ADC value measured with 13 mm square pads.

From the result of ADC distribution, electron *dE/dx* dependence of momentum and rejection factor of pion are evaluated on the assumption that energy loss depends only on the velocity. The track length sampled with the PHENIX-TPC is 50 cm. The rejection capability of PHENIX-TPC can be estimated with a simulation that incorporates the results of the measurements. π meson can be rejected by a factor of 11 in the momentum range of $p \leq$ 110 MeV/c using this type of TPC, when electron efficiency of 92 % is chosen.

5. Summary

A prototype TPC using CF_4 was developed for the PHENIX upgrade. The tracking resolution, the two hits resolution and the particle-identification capability were evaluated with beam at KEK. We achieved 100 μm of position resolution with 2.5 mm square pad.

References

[1] K. Adcox *el al.*, Nucl. Instrum. Methods. A **499** (2003) 469.
[2] T. Hatsuda, Y. Koike and S. Lee, Phys. Rev. D **47** (1993) 1225.
[3] http://www.phenix.bnl.gov/phenix/WWW/TPCHBD/
[4] T. Isobe *el al.*, CNS Annual Report 2003 (2002) 39.
[5] J.Va'vra *et al.*, Nucl. Instrum. Methods. **324** (1993) 113.

Electron Identification Capability of the Prototype Transition Radiation Detector for the LHC ALICE Experiment

T. Gunji, H. Hamagaki, K. Ozawa, M. Inuzuka, A. Andronic[a], O. Busch[a], C. Garabatos[a], H. Appelshäuser[b], T. Mahmoud[b] and B. Vulpescu[b], for the ALICE TRD Collaboration

Center for Nuclear Study, Graduate School of Science, University of Tokyo
[a]Gesellschaft für Schwerionenforschung, GSI, Darmstadt, Germany
[b]University of Heidelberg, Germany

1. Introduction

High energy heavy ion collision is a unique tool to study QCD phase transition from the ordinary hadronic matter to plasma of de-confined quarks and gluons (QGP) in a laboratory. ALICE [1] is an experiment under preparation at Large Hadron Collider (LHC) at CERN, optimized for the study of heavy ion collisions at $\sqrt{s_{NN}}$ = 5.5 TeV.

The Transition Radiation Detector (TRD) [2] will be installed in the ALICE experiment for the purposes of electron identification and charged particle tracking.

It is required for the ALICE TRD to satisfy the pion misidentification probability of less than 1%, which corresponds to pion rejection factor of more than 100.

2. Prototype TRD

Transition radiation (TR) [3] is emitted when a highly relativistic charged particle traverses the boundary between two media with different dielectric constants. TR yield depends on γ factor of the charge particle. More than one TR photon can be emitted when γ factor is more than $\sim$1000, which corresponds to the electron momentum of $\sim$0.5 GeV/c and the pion momentum of $\sim$140 GeV/c. The average energy of emitted photons is $\sim$10 keV and the emission angle is $\sim 1/\gamma$ with respect to the particle trajectory.

A prototype TRD was developed based on earlier measurements [2, 4]. TRD is composed of a radiator and a drift chamber mounted behind the radiator. The radiator consists of multi-layered media of irregular polypropylene (PP) fibers of diameter 17 μm and has a total thickness of 4.8 mm. The drift chamber has a drift region of 30 mm and an amplification region of 7 mm, and is operated with Xe+CO_2 (15%) gas mixture for an effective detection of TR.

To evaluate the electron identification capability and tracking capability, 4 prototype TRD's were developed and were tested at CERN PS in October, 2003. The mixed beams of electrons and pions from 1 GeV/c to 6 GeV/c were used. Electrons and pions were separated with two air-filled Cherenkov counters and a Lead Glass calorimeter. The pion contamination in the identified electron events was $\sim 0.1\%$.

Figure 1 shows a typical (left) and an average (right) pulse height distribution as a function of drift time. There is a great difference in signal patterns between electrons and pions. A large spike can be seen only in electron events around the end of drift time. This is due toa an absorption of TR photons in the drift chamber.

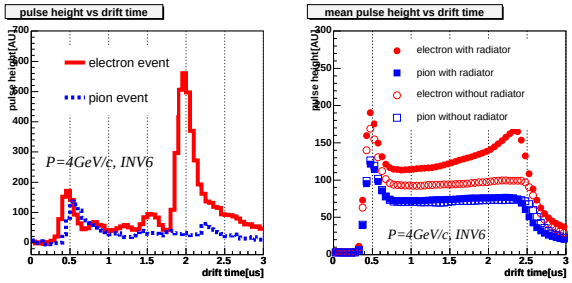

Figure 1. Pulse heights as a function of drift time for pions and electrons. Left and right panel show a typical and the average pulse height, respectively.

3. Analysis

Two analysis methods were applied to study the capability of electron identification. The Likelihood method has been applied in the analysis of electron identification with various TRD's [5]. The strategy and the analysis results are described in reference [6]. The pion rejection factor is achieved to be better than 100 for all momenta [6].

The second analysis method is Neural Network. The signal patterns are greatly different for electrons and pions as shown in Fig. 1. The existence of the large spike can be used to distinguish electrons from pions. Neural Network can be applied as a pattern recognition method. In this analysis, multi-layered feed forward network was used as shown in Fig. 2. The $6n$, $12n+1$ and 2 neurons were prepared for the

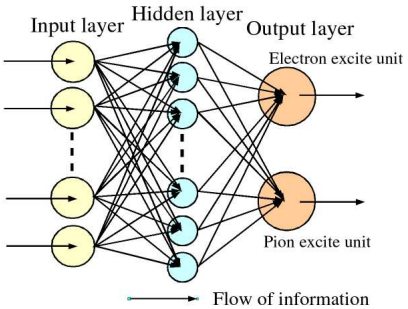

Figure 2. Multi-layered feed forward network applied in this analysis. Close circles correspond to neurons.

input, hidden and output layer, respectively. Here n means the number of TRD layers used to evaluate the pion rejection ($1 \leq n \leq 4$). One of the two neurons in output layer excites for electrons, called electron excite neuron, and the other for pions. Each neuron in input (hidden) layer connects to each neuron in hidden (output) layer with connec-

tion weights.

The input information fed into the input layer is described here in detail. Figure 3 shows pulse height distributions for electrons (solid) and pions (dashed) as a function of drift time. The drift time was divided into 6 regions. The integration of pulse heights in each time interval was fed into each neuron. Therefore, 6 (number of divided region) $\times$ n (number of TRD layers) neurons in input layer were prepared to evaluate the pion rejection for n TRD layers. The input information is the same as it was used in Likelihood analysis [6].

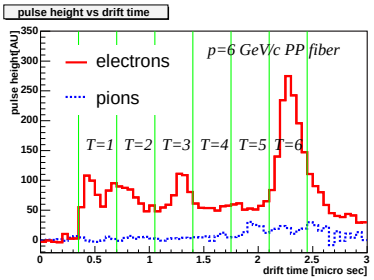

Figure 3. Pulse heights distributions as a function of drift time for electrons (solid) and pions (dashed). The drift region was divided into 6 regions.

Two data sets were prepared for electrons and pions. One was used for training network and the other was used to evaluate the pion rejection. Back-propagation algorithm [7] was used as the training algorithm. While the network is trained, the connection weights are updated for the output values to approach the expected values. The expected values of electron excite neuron are set to be 0.99 for electrons and 0.01 for pions.

Figure 4 shows the output distributions of electron excite neuron for training data after 10 (left) and 1000 (right) training cycles. Training cycle means how many times the training data is transfered to the network. The more times the network was trained, the clearer the separation became.

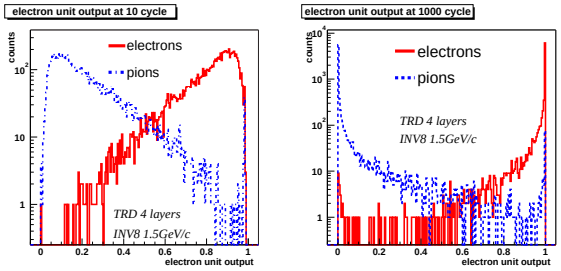

Figure 4. The output distributions of electron excite neuron at the training cycles of 10 (left) and 1000 (right). Solid and dashed line are for electrons and pions, respectively.

To evaluate the pion rejection, the other data set to evaluate the pion rejection was fed into the input layer. The output distributions of the electron excite neuron for 1 and 4 TRD layers are shown in Fig. 5. The arrow indicates the region where electron detection efficiency is 90%. Pion misidentification probability at electron detection efficiency of 90% is defined as the ratio of pion yields in that region to total pion yield. They become 31.0% and 2.1% for 1 and 4 TRD layers, respectively. After extrapolating to 6 TRD layers, the pion misidentification probability is achieved to be 0.32%, which corresponds to pion rejection factor of 313. The result of pion rejection factor based on Neural Network as a function of momentum is shown in Fig. 6. The result based on Likelihood method is also shown. Pion rejection factor is slightly improved by the Neural Network and it is demonstrated that Neural Network is useful for electron identification with TRD.

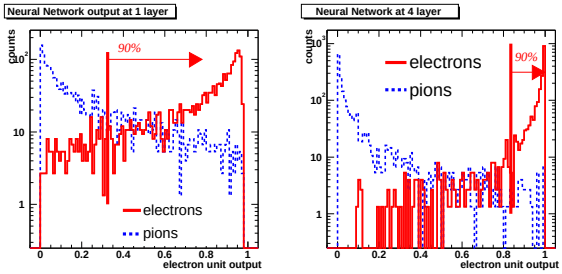

Figure 5. The output distributions of electron excite neuron for 1 (left) and 4 (right) TRD layers. Solid line and dashed line is for electrons and pions, respectively.

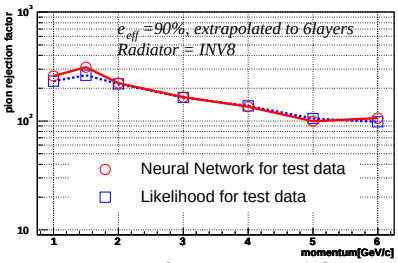

Figure 6. pion rejection factor extracted from Neural Network as a function of beam momentum (solid line). The likelihood results is also shown (dashed-line).

4. Summary

Electron identification capability of the prototype TRD has been studied by applying Likelihood method and Neural Network. Both analysis results show it meets the requirement of the ALICE TRD. Besides this result, it is demonstrated that Neural Network is also useful for the electron identification and that it will improve pion rejection by optimizing network structure and algorithm.

References

[1] ALICE Collaboration Technical Proposal, CERN/LHCC, 95-71.

[2] ALICE TRD Technical Design Report, CERN/LHCC, October 2001; http://www.gsi.de/˜alice/trdtdr.

[3] M.L. Cherry *et al*, Phys. Rev. D **10** (1974) 3594.

[4] A. Andronic *et al.*, Nucl. Instrum. Methods. A **498** (2003) 143.

[5] B. Dolgoshein, Nucl. Instrum. Methods. A **326** (1993) 434.

[6] T. Gunji *et al.*, CNS Annual Report 2002 (2003) 37.

[7] Carsten Peterson *et al*, Comput. Phys. Commun. **81** (1994) 185.

Development and Application of Gas Electron Multiplier (GEM)

M. Inuzuka, H. Hamagaki, K. Ozawa, T. Sakaguchi, F. Kajihara, T. Gunji, T. Isobe, N. Kurihara, S. Oda, Y. Yamaguchi, T. Tamagawa[a], S. Sawada[b] and S. Yokkaichi[a]

Center for Nuclear Study, Graduate School of Science, University of Tokyo
[a]RIKEN (The Institute of Physical and Chemical Research)
[b]High energy accelerator Research Organization (KEK)

1. Introduction

Gas Electron Multiplier (GEM) is a metalized polymer foil with holes [1]. The metal layers play a role of electrodes and a few hundred volts are applied between them. When a drift electron passes through the holes on a GEM, strong electric field inside the holes induces a cascade of electrons. This is the mechanism of the signal amplification by means of a GEM.

We succeeded in producing GEM foils using the plasma etching technology in Japan. In this note, development of GEMs and studies for applications to detectors in physics and medical fields are described.

2. Production of GEM and application to HBD

2.1. Production with the plasma etching method

The essential point in the production is the choice of technology for piercing metalized polymer foils. Hereafter, the GEMs produced at CERN and at CNS are referred to as 'CERN-GEM' and 'CNS-GEM', respectively.

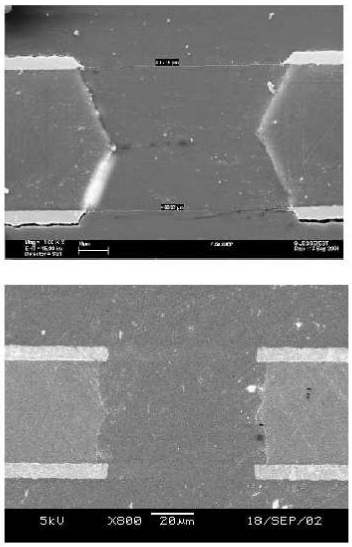

Figure 1. The upper and lower photographs are the hole of CERN- and CNS-GEM, respectively.

The standard CERN-GEM consists of $50\,\mu$m Kapton[1] coated with $5\,\mu$m copper, and the pitch and diameter of the holes are $140\,\mu$m and $70\,\mu$m, respectively [2]. After making holes on copper layers by conventional photolithography, the foil is immersed in a specific solvent, which dissolves Kapton. The CERN-GEM has holes with a double-conical shape (the upper photograph in Fig. 1).

[1]Tradename of Du Pont Co., Wilmington, DE, USA

On the other hand, CNS-GEMs were produced using the plasma etching method at Fuchigami Micro Co., Ltd.[2] [4]. The lower photograph in Fig. 1 shows a hole of CNS-GEM.

2.2. Gain characteristics and discharge problem

As was reported in the reference [4], the gain characteristics of CNS-GEMs were measured in argon mixtured gases. The performance of the CNS-GEM is comparable to that of CERN-GEM.

2.3. Improvement of plasma etching method

Since holes with a cylindrical shape might result in better electron transmission and less probability of charging-up [3], the plasma etching procedure has been re-optimized. Figure 2 shows a hole of new CNS-GEM. In total, 10 CNS-GEMs were produced; usually they can hold at more than $550\,$V in N_2 and stable operation is realized in argon mixtured gas. However, some of them were damaged during measurements. Detailed studies with more samples are necessary.

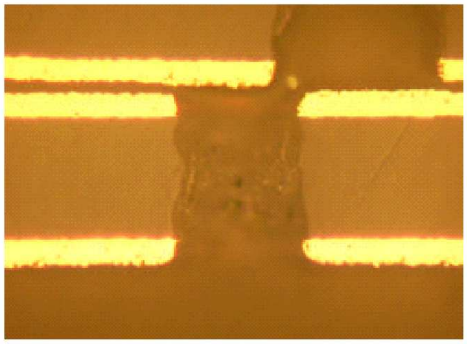

Figure 2. A hole of a new CNS-GEM.

3. Beam test of prototype HBD at KEK

In the PHENIX experiment, it is proposed to install a Hadron Blind Detector (HBD) in 2006. It is to improve electron identification capability and rejection of electron pairs from Dalitz decay and photon conversion. A schematic view of the HBD is shown in Fig. 3. The HBD is composed of (1) a Cherenkov radiator part and (2) a photon-to-electron convertor and an electron multiplication part. The latter is formed by three layers of GEM and the top surface is coated with CsI. When charged particles pass the detector, electrons are created above the top GEM due to energy loss. These electrons are drifted to the opposite direc-

[2] Fuchigami Micro Co., Ltd.: 3-1 Nanei Kagoshima 891-0122, Japan.

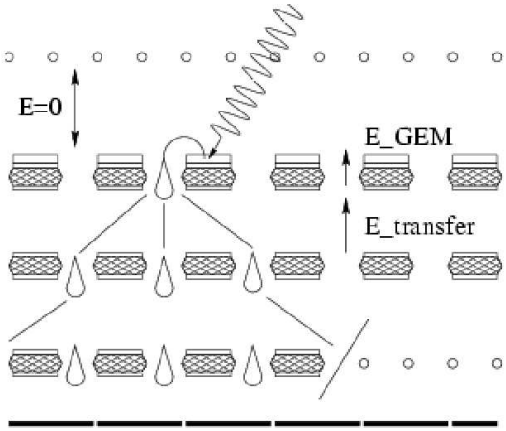

Figure 3. A schematic view of the HBD.

tion by applying the negative drift field. On the other hand, when electrons pass the radiator and emit Cherenkov lights, electrons are created on surface of CsI by photoelectric effect. These electrons are amplified by GEMs and detected at the readout pads. Thus, the HBD can identify electrons.

We constructed a prototype of HBD and tested it at the KEK testbeam facility (from June 25th to July 1st in 2003). The CsI evaporation was done by HAMAMATSU on CNS-GEMs. However, after the evaporation, the resistance between electrodes showed low values and could not be used in this beam test.

The measurements were carried out to check the haron blindness using CNS-GEMs without CsI evaporation. The gas filled in the detector was Ar(90%)-CH_4(10%) and V_{GEM} was 335 V. The drift field was controlled by applying voltage to the stainless mesh (3 mm upstream of the top GEM), V_{MESH}. Figure 4 shows the fraction of events detected by the HBD as a function of V_{MESH}. The circles and triangles in Fig. 4 are for 0.5 GeV of pions and protons, respectively. When $V_{MESH} = +200$ V, 97% of pions and protons were detected, while more than 95% were rejected when V_{MESH} is less than 0 V.

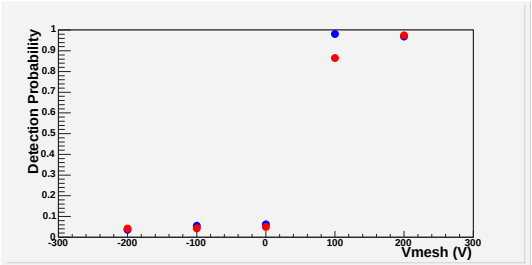

Figure 4. Detection probability as a function of V_MESH.

4. Application in medical field

Not only for the physics research, GEMs also could be powerful tools in the medical field, for example, two-dimensional X-ray radiography and radiation therapy beam monitoring. Considering the application in the medical field, it is necessary to detect high energy X-rays (about 100 keV), whose absorption length is the order of 100 m in one atomosperic Ar gas. In order to develop a detector with realistic size, one of the solutions is to choose heavy noble gas like Xe.

For this purpose, measurements with Xe was just started using CERN-GEMs. Figure 5 shows ADC spectra for V_{GEM} = 395, 400 and 405 V. The signal source was ^{55}Fe. Three peaks can be seen in the case of V_{GEM} = 405V. Assuming the peak at the highest ADC value corresponds to 5.9 keV, the rest two peaks can be explained as escape peaks of M- to L- and L- to K-shell transitions. However, the gain obtained from these results is an order of magnitude high compared with results by A.Orthen *et al* [6]. Further studies are ongoing.

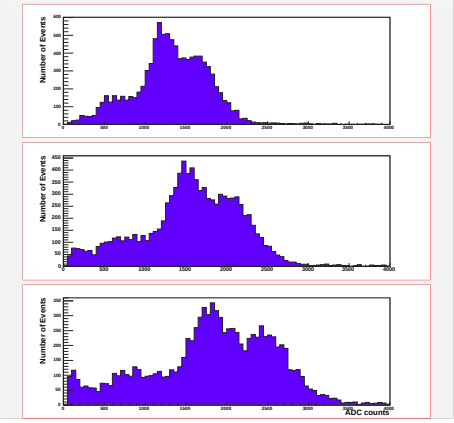

Figure 5. ADC spectra obtained from Xe gas.

5. Summary

The Gas Electron Multiplier, GEM, was produced using the plasma etching method. A prototype HBD was constructed and tested at the KEK testbeam facility. The performance of hadron blindness was confirmed. In addition, a study of gain characteristics using Xe was just started considering application to device in medical field.

References

[1] F. Sauli, Nucl. Instrum. Methods. A **386** (1997) 531.
[2] S. Bachmann *et al.*, Nucl. Instrum. and Methods. A **438** (1999) 376.
[3] F. Sauli *et al.*, IEEE Nuclear Science Symposium (Norfolk, November 12-14, 2002).
[4] M. Inuzuka, H. Hamagaki, K. Ozawa, T. Tamagawa and T. Isobe, Nucl. Instrum. and Methods. (in press).
[5] F. Sauli, CERN Yellow Report **77-09** (1997).
[6] A. Orthen et al., Nucl. Instrum. and Methods. A **512** (2003) 476.

Development of a Time Projection Chamber using Gas Electron Multipliers as Readout (GEM-TPC)

S.X. Oda, H. Hamagaki, K. Ozawa, M. Inuzuka, T. Isobe and Y.L. Yamaguchi[a]

Center for Nuclear Study, Graduate School of Science, University of Tokyo
[a] Waseda University

1. Introduction

At a high energy heavy ion collision experiment and a future e^+e^- linear collider, a central tracking detector with superb momentum resolution, good multi track separation and fine dE/dx measurement under high particle rate circumstances is needed. A time projection chamber (TPC) with micro-pattern gas detectors (MPGDs), such as gas electron multipliers (GEMs) or a Micromegas, is a leading candidate for the central tracking detector.

For signal amplification, a traditional TPC uses anode wires, while a TPC with GEM readout (GEM-TPC) uses GEMs. The GEM is a metalized $\sim$50 μm-thick polyimide foil with holes (see Fig. 1). The typical diameter and pitch of holes are 70 μm and 140 μm respectively. High electric fields are realized inside the holes with relatively low voltage difference between the both sides of the GEM, and the charge multiplication is induced inside the holes. The GEM can be used in multi structure, a double GEM or a triple GEM, for large gain ($\sim 10^4$) with low discharge probability. When cascaded electrons approach readout pads, positive charges are induced on the readout pads and negative charges flow into preamplifiers and are amplified.

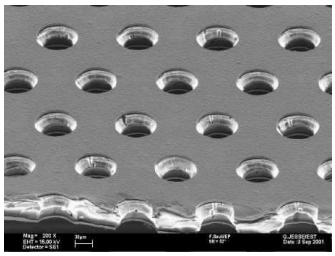

Figure 1. A microscope photograph of a GEM foil [1].

The GEM-TPC is expected to have improved position resolution than the traditional TPC. Since the GEM has two dimensional symmetry, dependence on incident angles of particles will be reduced than wire. And, because the intense electric field region will be limited in the holes, $\mathbf{E} \times \mathbf{B}$ effect is expected to be also reduced. Furthermore, the positive ion feedback to the drift region will be dramatically suppressed by structure of the GEM. Therefore gating grids will be unnecessary and the GEM-TPC can be realized with the low amount of material.

2. Development of a prototype of GEM-TPC

2.1. Structure of a prototype of GEM-TPC

A prototype of GEM-TPC has been constructed. It consists of an endcap and a field cage (36 cm length and 17$\times$17 cm^2). The endcap is shown in Fig. 2. The endcap can mount either a triple GEM (the effective area is 10$\times$10 cm^2) or wires on readout pads. The readout pads are made of gold-plated copper and those shapes are square (13$\times$13 mm^2). The field cage creates a uniform electric field to drift electrons produced by charged particles. The field cage consists of 115 gold-plated copper strips on FR4 boards. The strips are connected in series with 1 MΩ resistors. At the end of the resistor chain, resistors can be adjusted to equalize the potential of the field cage to that of the endcap on the surface of the top GEM. Since the area of the GEM is smaller than the cross section of the field cage, an end plate was added to prevent leakage of the electric field. High voltages are applied to the GEMs through connectors penetrated the endcap.

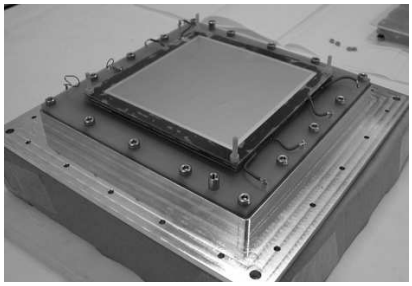

Figure 2. The endcap of the GEM-TPC with the triple GEM and the readout pads, without the end plate.

2.2. X-ray source test of the triple GEM

In order to verify the triple GEM mounted on the endcap works properly, ^{55}Fe X-ray (5.9 keV) signals were measured with Ar (90%) + CH_4 (10%) mixture (P10) gas and pure CF_4 gas at several points of V_{GEM}, the voltage difference between the both sides of the GEM. Charge sensitive preamplifiers were used in the measurement. The obtained spectrum with CF_4 is shown in Fig. 3. The energy resolu-

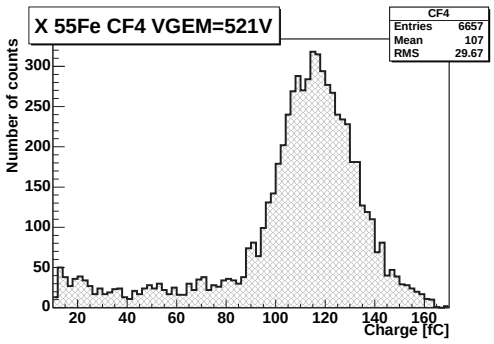

Figure 3. ^{55}Fe X-ray charge spectrum with CF_4 at $V_{GEM} = 521$ V.

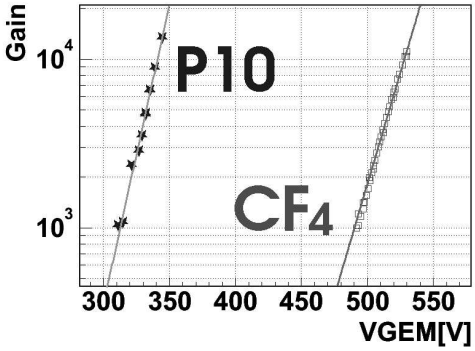

Figure 4. The gain curves of P10 and CF_4. The horizontal axis is the difference of voltages between both sides of a GEM and the vertical axis is the gain.

tion with P10 and CF_4 is 11% and 13% respectively. Gain curves of P10 and $CF_4$are shown in Fig. 4 and they agree with published results [2, 3].

2.3. Laser test of the prototype of the GEM-TPC

The GEM-TPC was tested with a nitrogen laser ($\lambda = 337$ nm) and P10 gas. The laser signals were divided into two parts. One part of signals entered the GEM-TPC and ionized gas. The created electrons drifted to the endcap, were multiplied in the GEMs and were collected on the readout pads. The rest of the laser signals entered a photo diode for trigger. Figure 5 shows the arrangement of the readout pads (top) and a snapshot of an oscilloscope (bottom). GEM-TPC signals coincide with a trigger signal. This is the first signal from our GEM-TPC.

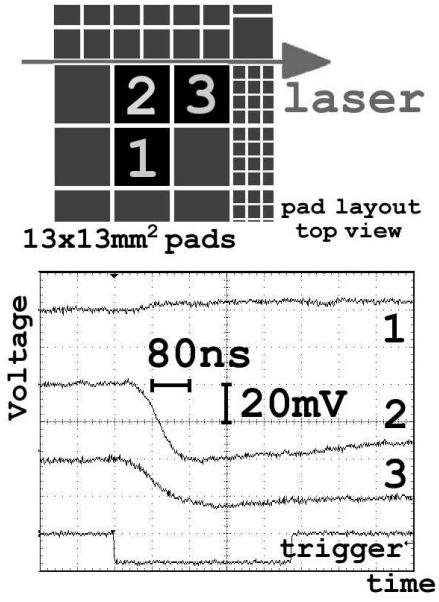

Figure 5. The arrangement of the readout pads (top). The first signal of the GEM-TPC with P10 gas (bottom). $V_{GEM} = 350$ V and $E_{drift} = 220$ V/cm.

3. Summary

We have constructed the prototype of the time projection chamber with GEM readout. It has been tested with a laser and it worked properly.

4. Outlook

In order to achieve better position resolution, the shape of readout pads will be modified from square to rectangular and chevron (zigzag) (see Fig. 6). Narrow strip pads are required for charge sharing with small diffusion gas, such as CF_4. Chevron pads will be more favorable for charge sharing than rectangle pads.

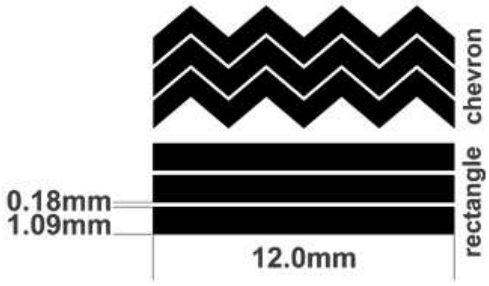

Figure 6. Shapes of new readout pads for the GEM-TPC.

A beam test will be performed at a secondary beam line of KEK 12 GeV proton synchrotron to test the performance of the GEM-TPC on May 2004. Test items are as follows;

- Efficiency
- Position resolution
- Two track separation power
- Space charge effect
- Dependence
  - Gas [P10, Ar (70%)+C_2H_6 (30%) and CF_4]
  - Pad shape (rectangle and chevron)

In order to achieve excellent spatial resolution, good two track separation and fine dE/dx measurements with large number of channels, high speed, low noise and compact readout electronics are needed.

References

[1] The Gas Detectors Development Group at CERN (http://gdd.web.cern.ch/GDD/).
[2] M. Inuzuka *et al.*, CNS Annual Report 2002 (2003) 35.
[3] A. Breskin *et al.*, Nucl. Instrum. Methods. A **483** (2002) 670.

Accelerator and Instrumentation

Improvement of the Hyper ECR Ion Source for Production of Metallic Ions and Extraction of Ion Beam

Y. Ohshiro, S. Watanabe, S. Yamaka and T. Katayama

Center for Nuclear Study, Graduate School of Science, University of Tokyo

1. Introduction

A Hyper ECR ion source [1] and a 10 GHz ECR ion source have been operated alternatively to deliver the beams for the RIKEN AVF cyclotron. The Hyper ECR ion source delivers gaseous ions such as $^{12}C^{4+}$, $^{13}C^{4+}$ and $^{14}N^{5+}$. In this year, a solid material insertion system (called a rod insertion system) and a beam extraction system (named an ion decelerator) were installed in the Hyper ECR ion source. With these devices, metallic ion beams, for example $^{24}Mg^{7+}$ and $^{7}Li^{2+}$ was extracted in the Hyper ECR ion source, which enabled to deliver the intense metallic ion beams to a CRIB [2].

2. Metallic ion production

The metallic ion was produced by a rod insertion method that is used routinely in the 10 GHz ECR ion source. A rod-shaped solid material is inserted near the ECR zone from the gas inlet side along the axis of the Hyper ECR ion source. The solid material was heated and ionized by the ECR plasma. The specifications of the rod insertion system are shown in Table 1.

We carried out the metallic ion production with the ion species of $^{24}Mg^{7+}$, $^{24}Mg^{5+}$ and $^{7}Li^{2+}$. The charged materials used the rod of a solidified MgO (in 6-cm long) and a crystal of LiF (in 5-cm long) for each ion production. After the rod was closed to the ECR plasma, the inside of the plasma chamber was baked for about four hours to remove residual gasses.

When the vacuum in the plasma chamber attained at the range of 10^{-7} Torr, the metallic ion was generated at the rod position to be apart about 20 mm from the boundary of ECR zone. The operating condition of the ECR ion source was as follows: the supporting gas used oxygen for magnesium ion and helium for lithium one. The RF (14.2 GHz) power was about 100 W. Two peaks of the mirror fields were 10.5 kG and 11.5 kG. The length of the ECR zone was about 7 cm. The beam intensities obtained as the initial test is summarized in Table 2.

Table 1. Specifications of the rod insertion system.

The attachable rod section	4 mm square
The attachable rod length	60 mm to 200 mm
Minimum operation speed	0.1 mm/h
Maximum operation speed	1.0 mm/h

Table 2. Metallic beam intensities obtained as initial test.

Ion species	$^{24}Mg^{7+}$	$^{24}Mg^{5+}$	$^{7}Li^{2+}$
Beam intensity (eμA)	3	5	10

3. Beam extraction by ion-decelerator

We replaced an extraction system from conventional type to the ion decelerator. The photograph of the new one is shown in Fig. 1. The electrodes goes and is arranged in the order of a negative electrode and a ground one from right-hand side. This unit is set near the anode electrode with the gap of about 45 mm between the anode electrode and the negative one. Beam goes through from right to left side.

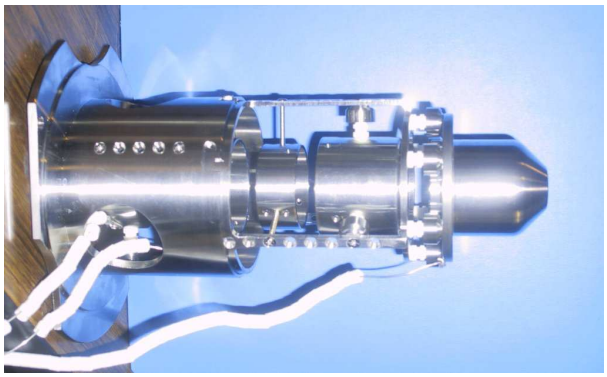

Figure 1. The decelerator unit set in the extraction chamber of the Hyper ECR ion source.

At this source, the ion beam has been extracted by the voltage of the range of 5 to 11 kV, because of these values are required by operating condition of the AVF cyclotron. With this new system, the extraction voltage can enhance up to 20 kV to increase the extraction beam intensity.

We investigated the voltage dependence of the beam intensity on the negative electrode, while the anode electrode that was 10 kV. In case of $^{14}N^{6+}$ and $^{14}N^{5+}$, the peak value of beam intensity was obtained on the negative electrode voltage of -5 kV (total 15 kV extraction) for $^{14}N^{6+}$, and -7 kV (total 17 kV one) for $^{14}N^{5+}$. Both ions, the beam intensity was found to increase nearly 2 times.

4. Conclusion

We completed the installation of the rod insertion and the ion deceleration system for the Hyper ECR ion source. It enabled to extract intense metallic ion beam from the Hyper ECR ion source.

References

[1] Y. Ohshiro *et al.*, RIKEN Accel. Prog. Rep. **36** (2003) 279.

[2] T. Teranishi *et al.*, CNS Annual Report 2001 (2002) 7.

RF Beam Buncher for the HiECR Ion Source

M. Watanabe[a], Y. Chiba[a], T. Katayama[a,b], T. Koseki[a], S. Yamaka[b], Y. Ohshiro[b] and S. Watanabe[b]

[a] *RIKEN (The Institute of Physical and Chemical Research)*

[b] *Center for Nuclear Study, Graduate School of Science, University of Tokyo*

1. Introduction

A broadband buncher cavity using MA (magnetic alloy) cores has been developed for an ion source named HiECR [1] in the CNS. The HiECR is intensively used for ion source research and also used for R&D's of ion beam monitors, which are applicable to the present and future cyclotrons. For the latter purpose, ion beam having bunched structure corresponding to the cyclotron frequencies is necessary.

We chose the Q-value of the buncher cavity less than 1 because of the required large frequency range from 18 to 45 MHz. In order to obtain a resonant frequency of 30 MHz, we adapted the cut core configuration [2, 3, 4] of MA to reduce the inductance of cavity.

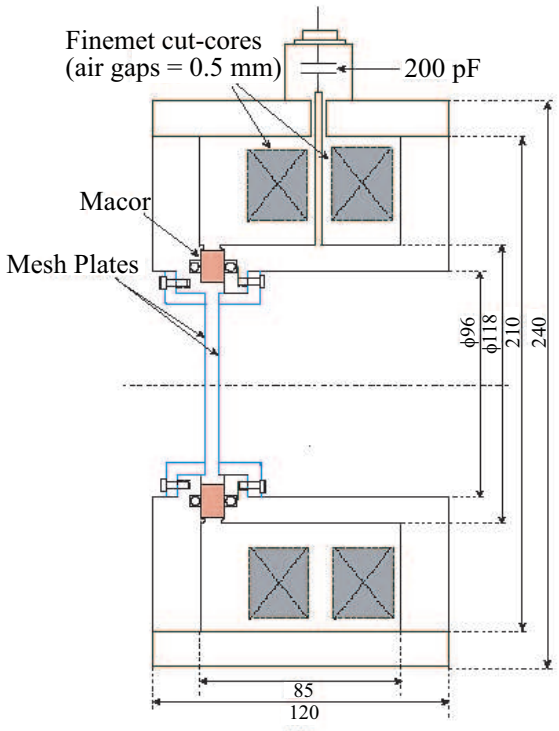

Figure 1. Cross-section of the buncher cavity.

2. Buncher cavity

Based on the rf characteristics measurement of MA cut cores [5], we designed and fabricated a compact buncher cavity. Figure 1 shows the cross sectional view of the cavity. Two parallel mesh plates made of copper are placed at the acceleration gap to increase the transit time factor. The mesh has hexagon shape [6] and distance between the mesh plates is 5 mm.

3. Beam test of the buncher cavity

The buncher cavity was installed in the beam transport line of the HiECR ion source system for performance study with real beams. Figure 2 shows typical beam current waveform using the buncher. The beam current was detected by a Faraday cup at 2.3 m down stream of the cavity. In this case, 10 keV proton beam with average current of 20 μA was used. Frequency and peak voltage of the rf cavity were 30 MHz and 150 V, respectively. As shown in the figure, beam structure of 30 MHz with the peak current of 32.5 μA was successfully obtained.

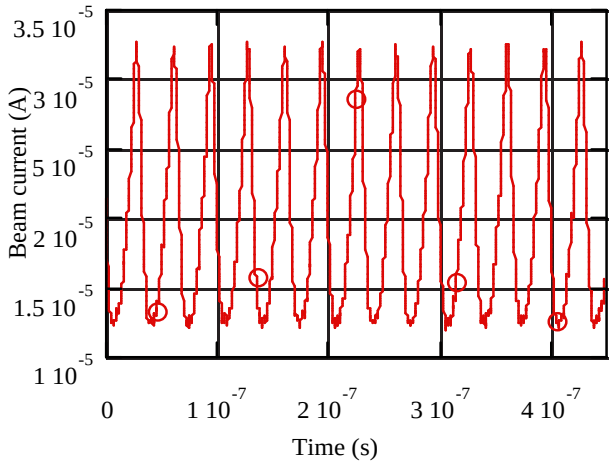

Figure 2. Bunched beam current waveform.

4. Summary

We have developed a buncher cavity using MA cut cores. It was installed in the beam transport line of the HiECR ion source system for the beam test. Beam structure of 30 MHz was successfully observed for 10 keV proton beam.

References

[1] S. Watanabe *et al.*, CNS Annual Report 2001 (2002) 47.

[2] M. Yoshii *et al.*, Proc. of EPAC2000 (2000) 984.

[3] J. Dey *et al.*, Proc. of PAC2001 (2001) 882.

[4] M. Watanabe *et al.*, RIKEN Accel. Prog. Rep. **36** (2003) 325.

[5] M. Watanabe *et al.*, Proc. of APAC 2004, Korea, to be published.

[6] K. Ikegami and A. Goto, RIKEN Accel. Prog. Rep. **22** (1988) 213.

Ion-milling Method for Strip Fabrication in Bi2223 for High Temperature Superconducting Application

S. Watanabe, T. Watanabe[a], T. Ikeda[a], Y. Ohshiro, S. Yamaka and T. Katayama

Center for Nuclear Study, Graduate School of Science, University of Tokyo
[a]RIKEN (The Institute of Physical and Chemical Research)

1. Introduction

A nondestructive beam current monitor based on the high temperature superconducting (HTS) technology has been developed [1]. Applied HTS material for the cylindrical current sensor is $Bi(Pb)_2$-Sr_2-Ca_2-Cu_3-O_x (Bi-2223) coated on a MgO substrate. The outer surface of cylindrical current sensor is divided by a slit. Separate outer surfaces are joined with a bridge to concentrate an image current from the ion beam. We have studied the bridge providing with a spiral coil structure. It is fabricated by the dry etching because order of 10-μm pitch of the spiral coil will be expected.

2. Ion milling method

A use of the beam from the HiECR ion source in the CNS is planned for milling the surface of the HTS material. Ion current density enabled it, as for the irradiation size of a beam, for this plan to realize 100 eμA/cm^2 by 10-mm diameter. The introductory mechanism of reactive gas is also examined so that ion beam milling may be performed early, and the kind of reactive gas was also examined to apply a reactive ion beam etching (RIBE). Since an irradiation sample was an oxide, it was examined also about the difference in each etching rate of a composition element (Bi, Sr, Ca, Cu and O). Although multi charged ion is taken out, deceleration electrode was considered in the irradiation system, and it enabled it to change the energy in this ion source.

3. Reaction chamber

A reaction chamber comprises a beam guide, gate valve, deceleration electrode, deflection electrode, vacuum pump, sample holder, Faraday cup, etc. Reactive-gas spraying equipment and a needle valve for controlling the etching rate on the surface of the sample are attached in the reaction chamber. A gas recovery instrument outside is equipped. XeF_2 as a neutral gas was already examined elsewhere for chemical etching. In Si, only in the case of an Ar^+ ion beam, XeF_2 has an etching rate remarkably early at a part for 70 Å/min compared with a part for 8 Å/min in the case of only Ar^+ ion beam [2]. We have introduced these physical and chemical reactions into the Bi2223. The reaction rate of a mask for preventing the ion beam irradiation plays a role to make fine slit pattern of Bi2223. The mask for the ion beam etching was tested using pure Ti slit for various ion beam milling.

4. Result

Ion milling of Bi2223 has been done with 10 kV Ar^{2+}, 40 eμA. The surface of irradiation sample is observed as Bi2223 layered grains. The layered grains mean a stack of flakes of Bi2223 with the sizes of $\sim$3-μm diameter. The reaction gas condition of XeF2 is of gas pressure = 6.2×10^{-6} Torr at 20°C (room temperature). Figure 1 shows etching depth of the surface of Bi2223. The etching depth of 5 μm and etching width of 100 μm are observed after beam irradiation time for 10 hours. The flatness of the surface seems to depend on the surface condition before the ion milling. We can observe the magnified surface with the EPMA (Electron Prove Micro-Analysis). It was observed that a flake of Bi2223 is melted and rolled due to the irradiation of ion beam. The composition of the irradiated Bi2223 is also analyzed by Specific X-ray photoelectron spectra. The quantity of the oxygen in the Bi2223 was measured by the EPMA.

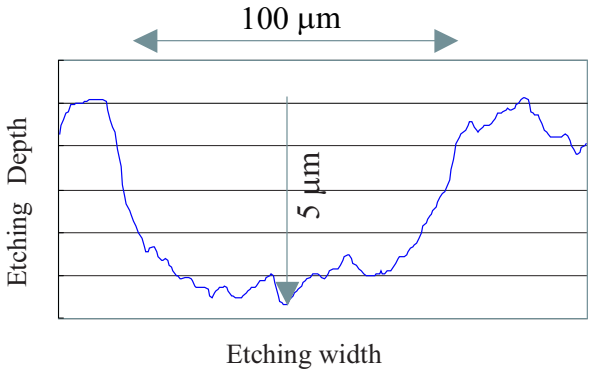

Figure 1. Etching depth of Bi2223 after Ar ion milling.

We have been studying the flatten beam irradiation to the sample, thin Bi2223 layers grain around 20-μm thickness, with increasing the irradiative ion beam current. The ion beam slit to make the pattern of spiral coil is one of the important issues. We have studied a thermal stress of the Ti slit in case of both the beam irradiation process and the machining process.

References

[1] T. Watanabe *et al.*, CNS Annual Report 2003 (2002) 71.
[2] T. Meguro and Y. Aoyagi, RIKEN Review **31** (2000) 48.

Study of Nano-Cluster Ion Source with Plasma-Gas-Aggregation Method

M. Imanaka, H. Arai[a], T. Nakagawa[b], C.-K. Chung[c], S.-M. Lee[c], Y. Ohshiro, S. Watanabe and T. Katayama

Center for Nuclear Study, Graduate School of Science, University of Tokyo
[a]Institute of Physics, University of Tsukuba
[b]RIKEN (The Institute of Physical and Chemical Research)
[c]Tsukuba Nanotechnology Co., Ltd.

1. Introduction

Science of nano-scaled structure is now a frontier of the solid state physics and electronics. For example, many researchers of solid state physics attempt to understand the evolution from atoms or molecules to bulk properties with increasing cluster size [1]. Understandably, the field of such clusters science depends strongly on the development of the nano-cluster ion source. Very often a development of the new techniques of the ion source gives rise to a quantum leap in the progress of the field.

Nano-cluster ion beam technology has been found to be able to offer solutions for a number of well-known problems associated with conventional monomer ion beam implantation [2]. Nano-cluster ion implantation has been found to offer implantation differences which are expected to lead to development of nano-cluster approaches as additional tools for device miniaturization.

Plasma-gas-aggregation is a very effective method to produce the large nano-clusters. Recently we have developed a magnetron type nano-cluster ion source, with plasma-gas-aggregation method, and successfully produced nano-cluster ion beam.

In this paper, we introduce the magnetron type nano-cluster ion source and experimental results that measured mass spectra of boron nano-cluster ions.

2. Experimental Setup

The schematic view of the magnetron type nano-cluster ion source is shown in Fig. 1(a). The nano-cluster ion source consists of a specially designed planar-type magnetron and an aggregation cell cooled by liquid nitrogen. Figure 1(b) shows schematically the magnetron head part. By suitable orientation of target magnets, a "race track" can be defined where electrons hop around at high speed. Target erosion by sputtering occurs within this track because ionization of the working gas is most intense above it.

The distance L between the magnetron and the exit slit (cell length) is controlled by a calibrated sliding rod attached the vacuum chamber. The aggregation cell has double cylindrical structure to allow cooling by direct contact with liquid nitrogen. Furthermore, at the end of the carrier gas stream, an iris diaphragm is installed to control the vapor pressure and stream velocity. Note that they are also controlled by adjusting the flow rate of the Ar and He gases with a mass flow controller. Generally, the gas aggregation process is performed under the vapor pressure of 0.1-2 Torr to obtain a sufficient high collision rate. The masses of produced nano-cluster ions are measured by Time Of Flight mass spectrometer (TOF-MS).

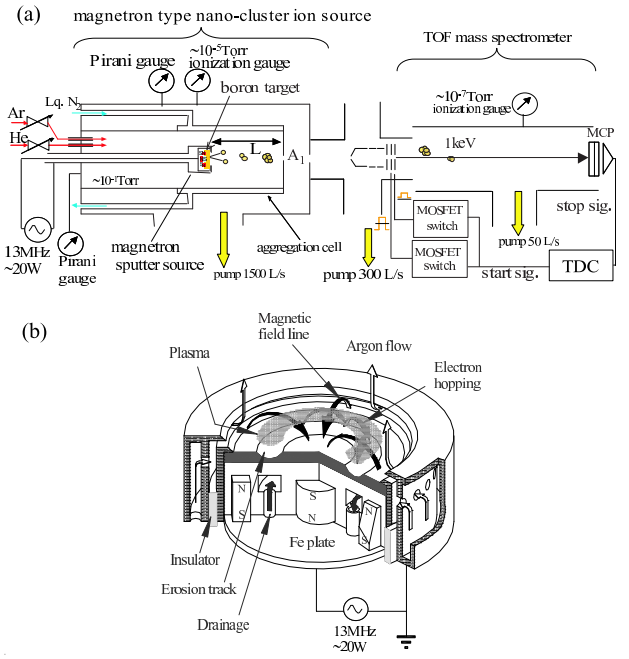

Figure 1. (a) Schematics of the magnetron nano-cluster ion source and TOF-MS system, and (b) schematic of magnetron sputter source.

Since the first report by Stephens [3], TOF mass spectrometry has become popular in the nano-cluster science. Several electrode of ion optics are driven with two MOSFET-switches synchronized with the start pulse. The total flight length is about 20 cm. The output signal from the micro channel plate (MCP) [4] is connected to the stop input of the multi-stop time to digital converter (TDC).

3. Results

Figure 2 shows a TOF mass spectrum of boron nano-cluster ions. The peaks of B^+, B_2He^+, B_3^+ and B_4^+ are identified. The reason why B_2^+ was not produced is that the binding energy between B and B^+ is very weak (0.8eV [5]). Additionally we can detect nano-cluster ions up to 150 amu, which corresponds to the mass of B_{13}^+, while the peaks around these masses can not be resolved.

The width of the peak in the mass spectrum Δm, that is proportional to square of the time distribution Δt, appearing on Fig. 2 is mostly caused by initial kinetic energy as acceleration of TOF-MS. Therefore, the initial kinetic en-

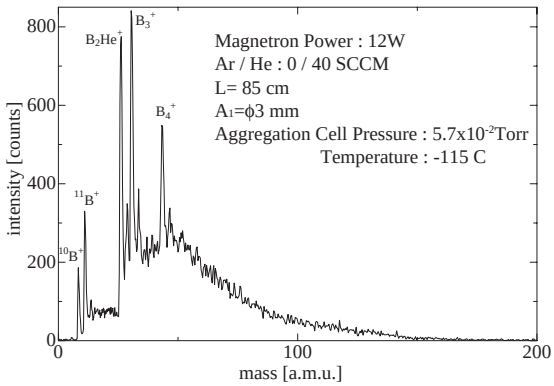

Figure 2. A mass spectrum of boron nano-cluster ions.

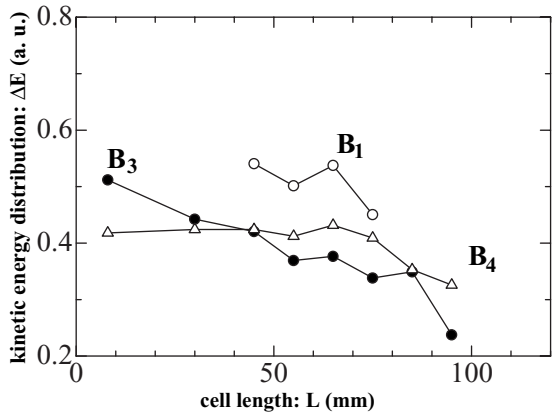

Figure 3. Relative energy distribution ΔE of B, B_3 and B_4 as a function of cell length L.

ergy distribution ΔE can be calculated from Δt. The calculated relative energy distributions ΔE of B, B_3 and B_4 as a function of cell length L are plotted in Fig. 3. The ΔE of all boron monomer and clusters decreases gradually with an increase of cell length L. These results suggest that boron nano-clusters are cooled by collision with condensation helium gas during the travel in aggregation cell. Consequently much kinetic energies of clusters are removed for longer L.

4. Conclusion

We succeeded to produce boron nano-cluster ion beam by using the nano-cluster ion source with plasma-gas-aggregation method. We recognized boron nano-clusters was cooled by collision with condensation He gas during traveling in the aggregation cell.

References

[1] H. Haberland, in Clusters of atoms and molecules I, edited by H. Haberland, Springer, Berlin (1995) 207.
[2] I. Yamada *et. al.*, Mater. Sci. Eng. R **34** (2001) 231.
[3] W. E. Stephens, Phys. Rev. **69** (1946) 691.
[4] J. L. Wizza, Nucl. Instrum. Methods. **162** (1979) 587.
[5] L. Hanley *et. al.*, J. Phys. Chem. **92** (1988) 5803.

Beam Dynamics and Instability during Final Beam Bunching for Heavy Ion Inertial Fusion

T. Kikuchi[a], T. Katayama, M. Nakajima[b] and K. Horioka[b]

Center for Nuclear Study, Graduate School of Science, University of Tokyo
[a]Department of Electric and Electronic Engineering, Utsunomiya University
[b]Department of Energy Sciences, Tokyo Institute of Technology

1. Introduction

Space-charge-dominated beam physics is crucial in heavy ion inertial fusion (HIF). In the HIF, energy of several MJ should be injected as a short time pulse to a fuel pellet. The target pellet irradiated by the energy driver is rapidly imploded. The implosion can cause a high energy density state at the center of the pellet, and a lot of thermonuclear reactions are expected under the state of the high temperature and density of the fuel plasma. The intense heavy-ion beam (HIB) is an influential candidate of the energy driver.

The required parameters for heavy ion beams are several GeV particle energy, 100 kA total current, and around 10 ns short pulse duration [1], and are far from those of conventional particle accelerator system. Therefore the beam dynamics and control are important research issues in HIF. In the final stage, the beam pulse must be longitudinally compressed from $\sim$100 to $\sim$10 ns [1, 2]. Induction voltage modulators, which have a precise waveform controllability, are proposed for this purpose [3]. For an effective pellet implosion, we should transport and compress the bunch of heavy ion beam with an emittance growth as low as possible. A final focus and beam irradiation are crucial, and a large emittance interferes the focusing to the small fuel pellet [4]. For this reason, the final beam bunching is a key technology in the HIF driver system.

Beam instability caused by a space charge oscillation imposes a limit on a strength of the HIB space charge effect. When the tune depression is lower than 0.4, the beam transport may be unstable due to the instability induced by the space charge effect [5]. In the region of final beam bunching, the intense HIB becomes the space-charge-dominated beam, and exceeds the threshold [6]. Not only the instability but also dilution of particle distribution can cause the emittance growth [7]. Nonequilibrium particle distribution will approach to a thermal equilibrium state during the final beam bunching.

In this study, we investigate the beam dynamics during the bunch compression in the final beam bunching and the final focus region. Multiparticle simulation using particle-in-cell (PIC) method with the longitudinal bunch compression model is carried out to investigate transverse particle behaviors [6, 8]. The emittance growth is observed and is compared with various types of the initial particle distribution. The particle distributions during the final beam bunching are also discussed by nonlinear field energy factors.

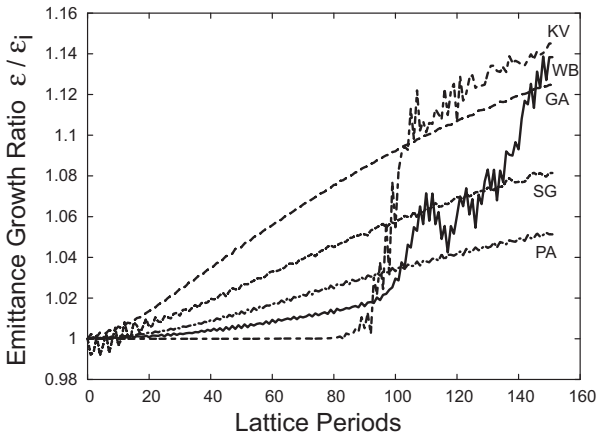

Figure 1. Emittance growth during the final beam bunching at each initial distribution.

2. Emittance growth during final beam bunching

The emittance value is used for the evaluations of beam transport quality. We define the average of unnormalized transverse rms emittance ϵ as

$$\epsilon = \frac{\epsilon_{x,rms} + \epsilon_{y,rms}}{2}, \tag{1}$$

where $\epsilon_{x,rms}$ and $\epsilon_{y,rms}$ are the unnormalized rms emittances for horizontal and vertical directions, respectively. The initial emittance is assumed as $\epsilon_{x,rms} = \epsilon_{y,rms} = \epsilon_i$ =10 mm mrad. The initial particle distributions are assumed as Kapchinskij-Vladimirskij (KV), waterbag (WB), Gaussian (GA), semi-Gaussian (SG), and parabolic (PA) distributions. At each initial distribution, the evolution of the emittance growth ϵ/ϵ_i, which indicates the ratio of the average emittance to the initial one at each lattice period, is shown in Fig. 1. As shown in Fig. 1, the emittance abruptly increases after 80 lattice periods in the case of the initial KV beam. Similar to the result of KV distribution, the emittance at the initial WB beam is steeply increased after 90 lattice periods. These rapid emittance increases are confirmed as a result of the beam instability due to the strong space charge effect during the final beam bunching [6]. On the other hand, the initial GA, SG, and PA beams cause the gradual increase of the emittance without abrupt growth. The final emittance growth ratios at 150 lattice periods are around 1.15, 1.14, 1.12, 1.08 and 1.05 in the initially KV, WB, GA, SG, and PA distributed beams, respectively.

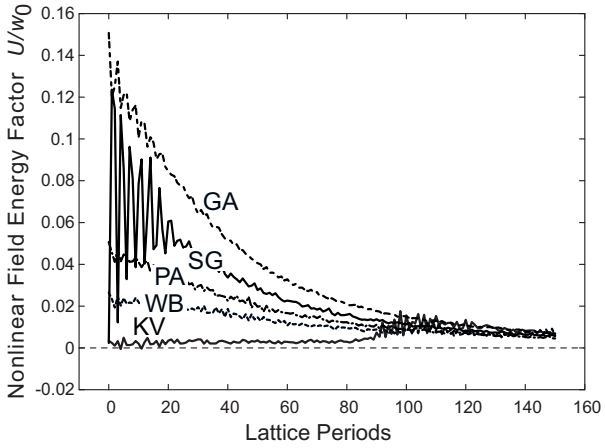

Figure 2. Nonlinear field energy factor during the final beam bunching at various initial distributions.

3. Particle distributions during final beam bunching

The particle distribution inside one beam is also important for the uniformity of beam irradiation in a low-number beam system [4]. As a figure of merit for the uniformity of charge distribution in real space inside one beam, the nonlinear field energy factor is defined by U/w_0 [9, 10]. The field energy difference U is given by

$$U = w_n - w_u, \tag{2}$$

where w_n and w_u are the field energies per unit length in the cases of nonuniform and uniform beams, respectively. The field energy per unit length within the actual beam volume is written as [9, 10]

$$w_0 = \frac{I^2}{16\,\pi\,\epsilon_0\,v_z^2}, \tag{3}$$

where I is the beam current, ϵ_0 is the permittivity of free space, and v_z is the longitudinal beam velocity, respectively. The nonlinear field energy factor expresses the degree of uniform charge distribution in real space, i.e., the charged particles are distributed uniformly if $U/w_0 = 0$. Figure 2 shows the nonlinear field energy factor given by PIC simulations during the longitudinal bunch compression [11]. Although each of the distributed beams has various nonlinear field energy factor at the initial condition, the factors approach zero after the final beam bunching as shown in Fig. 2. As a result, the transverse particle distribution in real space approaches uniform density during the final beam bunching [11].

4. Summary

In this study, the transverse beam dynamics was investigated during the final beam bunching in a HIF driver system. The transverse PIC simulation with the increase in the beam current was carried out for the study of the beam transport as a model of the longitudinal bunch compression.

Although the initially KV and WB distributed beams cause an abrupt emittance growth due to the instability induced by the space charge effect, it is expected that the initial GA, SG, and PA beams may pass through the final bunching region without the instability excited by space charge oscillation. The emittance growth is estimated to be 15% at the highest in this study.

The nonlinear field energy factors indicated that the transverse particle distribution inside a beam bunch approaches uniform after the final beam bunching. The particle distribution after the final beam bunching becomes independent of the initial distribution.

References

[1] J.J. Barnard, *et al.*, Nucl. Instrum. Methods. A **415** (1998) 218.
[2] J.J. Barnard, *et al.*, Phys. Fluids B **5** (1993) 2698.
[3] K. Horioka, *et al.*, Nucl. Instrum. Methods. A **415** (1998) 291.
[4] T. Someya, A.I. Ogoyski, S. Kawata and T. Sasaki, Phys. Rev. ST Accel. Beams **7** (2004) 044701.
[5] I. Hofmann, *et al.*, Part. Accel. **13** (1983) 145.
[6] T. Kikuchi, M. Nakajima, K. Horioka and T. Katayama, Phys. Rev. ST Accel. Beams **7** (2004) 034201.
[7] T. Kikuchi, M. Nakajima and K. Horioka, J. Plasma Fusion Res. **79** (2003) 105.
[8] S.M. Lund, O. Boine-Frankenheim, G. Franchetti, I. Hofmann and P. Spiller, Proceedings of the 1999 Particle Accelerator Conference, New York, March 1999, p.1785.
[9] M. Reiser, *Theory and Design of Charged Particle Beams*, Wiley, New York, (1994).
[10]M. Reiser, J. Appl. Phys **70** (1991) 1919.
[11]T. Kikuchi, M. Nakajima, K. Horioka and T. Katayama, J. Plasma Fusion Res. **80** (2004) 87.

Feasibility Study of Mass Measurement Using the RIKEN Cyclotrons

M. Fukuda[ac], S. Kubono[a], T. Teranishi[d], M. Notani[a], S. Nishimura[b], M. Nishimura[b], M. Terasawa[a], T. Suda[b], S. Kato[e], E. Ideguchi[a] and A. Goto[b]

[a] *Center for Nuclear Study, Graduate School of Science, University of Tokyo*
[b] *RIKEN (The Institute of Physical and Chemical Research)*
[c] *Takasaki Radiation Chemistry Research Establishment, JAERI*
[d] *Department of Physics, Kyushu University*
[e] *Department of Physics, Yamagata University*

1. Introduction

Investigation of heavy-element nucleosynthesis [1] is required for understanding the mechanism of stellar events and cosmo-chronology. The rapid neutron capture process (r-process) is one of the dominant process for the heavy element nucleosynthesis. The r-process path runs in a very high neutron?density region far away from the stable nuclei. Difficulties lie in experimental simulation of the nucleosynthesis in the r-process using accelerators, since heavy neutron-rich nuclei with very short life time are synthesized one after another by neutron capture before occurring beta-decay. Not only basic parameters of masses and half lives but also level densities and neutron capture rates should be determined to investigate the r-process path.

Mass resolution less than $\Delta M/M = 1 \times 10^{-5}$ is required to identify the neutron-rich nuclei in the r-process region. The mass resolution of a typical time-of-flight (TOF) method, one of mass analysis techniques, is limited to around 1×10^{-4} by the length of the flight path and the time resolution of a particle detector system. In order to improve the precision of the mass analysis using the TOF method, a cyclotron can be used as a high resolution mass spectrometer, since a total flight path length amounts to a few kilometers [2]. The precision in the measurement of the mass difference achieved at GANIL was estimated to be better than 10^{-6}.

In this work, feasibility of the mass analysis using the RI beam factory (RIBF) at RIKEN, has been explored for the identification of neutron-rich nuclei. The most possible system is a coupling of a K980-MeV ring cyclotron (IRC) and a K2500-MeV superconducting ring cyclotron (SRC). The mass resolution of the SRC has been estimated from its design parameters.

2. Principles of the TOF Mass Analysis Combined with a Cyclotron

In general, the flight time of particles is expressed by

$$t = \frac{m_0}{p} LM, \tag{1}$$

where m_0 is the atomic mass unit, p a momentum, L a flight path length, M a mass number. Assuming that the momentum and the flight path length are the same for any particles passing through a momentum analyzer, the mass difference

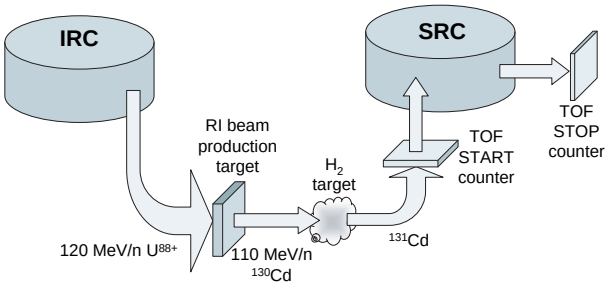

Figure 1. Schematic diagram of the mass analysis system using the SRC.

of the particles is given by the flight time difference as

$$\frac{\Delta M}{M} = \frac{\Delta t}{t}. \tag{2}$$

Higher mass resolution can be obtained by improving the resolution of a flight time measurement and by increasing the flight time, namely, the flight path length.

A cyclotron is a high resolution mass spectrometer with a long flight path length. A particle revolution time in a cyclotron is kept constant by an isochronous condition given by

$$2\pi \frac{f_{RF}}{h} = \frac{B_0}{m_0 c^2} \frac{Q}{M}, \tag{3}$$

where f_{RF} is a radio frequency, B_0 an averaged magnetic field, h an acceleration harmonic number, Q a charge state of a particle. A flight time from injection to extraction in a cyclotron, that is, the total revolution time, is proportional to a total turn number, given by

$$t = N \frac{h}{f_{RF}}, \tag{4}$$

where N is a total turn number. ¿From the Eqs. (2) and (4), the resolution of the mass-to-charge ratio can be evaluated from

$$\frac{\Delta(M/Q)}{M/Q} = \frac{f_{RF}}{hN} \Delta t. \tag{5}$$

In this case, the Δt is given by a time resolution of a particle detection system.

3. Mass Resolution Estimation for the IRC and the SRC

A schematic diagram of the TOF mass analysis system is shown in Fig.1. RI beams used for the r-process path investigation will be generated by projectile fragmentation using

a primary 120 MeV/nucleon U^{88+} beam extracted from the IRC. For example, the neutron-rich nuclei like ^{131}Cd will be obtained by the nuclear reaction of $H_2(^{130}Cd,p)^{131}Cd$, using a 100 MeV/nucleon ^{130}Cd beam produced by the 120 MeV/nucleon U^{88+} beam. The mass analysis for identification of the neutron-rich nuclei will be carried out by the TOF method combined with the SRC.

The main parameters of the SRC are listed in Table 1. Assuming that the time resolution of the detector system is Δt = 100 ps in the Eq. (5), the mass-to-charge ratio resolution of the SRC is estimated to be 1.4×10^{-6}. This resolution meets the requirement for the identification of the neutron-rich nucleus.

A detailed design of the TOF mass analysis system is in progress.

Table 1. Parameters of the SRC.

K-number	2500
Sector number	6
Diameter (cm)	1900
Maximum magnetic field (T)	3.8
Average injection radius (m)	3.56
Average extraction radius (m)	5.36
Acceleration frequency (MHz)	18 to 38
Harmonics	6
Cavity number (fundamental)	4
Cavity number (flattop)	1
Cavity voltage (kV/cavity)	500
Acceleration voltage (kV/turn)	2000
Accelerated Ion : Cd	131
Charge state	48
Energy (MeV/nucleon)	350
Acceleration frequency (MHz)	36.7

References

[1] S. Kubono, Nucl. Phys. A **693** (2001) 221.

[2] G. Auger *et.al.*, Nucl. Instrum. Methods. A **350** (1994) 235.

Velocity Separation Test of CRIB Wien Filter

T. Teranishi, S. Kubono, J.J. He, M. Notani, N. Yamazaki, M. Niikura, S. Nishimura[a], M. Nishimura[a] and S. Michimasa[a]

Center for Nuclear Study, Graduate School of Science, University of Tokyo
[a]RIKEN (The Institute of Physical and Chemical Research)

1. Introduction

A Wien filter system was developed for the CRIB radioactive-ion beam separator [1, 2, 3, 4]. The CRIB separator has a momentum dispersive focal plane (F1), where a slit is set to select a magnetic rigidity ($B\rho$) of particles. The second focal plane F2 is designed to be achromatic and used as a site for experiments. Recently, the Wien filter system was built as an extension of CRIB after F2. The Wien filter system is 5-m long and consists of four quadrupole (Q) magnets and a velocity separation section of 1.5-m long placed between the second and the third Q magnets. At the velocity separation section, a magnetic field and an electric field are superimposed perpendicularly to each other. The new focal plane after the Wien filter system is called F3. Ions that reach F2 have roughly the same magnetic rigidity. Therefore, with the velocity separation after F2, CRIB can select ions by the mass-to-charge ratio A/q. If a secondary ion of interest and a major contaminant have different A/q, the beam purity can be much improved at F3. This paper reports the first beam test of the Wien filter system.

2. Beam Test of the Wien Filter System

For the first beam test, we avoided handling of extremely high voltages and used a relatively low electric field of $F = 12.3$ kV/cm (± 49 kV for the 8-cm gap), which was about 1/4 of the maximum. For this reason, an ^{14}O(8+) secondary beam of $E/A = 7.1$ MeV was chosen as a test beam. The ^{14}O beam was produced by using the ^{14}N(p,n)^{14}O reaction in inverse kinematics. The setup for the ^{14}O beam production was almost the same as those described in Refs. [5, 6]. The momentum width of ^{14}O was set to be 2% (FWHM) by the slit at F1. No energy degrader was inserted at F1. A major contaminant in the secondary beam at F2 was ^{14}N(7+) at E/A = 5.5 MeV, with the same $B\rho$ as ^{14}O. The origin of the ^{14}N contaminant is scattering of the ^{14}N primary beam at inner walls of the beam line and the separator. The velocity of ^{14}N is 12.5 % smaller than that of ^{14}O. As shown below, $F = 12.3$ kV/cm was large enough to separate ^{14}O from ^{14}N. The magnetic field of the velocity separation section was set to be 0.032 T.

Figure 1 shows a ray-trace simulation of the Wien filter system for the present case. In the simulation, trajectories of ions were calculated by the equation of motion for ions in electric and magnetic fields. For Q magnets, uniform Q fields with effective boundaries were assumed. For the dipole magnet, we used a real fringing field based on a hall-probe measurement. The fringing electric field by the electrodes was calculated by the POISSON code [7]. As shown in Fig. 1, the simulation gave an ^{14}O-^{14}N separation of 2.6 cm at F3.

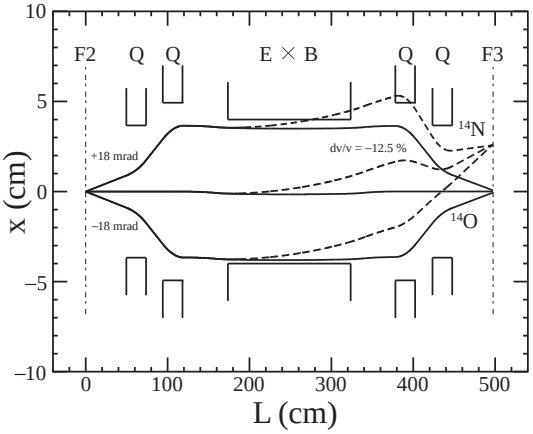

Figure 1. Ray-trace simulation of the Wien filter system on the horizontal plane for the present beam test. The electric field at the velocity separation section is parallel to the x-axis. The superimposed magnetic field is normal to the plane.

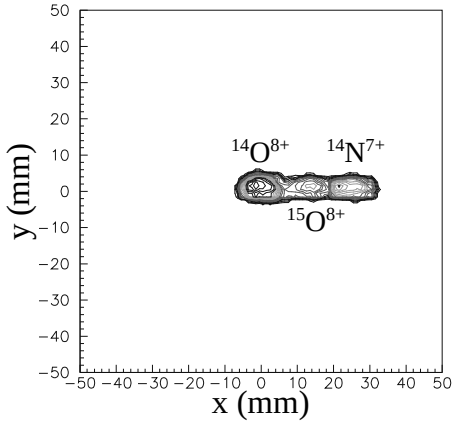

Figure 2. Beam spot image measured by a PPAC at F3 after the Wien filter system.

Figure 2 shows the actual image of beam spots measured in the beam test by using a parallel-plate avalanche counter (PPAC) [8] at F3. The most intense spot at the center is ^{14}O and the spot at $x \sim 2.5$ cm is ^{14}N, as expected by the simulation. A weak beam spot of ^{15}O(8+) is seen between the ^{14}O and ^{14}N spots. The contaminant of ^{15}O is produced by background reactions at the production target. The size of ^{14}O spot was about 0.5 cm diameter (FWHM), which was almost the same as the spot size at F2, because both the horizontal and vertical magnifications were 1.0 from F2 to F3.

The velocity dispersion at F3 was 0.20 cm/% (= 2.5 cm /

12.5 %) for $F = 12.3$ kV/cm and $E/q = 12.5$ MeV. Note that the velocity dispersion is proportional to both of F and q/E. For the present beam, we may expect the maximum dispersion of 0.81 cm/% with the maximum electric field of 50 kV/cm.

3. Summary

The first beam test of the CRIB Wien filter system was successfully performed. We achieved a focusing condition at the new focal plane of F3 after the Wien filter system. The velocity separating power was tested using the ^{14}O and ^{14}N ions with the same magnetic rigidity. By setting a slit at F3, we can have an ^{14}O beam of 100% purity. Further tests with higher voltages and heavier ions will be performed.

References

[1] T. Teranishi *et al.*, Nucl. Phys. A **718** (2003) 207c.
[2] S. Kubono *et al.*, Eur. Phys. J. A **13** (2002) 217.
[3] T. Teranishi et al., CNS-REP-39 (2001).
[4] J.J. He *et al.*, CNS Annual Report 2002 (2003) 51.
[5] K. Ue *et al.*, CNS Annual Report 2001 (2002) 49.
[6] M. Notani *et al.*, CNS Annual Report 2002 (2003) 19.
[7] POISSON, Los Alamos Accelerator Code Group.
[8] H. Kumagai *et al.*, Nucl. Instrum. Methods. A **470** (2001) 562.

Polarization and Density Calibration of the Spin-Exchange Type Polarized ^{3}He Target at CNS

K. Itoh[a], T. Uesaka[b] and T. Wakui[b]

[a] *Graduate School of Science and Engineering, Saitama University*
[b] *Center for Nuclear Study, Graduate School of Science, University of Tokyo*

1. Introduction

We have been developing a spin-exchange type polarized ^{3}He target. In 2002, we have constructed the target system and measured an enhancement of the ^{3}He polarization with the adiabatic-fast-passage(AFP)-NMR method which provides only a relative value of polarization [1].

In order to determine the absolute value of the ^{3}He polarization, frequency shift measurement of the Rb electron spin resonance (ESR) is performed. It is known that the frequency shift is proportional to the ^{3}He density and ^{3}He polarization [2]. Thus, the absolute value of ^{3}He polarization can be deduced by measuring the ESR frequency shift for the cell in which the ^{3}He density is known.

To measure the ^{3}He density after the gas was enclosed, the pressure broadening measurement is newly introduced. In the presence of high pressure foreign gas, the spectral width of Rb is broaden proportional to the gas density [3].

2. Target density measurement

We performed the pressure broadening measurement for the Rb D_1 line (794.7 nm). The D_1 spectral line shape of Rb in several atoms of ^{3}He gas is written as follows [4].

$$I(\nu) = \frac{A[1 + 0.664 \cdot 2\pi T_d(\nu - \nu_c)]}{(\nu - \nu_c)^2 + (\gamma/2)^2} \qquad (1)$$

The coefficient A is a constant, ν is a frequency of the laser light, ν_c is a resonant frequency, T_d is a dispersion-like asymmetry coefficient, and γ is a spectral width which is sum of the natural width, doppler width, and pressure broadening width. We can obtain the density of ^{3}He atoms in a cell by measuring the width.

Figure 1 shows the experimental setup to measure the pressure broadening.

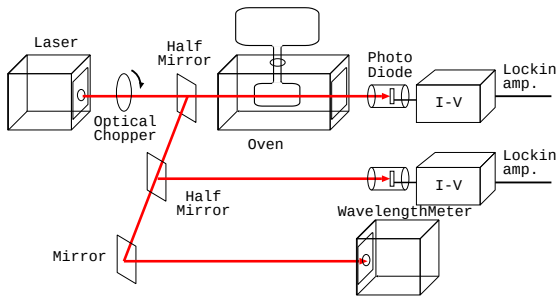

Figure 1. Configuration of the pressure broad measurement. Three arrows show the passes of the light.

Tunable diode laser with external cavity (NewFocus Model6312) was installed. The maximum sweep wavelength range is 790-800 nm. For a cell that the pressure is about 3 atoms, the sweep wavelength range of more than 2 nm is required. It is achieved for a cell in which 10 atoms of ^{3}He are filled, which we plan to prepare.

The laser light is chopped at a frequency of 117 Hz by an optical chopper (Terahertz Technologies C-995) and splitted into three. They are used to measure the density, to measure the shift of the laser power when the wavelength is swept, and to measure the frequency of the light. The first one is pass through the cell and the transmission of the light is measured by using a photodiode (Hamamatu S1337-1010BR). The second one is directly injected into a photodiode. Each signal is measured with a lock-in amplifier referenced to a signal synchronized with the chopping frequency. The last one is detected by a wavelength meter. The cell in an oven is heated up to about 100 °C to vaporize Rb atoms.

A typical spectrum is shown in Fig.2. The solid line

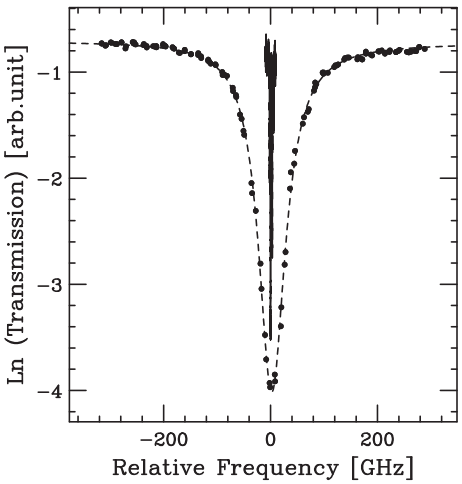

Figure 2. Rb D_1 spectrum for the cell without foreign gas (solid line around the 0 GHz) and with 3 atoms of ^{3}He gas (closed symbols and broken line).

around the 0 GHz shows the spectrum for the cell without foreign gases. The spectrum shows only the contribution of the natural width and doppler width, which are estimated to be less than 10 MHz and 0.3 GHz, respectively. The closed symbol shows the result for the cell with 3 atoms of ^{3}He gas, and the broken line shows the fitting result of these data with Eq. (1).

The coefficient of the spectral width of Rb D_1 line and the density of ^{3}He gas was measured by Romalis *et al.* and

the value was (6.95 $\pm$ 0.11) $\times 10^{-19}$ GHz·cm^3/atoms [4]. The measured width of the Rb and ^{3}He gas was 60.6 $\pm$ 0.6 GHz and resulting density was (8.70 $\pm$ 0.16) $\times$ 10^{19} atoms/cm^3.

3. Polarization calibration measurement

The ESR frequency of Rb atoms corresponds to the Zeeman splitting energy of two hyperfine levels. The ESR frequency of Rb atoms shifts from the Zeeman frequency due to the hyperfine interaction with polarized ^{3}He [2]. The shift is proportional to the ^{3}He polarization, the ^{3}He density, and the temperature dependent coefficient κ_0. The last one was measured with the uncertainty of 1.5% and written as $\kappa_0 = 4.52 + 0.00934 \times T(^\circ\mathrm{C})$ [2].

Figure 3 shows the experimental setup of the Rb ESR shift measurement.

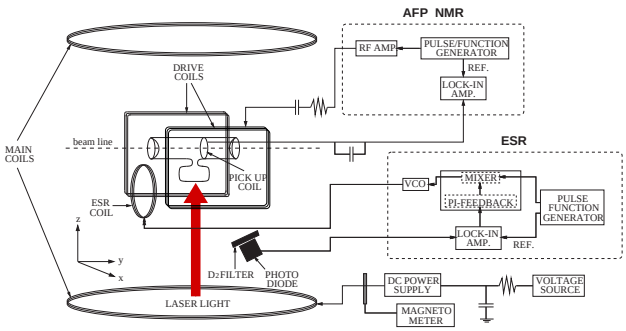

Figure 3. Configuration of the ESR frequency shift measurement.

The cell placed in a magnetic field is illuminated by the left-circularly polarized laser light. Rb atoms are optically pumped into the $F = 3, m = -3$ state by the light and they can not absorb the circularly polarized photon. F and m denotes the total angular momentum of the Rb atoms and the magnetic quantum number of the Rb atoms, respectively.

The ESR coil is used to apply a RF field which induces ESR. The RF field is generated by a voltage controlled oscillator (VCO) and the frequency is modulated in the range of 25 kHz. The frequency of 9.19 MHz corresponds to the Rb energy splitting between $F = 3$, $m = -3$ and $F = 3$, $m = -2$ state at the holding field of 20 G. Applying the RF field which induces the $m = -3 \rightarrow m = -2$ transition, the population in the $m = -2$ state is increased. They can absorb the circularly polarized laser light and subsequently decay back to the grand state by emitting fluorescence photons. These photons are detected by a photodiode with a narrow (1.5nm FWHM) optical band-pass filter. The occurrence of ESR can be thus monitored by detecting the enhancement of fluorescence light. The fluorescence intensity signal is detected by a lock-in amplifier referenced to the modulation frequency. To keep the ESR frequnecy, we use a proportional-integral feedback system. Monitored fluorescence intensity is used to lock the RF frequency to the ESR frequency. The locked frequency is measured with a counter.

We measured ESR frequency difference between spin up and down state, which corresponds to twice of the ESR frequency shift. AFP-NMR measurement was done before and after a ESR frequency measurement. Figure 4 shows the correlation of the measured NMR voltage and the ESR frequency shift. The open circle shows a result of a set of ESR frequency shift measurement,and the solid line shows the fitting result for the 50 measurements.

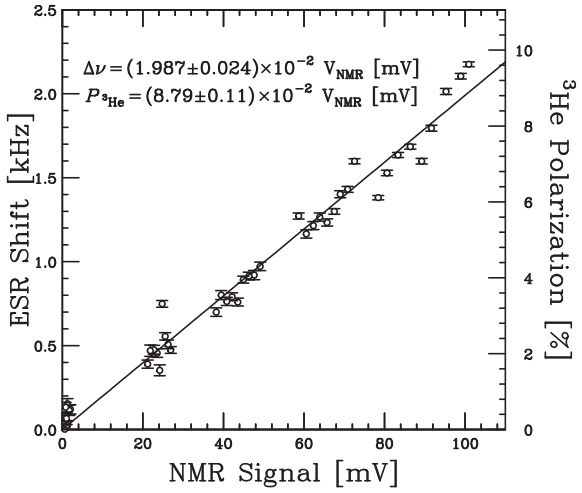

Figure 4. Correlation of the AFP-NMR amplitude and the ESR frequency shift, and the absolute value of polarization.

The resulting calibration coefficient of AFP-NMR and ESR frequency shift is (1.987 $\pm$ 0.024) $\times$ 10^{-2} kHz/mV. If ^{3}He is completely polarized, the frequency shift is 22.6 kHz for the ^{3}He density of 8.7$\times 10^{-19}$ atoms/cm^3. Thus coefficient of NMR and ^{3}He polarization is deduced to (8.79 $\pm$ 0.11 $\pm$ 0.26) $\times$ 10^{-2} mV^{-1}. The systematic error of the coefficient is estimated about 3%. The main origin of the error is uncertainly of cell temperature.

4. Summary

High precision measurement system of target density and absolute polarization has been constructed. The error of measured density and polarization is 2% and 4%, respectively.

References

[1] K. Itoh *et al*, CNS Annual Report 2002 (2002) 62.
[2] M.V. Romalis and G.D. Cates, Phys. Rev. A **58** (1998) 3004.
[3] J. Szudy and W.E. Barylis, Phys. Rep. **266** (1996) 127.
[4] M.V. Romalis, E. Miron and G.D. Cates, Phys. Rev. A **56** (1997) 4569.

Dependence of Polarization on Laser Power in CNS Polarized Proton Target

T. Wakui[a], M. Hatano[a,b], H. Sakai[a,b], T. Uesaka[a] and A. Tamii[b]

[a] *Center for Nuclear Study, Graduate School of Science, University of Tokyo*
[b] *Department of Physics, University of Tokyo*

1. Introduction

A polarized solid proton target using a crystal of naphthalene doped with pentacene has been developed for $\vec{p}$-RI scattering experiments. In the crystal, pentacene molecules are optically aligned in the photo-excited triplet state, and then the population difference between two sublevels among the triplet state is transferred to protons by microwaves [1]. The target was used in the first experiment with an unstable ^{6}He beam in July 2003 at RIKEN Accelerator Research Facility [2, 3].

As described in the previous report [4], we have obtained proton polarization of 37% in 0.3 T at 100 K. In this experiment, the laser power for the optical excitation was 200 μJ/pulse, which was insufficient to induce the excitation of all pentacene molecules in the crystal, because the number of photons was 10 times smaller than that of pentacene. The polarization rate is therefore expected to increase with increasing the average laser power unless absorption transition is saturated. On the other hand, a higher laser power will increase also the relaxation rate of proton polarization. Since the degree of proton polarization is a result of competition between the polarization and the relaxation rates, an optimum laser power should be found for attaining a higher proton polarization.

To investigate an optimum condition for the laser power, we have measured dependence of polarization and relaxation rates on the laser power [5]. In this measurements, a proton polarizing system with a cylindrical microwave cavity [6] has been used. The laser was an Ar-ion laser having the maximum power of 10 W for the wavelength of 514 nm. The laser was operated with the repetition rate of 1 kHz and the pulse duration of 20 μs. By using the results, we estimated the attainable proton polarization. In this report, we describe results of the measurements and the estimation.

2. Polarization rate

The proton polarization, P, increases with time during the polarization buildup process:

$$P = \frac{A}{A+\Gamma_p}\overline{P_e}\{1-\exp[-(A+\Gamma_p)t]\}, \qquad (1)$$

where $\overline{P_e}$ is the average population difference between two sublevels in the triplet state, Γ_p the total relaxation rate of proton spins, and A the polarization transfer rate which is proportional to the average population in the triplet state. The polarization rate derived from Eq. (1) reduces to

$$\frac{dP}{dt} = A\overline{P_e}, \qquad (2)$$

as long as $(A+\Gamma_p)t$ is sufficiently smaller than unity. We can thus determine the polarization rate by measuring the proton polarization at short times.

Figure 1 shows the polarization rate as a function of the laser power measured at the immediate output of the Ar-ion laser. The polarization rate was obtained by measuring the polarization at t=0.08 h to ensure that the value of $(A+\Gamma)t$ was always less than 0.06. The polarization rate increases almost linearly with increasing the average laser power. The offset of a linear fit is consistent with zero within error bars. The proportionality coefficient is 7.48±0.26.

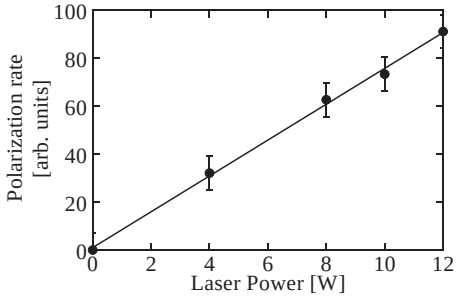

Figure 1. Polarization rate as a function of the laser power.

3. Relaxation rate

During the buildup process, the relaxation of proton spins is caused by several sources, and the total relaxation rate is the sum of the intrinsic relaxation rate, Γ_I, the rate due to pentacene on the photo-excited triplet state, Γ_T, and the rate due to a cumulative effect of laser irradiation, Γ_L:

$$\Gamma_p = \Gamma_I + \Gamma_T + \Gamma_L. \qquad (3)$$

The intrinsic relaxation of proton spins in a target crystal below 250 K is mainly due to the fluctuating field produced by paramagnetic impurities, and Γ_I at 100 K for the crystal used in this experiment was (6.2±0.1)×10^{-2} h^{-1}. Relaxation due to pentacene in the photo-excited triplet state is caused by interaction between triplet and proton spins. Since the population of pentacene on the triplet state is proportional to laser power unless transition is saturated, Γ_T will increase linearly with increasing the laser power.

In addition to these sources, we have found a cumulative effect of laser irradiation. After laser irradiation, the relaxation rate measured without laser irradiation was increased compared with the intrinsic relaxation rate. Figure 2 shows Γ_L as a function of the product of laser power and time for laser irradiation, Γ_L which was obtained from the relaxation rate measured without laser irradiation by subtracting the intrinsic relaxation rate. The solid line shows the least-squares fit of a linear function. The proportionality constant was (1.1±0.5)×10^{-3} W^{-1}h^{-2}. The cause of the effect has not been understood.

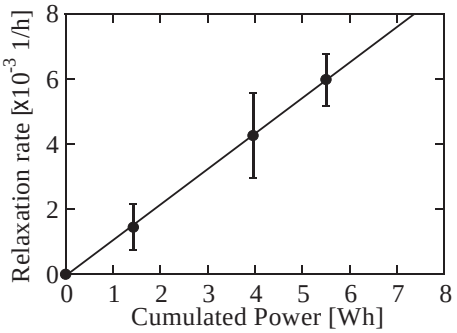

Figure 2. Relaxation rate due to a cumulative effect of laser irradiation.

During laser irradiation, some of excited pentacene molecules decay to the ground state non-radiatively and dissipate its excitation energy as heat. Since Γ_I increases quadratically with temperature, the effect of the non-radiative decay on Γ_I might be serious at higher laser power. Figure 3 shows Γ_T as a function of the laser power. The relaxation rate was obtained from the measured relaxation rate by subtracting the intrinsic relaxation rate and the rate due to the cumulative effect. The relaxation rate increases almost linearly with the laser power. This would be attributed mainly due to the increase of the number of pentacene in the triplet state. Since the relaxation rate shows no apparent quadratic increase, the heat due to the non-radiative decay has negligible effect on the relaxation in the range of the present measurement.

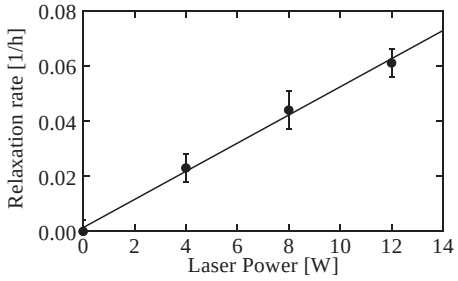

Figure 3. Relaxation rate due to pentacene in the photo-excited triplet state. The intrinsic relaxation rate and the rate due to the cumulative effect are subtracted.

4. Proton polarization

By using the measured polarization and relaxation rates, we estimate the attainable proton polarization. At first the values of $A\overline{P_e}$ in Fig. 1 has to be calibrated to the absolute values. For the calibration, the evolution of the polarization shown in the previous report was fitted to Eq. (1). Since the laser parameters, such as repetition rate and pulse duration, in the present experiment were the same as the previous ones, we can assume that the rates of polarization transfer and of relaxation induced by laser irradiation are equivalent to the previous ones. ¿From the fitted values, $A\overline{P_e}$ for the laser power of 8 W in the previous experiment was obtained as (9.0±0.8)$\times 10^{-2}$ h^{-1}, and the resulting calibration factor for the $A\overline{P_e}$ in Fig. 1 was (1.4±0.1)$\times 10^{-3}$. The $\overline{P_e}$ was obtained as 66±5%.

Figure 4 shows the attainable proton polarization predicted by the first term in Eq. (1). In this calculation, the relaxation due to the cumulative effect was assumed to be 2.6×10^{-3}, which corresponds to the irradiation time of 15 hours. The polarization increases quickly with the laser current and tends to saturate at approximately 45%.

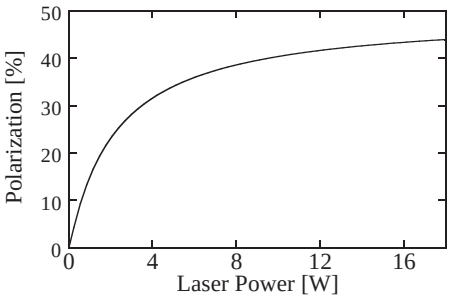

Figure 4. The proton polarization predicted by Eq. (1) for the repetition rate of 1 kHz and the pulse duration of 20 μs.

To attain a higher proton polarization, further study for obtaining dependence of proton polarization on other laser parameters, such as the pulse duration and the repetition rate, is required, because the pulse duration affects $\overline{P_e}$, which gives the limit of proton polarization, and the repetition rate has an influence on A.

5. Summary

We have measured the polarization and relaxation rates to find an optimal condition for polarizing proton. We have also estimated the attainable proton polarization, and the maximum polarization is predicted as 45% for the repetition rate of 1 kHz and the pulse duration of 20 μs.

References

[1] A. Henstra *et al.*, Phys. Lett. A **134** (1988) 134.
[2] T. Uesaka *et al.*, Nucl. Instrum. Methods. A **526** (2004) 186.
[3] T. Uesaka *et al.*, CNS Annual Report 2003 (2004) 17.
[4] T. Wakui *et al.*, CNS Annual Report 2002 (2003) 49.
[5] T. Wakui *et al.*, Nucl. Instrum. Methods. A **526** (2004) 182.
[6] T. Wakui *et al.*, RIKEN Accel. Prog. Rep. **34** (2001) 149.

Liquid Hydrogen Target for EPR Pardox Experiment at SMART

T. Ikeda, K. Itoh, T. Kawabata[a], H. Saito[b], H. Sakai[a,b], T. Uesaka[a] and K. Yako[b]

Department of Physics, Saitama University
[a]*Center for Nuclear Study, Graduate School of Science, University of Tokyo*
[b]*Department of Physics, University of Tokyo*

Einstein Podolsky Rosen (EPR) paradox is one of the most fundamental problems in quantum mechanics. We have tackled this problem by measuring the spin correlation between two protons coupled into the $^1S_0$ state, which are emitted from the (d, ^{2}He) reaction at intermediate energy [1].

As a target for the (d, ^{2}He) reaction to produce spin-singlet proton pairs, hydrogen is the most appropriate material because of the simplicity in the reaction mechanism. For the reliable measurement, fully dense and pure hydrogen target is required. Thus, we developed a liquid hydrogen target for the EPR paradox experiment.

The target system consisted of a cryogenic refrigerator, a target cell, a thermal shield, and driving gears for moving and rotating the target (Fig. 1). The target cell was attached to the cold head of the cryogenic refrigerator and installed in the scattering chamber of the SMART spectrograph in the E4 experimental hall at RIKEN. The target cell was made of aluminum to keep the high thermal conductance and to avoid radio-activation by the beam halo. The thermal shield made of aluminum was attached to the first stage of the refrigerator in order to avoid the thermal radiation effect from surrounding materials at room temperature.

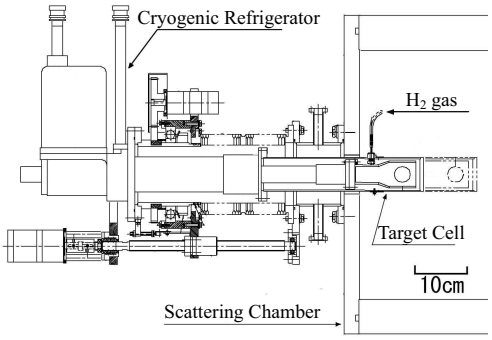

Figure 1. Liquid hydrogen target system.

From the estimated production rate of ^{2}He and the true-to-accidental ratio in the coincidence measurement of two protons, the target thickness was determined to be 70 mg/cm^2. Aramid films with a diameter of 20 mm and a thickness of 12.5 μm were used as the window foil of the target cell.

The present liquid hydrogen target was tested by using a 270-MeV deuteron beam accelerated by the RIKEN ring cyclotron. During the experiment, the temperature and inner pressure of the target cell were kept at 15 K and 0.4 atm as shown in Fig. 2. Several peaks were observed in the target temperature and vacuum in the scattering chamber whenever the target position was moved. The reason of this phenomenon is still unclear. Figure 2 indicates that the fluctuation of target temperature was very small unless the target position changed.

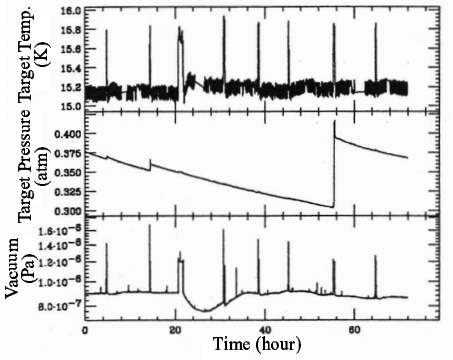

Figure 2. Target temperature, inner pressure and vacuum in the scattering chamber.

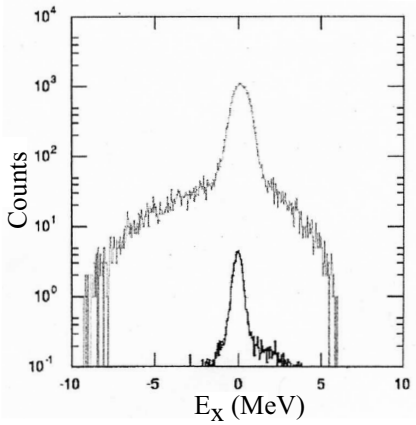

Figure 3. Excitation energy spectra of the remaining neutron in the ^{1}H(d, ^{2}He) reaction. The gray line shows the spectrum obtained by using the target cell filled by the liquid hydrogen, while the black line shows the spectrum by the empty target cell.

The excitation energy spectra for the remaining neutron in the ^{1}H(d, ^{2}He) reaction are shown in Fig. 3. It is found that the ratio of true events from liquid hydrogen to background events from the aramid window foil is better than 100, and the background from the aramid foil is negligible. From this test experiment, we concluded that the present liquid hydrogen target with a high stability and a high S/N ratio could be successfully used in the EPR paradox experiment.

References

[1] T. Saito *et al.*, CNS Annual Report 2003 (2004) 19.

Gamma-Ray Detector Array with Position and Energy Sensitivity (GRAPE)

S. Shimoura, E. Ideguchi, M. Kurokawa[a], T. Fukuchi, H. Baba[b], S. Ota[c], M. Tamaki, M. Niikura and H. Sakai

Center for Nuclear Study, Graduate School of Science, University of Tokyo
[a] *RIKEN (The Institute of Physical and Chemical Research)*
[b] *Department of Physics, Rikkyo University*
[c] *Department of Physics, Kyoto University*

The GRAPE (**G**amma-**R**ay detector **A**rray with **P**osition and **E**nergy sensitivity) has been developed since 2000 for high-resolution in-beam γ-ray spectroscopy using Radioactive Ion (RI) beams (Fig. 1). In order to overcome the Doppler broadening from the moving γ-ray emitters, the array was designed to have position sensitivities in the detector material (Germanium crystal). The total array consists of 18 detectors each of which contains two Ge planar-type crystals with 3×3 segmented electrodes [1]. The planar structure and the segmented electrodes enable us to extract the position information based on a pulse-shape analysis. The resolution for the Doppler shift correction can be achieved less than 1% for v/c = 0.3 emitters for the closed pack configuration of the detectors, where a total efficiency ($\epsilon\Omega$) of 5% for 1 MeV γ is expected.

The followings are the progresses in this year:

- The nickname of the array was decided to be GRAPE.
- Simulation procedure for the pulse-shape was established [2].
- The first-phase electronics using conventional analog techniques for the pulse-shape analysis have been completed for all the 18 detectors.
- A testbench was constructed for the automatic measurements of the characteristics of each detector [3]. The geometrical positions of the Ge crystals in the detectors were measured and databased.
- Overall performances for the Doppler correction were evaluated by using the data of the first (July 2002; 6 detectors) and the second (July 2003; 14 detectors) physics experiments [4, 5].
- Total system was used for the measurement of the fusion reaction of low-energy RI beams on Be target [6].
- For the second-phase data aquisition, a small system where pulse shapes are sampled with flash ADCs was constructed. R&D of pulse shape analysis based an artificial neural network alogorithm was initiated by using the digital pulse-shape data [7].
- A maintenance equipment having an oil-free vacuum system was constructed.

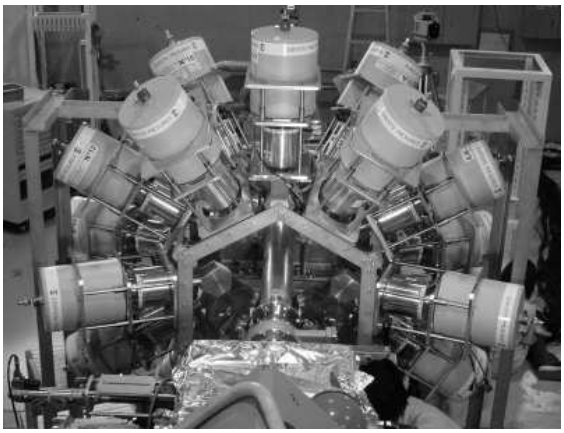

Figure 1. The GRAPE.

In 2004, we will perform the following two physics experiments by using the GRAPE:

- Single-particle structures of the neutron-rich nuclei in the island-of-inversion ($N \sim 20$ and $Z \sim 12$) will be studied by using in-beam spectroscopy of excited states produced by nucleon transfer reactions (α,t) and (α,^{3}He).
- High-spin states in the $N \sim 28$ and $Z \sim 20$ region will be studied by measuring γ-rays from nuclei produced by fusion reaction with low-energy neutron-rich RI beams.

We will also continue the R&D of the digital signal processing and analysis system not only for making tuning procedures easier but also for three-dimensional position determination.

References

[1] S. Shimoura *et al.*, CNS Annual Report 2001 (2002) 5.
[2] M. Kurokawa *et al.*, IEEE Trans. Nucl. Sci. **50** (2003) 1309.
[3] T. Fukuchi *et al.*, CNS Annual Report 2003 (2004) 88.
[4] S. Shimoura, Nucl. Instrum. Methods. A **525** (2004) 188.
[5] C. Ishida *et al.*, CNS Annual Report 2003 (2004) 9.
[6] M. Niikura *et al.*, CNS Annual Report 2003 (2004) 11.
[7] T. Fukuchi *et al.*, CNS Annual Report 2003 (2004) 90.

Development of Testbech for the Gamma-Ray Detector Array with Position and Energy Sensitivity (GRAPE)

T. Fukuchi, S. Shimoura, E. Ideguchi, M. Kurokawa[a], H. Baba, S. Ota[b], M. Tamaki and M. Niikura

Center for Nuclear Study, Graduate School of Science, University of Tokyo
[a]RIKEN(the Institute for Physical and Chemical Research)
[b]Department of Physics, Kyoto University

1. Introduction

We have been developing the Gamma-Ray detector Array with Position and Energy sensitivity (GRAPE) which is mainly used for detecting γ-rays emitted from fast moving nuclei [1]. The GRAPE consists of 18 high-purity germanium (Ge) detectors. All detectors have two planar-type Ge crystals (60 mm in diameter and 20-mm thickness). The electrode of Ge crystal is segmented in 3×3 as shown in Fig. 1. These Ge detectors were manufactured by the company Eurisys Measures.

To investigate the detector character and performance, a detector testbench has been developed. The detector testbench is also a powerful tool of long time sampling for pulse shape analysis [2] with flash-ADC. The measurement of crystal geometry in cryostat has been performed using the detector testbench. The information of the crystal geometry is necessary to achieve an accurate energy correction of Doppler-shifted γ-rays radiated from flying nuclei.

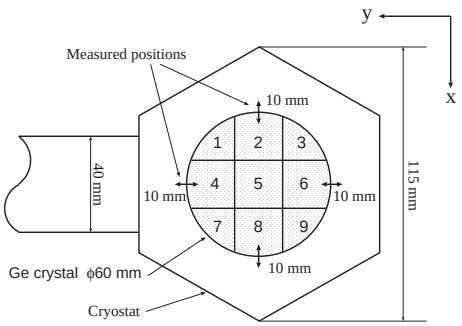

Figure 1. Schematic view of the segmented Ge detector crystal and a part of cryostat. The measured positions are shown by arrows. Numbers are given to identify each segmented electrode.

2. Detector Testbench

The detector testbench is composed of two linear-motion sliders which move with an accuracy of 1/100 mm by the stepping motors. A led collimator is mounted on the sliders and moves in a vertical plane of 20×20 cm^2. To scan from various direction, the testbench has a detector mount and several slider mount positions. Figure 2 shows a photograph of the detector testbench. Since the intensity of the collimated γ-ray is weak, scanning whole volume of the crystal requires a few days to collect enough events. To process a data acquisition (DAQ) and motion control(MC) of the sliders automatically, a Linux-based personal computer and a VME control system manage both DAQ and MC. The detector testbench enables automatic and accurate measurements.

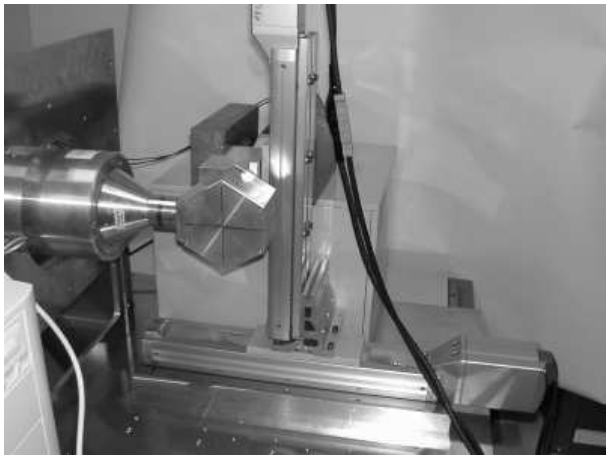

Figure 2. A photograph of the detector testbench and a head part of the Ge detector.

3. Measurement of the Crystal Geometry

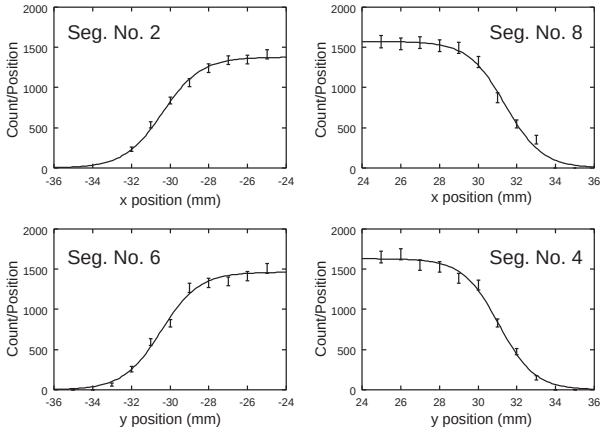

Figure 3. A sample of measured data and fitted curves (detector number 1, side A).The axis directions of x and y are shown in Fig. 1. The center of the cryostat is the origin.

The measurement of the crystal geometry in a cryostat have been performed using the detector testbench. Four edges in a crystal were scanned. On each edges, positions of every 1 mm interval were measured. These measured posi-

tions are shown in Fig. 1 by arrows. The measurements were performed using a ^{22}Na γ-ray source with a led collimator which has 100-mm thickness and a hole of 1 mm in diameter. The source used had an activity of about 3.7 Mbq providing a detector counting rate of about 500 Hz. Energy signals were taken from each segment with ADCs. The ADCs were triggered by total signal. The data for one position was collected for 15 minutes. One crystal measurement took about 11 hours. Two crystals in a detector were named side A and B to identify, and measured separately. The crystal geometry was deduced from 511 keV photopeak counts. Because of the finite size of the collimator and the Compton scattering effect, the photopeak counts increase gradually at the edge of crystal. The photopeak counts were fitted using a function :

$$\mathrm{F(x)} = \frac{a}{1 + \exp\{b(x-c)\}}$$

where x is a collimator position, a, b and c are free parameters and determined by a least mean square fit. The sample results of the measured data and fits are shown in Fig. 3. The crystal geometry was deduced from the average value of parameter c of each edge. The all deviations of the crystal center are summarized in Table 1. All values have a statistical errors of $\pm$0.1 mm and the systematic errors $\pm$0.3 mm.

Table 1. A summary of crystal misorientation in the cryostat. The x and y axis directions are shown in Fig. 1.

Detector Number	Side A x (mm)	Side A y (mm)	Side B x (mm)	Side B y (mm)
1	0.5	0.3	0.4	0.1
2	0.6	– 0.3	0.6	0.3
3	0.2	0.5	0.5	0.3
4	– 0.3	0.0	1.1	– 0.1
5	– 0.4	– 0.5	– 0.1	– 0.2
6	0.3	0.0	0.5	0.2
7	0.6	– 0.5	0.0	0.4
8	0.3	0.3	0.2	0.2
9	0.6	0.2	0.7	0.0
10	0.6	– 0.1	1.1	0.0
11	1.3	– 0.6	0.0	0.3
12	0.8	0.0	0.8	0.1
13	0.7	– 1.0	0.3	0.1
14	0.0	0.7	0.7	– 0.1
15	– 0.1	– 0.8	0.0	0.2
16	– 1.6	– 0.1	0.3	0.1
17	– 1.4	0.2	0.2	– 0.3
18	0.4	0.1	0.1	0.1
19	0.2	0.3	0.4	0.4

References

[1] S. Shimoura *et al.*, CNS Annual Report 2001 (2002) 5.

[2] M. Kurokawa *et al.*, IEEE Trans. Nucl. Sci. **50** (2003) 1309.

Development of Position Sensitive Ge Detector using the Neural Network

T. Fukuchi, S. Shimoura, E. Ideguchi, M. Kurokawa[a], H. Baba, S. Ota[b],
M. Tamaki and M. Niikura,

Center for Nuclear Study, Graduate School of Science, University of Tokyo
[a]RIKEN(the Institute for Physical and Chemical Research)
[b]Department of Physics, Kyoto University

1. Introduction

An artificial neural network (ANN) algorithm has been used in a wide variety of data processing application. Neural network computing is analogous to biological neural systems. The ANN algorithm was applied to the pulse shape analysis for a germanium (Ge) detector which is a component of the GRAPE (Gamma-Ray detector Array with Position and Energy sensitivity) [1]. The GRAPE is mainly used for detecting gamma-rays emitted from fast moving nuclei. An advantage of ANN technique is rapid pattern recognition with an appropriate training in advance. We aim to extract the interacting position of gamma-rays online using the ANN algorithm.

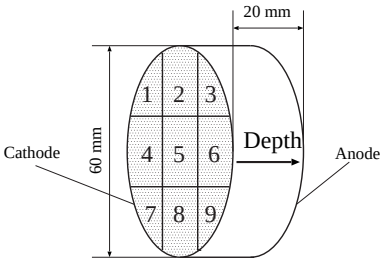

Figure 1. Schematic view of the segmented Ge detector crystal. Numbers are given to identify each segmented electrodes.

2. Measurement

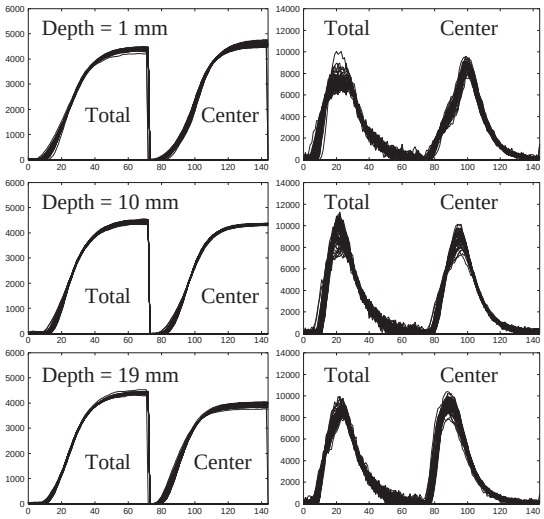

Figure 2. Measured pulse shapes of total signal, center segment signal (right) and these differential (right). Interaction depth are indicated in each spectrum.

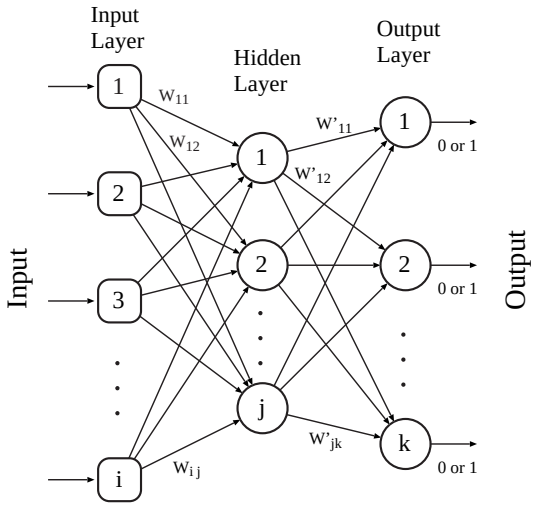

Figure 3. Structure of neural network in pulse shape analyses. In this analysis, the structure of ANN was composed of 288 input layers, 4 hidden layers and 4 output layers.

In odder to make a supervisory data set for training the ANN, the pulse shape sampling was performed using a VME SIS3300 flash-ADCs. The SIS3300 are eight channel ADC/digitizer with a sampling rate of 100 MHz and a resolution of 14-bit in an input range of ± 2.5 V.

A Ge crystal has a planer geometry with a 60 mm diameter and a thickness of 20 mm. The cathode is divided into nine segments as shown in Fig.1 The analog summation of all the nine cathode signals are referred as total signal which is equivalent to the signal from the anode [2].

In this measurement, total and center segment (number 5) signals were taken. The signals from the crystal are amplified by the charge-sensitive pre-amplifiers. After pre-amplifiers, operational amplifiers were used for matching with dynamic range of flash-ADCs. The pulse shapes in the rising 720 ns were taken by flash-ADCs. The data set of 16 different interaction depth was stored for ANN training using a detector testbench [3]. In this measurement, collimated gamma-ray source of a ^{22}Na was used.

About 1000 count of the full energy deposited events (1275 keV) were stored for each depth. All events have depth tags which correspond to the collimator positions for ANN training. Figure 2 shows measured pulse shape spectra(left) and those of differential spectra(right) of different interaction depth. Because collimated gamma-ray has finite size, the measured pulse shapes have some variations.

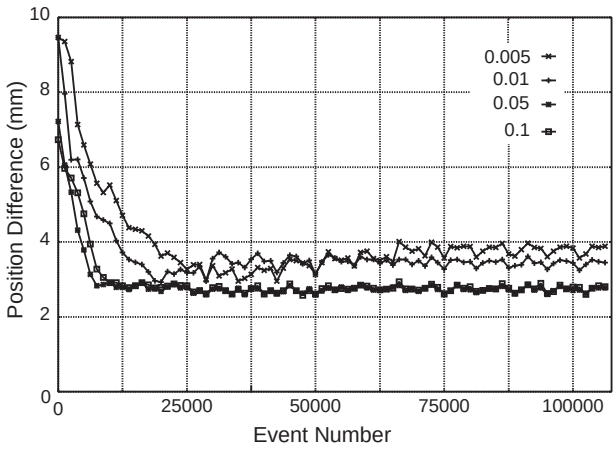

Figure 4. Results of ANN outputs. The progress of the training versus difference between inputs and outputs. Each line shows results of different training efficiency parameter.

3. ANN Analysis and Result

The ANN is composed of an input layer, one or more hidden layer and an output layer. Each layer includes neurons which are connected to all the neurons of a successive layer. Each connection has its own weight and each neuron discriminates output from summation of input values multiplied by the weight. Figure 3 shows schematic view of the ANN. All calculations were executed on the software by a personal computer.

The weights of each conection are modified thorough a training procedure. The training of the ANN can be performed with a back-propagation (BP) algorithm. In this algorithm, example data set whose outputs are known are used as input data. The calculated output is then compared with the known output. The difference between the two outputs is then back-propagated to modify the weights. Such an interactive procedure is continued until the difference becomes desirably small.

In this analysis, the structure of ANN was composed of 288 input parameters, 4 neurons in hidden layer and output layer. For input parameter of ANN, total, center segment and these differential amplitudes were used. Each pulse shape has 72 parameters. Normalized input parameters were provided to each neuron of the input layer of the ANN. The interacting depth comes out from output layer as Boolean value. The numbers of neurons in hidden layer was determined through trial and error to be optimal.

Output results are given in Fig. 4. The vertical axis is the difference between input and output depth values. The horizontal axis (event number) means progress of the ANN training. Four lines in the graph show results of different training efficiency parameter (0.01 - 0.005) which is a factor of the weight modification. The figure shows that the training in effective until 25,000 events, while the further training is ineffective or even harmful.

Extraction of the three-dimensional interacting position using the transient signals which appear in the neighbors of interacting segment are now in progress.

References

[1] S. Shimoura *et al.*, CNS Annual Report 2001 (2002) 5.
[2] M. Kurokawa *et al.*, IEEE Trans. Nucl. Sci. **50** (2003) 1309.
[3] T. Fukuchi *el al.*, CNS Annual Report 2003 (2004) 88.

Theoretical Nuclear Physics

Large Scale Nuclear Structure Calculations in CNS

N. Shimizu[a], T. Otsuka[a,b,c], N. Itagaki[a], T. Mizusaki[d], M. Honma[e] and Y. Utsuno[f]

[a] *Department of Physics, University of Tokyo*
[b] *Center for Nuclear Study, Graduate School of Science, University of Tokyo*
[c] *RIKEN (The Institute of Physical and Chemical Research)*
[d] *Institute of Natural Sciences, Senshu University*
[e] *Center for Mathematical Sciences, University of Aizu*
[f] *Japan Atomic Energy Research Institute*

1. Introduction

The CNS has started theoretical studies since the year 2001. Here, we describe one of the major theoretical activities, the project of large-scale nuclear structure calculation. This project has been carried out based on a collaboration agreement between CNS and RIKEN Accelerator Research Facility (RARF) [1, 2]. In 2003, we studied not only the shell model calculation utilizing the Monte-Carlo technique, but also more general nuclear structure calculation.

At the beginning of this project, we have mainly used the nuclear shell model to explore the structure of exotic (unstable) nuclei. The large-scale shell model calculation can provide precisely the properties, excitation schemes and transition probabilities of the low-lying states of a nucleus. However, it requires the diagonalization of the Hamiltonian matrix which has huge dimension (e.g. 10^{14} for ^{150}Ba). In order to do such large-scale nuclear structure calculation including the shell model calculation, we have started this project and introduced massive parallel computers. We mention the installation of the computers in Sec.2 and the physical aspect of this project in Sec.3.

2. Computer Systems

Two parallel computer systems have been installed by the end of the academic year 2003. One is comprised of the Alpha CPUs: 52 of 1 GHz Alpha ev68 CPUs (installed in the academic year 2001), 64 of 1.2 GHz Alpha ev68 CPUs (2002) and 64 of 1.15GHz Alpha ev7 CPUs (2003). Figure 1 shows a photograph of this parallel computer system, called Alphleet-2, which was built primarily by Hewlett-Packard Inc. and Mitsubishi Space Software Inc.

The second parallel computer system was built primarily by Cray Japan Inc. and Mitsubishi Space Software Inc. and comprised of Intel Xeon CPUs: 30 of 2.8GHz CPUs (2002) and 6 of 3.2GHz CPUs (2003).

These computers are placed at the Linac Building, Room B01, Wako, RIKEN. This room is always monitored by four cameras, one smoke detector and many thermometers involved by each computer for disaster prevention. The pictures taken by these cameras can be seen from anywhere through the Internet. As soon as the smoke detector finds something wrong, all the computers are forced to be halted and it notifies all the administrators of the warning message with telephone and e-mail. Thus, the systems can be run quite safely without human attendance.

Figure 1. A photograph of the parallel computer system Alphleet-2 comprised of 170 Alpha CPUs. Four racks on the right end were added in 2003 and comprised of 64 CPUs and 96 GB main memory.

3. Theoretical Methods and Achievements

The scientific purpose of the project is to study a huge variety of nuclear structure by means of the various ways of nuclear structure calculations. In order to obtain wave function of states, we use the shell model calculation for heavy nuclei ($N > 20$) and the molecular-orbit approach for light nuclei ($N \simeq 10$). In addition, the study of the nuclear force is also required. We describe various topics of this project in the following.

The shell-model calculation with exact diagonalization predicts precise physical quantities of low-lying states. However, the range of its application is strongly limited by the dimension of the Hamiltonian matrix practically. One of the authors (T. Mizusaki) wrote the MSHELL code [3] for exact diagonalization method. In addition, he introduced a new extrapolation method [4] based on the MSHELL code in order to obtain the nuclear structure, whose wave function cannot be provided exactly. In this method, the energies of truncated spaces are well described as a function of energy variances, and exact energies can be obtained by the extrapolation.

Another method to obtain the nuclear structure, whose wave function cannot be provided exactly, is the Monte Carlo Shell Model [5]. The MCSM enables us to carry out shell-model calculations for low-lying states of virtually all nuclei. We discussed the sd-pf-shell nuclei and pf-shell

nuclei [6, 7, 8] using the MCSM,

Recently, the structure of neutron-rich nuclei was studied experimentally, and new magic numbers have been observed [9]. By the analysis of the shell-model calculations, we show the origin of the evolution of shell structure and magic numbers of exotic nuclei is the spin-isospin dependent parts of the nucleon-nucleon interaction in nuclei [10].

In the shell model calculation, an atomic nucleus is one of quantum many body systems and it has been of interest to investigate the spectroscopic properties of many-body systems provided by random shell-model Hamiltonians. This investigation is one of major topics of quantum chaos. We studied the ground state properties provided by the random interaction, and showed the dynamical symmetry and quantum chaos are deeply related with each other in Ref. [11].

On the other side, the molecular-orbital approach becomes more important for the study of light nuclei (A $\simeq$ 10). The shell model study, in which the spherical harmonic oscillator potential is assumed, cannot be applied to the study of such extremely exotic nuclei. The molecular-orbital model is essential for our activity to cover the whole region of the nuclear chart. Itagaki wrote the computer code for this model and revealed that ^{14}C could have 3-α plus 2-n structure [12].

4. Summary

We published or submitted [4, 6, 7, 8, 10, 11, 12] in academic year 2003, and some more are being prepared for submissions. We began to study not only the shell-model calculation of the exotic nuclear structure around pf-shell nuclei, but also the various topics including the light exotic nuclei using the molecular-orbital model and the quantum chaos with the random shell-model interaction. The increase in the computer performance, which is described in Sec.2, was essential for the achievements discussed in Sec.3.

References

[1] Grant-in-Aid for Specially Promoted Research (13002001) from the Ministry of Education, Science, Sport, Culture and Technology.

[2] T. Otsuka, N. Shimizu and S. Shimoura, CNS Annual Report, (2002) 81.

[3] T. Mizusaki, RIKEN Accel. Prog. Rep. **33** (2000) 14.

[4] T. Mizusaki and M. Imada, Phys. Rev. C **67**, (2003) 041301.

[5] T. Otsuka, M. Honma, T. Mizusaki, N. Shimizu and Y. Utsuno, Prog. Part. Nucl. Phys. **47** (2001) 319.

[6] A.F. Lisetskiy, N. Pietralla, M. Honma, A. Schmidt, I. Schneider, A. Gade, P. von Brentano, T. Otsuka, T. Mizusaki and B.A. Brown, Phys. Rev. C **68** (2003) 034316.

[7] S.N. Liddick, P.F. Mantica, R.V.F. Janssens, R. Broda, B.A. Brown, M.P. Carpenter, B. Fornal, M. Honma, T. Mizusaki, A.C. Morton, W.F. Mueller, T. Otsuka, J. Pavan, A. Stolz, S.L. Tabor, B.E. Tomlin and M. Wiedeking, Phys. Rev. Lett. **92** (2004) 072502.

[8] M. Honma, T. Otsuka, B. A. Brown and T. Mizusaki, Phys. Rev. C. **69** (2004) 034335.

[9] A. Ozawa, T. Kobayashi, T. Suzuki, K. Yoshida and I. Tanihata, Phys. Rev. Lett. **84** (2000) 5493.

[10] T. Otsuka, Nucl. Phys. A **722** (2003) 347c.

[11] T. Otsuka and N. Shimizu, AIP Conference Proceedings, to be published.

[12] N. Itagaki, T. Otsuka, K. Ikeda and S. Okabe, Phys. Rev. Lett. **92** (2004) 142501.

Other Activities

The Second CNS International Summer School (CISS03)

T. Uesaka[a] T. Otsuka,[b] Y. Koike[a,c] and H. Sakai[a,b]

[a]*Center for Nuclear Study, Graduate School of Science, University of Tokyo*
[b]*Department of Physics, Graduate School of Science, University of Tokyo, .*
[c]*Department of Physics, Hosei University, .*

The 2nd CNS International Summer School (CISS03) was held at the Wako campus of the Center for Nuclear Study (CNS), the University of Tokyo, in the period of September 16 – 20, 2003.

This summer school is the second one in the series which aimed at providing graduate students and postdocs with basic knowledge and perspectives of nuclear physics. "*Nuclear Force and Nuclear Structure*" was chosen for a central subject of this year. Interesting lectures on the subject were given in many different views: from few-nucleon systems to infinite system, from quantumchromodynamics to effective interactions in nuclei, and from neutron/proton rich nuclei to hypernuclei. Lectures on relevant topics, nuclear study with low/high energy radioactive isotope beams, nuclear reaction theory, and quark gluon plasma, were also given.
The list of lecturers and the titles of lectures are shown below.

Y. Akaishi(KEK)	"Tensor Force Effects in Model and Real Spaces / Λ-Σ Couplings in Asymmetric Hyper Nuclei"
Kenneth Amos (Melbourne, Australia)	"Theories and predictions of nucleon-nucleus scattering"
H. Hamagaki (CNS)	"Selected topics from experimental studies at RHIC"
T. Hatsuda (Tokyo)	"QCD and Chiral Symmetry"
M. Honma (Aizu)	"Effective interactions in shell-model calculations"
S. Kubono (CNS)	"Study of Stellar Reactions with Low-Energy RI Beams in Nuclear Astrophysics"
T. Motobayashi (RIKEN)	"Nuclear-structure studies with fast exotic beams"
T. Nilsson (CERN, Switzerland)	"Physics with radioactive beams at CERN-ISOLDE"
V. R. Pandharipande (Illiois, USA)	"Many-Body Theory of Nuclei and Nuclear Matter"
H. Sakai (Tokyo)	"Looking for three-body forces by the nucleon-deuteron elastic scattering at intermediate energy"

This year, 84 attendances were gathered together from 8 countries: Among them, 10 attendances were from Asian countries, China, Korea, Bangladesh, Taiwan. Domestic attendances were from 14 universities and 3 institutes over the country.

In the closing ceremony, foreign lecturers announced that they would award prizes to the excellent talks in the student session. Since they prepared the prize in secret, no student had known about the prize before the closing. The students who got the unexpected present were H. Kuboki (Tokyo), Y. Shimbara (Osaka), K. Nakanishi (Osaka), and W. T. Chiang (Academia Sinica, Taiwan). All the attendance celebrated the prize winners and admired the lecturers for their impressive gifts.

All the information concerning the summer school, including lecture notes, is open for access at the following URL:

http://www.cns.s.u-tokyo.ac.jp/summerschool/

The organizers thank all the attendances and all the members of the CNS who supported the summer school. They are also grateful to RIKEN for their supports in the preparation of the school. This school was supported in part by the International Exchange Program of Graduate School of Science, the University of Tokyo.

Nuclear Scattering Experiments for Education of Undergraduate Students

K. Yako[a], T. Kawabata[b], M. Sasano[a], H. Sakai[a,b] and S. Shimoura[b]

[a] *Department of Physics, University of Tokyo, Tokyo*

[b] *Center for Nuclear Study, Graduate School of Science, University of Tokyo*

Nuclear scattering experiments have been performed for education of undergraduate students of the University of Tokyo as a part of the curriculum of experimental physics. This program is aiming at providing undergraduate students of an opportunity to learn how to study the world of $< 10^{-14}$ m by using an ion beam from an accelerator and basic experimental equipment.

In this year 22 students have participated in four beam times. They used an α beam at $E_\alpha = 6.5$ MeV/A accelerated by the AVF cyclotron and the CRIB beam line in the E7 experimental hall at RIKEN. In each experiment, students were divided into two groups and took one of the following two subjects;

1. Measurement of elastic scattering of α particles from ^{197}Au nucleus.

2. Measurement of gamma-rays emitted in the cascade decay of the rotational bands in ^{154}Gd and ^{184}Os nuclei.

Before the experiment, they learned the operation of the semiconductor detectors at the Hongo campus and took a radiation safety course at RIKEN.

In the $\alpha + {}^{197}$Au measurement, the α particles scattered from a 2.3 mg/cm^2 thick Au foil were detected by a silicon PIN-diode with a thickness of 50 μm located 11 cm away from the target. A plastic collimator with a diameter of 6 mm were attached on the silicon detector. The energy spectrum of the scattered α particles was recorded by a multi-channel analyzer (MCA) system. The beam was stopped by a Faraday cup in the scattering chamber and the charge was measured by a current integrator. The cross section of the reaction was measured typically in the angular region of $\theta_{\rm lab} = 30$–130°. The obtained data were compared with the Rutherford scattering cross sections. The size of gold nucleus has been discussed by taking account of the nuclear potential with a simple square-well shape or the Woods-Saxon shape. Some of the students calculated the angular distribution by the distorted wave Born approximation with a Coulomb wave function and a realistic nuclear potential.

In the measurement of the rotational bands, excited states in ^{154}Gd and ^{184}Os nuclei have been populated by the ^{152}Sm$(\alpha, 2n)$ and ^{182}W$(\alpha, 2n)$ reactions, respectively. The gamma-rays from the cascade decay of the rotational bands were measured by a high purity germanium (HPGe) detector. The gain and the efficiency of the detector system have been calibrated with a ^{152}Eu standard gamma-ray source. Since the target material was glued onto an aluminum plate, a background measurement was also performed by using a dummy target with glue on aluminum backing. Typical spectra are shown in Fig. 1. Four or five gamma-ray peaks from the rotational bands have been identified according to the level scheme. The moment of inertia and the deformation parameters of the excited states have been discussed by using a classical rigid rotor model and a irrotational fluid model. It has been found that the reality lies between the two extreme models. Some students calculated the moment of inertia employing the cranking model and obtained a good agreement with the data. Others discussed the initial population among the levels of the rotational band taking account of the effect of internal conversion.

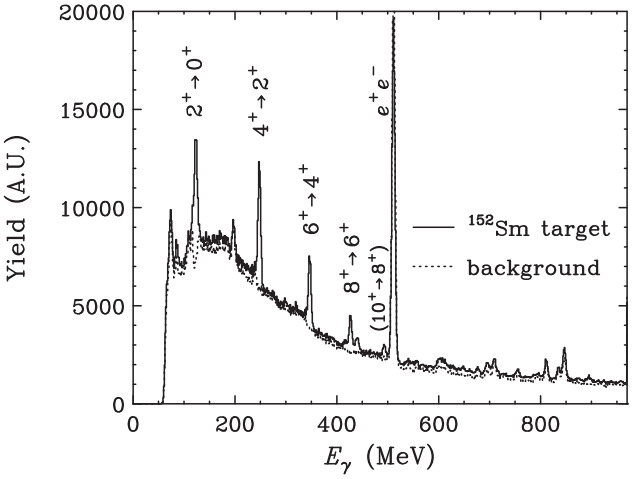

Figure 1. Energy spectrum of gamma-rays from ^{152}Sm(α, X) reaction. The peaks due to the cascade decay of the rotational band of ^{154}Gd are observed.

For most of the students it was the first time to use such large experimental equipment. This program had a strong impact on them. On the spot they became more eagar to learn the operation of the semiconductor detectors as well as other basic things about the experimental nuclear physics. We believe they also enjoyed the process to extract physics from the data by using simple tractable models.

The authors acknowledge S. Kubono and T. Teranishi for improving the work environment around the scattering chamber.

Appendices

Symposia, Workshops, Seminars, and PAC
CNS Reports
Publication List
Talks and Presentations
Personnel

Symposia, Workshops, Seminars and PAC

A. Symposia

1. International Symposium on "Origin of Matter and Evolution of Galaxies 2003" (OMEG03)
   November 17–19, 2003, Nishina Memorial Hall at RIKEN Wako Campus, Japan.

   This is a nuclear astrophysics symposium being held periodically, started back in 1988 as a collaboration of RIKEN accelerator research facility (RARF) and Institute for Nuclear Study, the former institute of CNS. The symposium focused on recent astronomical observations, various progresses in models for the universe as well as both in theoretical and experimental nuclear physics, which includes a successful operation of the CNS low-energy RI beam separator CRIB that provides a variety of RI beams for nuclear astrophysics experiments. The discussion extended to the scope of the fields relevant, specifically the experimental programs to be made at the RIBF project at RIKEN. The symposium was hosted by CNS, RARF and National Astronomical Observatory of Japan, and participated in by 105 scientists including 20 persons from outside of Japan. The proceedings of the symposium will be published from the World Scientific Publishing Co. in Singapore.

   Organizers: S. Kubono (CNS), T. Kajino (RIKEN), T. Kishida (RIKEN), T. Motobayashi (RIKEN), K. Nomoto (Tokyo) and M. Terasawa (CNS).

2. CNS-RIKEN Joint Symposium on "Frontier of gamma-ray spectroscopy and its application (GAMMA04)"
   March 18–19, 2004, Nishina Memorial Hall at RIKEN Wako Campus, Japan.

   This symposium was held for the period of March 18–19, 2004, at Nishina hall in RIKEN, Wako, Saitama, Japan. It was co-hosted by CNS and RIKEN. The purpose of the symposium was to discuss recent progress in the field of gamma-ray spectroscopy in both high spin and high isospin as well as recent development of advanced gamma-ray detectors. More than 60 people, including 7 from abroad,participated in the symposium, and good presentations and valuablediscussions were made. Details of the symposium is described in the following web-page; http://www.cns.s.u-tokyo.ac.jp/gamma04/

   Organizers: E. Ideguchi (Chair, CNS), T. Motobayashi (RIKEN), S. Shimoura (CNS), H. Tamura (Tohoku), T. Ishii (JAERI), T. Otsuka (Tokyo), K. Asahi (RIKEN/TIT), H. Watanabe (RIKEN), N. Aoi (RIKEN).

B. Workshops

1. International Workshop on"Beam Cooling and Related Topics"
   May 19–23, 2003, Hotel Mt. Fuji, Yamanashi, Japan.

   Review of beam cooling and the related physics were presented. It was stressed that the new discoveries of nuclear, particle and atomic physics were performed with the aid of beam cooling technique. Also the details of electron cooling, stochastic cooling, laser cooling and muon cooling were presented. The future prospect of beam cooling were discussed to make a breakthrough to the new science. Participants were counted 120, from 8 countries. The workshop was sponsored by the University of Tokyo and RIKEN.

   Organizers: T. Katayama (Chair, CNS/RIKEN), Y. Mori (KEK), A. Noda (Kyoto), K. Noda (NIRS), H. Okamoto (Hiroshima), T. Tanabe (KEK), Y. Yamazaki (RIKEN/Tokyo), Y. Yano (RIKEN), T. Kikuchi (Tokyo), T. Koseki (RIKEN), M. Nishiura (NIFS), M. Okamura (RIKEN), S. Ozawa (RIKEN), S. Watanabe (CNS), M. Takanaka (RIKEN), H. Tsutsui (RIKEN), M. Watanabe (RIKEN), T. Watanabe (RIKEN), M. Takano (RIKEN).

2. Symposium and Workshop on "the Quark-Gluon Plasma and Heavy-Ion Physics at RHIC and LHC", July 25, 2003, School of Science Build. 4(room 1220), University of Tokyo, Tokyo, Japan.

   With two famous theorists H. Satz (Bielfeld) and X-N. Wang (LBNL), a small workshop was held to overview the progress at RHIC and to discuss physics possibilities at LHC.

Participants: about 30
Organizers: H. Hamagaki(CNS), T. Hatsuda(Tokyo), T. Matsui(Tokyo).

3. Workshop on "Perspectives of Polarization in RI-beam Induced Reactions", March 2–4, 2004, CNS Wako Campus, Saitama, Japan.

   The purpose of this workshop was to discuss possible physical knowledge to be gained via polarization measurements in RI beam induced reactions and to establish directions in future experimental investigations with RI beams and polarized targets. Experimental plans and polarized target technology employed at CNS/RIKEN, HRIBF/PSI, and EURISOL were discussed.

   Organizers: T. Uesaka (CNS), T. Wakui (CNS), T. Kawabata (CNS), H. Sakai (CNS/Tokyo)

C. CNS Seminars

1. "r-Process Nucleosynthesis in the Neutrino-Driven Winds from Rotating Proto-Neutron Star",
   T. Yamazaki (Department of Astronomy, Kyoto University), June 4, 2003.
2. "Measurements of Eu Isotope Abundances in Metal-Deficient Stars",
   W. Aoki (National Astronomical Observatory of Japan), July 9, 2003.

D. CNS Program Advisory Committee

1. The 4th CNS PAC meeting
   December 8, 2003.

   The CNS Program Advisory Committee considered 7 proposals for 45 days of beam time. The PAC recommended allocation of $26.5 + 6$ (conditional) days for 6 experiments.

   Approved Proposals

   (a) T. Katayama: Interaction of Heavy Ion Beams with Laser-Excited Plasma (2.5 days)
   (b) T. Teranishi: Search for Proton Resonant States via the $^{14}\mathrm{O} + p$ and $^{13}\mathrm{N} + p$ Elastic Scatterings (9 days)
   (c) A. Odahara: Search for Isomer States in $N = 51$ Nuclei by Fusion Reaction of Unstable Nuclear Beam ^{17}N ($2 + 6$ (conditional) days)
   (d) M. Nishimura: Reaction Cross Sections of Nuclear-Astrophysical Interest Studied with $^{8}\mathrm{Li}$ Beam (3 days)
   (e) Zs. Fülöp: Half-life Measurement of $^{39}\mathrm{Ar}$ using Radioactive Beam Implantation (2 days)
   (f) M. Dasgupta: Dependence on Neutron Excess of Inhibition of Fusion by Quasi-Fission (8 days)

CNS Reports

#58 "Structure of the Unbound ^{11}N Nucleus by the (^{3}He, ^{6}He) Reaction"
V. Guimarães, S. Kubono, F.C. Barker, M. Hosaka, S.C. Jeong, I. Katayama, T. Miyachi, T. Nomura, M.H. Tanaka, Y. Fuchi, H. Kawasima, S. Kato, C.C. Yun, K. Ito, H. Orihara, T. Terakawa, T. Kishida, Y. Pu, S. Hamada, M. Hirai and H. Miyatake, Apr. 2003.

#59 "CNS Annual Report 2002"
edited by T. Uesaka and N. Suzuki, Jul. 2003.

#60 "Direct Mesurement of the Astrophysical Preaction ^{14}O(α, p)^{17}F"
M. Notani, S. Kubono, T. Teranishi, Y. Yanagisawa, S. Michimasa, K. Ue, J.J. He, H. Iwasaki, H. Baba, M. Tamaki, T. Minemura, S. Shimoura, N. Hokoiwa, Y. Wakabayashi, T. Sasaki, T. Fukuchi, A. Odawara, Y. Gono, Zs. Fülöp, E.K. Lee, K.I. Hahn, J.Y. Moon, C.C. Yun, J.H. Lee, C.S. Lee and S. Kato, Jan. 2003.

Publication List

A. Original Papers

1. K. Adcox *et al.* (PHENIX Collaboration): "PHENIX detector overview", Nucl. Instrum. Methods. A **499** (2003) 469–479.

2. M. Aizawa *et al.* (PHENIX Collaboration): "PHENIX central arm particle I.D. detectors", Nucl. Instrum. Methods. A **499** (2003) 508–520.

3. K. Adcox *et al.* (PHENIX Collaboration): "Centrality Dependence of the High $p_{\rm T}$ Charged Hadron Suppression in Au+Au collisions at $\sqrt{s_{NN}} = 130$ GeV", Phys. Lett. B **561** (2003) 82–92.

4. S.S. Adler *et al.* (PHENIX Collaboration): "Suppressed π^0 Production at Large Transverse Momentum in Central Au+Au Collisions at $\sqrt{s_{NN}} = 200$ GeV", Phys. Rev. Lett. **91** (2003) 072301.

5. S.S. Adler *et al.* (PHENIX Collaboration): "Absence of Suppression in Particle Production at Large Transverse Momentum in $\sqrt{s_{NN}} = 200$ GeV $d+{\rm Au}$ Collisions", Phys. Rev. Lett. **91** (2003) 072303.

6. S.S. Adler *et al.* (PHENIX Collaboration): "Scaling properties of proton and anti-proton production in $\sqrt{s_{NN}} =$ 200 GeV Au + Au collisions", Phys. Rev. Lett. **91** (2003) 172301.

7. S.S. Adler *et al.* (PHENIX Collaboration): "Elliptic Flow of Identified Hadrons in Au+Au Collisions at $\sqrt{s_{NN}} =$ 200 GeV", Phys. Rev. Lett. **91** (2003) 182301.

8. S.S. Adler *et al.* (PHENIX Collaboration): "Mid-Rapidity Neutral Pion Production in Proton-Proton Collisions at $\sqrt{s_{NN}} = 200$ GeV", Phys. Rev. Lett. **91** (2003) 241803.

9. S.S. Adler *et al.* (PHENIX Collaboration): "J/ψ Production in Au-Au Collisions at $\sqrt{s_{NN}} = 200$ GeV at the Relativistic Heavy Ion Collider", Phys. Rev. C **69** (2004) 014901.

10. S.S. Adler *et al.* (PHENIX Collaboration): "J/ψ production from proton-proton collisions at $\sqrt{s} = 200$ GeV", Phys. Rev. Lett. **92** (2004) 051802.

11. K. Adcox *et al.* (PHENIX Collaboration): "Single Identified Hadron Spectra from $\sqrt{s_{NN}} = 130$ GeV Au+Au Collisions", Phys. Rev. C **69** (2004) 024904.

12. S.S. Adler *et al.* (PHENIX Collaboration): "Identified Charged Particle Spectra and Yields in Au+Au Collisions at $\sqrt{s_{NN}} = 200$ GeV", Phys. Rev. C **69** (2004) 034909.

13. S.S. Adler *et al.* (PHENIX Collaboration): "High-$p_{\rm T}$ Charged Hadron Suppression in Au+Au Collisions at $\sqrt{s_{NN}} =$ 200 GeV", Phys. Rev. C **69** (2004) 034910.

14. H. Amemiya, T. Tanabe and T. Katayama: "Cooling of Ions by Cold Electron through Coulomb Collisions", J. of Phys. Soc. of Japan **73** (2004) 617.

15. S. Bishop, R.E. Azuma, L. Buchmann, A.A. Chen, M.L. Chatterjee, J.M. D'Auria, S. Engel, D. Gigliotti, U. Greife, M. Hernanz, D. Hunter, A. Hussein, D. Hutcheon, C. Jewett, J. Jose, J. King, S. Kubono, A.M. Laird, M. Lamey, R. Lewis, W. Liu, S. Michimasa, A. Olin, D. Ottewell, P.D. Parker, J.G. Rogers, F. Strieder, C. Wrede: "The ^{21}Na(p,γ)^{22}Mg Reaction and Oxygen-Neon Novae", Phys. Rev. Lett. **90** (2003) 162501; Phys. Rev. Lett. **90** (2003) 229902.

16. C.J. Chiara, E. Ideguchi, M. Devlin, D.R. LaFosse, F. Lerma, W. Reviol, S.K. Ryu, D.G. Sarantites, C. Baktash, A. Galindo-Uribarri, M.P. Carpenter, R.V.F. Janssens, T. Lauritsen, C.J. Lister, P. Reiter, D. Seweryniak, P. Fallon, A. Gorgen, A.O. Macchiavelli, D. Rudolph: "Transition quadrupole moments in the superdeformed band of ^{40}Ca", Phys. Rev. C **67** (2003) 041303.

17. Z. Elekes, Zs. Dombrádi, A. Krasznahorkay, H. Baba, M. Csatlós, L. Csige, N. Fukuda, Zs. Fülöp, Z. Gácsi, J. Gulyás, N. Iwasa, H. Kinugawa, S. Kubono, M. Kurokawa, X. Liu, S. Michimasa, T. Minemura, T. Motobayashi, A. Ozawa, A. Saito, S. Shimoura, S. Takeuchi, I. Tanihata, P. Thirolf, Y. Yanagisawa, K. Yoshida: "Decoupling of Valence Neutrons from the Core in ^{16}C", Phys. Lett. B **586** (2004) 34–40.

18. Y. Fujita, Y. Shimbara, A. F. Lisetskiy, T. Adachi, G.P.A. Berg, P. von Brentano, H. Fujimura, H. Fujita, K. Hatanaka, J. Kamiya, T. Kawabata, H. Nakada, K. Nakanishi, Y. Shimizu, M. Uchida, M. Yosoi: "Analogous Gamow-Teller and $M1$ transitions in ^{26}Mg, ^{26}Al, and ^{26}Si", Phys. Rev. C **67** (2003) 064312.

19. V. Guimarães, S. Kubono, F. C. Barker, M. Hosaka, S. C. Jeong, I. Katayama, T. Miyachi, T. Nomura, M. H. Tanaka, Y. Fuchi, H. Kawashima, S. Kato, C.C. Yun, K. Ito, H. Orihara, T. Terakawa, T. Kishida, Y. Pu, S. Hamada, M. Hirai, and H. Miyatake: "Study of the Unbound ^{11}N Nucleus by the (^{3}He, ^{6}He) Reaction", Phys. Rev. C **67** (2003) 064601.

20. K. Hara, T. Adachi, H. Akimune, I. Daito, H. Fujimura, Y. Fujita, M. Fujiwara, K. Fushimi, K.Y. Hara, M.N. Harakeh, K. Ichihara, T. Ishikawa, J. Janecke, J. Kamiya, T. Kawabata, K. Kawase, K. Nakanishi, Y. Sakemi, Y. Shimbara, Y. Shimizu, M. Uchida, H.P. Yoshida, M. Yosoi, R.G.T. Zegers: "Microscopic structure of the Gamow-Teller resonance in ^{58}Cu", Phys. Rev. C **68** (2003) 064612.

21. M. Honma, T. Otsuka, B.A. Brown and T. Mizusaki: "New effective interaction for pf-shell nuclei and its implications for the stability of the $N = Z = 28$ closed core", Phys. Rev. C **69** (2004) 034335.

22. N. Imai, H.J. Ong, N. Aoi, H. Sakurai, K. Demichi, H. Kawasaki, H. Baba, Zs. Dombrádi, Z. Elekes, N. Fukuda, Zs. Fülöp, A. Gelberg, T. Gomi, H. Hasegawa, K. Ishikawa, H. Iwasaki, E. Kaneko, S. Kanno, T. Kishida, Y. Kondo, T. Kubo, K. Kurita, S. Michimasa, T. Minemura, M. Miura, T. Motobayashi, T. Nakamura, M. Notani, T.K. Onishi, A. Saito, S. Shimoura, T. Sugimoto, M.K. Suzuki, E. Takeshita, S. Takeuchi, M. Tamaki, K. Yamada, K. Yoneda, H. Watanabe, M. Ishihara: "Anomalously hindered $E2$ strength B($E2; 2_1^+ \rightarrow 0^+$) in ^{16}C", Phys. Rev. Lett. **92** (2004) 062501.

23. M. Inuzuka, H. Hamagaki, K. Ozawa, T. Tamagawa and T. Isobe: "Gas electron multiplier produced with the plasma etching method", Nucl. Instrum. Methods. A **525** (2004) 529–534.

24. M. Itoh, H. Sakaguchi, M. Uchida, T. Ishikawa, T. Kawabata, T. Murakami, H. Takeda, T. Taki, S. Terashima, N. Tsukahara, Y. Yasuda, M. Yosoi, U. Garg, M. Hedden, B. Kharraja, M. Koss, B.K. Nayak, S. Zhu, H. Fujimura, M. Fujiwara, K. Hara, H.P. Yoshida, H. Akimune, M. N. Harakeh, M. Volkerts: "Systematic study of $L \leq 3$ giant resonances in Sm isotopes via multipole decomposition analysis", Phys. Rev. C **68** (2003) 064602.

25. N. Iwasa, T. Motobayashi, H. Sakurai, H. Akiyoshi, Y. Ando, N. Aoi, H. Baba, N. Fukuda, Zs. Fülöp, U. Futakami, T. Gomi, Y. Higurashi, K. Ieki, H. Iwasaki, T. Kubo, S. Kubono, H. Kinugawa, H. Kumagai, M. Kunibu, S. Michimasa, T. Minemura, H. Murakami, K. Sagara, A. Saito, S. Shimoura, S. Takeuchi, Y. Yanagisawa, K. Yoneda, M. Ishihara: "In-beam γ spectroscopy of ^{34}Si with deuteron inelastic scattering using reverse kinematics", Phys. Rev. C **67** (2003) 064315.

26. J. Kamiya, K. Hatanaka, T. Adachi, K. Fujita, K. Hara, T. Kawabata, T. Noro, H. Sakaguchi, N. Sakamoto, Y. Sakemi, Y. Shimbara, Y. Shimizu, S. Terashima, M. Uchida, T. Wakasa, Y. Yasuda, H. P. Yoshida, M. Yosoi: "Calibration of the effective analyzing power for a ^{3}He polarimeter at 443 MeV", Nucl. Instrum. Methods. A **507** (2003) 703.

27. J. Kamiya, K. Hatanaka, T. Adachi, F. Fujita, K. Hara, T. Kawabata, T. Noro, H. Sakaguchi, N. Sakamoto, Y. Sakemi, Y. Shimbara, H. Shimizu, S. Terashima, M. Uchida, T. Wakasa, Y. Yasuda, H. P. Yoshida, M. Yosoi: "Cross section and induced polarization in ^{3}He elastic scattering at 443 MeV", Phys. Rev. C **67** (2003) 064612.

28. T. Katayama, T. Suda and I. Tanihata: "Status of MUSES Project and Electron RI Collider at RIKEN" Physica Scripta. **T104**, (2003) 129–143.

29. T. Kikuchi, M. Nakajima, K. Horioka, T. Katayama: "Transverse particle distribution of intense beams after final bunching for heavy ion inertial fusion", J. Plasma Fusion Res. **80** (2004) 87–88.

30. T. Kikuchi, M. Nakajima, K. Horioka, T. Katayama: "Beam instability induced by space charge oscillation during final beam bunching for heavy ion inertial fusion", Phys. Rev. ST Accel. Beams **7** (2004) 034201.

31. A. Kozlov, I. Ravinovich, L. Shekhtman, Z. Fraenkel, M. Inuzuka and I. Tserruya: "Development of a triple GEM UV-photon detector operated in pure CF4 for the PHENIX experiment", Nucl. Instrum. Methods. A **523** (2004) 345–354.

32. S. Kubono, K. Abe, S. Kato, T. Teranishi, M. Kurokawa, X. Liu, N. Imai, K. Kumagai, P. Strasser, M. H. Tanaka, Y. Fuchi, C.S. Lee, Y.K. Kwon, L. Lee, J.H. Ha, and Y.K. Kim: "Determination of the Subthreshold State Contribution in ^{13}C(α, n) ^{16}O, the Main Neutron-Source Reaction for the s-Process", Phys. Rev. Lett. **90** (2003) 062501.

33. M. Kurokawa, S. Shimoura, H. Iwasaki, H. Baba, S. Michimasa, S. Ota, H. Murakami, H. Sakai: "Pulse Shape Simulation and Analysis of Segmented Ge Detectors for Position Extraction", IEEE Trans. Nucl. Sci. **50** (2003) 1309–1316.

34. S.N. Liddick, P.F. Mantica, R.V.F. Janssens, R. Broda, B.A. Brown, M.P. Carpenter, B. Fornal, M. Honma, T. Mizusaki, A.C. Morton, W.F. Mueller, T. Otsuka, J. Pavan, A. Stolz, S.L. Tabor, B.E. Tomlin, and M. Wiedeking: "Lowest Excitations in ^{56}Ti and the predicted $N = 34$ shell closure", Phys. Rev. Lett. **92** (2004) 072502.

35. A.F. Lisetskiy, N. Pietralla, M. Honma, A. Schmidt, I. Schneider, A. Gade, P. von Brentano, T. Otsuka, T. Mizusaki, and B.A. Brown: "Experimental evidence for ^{56}Ni-core breaking from the low-spin structure of the $N = Z$ nucleus $^{58}_{29}$Cu$_{29}$", Phys. Rev. C **68** (2003) 034316.

36. M. Sekimoto, J. Chiba, H. Funahashi, H. Hamagaki, M. Ieiri, M. Ishino, M. Kitaguchi, S. Mihara, T. Miyashita, T. Murakami, R. Muto, M. Naruki, M. Nomachi, K. Ozawa, F. Sakuma, O. Sasaki, T. Tabaru, K. H. Tanaka, S. Yamada, S. Yokkaichi, Y. Yoshimura, H. En'yo: "Spectrometer for measurements of ϕ mesons in nuclear matter produced through 12-GeV p + A reactions", Nucl. Instrum. Methods. A **516** (2004) 390–405.

37. S. Shimoura, A. Saito, T. Minemura, Y.U. Matsuyama, H. Baba, H. Akiyoshi, N. Aoi, T. Gomi, Y. Higurashi, K. Ieki, N. Imai, N. Iwasa, H. Iwasaki, S. Kanno, S. Kubono, M. Kunibu, S. Michimasa, T. Motobayashi, T. Nakamura, H. Sakurai, M. Serata, E. Takeshita, S. Takeuchi, T. Teranishi, K. Ue, K. Yamada, Y. Yanagisawa, M. Ishihara, N. Itagaki: "Isomeric 0^+ state in ^{12}Be", Phys. Lett. B **560** (2003) 31–36.

38. T. Suzuki, R. Fujimoto and T. Otsuka: "Gamow-Teller transitions and magnetic properties of nuclei and shell evolution", Phys. Rev. C **67** (2003) 044302.

39. T. Teranishi, S. Kubono, S. Shimoura, M. Notani, Y. Yanagisawa, S. Michimasa, K. Ue, H. Iwasaki, M. Kurokawa, Y. Satou, T. Morikawa, A. Saito, H. Baba, J. H. Lee, C. S. Lee, Zs. Fülöp, and S. Kato: "Study of Resonance States in ^{12}N Using a Radioactive Ion Beam of ^{11}C", Phys. Lett. B **556** (2003) 27–32.

40. H. Watanabe, H. Ueno, D. Kameda, W. Sato, A. Yoshimi, H. Miyoshi, T. Kishida, Y. Kobayashi, A. Odahara, Y. Gono, K. Asahi: "g-Factor of the high-spin isomer in ^{149}Dy and a multi-quasiparticle configuration caused by the $N = 82$ core excitations", Nucl. Phys. A **728** (2003) 365-378.

41. H. Watanabe, Y. Wakabayashi, Y. Gono, T. Fukuchi, H. Ueno, W. Sato, A. Yoshimi, D. Kameda, H. Miyoshi, T. Kishida, Y. Kobayashi, T. Morikawa, S. Motomura, O. Kashiyama, K. Saito, A. Odahara, K. Asahi: "Lifetime of a new high-spin isomer in ^{150}Dy", Eur. Phys. J. A **19** (2004) 163.

42. K. Yamada, T. Motobayashi, H. Akiyoshi, N. Aoi, Zs, Fülöp, T. Gomi, Y. Higurashi, N. Imai, N. Iwasa, H. Iwasaki, Y. Iwata, H. Kobayashi, M. Kurokawa, Z. Liu, T. Minemura, S. Ozawa, H. Sakurai, M. Serata, S. Shimoura, S. Takeuchi, T. Teranishi, Y. Yanagisawa, K. Yoshida, M. Ishihara: "$E1$ strength of the subthreshold $3/2^+$ state in ^{15}O studied by Coulomb excitation", Phys. Lett. B **579** (2004) 265–270.

43. Y. Yanagisawa, M. Notani, H. Sakurai, M. Kunibu, H. Akiyoshi, N. Aoi, H. Baba, K. Demichi, N. Fukuda, H. Hasegawa, Y. Higurashi, M. Ishihara, N. Iwasa, H. Iwasaki, T. Gomi, S. Kanno, M. Kurokawa, Y.U. Matsuyama, S. Michimasa, T. Minemura, T. Mizoi, T. Nakamura, A. Saito, M. Serata, S. Shimoura, T. Sugimoto, E. Takeshita, S. Takeuchi, K. Ue, K. Yamada, K. Yoneda, T. Motobayashi: "The first excited state of ^{30}Ne studied by proton inelastic scattering in reversed kinematics", Phys. Lett. B **566** (2003) 84–89.

44. R.G.T. Zegers, H. Abend, H. Akimune, A.M. van den Berg, H. Fujimura, H. Fujita, Y. Fujita, M. Fujiwara, S. Gales, K. Hara, M.N. Harakeh, T. Ishikawa, T. Kawabata, K. Kawase, T. Mibe, K. Nakanishi, S. Nakayama, H. Toyokawa, M. Uchida, T. Yamagata, K. Yamasaki, M. Yosoi: "Excitation and Decay of the Isovector Giant Monopole Resonances via the ^{208}Pb(^{3}He, tp) Reaction at 410 MeV", Phys. Rev. Lett. **90** (2003) 202501.

B. Proceedings

1. N.N. Ajitanand, for the PHENIX Collaboration: "Two Particle Azimuthal Correlation Measurement in PHENIX", Proc. of the 16th International Conference on Ultra-Relativistic Nucleus-Nucleus Collisions (QM2002), Jul. 18–24, 2002, Nantes, France, Nucl. Phys. A **715** (2003) 765c–768c.

2. R. Averbeck, for the PHENIX Collaboration: "Single leptons from heavy flavor decays at RHIC", Proc. of the 16th International Conference on Ultra-Relativistic Nucleus-Nucleus Collisions (QM2002), Jul. 18–24, 2002, Nantes, France, Nucl. Phys. A **715** (2003) 695c–698c.

3. A. Bazilevsky, for the PHENIX Collaboration: "Charged Particle Multiplicity and Transverse Energy Measurements in Au-Au collisions in PHENIX at RHIC", Proc. of the 16th International Conference on Ultra-Relativistic Nucleus-Nucleus Collisions (QM2002), Jul. 18–24, 2002, Nantes, France, Nucl. Phys. A **715** (2003) 486c–489c.

4. J.M. Burward-Hoy, for the PHENIX Collaboration: "Source Parameters from Identified Hadron Spectra and HBT Radii for Au-Au Collisions at $\sqrt{s_{NN}} = 200$ GeV in PHENIX", Proc. of the 16th International Conference on Ultra-Relativistic Nucleus-Nucleus Collisions (QM2002), Jul. 18–24, 2002, Nantes, France, Nucl. Phys. A **715** (2003) 498c–501c.

5. T. Chujo, for the PHENIX Collaboration: "Results on Identified Hadrons from the PHENIX Experiment at RHIC", Proc. of the 16th International Conference on Ultra-Relativistic Nucleus-Nucleus Collisions (QM2002), Jul. 18–24 ,2002, Nantes, France, Nucl. Phys. A **715** (2003) 151c–160c.

6. M. Chiu, for the PHENIX Collaboration: "Charged Particle Angular Correlations from Leading Photons at RHIC", Proc. of the 16th International Conference on Ultra-Relativistic Nucleus-Nucleus Collisions (QM2002), Jul. 18–24, 2002, Nantes, France, Nucl. Phys. A **715** (2003) 761c–764c.

7. D. d'Enterria, for the PHENIX Collaboration: "High-$p_{\rm T}$ π^0 suppression in Au+Au collisions at $\sqrt{s_{NN}} = 200$ GeV", Proc. of the 16th International Conference on Ultra-Relativistic Nucleus-Nucleus Collisions (QM2002), Jul. 18–24, 2002, Nantes, France, Nucl. Phys. A **715** (2003) 749c–752c.

8. A. Enokizono, for the PHENIX Collaboration: "Two-particle correlations measured by PHENIX in Au-Au collisions at $\sqrt{s_{NN}} = 200$ GeV", Proc. of the 16th International Conference on Ultra-Relativistic Nucleus-Nucleus Collisions (QM2002), Jul. 18–24, 2002, Nantes, France, Nucl. Phys. A **715** (2003) 595c–598c.

9. ShinIchi Esumi, for the PHENIX Collaboration: "Identified charged particle azimuthal anisotropy in PHENIX at RHIC", Proc. of the 16th International Conference on Ultra-Relativistic Nucleus-Nucleus Collisions (QM2002), Jul. 18–24, 2002, Nantes, France, Nucl. Phys. A **715** (2003) 599c–602c.

10. A.D. Frawleyb, for the PHENIX Collaboration: "$J/\Psi \rightarrow ee$ and $J/\Psi \rightarrow \mu\mu$ Measurements in *AuAu* and *pp* Collisions at $\sqrt{s_{NN}} = 200$ GeV", Proc. of the 16th International Conference on Ultra-Relativistic Nucleus-Nucleus Collisions (QM2002), Jul. 18–24, 2002, Nantes, France, Nucl. Phys. A **715** (2003) 687c–690c.

11. S. Mioduszewski, for the PHENIX Collaboration: "High p_T Measurements from PHENIX", Proc. of the 16th International Conference on Ultra-Relativistic Nucleus-Nucleus Collisions (QM2002), Nantes, France, Jul. 18–24, 2002, Nucl. Phys. A **715** (2003) 199c–208c.

12. Debsankar Mukhopadhyay, for the PHENIX Collaboration: "ϕ meson production in Au-Au collisions at $\sqrt{s_{NN}} = 200$ GeV", Proc. of the 16th International Conference on Ultra-Relativistic Nucleus-Nucleus Collisions (QM2002), Jul. 18–24, 2002, Nantes, France, Nucl. Phys. A **715** (2003) 494c–497c.

13. J.L. Nagle, for the PHENIX Collaboration: "Leptonic Observables in Ultra-Relativistic Heavy-Ion Collisions", Proc. of the 16th International Conference on Ultra-Relativistic Nucleus-Nucleus Collisions (QM2002), Jul. 18–24, 2002, Nantes, France, Nucl. Phys. A **715** (2003) 252c–261c.

14. J. Nystrand, for the PHENIX Collaboration: "Charge Fluctuations at Mid-Rapidity in Au+Au Collisions in the PHENIX experiment at RHIC", Proc. of the 16th International Conference on Ultra-Relativistic Nucleus-Nucleus Collisions (QM2002), Jul. 18–24, 2002, Nantes, France, Nucl. Phys. A **715** (2003) 603c–606c.

15. Klaus Reygers, for the PHENIX Collaboration: "Results on Photon Production in Au+Au Collisions at RHIC", Proc. of the 16th International Conference on Ultra-Relativistic Nucleus-Nucleus Collisions (QM2002), Jul. 18–24, 2002, Nantes, France, Nucl. Phys. A **715** (2003) 683c–686c.

16. T. Sakaguchi, for the PHENIX Collaboration: "High p_T identified hadron ratios in $\sqrt{s_{NN}} = 200$ GeV Au+Au Collisions", Proc. of the 16th International Conference on Ultra-Relativistic Nucleus-Nucleus Collisions (QM2002), Jul. 18–24, 2002, Nantes, France, Nucl. Phys. A **715** (2003) 757c–760c.

17. H. Torii, for the PHENIX Collaboration: "Measurement of the neutral pion cross section in proton-proton collisions at $\sqrt{s} = 200$ GeV with PHENIX", Proc. of the 16th International Conference on Ultra-Relativistic Nucleus-Nucleus Collisions (QM2002), Jul. 18–24, 2002, Nantes, France, Nucl. Phys. A **715** (2003) 753c–756c.

18. R.E. Azuma, S. Bishop, L. Buchmann, M.L. Chatterjee, A.A. Chen, J.M. D'Auria, T. Davinson, S. Engel, B.R. Fulton, D. Gigliotti, U. Greife, D. Groombridge, D. Hunter, A. Hussein, D. Hutcheon, C. Jewett, J.D. King, N. Khan, S. Kubono, A.M. Laird, M. Lamey, R. Lewis, L. Ling, W. Liu, S. Michimasa, A.S. Murphy, A. Olin, D. Ottewell, P. Parker, J. Pearson, I. Roberts, A. Robinson, J.G. Rogers, G. Roy, C. Ruiz, F. Sarazin, A.C. Shotter, H. Sprenger, F. Strieder, P. Walden, P.J. Woods, C. Wrede: "Results of ^{21}Na + p Experiments at ISAC", Proc. of Int. Symp. Nuclei in the Cosmos VII, Jul. 8–12, 2002, Fuji-Yoshida, Japan, Nucl. Phys. A **718** (2003) 119c–126c.

19. S. Bishop, R. Azuma, L. Buchmann, A.A. Chen, M.L. Chatterjee, J.M. D'Auria, S. Engel, D. Gigliotti, U. Greife, D. Hunter, A. Hussein, D. Hutcheon, C. Jewett, J. King, S. Kubono, M. Lamey, R. Lewis, W. Liu, S. Michimasa, A. Olin, D. Ottewell, P.D. Parker, J. Rogers, C. Wrede: "Nuclear Astrophysics Studies at DRAGON: the ^{21}Na(p,γ)^{22}Mg Reaction and Oxygen-Neon Novae", Proc. of Int. Symp. Nuclei in the Cosmos VII, Jul. 8–12, 2002, Fuji-Yoshida, Japan, Nucl. Phys. A **718** (2003) 263c–268c.

20. Zs. Fülöp, L. Bartha, Gy. Gyurky, E. Somorjai, S. Kubono, H. Kudo and D. Kaji: "The Half-Life of ^{148}Gd", Proc. of Int. Symp. Nuclei in the Cosmos VII, Jul. 8–12, 2002, Fuji-Yoshida, Japan, Nucl. Phys. A **718** (2003) 688c–690c.

21. T. Gomi, T. Motobayashi, K. Yoneda, S. Kanno, N. Aoi, Y. Ando, H. Baba, K. Demichi, Zs. Fülöp, U. Futakami, H. Hasegawa, Y. Higurashi, K. Ieki, N. Imai, N. Iwasa, H. Iwasaki, T. Kubo, S. Kubono, M. Kunibu, Y.U. Matsuyama, S. Michimasa, T. Minemura, H. Murakami, T. Nakamura, A. Saito, H. Sakurai, M. Serata, S. Shimoura, T. Sugimoto, E. Takeshita, S. Takeuchi, K. Ue, K. Yamada, Y. Yanagisawa, A. Yoshida, M. Ishihara: "Study of the ^{22}Mg(p,γ)^{23}Al reaction with the Coulomb-dissociation method", Proc. of Int. Symp. Nuclei in the Cosmos VII, Jul. 8–12, 2002, Fuji-Yoshida, Japan,eds. S. Kubono, Nucl. Phys. A **718** (2003) 508c–509c.

22. S. Kato, K. Abe, S. Kubono, T. Teranishi, M. Kurokawa, X. Liu, P. Strasser, N. Imai, K. Kumagai, C. S. Lee, Y. K. Kwon, C. Lee, J.H. Ha, Y.K. Kim, M.H. Tanaka and Y. Fuchi: "Determination of the Sub-Threshold Contribution in the ^{13}C(α,n) ^{16}O Reaction for the Neutrons of s-Process", Proc. of Int. Symp. Nuclei in the Cosmos VII, Jul. 8–12, 2002, Fuji-Yoshida, Japan, Nucl. Phys. A **718** (2003) 189c–192c.

23. S. Michimasa, S. Kubono, S.H. Park, T. Teranishi, Y. Yanagisawa, N. Imai, Zs. Fülöp, X. Liu, T. Minemura, C.C. Yun, J.M. D'Auria, K.P. Jackson: "Study on the ^{21}Na(p,γ)^{22}Mg Stellar Reaction by the (p,t) Reaction", Proc. of Int. Symp. Nuclei in the Cosmos VII, Jul. 8–12, 2002, Fuji-Yoshida, Japan, Nucl. Phys. A **718** (2003) 581c–583c.

24. T. Teranishi, S. Kubono, S. Shimoura, M. Notani, Y. Yanagisawa, S. Michimasa, K. Ue, H. Iwasaki, M. Kurokawa, Y. Satou, T. Morikawa, A. Saito, H. Baba, J.H. Lee, C.S. Lee, Zs. Fülöp, S. Kato: "Experimental Studies Using a Low-Energy RI Beam Separator at CNS", Proc. of Int. Symp. Nuclei in the Cosmos VII, Jul. 8–12, 2002, Fuji-Yoshida, Japan, Nucl. Phys. A **718** (2003) 207c–213c.

25. Z. Elekes, G. Kalinka, Zs. Fülöp, J. Gál, J. Molnár, G. Hegyesi, D. Novák, J. Végh, T. Motobayashi, A. Saito, and Y. Yanagisawa: "Optimization of the performance of a CsI(Tl) scintillator + Si PIN photodiode detector for medium-energy light-charged particle hybrid array", Proc. of the 17th International Nuclear Physics Divisional Conference of the European Physics Society "Nuclear Physics in Astrophysics", Sep. 30–Oct. 4, 2002, Debrecen, Hungary, Nucl. Phys. A **719** (2003) 316c–321c.

26. T. Teranishi, S. Kubono, S. Shimoura, M. Notani, Y. Yanagisawa, S. Michimasa, K. Ue, H. Iwasaki, M. Kurokawa, Y. Satou, T. Morikawa, A. Saito, H. Baba, J.H. Lee, C.S. Lee, Zs. Fülöp, S. Kato: "Study of resonance states using a low-energy RI beam separator at CNS", Proc. of the 17th International Nuclear Physics Divisional Conference of the European Physics Society "Nuclear Physics in Astrophysics", Sep. 30–Oct. 4, 2002, Debrecen, Hungary, Nucl. Phys. A **719** (2003) 253c–256c.

27. T. Chujo, for the PHENIX Collaboration: "Results on Identified Charged Hadrons from the PHENIX Experiment at RHIC", Proc. of the 16th International Conference on Particles and Nuclei (PANIC'02), Sep. 30–Oct.4, 2002, Osaka, Japan, Nucl. Phys. A **721** (2003) 273c–276c.

28. ShinIchi Esumi, for the PHENIX Collaboration: “Event anisotropy measurement in 200 GeV Au+Au collisions at RHIC-PHENIX experiment”, Proc. of the 16th International Conference on Particles and Nuclei (PANIC’02), Sep. 30–Oct. 4, 2002, Osaka, Japan, Nucl. Phys. A **721** (2003) 269c–272c.

29. Y. Goto, for the PHENIX Collaboration: “Neutral Pion Measurements in Polarized Proton Collisions from PHENIX at RHIC”, Proc. of the 16th International Conference on Particles and Nuclei (PANIC’02), Sep. 30–Oct. 4, 2002, Osaka, Japan, Nucl. Phys. A **721** (2003) 360c–363c.

30. J. Lajoie, for the PHENIX Collaboration: “Recent Results from the PHENIX Experiment at RHIC”, Proc. of the 16th International Conference on Particles and Nuclei (PANIC’02), Sep. 30–Oct. 4, 2002, Osaka, Japan, Nucl. Phys. A **721** (2003) 221c–226c.

31. M. Naruki, J. Chiba, H. En’yo, H. Funahashi, H. Hamagaki, M. Ieiri, M. Ishino, H. Kanda, M. Kitaguchi, S. Mihara, T. Miyashita, T. Murakami, R. Muto, M. Nomachi, K. Ozawa, F. Sakuma, O. Sasaki, H.D. Sato, M. Sekimoto, T. Tabaru, K.H. Tanaka, S. Yadama, S. Yokkaichi, Y. Yoshimura: “Measurement of Invariant Mass Spectra of Vector Meson Decaying in Nuclear Matter”, Proc. of the 16th International Conference on Particles and Nuclei (PANIC’02), Sep. 30–Oct. 4, 2002, Osaka, Japan, Nucl. Phys. A **721** (2003) 297c–300c.

32. K. Ozawa, for the PHENIX Collaboration: “Measurement of $J/\Psi \to ee$ in Au+Au collisions at $\sqrt{s_{NN}} = 200$ GeV at RHIC-PHENIX”, Proc. of the 16th International Conference on Particles and Nuclei (PANIC’02), Sep. 30–Oct. 4, 2002, Osaka, Japan, Nucl. Phys. A **721** (2003) 257c–260c.

33. K. Sekiguchi, H. Sakai, H. Okamura, A. Tamii, T. Uesaka, K. Suda, N. Sakamoto, T. Wakasa, Y. Satou, T. Ohnishi, K. Yakou, S. Sakoda, H. Kato, Y. Maeda, M. Hatano, J. Nishikawa, T. Saito, N. Uchigashima, N. Kalantar-Nayestanaki, and K. Ermisch: “Polarization transfer measurement for d-p scattering and three nucleon force effects”, Proc. of the 16th International Conference on Particles and Nuclei Sep. 30–Oct. 4, 2002, Osaka, Japan, Nucl. Phys. A **721** (2003) 637c–640c.

34. S. Kubono, T. Teranishi, and S. Kato: “Low-Energy Nuclear Reaction Studies with RI Beams in Nuclear Astrophysics”, Proc. the International Symposium on Physics of Unstable Nuclei, Nov. 20–25, Halong Bay, Vietnam, Nucl. Phys. A **722** (2003) 17c–23c.

35. T. Nakamura, N. Fukuda, N. Aoi, H. Iwasaki, T. Kobayashi, T. Kubo, A. Mengoni, M. Notani, H. Otsu, H. Sakurai, S. Shimoura, T. Teranishi, Y.X. Watanabe, K. Yoneda, M. Ishihara: “Coulomb dissociation of halo nuclei”, Proc. the International Symposium on Physics of Unstable Nuclei (ISPUN02), Nov. 20–25, Halong Bay, Vietnam, Nucl. Phys. A **722** (2003) 301c–307c.

36. S. Shimoura: “Spectroscopy of exotic nuclei using intermediate-energy direct reaction”, Proc. the International Symposium on Physics of Unstable Nuclei (ISPUN02), Nov. 20–25, Halong Bay, Vietnam, Nucl. Phys. A **722** (2003) 164c–169c.

37. T. Otsuka: “Shell Evolution and Structure of Exotic Nuclei”, Proc. of the 8th International Conference on Nucleus-Nucleus Collisions, Jun. 17–21, 2003, Moscow, Russia, Nucl. Phys. A **734**, (2004) 365–368.

38. T. Saito, M. Hatano, H. Kato, Y. Maeda, H. Sakai, S. Sakoda, A. Tamii, N. Uchigashima, V. P. Ladygin, A. Yu. Isupov, N. B. Ladygina, A. I. Malakhov, S. G. Reznikov, T. Uesaka, K. Yako, T. Ohnishi, N. Sakamoto, K. Sekiguchi, H. Kumasaka, J. Nishikawa, H. Okamura, K. Suda and R. Suzuki: “Measurement of the Analyzing Powers for the $\vec{d}d \longrightarrow {}^3\mathrm{H}en$ and $\vec{d}d \longrightarrow {}^3\mathrm{H}p$ Reactions at Intermediate Energies”, Proc. of the Second Asia Pacific Conference on Few- Body Problems in Physics (APFB02), Aug. 27- 30, 2002, Shanghai, Chaina, Modern Physics Letters A **18** (2003) 294–297.

39. A. Tamii, M. Hatano, H. Kato, Y. Maeda, T. Saito, H. Sakai, S. Sakoda, N. Uchigashima, K. Hatanaka, D. Hirooka, J. Kamiya, T. Wakasa, K. Yako, K. Sekiguchi and T. Uesaka: “Search for Super-Narrow Dibaryon Resonances by the $pd \to pd\mathrm{X}$ and $pd \to pp\mathrm{X}$ Reactions”, Proc. of the Second Asia Pacific Conference on Few-Body Problems in Physics (APFB02), Aug. 27–30, 2002, Shanghai, Chaina, Modern Physics Letters A **18** (2003) 410–413.

40. T. Otsuka: “Frontiers of the Nuclear Shell Model”, Proc. of Conference on Frontiers of Nuclear Structure, Jul. 29–Aug. 2, 2002, Berkeley, USA, AIP Conf. Proc. **656** (2003) 190–196.

41. H. Okamura, T. Uesaka, K. Suda, H. Kumasaka, R. Suzuki, A. Tamii, N. Sakamoto, and H. Sakai: “Model Independent Spin Parity Determination by the $(d, {}^2\mathrm{He})$ Reaction and Possible Evidence for a 0^- State in ${}^{12}\mathrm{B}$”, Proc. of 15th International Spin Physics Symposium (SPIN2002), Sep. 9–14, 2002, New York, USA, AIP Conf. Proc. **675** (2003) 671–675.

42. T. Kawabata, H. Akimune, G.P.A. Berg, B.A. Brown, H. Fujimura, H. Fujita, Y. Fujita, M. Fujiwara, K. Hara, K. Hatanaka, K. Hosono, T. Ishikawa, M. Itoh, J. Kamiya, M. Nakamura, T. Noro, E. Obayashi, H. Sakaguchi, Y. Shimbara, H. Takeda, T. Taki, A. Tamii, H. Toyokawa, M. Uchida, H. Ueno, T. Wakasa, K. Yamasaki, Y. Yasuda, H. P. Yoshida, M. Yosoi: "Polarization Transfer in the ^{16}O(p, p') Reaction at Forward Angles and Structure of the Spin-dipole Resonances", Proc. of 15th International Spin Physics Symposium (SPIN2002), Sep. 9–14, 2002, New York, USA, AIP Conf. Proc. **675** (2003) 681–685.

43. T. Saito, V. P. Ladygin, T. Uesaka, M. Hatano, A. Yu. Isupov, H. Kato, H. Kumasaka, N. B. Ladygina, Y. Maeda, A. I. Malakhov, J. Nishikawa, T. Ohnishi, H. Okamura, S. G. Reznikov, H. Sakai, N. Sakamoto, S. Sakoda, K. Sekiguchi, K. Suda, R. Suzuki, A. Tamii, N. Uchigashima, and K. Yako: "Study of ^{3}He (^{3}H) Spin Structure via $\vec{d}\vec{d} \longrightarrow {}^3\mathrm{He}n({}^3\mathrm{H}p)$ Reaction", Proc. of 15th International Spin Physics Symposium (SPIN2002), Sep. 9–14, 2002, New York, USA, AIP Conf. Proc. **675** (2003) 715–719.

44. Y. Satou, S. Ishida, H. Kato, H. Sakai, H. Okamura, N. Sakamoto, T. Uesaka, A. Tamii, T. Wakasa, T. Ohnishi, K. Sekiguchi, K. Yako, K. Suda, M. Hatano, Y. Maeda, and T. Ichihara: "Isoscalar Spin Response in the Continuum Studied via the $^{12}\mathrm{C}(\vec{d}, \vec{d'})$ Reaction at 270 MeV", Proc. of 15th International Spin Physics Symposium (SPIN2002), Sep. 9–14, 2002, New York, USA, AIP Conf. Proc. **675** (2003) 696–699.

45. K. Sekiguchi, H. Sakai, H. Okamura, A. Tamii, T. Uesaka, K. Suda, N. Sakamoto, T. Wakasa, Y. Satou, T. Ohnishi, K. Yakou, S. Sakoda, H. Kato, Y. Maeda, M. Hatano, J. Nishikawa, T. Saito, N. Uchigashima, N. Kalantar-Nayestanaki, and K. Ermisch: "Polarization Transfer Measurement for d-p Elastic Scattering — a Probe for Three Nucleon Force Properties —", Proc. of 15th International Spin Physics Symposium (SPIN2002), Sep. 9–14, 2002, New York, USA, AIP Conf. Proc. **675** (2003) 711–714.

46. T. Wakui, M. Hatano, H. Sakai, A. Tamii and T. Uesaka: "Polarized Solid Proton Target for RI Beam Experiments", Proc. of 15th International Spin Physics Symposium (SPIN2002), Sep. 9–14, 2002, New York, USA, AIP Conf. Proc. **675** (2003) 911–915.

47. T. Teranishi, S. Kubono, J.J. He, M. Notani, T. Fukuchi, S. Michimasa, S. Shimoura, S. Nishimura, M. Nishimura, Y. Yanagisawa, M. Kurokawa, Y. Wakabayashi, N. Hokoiwa, Y. Gono, T. Morikawa, A. Odahara, H. Ishiyama, Y.X. Watanabe, T. Hashimoto, T. Ishikawa, M.H. Tanaka, H. Miyatake, J.Y. Moon, J.H. Lee, J.C. Kim, C.S. Lee, V. Guimaraes, R.F. Lihitenthaler, H. Baba, A. Saito, K. Sato, T. Kawamura, S. Kato, H. Iwasaki, K. Ue, Y. Satou, and Z. Fülöp: "Low-Energy Radioactive-Ion Beam Separator at CNS and Resonance Scattering Experiments", Proc. of Tours Symposium on Nuclear Physics V, Aug. 26–29, 2003, Tours, France, AIP Conf. Proc. **704** (2004) 447.

48. T. Otsuka: "Shell model results for exotic nuclei", Proc. of Conference on Nuclear Structure with Large Gamma-Arrays: Status & Perspectives, Sep. 23–27, 2002, Legnaro-Padva, Italy, Eur. Phys. J. A **20** (2004) 69–73 .

49. S. Shimoura: "In-Beam Spectroscopy of Exotic Nuclei Using Direct Reaction of RI Beams", Proc. the Symposium for the 30th Anniversary of Nuclear Physics Division of the Korean Physical Society, Oct. 24–25, 2002, Seoul, Korea, J. Korean Phys. Soc. **43** (2003) S83–S86.

50. T. Watanabe, S. Watanabe, T. Ikeda, M. Kase, Y. Sasaki, T. Kawaguchi and T. Katayama: "Prototype of Highly Sensitive Cryogenic Current Comparater with HTS SQUID and HTS Magnetic Shield", Proc. of the 6th European Conference on Applied Superconductivity (EUCAS), Sep. 14–18, Sorrento, Italy, Supercond. Sci. Technol. **17** (2004) s450–s455.

51. E. Ideguchi, H. Madokoro, D.G. Sarantites, W. Reviol, C.J. Chiara, M. Devlin, R.V.F. Janssens, M.P. Carpenter, T. Lauritsen, C.J. Lister, P. Reiter, D. Seweryniak, C. Baktash, A. Galindo-Uribarri, D. Rudolph, A. Axelsson, M. Weiszflog, D.R. Lafosse: "Collective Structures in the Doubly Magic Nucleus ^{40}Ca", Proc. of the international symposium on Frontiers of Collective Motions (CM2002), Nov. 6–9, 2002, Aizu-Wakamatsu, Japan, ed. by H. Sagawa and H. Iwasaki, World Scientific (2003) pp. 343–348.

52. H. Iwasaki: "Low-lying Structure of Neutron-rich Nuclei around $N = 8$ and 20 from In-beam Gamma-ray Spectroscopy", Proc. of the international symposium on Frontiers of Collective Motions (CM2002), Nov. 6–9, 2002, Aizu-Wakamatsu, Japan, ed. by H. Sagawa and H. Iwasaki, World Scientific (2003) pp. 337–342.

53. A. Odahara, T. Fukuchi, Y. Gono, H. Watanabe, E. Ideguchi, T. Kishida, H. Sagawa: "High-spin isomers in $N = 83$ isotones", Proc. of the International Symposium on "Frontiers of Collective Motions (CM2002)", Nov. 6–9, 2002, Aizu-Wakamatsu, Japan, ed. by H. Sagawa and H. Iwasaki, World Scientific (2003) pp. 349–354.

54. S. Kubono, S. Michimasa, T. Teranishi, Y. Yanagisawa, Zs. Fülöp, X. Liu, K. Kumagai, K. Abe, C.C. Yun, S. Watanabe, N. Yamazaki, Y. Ohshiro, M. Kurokawa, P. Strasser, K.I. Hahn, T. Kishida, N. Imai, S. Kato, Y. Fuchi, and M.H. Tanaka: "Nuclear Astrophysics Project with a New Low-Energy RIB Separator CRIB—Study of a Critical Stellar Reaction ^{15}O$(\alpha,\gamma)^{19}$Ne—", Proc. of the International Symposium on Origin of Matter and Evolution of Galaxies, Jan. 19–21, 2000, Tokyo, Japan, ed. by T. Kajino, S. Kubono, K. Nomoto and I. Tanihata, World Scientific (2003) pp. 171–178.

55. M. Imanaka, H. Arai, T. Nakagawa, Y. Ohshiro, S. Watanabe and T. Katayama: "Nano-Cluster Ion Source by Plasma-Gas-Aggregation", Proc. of the 14th Symp. on Accel. Sci. and Technology, Nov. 11–13, 2003, KEK, Tsukuba, Japan, (2003) 509–511.

56. Y. Ohshiro, S. Watanabe, S. Yamaka, S. Kubono, and T. Katayama: "Installation of Hyper ECR Ion Source in the RIKEN AVF Cyclotron", Proc. of the 14th Symp. on Accel. Sci. and Technology, Nov. 11–13, 2003, KEK, Tsukuba, Japan, (2003) 164–166.

57. S. Watanabe, Y. Ohshiro, T. Katayama, T. Watanabe, and T. Ikeda: "The possibility of the ion beam machining of the high temperature superconductor Bi2223", Proc. of the 14th Symp. on Accel. Sci. and Technology, Nov. 11–13, 2003, KEK, Tsukuba, Japan, (2003) 575–577.

58. T. Watanabe, S. Watanabe, T. Ikeda, T. Katayama, M. Kase, T. Kawaguchi, and Y. Sasaki: "Development of Highly Sensitive and Nondestructive Beam Current Monitor with HTS SQUID and HTS Magnetic Shield", Proc. of the 14th Symp. on Accel. Sci. and Technology, Nov. 11–13, 2003, KEK, Tsukuba, Japan, (2003) 99–101.

C. Theses

1. T. Gunji: "Study of Electron Identification Capability of the ALICE Transition Radiation Detector", Master Thesis, University of Tokyo, March (2004).

2. T. Isobe: "Development of Time Projection Chamber for Experiments with Heavy Ion Collisions", Master Thesis, University of Tokyo, March (2004).

3. K. Itoh: "Polarization and Density Measurement of Polarized ^{3}He Target", Master Thesis, Saitama University, March (2004).

4. N. Kurihara: "Development of Readout Electronics for Aerogel Counter at RHIC-PHENIX", Master Thesis, University of Tokyo, March (2004).

5. M. Tamaki: "Study of excited states in ^{22}O via α inelastic scatterings", Master Thesis, University of Tokyo, March (2004).

D. Other Publications

1. K. Ozawa, H. En'yo: "Origin of the Dynamical Mass in QCD – An Approach using vector mesons in nuclei", BUTSURI **59** (2004) 172–174.

2. 浜垣　秀樹：「クオーク－グルーオンプラズマが見えた？」、パリティ 1 月号 (2004) 43–45.

Talks and Presentations

A. Conferences

1. H. Arai, G. Arzumanyan, Y. Higurashi, M. Imanaka, M. Kidera, M. Kase, T. Nakagawa, G. Shirkov, and Y. Yano: "ECR Developments in RIKEN", The 10th International Conference of Ion Sources, Sep. 8–13, 2003, JINR, Dubna, Russia.

2. H. Baba, S. Shimoura, A. Saito, T. Minemura, Y. U. Matsuyama, H. Akiyoshi, N. Aoi, T. Gomi, Y. Higurashi, K. Ieki, N. Imai, N. Iwasa, H. Iwasaki, S. Kanno, S. Kubono, M. Kunibu, S. Michimasa, T. Motobayashi, T. Nakamura, H. Sakurai, M. Serata, E. Takeshita, S. Takeuchi, T. Teranishi, K. Ue, K. Yamada,and Y. Yanagisawa (Poster): "Invariant-mass spectroscopy of ^{14}O via the (α, α') reaction", International Symposium on A New Era of Nuclear Structure Physics (NENS03), Nov. 19–22, 2003, Kurokawa Village, Niigata, Japan.

3. T. Fukuchi, Y. Gono, A. Odahara, H. Watanabe, S. Tanaka, M. Inoue, Y. Wakabayashi, T. Sasaki, M. Kibe, N. Hokoiwa, T. Shinozuka, M. Fujita, A. Yamazaki, T. Sonoda, C.S. Lee, Y.K. Kwon and J.H. Lee (Poster):"High-Spin Isomer in ^{93}Mo", International Symposium on A New Era of Nuclear Structure Physics (NENS03), Nov. 19–22, 2003, Kurokawa Village, Niigata, Japan.

4. T. Fukuchi, Y. Gono, A. Odahara, H. Watanabe, S. Tanaka, M. Inoue, Y. Wakabayashi, T. Sasaki, M. Kibe, N. Hokoiwa, T. Shinozuka, M. Fujita, A. Yamazaki, T. Sonoda, C.S. Lee, Y.K. Kwon and J.H. Lee: "High-Spin Isomer in ^{93}Mo", CNS-RIKEN Joint Symposium on Frontier of Gamma-ray Spectroscopy and its Application (GAMMA04), Mar. 18–19, 2004, RIKEN, Wako, Japan

5. M. Hatano, T. Wakui, T. Uesaka, H. Sakai, A. Tamii: "Design and Performance of the Polarized Solid Proton Target for the RI Beam Experiments", 10th International Workshop on Polarized Sources and Targets, Sep. 22–26, 2003, Novosibirsk, Russia.

6. J.J. He, S. Kubono, T. Teranishi, M. Notani, H. Baba, S. Nishimura, J.Y. Moon M. Nishimura, S. Michimasa, H. Iwasaki, Y. Yanagisawa, N. Hokoiwa, M. Kibe, J.H. Lee, S. Kato, Y. Gono and C. S. Lee (Poster): "Resonance scattering of ^{22}Mg and ^{21}Na RI beams on the H target", Origin of Matter and Evolution of the Galaxies (OMEG08), Nov. 17–19, 2003, RIKEN, Wako, Japan.

7. J.J. He, S. Kubono, T. Teranishi, M. Notani, H. Baba, S. Nishimura, J.Y. Moon, M. Nishimura, S. Michimasa, H. Iwasaki, Y. Yanagisawa, N. Hokoiwa, M. Kibe, J.H. Lee, S. Kato, Y. Gono and C.S. Lee: "Study of Astrophysical Relevant Resonant States in ^{23}Al and ^{22}Mg using RI beams at CRIB", The Fifth Japan China Joint Nuclear Physics Symposium (JCNP2004), Mar. 7–11, 2004, Kyushu University, Fukuoka, Japan.

8. J.J. He, S. Kubono, T. Teranishi M. Notani, H. Baba, S. Nishimura, J.Y. Moon, M. Nishimura, S. Michimasa, H. Iwasaki, Y. Yanagisawa, N. Hokoiwa, M. Kibe, J.H. Lee, S. Kato, Y. Gono and C.S. Lee: "Study of proton resonant states of astrophysical interest in ^{23}Al using RI beams at CNS", The Fifth Japan China Joint Nuclear Physics Symposium (JCNP2004), Mar. 7–11, 2004, Kyushu University, Fukuoka, Japan.

9. E. Ideguchi: "Study of high-spin states by using secondary fusion reaction", CNS-RIKEN Joint Symposium on Frontier of Gamma-ray Spectroscopy and its Application (GAMMA04), Mar. 18–19, 2004, RIKEN, Wako, Japan.

10. E. Ideguchi (Invited): "Study of high-spin states in Ca region by using low-energy secondary beam", Sweden-Japan Joint Symposium on Accelerator Science and Accelerator Based Sciences, Jan. 6–7, 2004. University of Tokyo, Tokyo, Japan.

11. M. Imanaka, H. Arai, T. Katayama, T. Nakagawa, Y. Ohshiro, and S. Watanabe: "Nanocluster Ion Source by Plasma-Gas-Aggregation", The 10th International Conference of Ion Sources, Sep. 8–13, 2003, JINR, Dubna, Russia.

12. M. Imanaka, H. Arai, T. Nakagawa, Y. Ohshiro, S. Watanabe, and T. Katayama (Poster): "Nano-Cluster Ion Source By Plasma-Gas-Aggregation", 14th Symp. on Accel. Sci. and Technology, Nov. 11–13, 2003, KEK, Tsukuba, Japan.

13. M. Inuzuka, H. Hamagaki, K. Ozawa, T. Sakaguchi, T. Tamagawa, F. Kajihara, T. Isobe, T. Gunji, N. Kurihara, S. Oda, Y. Yamaguchi, S. Sawada, S. Yokkaichi: "Gas Electron Multiplier (GEM) produced with the Plasma Etching Mehotd", Quark Matter 2004 Conference, Jan. 13, 2004, Oakland, USA.

14. T. Isobe, H. Hamagaki, K. Ozawa, M. Inuzuka, T. Sakaguchi, F. Kajihara, T. Gunji, N. Kurihara, S. Yokkaichi, and S. Sawada: "Development of a prototype TPC with CF4 & GEM readout for heavy ion collision", 2003 IEEE Nuclear Science Symposium and Medical Imaging Conference, Oct. 19–25, 2003, Portland, USA.

15. T. Katayama (Invited): "Electron RI Collider and Internal Target Operation of RIKEN Storage Ring Project", International Workshop on Beam Cooling and Related Topics, Yamanaka, Japan, May. 19–23, 2003.

16. T. Kawabata, H. Akimune, H. Fujimura, H. Fujita, Y. Fujita, M. Fujiwara, K. Hara, K. Y. Hara, K. Hatanaka, T. Ishikawa, M. Itoh, J. Kamiya, M. Nakamura, H. Sakaguchi, Y. Shimbara, H. Takeda, A. Tamii, T. Noro, H. Toyokawa, M. Uchida, T. Wakasa, Y. Yasuda, H. P. Yoshida, M. Yosoi (Invited): "Weak Isoscalar Response of ^{11}B", International Conference on Nuclear Structure and Related Topics (NSRT03), Sep. 2–6, 2003, Dubna, Russia.

17. T. Kawabata: "$M1$ transition strengths in ^{11}B", "Spin observables in nucleon-knockout reactions", International Workshop on Perspectives of Polarization in RI beam Induced Reactions, Mar. 2-6, 2004, Wako, Japan.

18. T. Kikuchi, M. Nakajima, K. Horioka, T. Katayama: "Emittance growth due to bunch compression in final buncher for HIF", Third International Conference on Inertial Fusion Sciences and Applications (IFSA2003), Sep. 7–12, 2003, Monterey, USA.

19. T. Kikuchi, T. Katayama, M. Nakajima, K. Horioka: "Beam dynamics and instability in final beam bunching for heavy ion inertial fusion", 14th Symposium on Accelerator Science and Technology, Nov. 11–13, 2003, Tsukuba, Japan.

20. T. Kikuchi, M. Nakajima, K. Horioka, T. Katayama: "Emittance growth and particle distributions during final beam bunching in heavy ion fusion driver", The 3rd Asian Particle Accelerator Conference (APAC2004), Mar. 22–26, 2004, Gyeongju, Korea.

21. T. Kikuchi, S.M. Lund, T. Katayama: "Possible parameters for bunch compression in a ring in future RIKEN projects", The 3rd Asian Particle Accelerator Conference (APAC2004), Mar. 22–26, 2004, Gyeongju, Korea.

22. S. Kubono: "Experimental Study of nuclear reactions under explosive phenomena in the Universe", Workshop on Photo-Induced Reactions, Mar. 18–19, 2004, Kansai JAERI, Kizu, Kyoto, Japan.

23. S. Michimasa, S. Shimoura, H. Iwasaki, M. Tamaki, N. Aoi, H. Baba, N. Iwasa, S. Kanno, S. Kubono, K. Kurita, M. Kurokawa, T. Minemura, T. Motobayashi, M. Notani, H.J. Ong, S. Ota, A. Saito, H. Sakurai, S. Takeuchi, E. Takashita, Y. Yanagisawa and A. Yoshida: "Measurement of Excited States in ^{23}F by Proton Transfer and Inelastic Scattering", International Conference on Direct Reactions with Exotic Beams (DREB2003), Jul. 10–12, 2003, Surrey, UK.

24. S. Michimasa, S. Shimoura, H. Iwasaki, M. Tamaki, N. Aoi, H. Baba, N. Iwasa, S. Kanno, S. Kubono, K. Kurita, M. Kurokawa, T. Minemura, T. Motobayashi, M. Notani, H.J. Ong, S. Ota, A. Saito, H. Sakurai, S. Takeuchi, E. Takashita, Y. Yanagisawa and A. Yoshida: "In-Beam Gamma-ray Spectroscopy of Neutron-rich Nucleus ^{23}F", CNS-RIKEN Joint Symposium on Frontier of Gamma-ray Spectroscopy and its Application (GAMMA04), Mar. 18–19, 2004, RIKEN, Wako, Japan.

25. S. Michimasa, S. Shimoura, H. Iwasaki, M. Tamaki, N. Aoi, H. Baba, N. Iwasa, S. Kanno, S. Kubono, K. Kurita, M. Kurokawa, T. Minemura, T. Motobayashi, M. Notani, H.J. Ong, S. Ota, A. Saito, H. Sakurai, S. Takeuchi, E. Takashita, Y. Yanagisawa and A. Yoshida: "Gamma-ray Spectroscopy of ^{23}F with Proton Transfer Reaction", The Fifth Japan China Joint Nuclear Physics Symposium, Mar. 7–10, 2004, Fukuoka, Japan.

26. J.Y. Moon, C.S. Lee, J.H. Lee, C.C. Yun, J.C. Kim, M. Youn, S. Kubono, T. Teranishi, J.J. He, M. Notani, S. Nishimura, M. Nishimura, V. Guimarães, R.F. Lihitenthaler and S. Kato (Poster): "Study of proton resonances in ^{26}Si and ^{27}P by the elastic scattering of ^{1}H(^{25}Al,p)^{25}Al, ^{1}H(^{26}Si,p)^{26}Si", Origin of Matter and Evolution of the Galaxies (OMEG03), Nov. 17–19, 2003, RIKEN, Wako, Japan.

27. M. Notani, S. Kubono, T. Teranishi, Y. Yanagisawa,S. Michimasa, K. Ue, J.J. He, H. Iwasaki, H. Baba, M. Tamaki, T. Minemura, S. Shimoura, N. Hokoiwa, Y. Wakabayashi, T. Sasaki, T. Fukuchi, A. Odahara, Y. Gono, Zs. Fülöp, E.K. Lee, K.I. Hahn, J.Y. Moon, C.C. Yun, J.H. Lee, C.S. Lee and S. Kato: "Direct measurement of the astrophysical reaction ^{14}O$(\alpha, p)^{17}$F", Origin of Matter and Evolution of the Galaxies (OMEG03), Nov. 17–19, 2003, RIKEN, Wako, Japan.

28. M. Notani, S. Kubono, T. Teranishi, Y. Yanagisawa,S. Michimasa, K. Ue, J.J. He, H. Iwasaki, H. Baba, M. Tamaki, T. Minemura, S. Shimoura, N. Hokoiwa, Y. Wakabayashi, T. Sasaki, T. Fukuchi, A. Odahara, Y. Gono, Zs. Fülöp, E.K. Lee, K.I. Hahn, J.Y. Moon, C.C. Yun, J.H. Lee, C.S. Lee and S. Kato: "Direct measurement of the astrophysical reaction ^{14}O$(\alpha, p)^{17}$F", The Sixth International Conference on Radioactive Nuclear Beams (RNB6), Sep. 22–26, 2003, Argonne, USA.

29. M. Notani, S. Kubono, T. Teranishi, Y. Yanagisawa,S. Michimasa, K. Ue, J.J. He, H. Iwasaki, H. Baba, M. Tamaki, T. Minemura, S. Shimoura, N. Hokoiwa, Y. Wakabayashi, T. Sasaki, T. Fukuchi, A. Odahara, Y. Gono, Zs. Fülöp, E.K. Lee, K.I. Hahn, J.Y. Moon, C.C. Yun, J.H. Lee, C.S. Lee and S. Kato: "Direct measurement of the astrophysical reaction ^{14}O$(\alpha, p)^{17}$F", The Eighth International Conference on Clustering Aspects of Nuclear Structure and Dynamics (Cluster8), Nov. 24–29, 2003, Nara, Japan.

30. A. Odahara, Y. Gono, Y. Wakabayashi, N. Hokoiwa, M. Kibe, T. Fukuchi, T. Teranishi, S. Kubono, M. Notani, S. Michimasa, J.J. He, S. Shimoura, E. Ideguchi, Y. Yanagisawa, H. Watanabe, T. Kishida, S. Nishimura, M. Nishimura, H. Baba, H. Iwasaki, J. Y. Moon, S. Kato and H. Sagawa: "Development of Unstable Nuclear Beam ^{17}N to Search for High-Spin Isomers in $N = 51$ Isotones", International Symposium on A New Era of Nuclear Structure Physics (NENS03), Nov. 19–22, 2003, Niigata, Japan.

31. A. Odahara, Y. Gono, E. Ideguchi, H. Watanabe, T. Fukuchi and H. Sagawa: "High Spin Shape Isomers in $N = 83$ Isotones", The Fifth Japan China joint Nuclear Physics Symposium, Mar. 7–10, 2004, Fukuoka, Japan.

32. A. Odahara, Y. Gono, Y. Wakabayashi, T. Fukuchi, N. Hokoiwa, M. Kibe, T. Teranishi, S. Kubono, M. Notani, Y. Yanagisawa, S. Michimasa, J.J. He, H. Iwasaki, S. Shimoura, H. Watanabe, T. Kishida, E. Ideguchi, H. Baba, S. Nishimura, M. Nishimura, J.Y. Moon, S. Kato and H. Sagawa: "Gamma-Ray Spectroscopy by Secondary Fusion Reactions using CRIB", CNS-RIKEN Joint Symposium on Frontier of gamma-ray spectroscopy and its application, Mar. 18–19, 2004, RIKEN, Wako, Japan.

33. Y. Ohshiro, S. Watanabe, S. Yamaka, S. Kubono, and T. Katayama (Poster): "Installation of Hyper ECR Ion Source in the RIKEN AVF Cyclotron ", 14th Symp. on Accel. Sci. and Technology, Nov. 11–13, 2003, KEK, Tsukuba, Japan.

34. S. Ota, S. Shimoura, H. Iwasaki, M. Kurokawa, K. Demichi, S. Michimasa, S. Kubono, T. Teranishi, M. Notani, N. Iwasa, Y. Yanagisawa, T. Minemura, T. Motobayashi, S. Takeuchi, T. Gomi, K. Yamada, A. Saito, H. Baba, Y.U. Matsuyama, S. Kanno, E. Takeshita, K. Hasegawa, H. Sakurai, N. Aoi, T. Murakami, M. Tamaki, E. Ideguchi, T. Fukuchi, A. Odahara, K. Kurita, K. Miller, Z. Elekes, M. Ishihara: "Proton transfer reaction ^{4}He(^{12}Be,^{13}B) at 50A MeV", International Conference on Direct Reactions with Exotic Beams (DREB2003), Jul. 10–12, 2003, Surrey, UK.

35. S. Ota, T. Murakami, S. Shimoura, S. Michimasa, S. Kubono, T. Teranishi, M. Notani, M. Tamaki, E. Ideguchi, T. Fukuchi, H. Iwasaki, H. Sakurai, N. Aoi, M. Kurokawa, T. Motobayashi, Y. Yanagisawa, T. Minemura, S. Takeuchi, Z. Elekes, M. Ishihara, T. Gomi, K. Yamada, A. Saito, H. Baba, Y.U. Matsuyama, S. Kanno, E. Takeshita, K. Demichi, H. Hasegawa, K. Kurita, A. Odahara, K. Miller: "Spectroscopy of ^{13}B via ^{4}He(^{12}Be,^{13}Bγ) Reaction", International Symposium on A New Era of Nuclear Structure Physics (NENS03), Nov. 19–22, 2003, Kurokawa Village, Niigata, Japan.

36. T. Otsuka (Invited): "Shell and cluster structures of exotic nuclei", Theory Symposium on Rare Isotope Accelerator Science, Apr. 28–May 2, 2003, Argonne, USA.

37. T. Otsuka (Invited): "Evolution of shell structure and nuclear force", Int. Conf. on Relativistic Structure Models for the Physics of Radioactive Nuclear Beams, May 12–16, 2003, Bad Honnef, Germany.

38. T. Otsuka (Invited): "Shells in nuclei on and far from stability", Int. Workshop on Recent Advances in the Nuclear Shell Model, Jun. 29–Jul. 12, 2003, Trento, Italy.

39. T. Otsuka (Invited): "Mechanisms of Shell Evolution and Structure of Exotic Nuclei", Int. Conf. on the Labyrinth in Nuclclear Structure, Jul. 13–19, 2003, Crete, Greece.

40. T. Otsuka (Invited): “Perspectives of the shell model”, Int. Symp. A New Era of Nuclear Structure Physics, Nov. 19–22, 2003, Niigata, Japan.

41. T. Otsuka (Invited): “Single-particle states in exotic nuclei”, Int. Workshop on Spectroscopic Factors, Mar 2–12, 2004, Trento, Italy.

42. T. Otsuka (Invited): “Shell Evolution in Exotic Nuclei”, Fifth Japan-China Joint Nuclear Physics Symposium, Mar 7–10, 2004, Fukuoka, Japan.

43. K. Ozawa for the PHENIX collaboration (Poster): “Measurements of $J/\Psi \rightarrow e^+e^-$ in Au+Au Collisions at $\sqrt{s_{NN}}$ =200 GeV”, Quark Matter 2004, Jan. 11–17, 2004, Oakland, USA.

44. A. Saito, S. Shimoura, S. Takeuchi, T. Motobayashi, T. Minemura, Y. U. Matsuyama, H. Baba, H. Akiyoshi, Y. Ando, N. Aoi, Zs. Fülöp, T. Gomi, Y. Higurashi, M. Hirai, K. Ieki, N. Imai, N. Iwasa, H. Iwasaki, Y. Iwata, S. Kanno, H. Kobayashi, S. Kubono, M. Kunibu, M. Kurokawa, Z. Liu, S. Michimasa, T. Nakamura, S. Ozawa, H. Sakurai, M. Serata, E. Takeshita, T. Teranishi, K. Ue, K. Yamada, Y. Yanagisawa, and M. Ishihara: “Molecular States in Neutron-Rich Beryllium Isotopes”, The 8th International Conference on Clustering Aspects of Nuclear Structure and Dynamics, Nov. 24–29, 2003, Nara, Japan.

45. T. Sakaguchi for the PHENIX Collaboration: “Searching for non-hadronic sources of photons in Au+Au collisions at $\sqrt{s_{NN}}$= 200 GeV at RHIC-PHENIX”, Awarded Poster Presentation at the Quark Matter 2004 Conference, Jan. 13, 2004, Oakland, USA.

46. S. Shimoura: “Spectroscopy of Light Exotic Nuclei through Direct Reaction with Inverse Kinematics”, International Conference on Direct Reactions with Exotic Beams (DREB2003), Jul. 10–12, 2003, Surrey, UK.

47. S. Shimoura (Invited): “Position Sensitivity of Ge Detectors and its Applications to In-beam Nuclear Spectroscopy”, International Conference on Imaging Techniques in Subatomic Physics, Astrophysics, Medicine, Biology and Industry (Imaging2003), Jun. 24–27, 2003, Stockholm, Sweden.

48. S. Shimoura (Invited): “Excited States in Exotic Nuclei Populated by Direct Reactions of RI Beams”, The 8th International Conference on Clustering Aspects of Nuclear Structure and Dynamics, Nov. 24–29, 2003, Nara, Japan.

49. S. Shimoura (Invited): “Proton single-particle states in neutron-rich nuclei via (α, t) reactions at intermediate energy”, ECT* workshop on Spectroscopic Factors, Mar. 2–12, 2004, Trento, Italy.

50. S. Shimoura (Invited): “Measurements of Excited States in Light Unstable Nuclei”, KEK Workshop on New Developments in Nuclear Physics apart from the Stable Nuclei, Mar. 15–17, 2004, KEK, Tsukuba, Japan.

51. S. Shimoura: “Excited States in Light Unstable Nuclei via Direct Reactions”, RCNP Workshop on Nuclear Forces and Nuclear Structure, Mar. 22–24, 2004, RCNP, Osaka, Japan.

52. T. Teranishi, S. Kubono, J.J. He, M. Notani, T. Fukuchi, S. Michimasa, S. Shimoura, S. Nishimura, M. Nishimura, Y. Yanagisawa, M. Kurokawa, Y. Wakabayashi, N. Hokoiwa, Y. Gono, T. Morikawa, A. Odahara, H. Ishiyama, Y.X. Watanabe, T. Hashimoto, T. Ishikawa, M.H. Tanaka, H. Miyatake, J.Y. Moon, J.H. Lee, J.C. Kim, C.S. Lee, V. Guimarães, R.F. Lihitenthaler, H. Baba, A. Saito, K. Sato, T. Kawamura, S. Kato, H. Iwasaki, K. Ue, Y. Satou, and Z. Fülöp: “Low-Energy Radioactive-Ion Beam Separator at CNS and Resonance Scattering Experiments”: Tours Symposium on Nuclear Physics V, Aug. 26–29, 2003, Tours, France.

53. T. Teranishi, S. Kubono, J.J. He, M. Notani, T. Fukuchi, S. Michimasa, S. Shimoura, S. Nishimura, M. Nishimura, Y. Wakabayashi, N. Hokoiwa, Y. Gono, A. Odahara, H. Ishiyama, Y.X. Watanabe, T. Hashimoto, T. Ishikawa, M.H. Tanaka, H. Miyatake, J.Y. Moon, J.C. Kim, C.S. Lee, V. Guimarães, R.F. Lihitenthaler, H. Baba, K. Sato, T. Kawamura, and S. Kato: “Elastic Resonance Scattering of ^{23}Mg+p Origin of Matter and Evolution of the Galaxies”, Nov. 17–19, 2003, RIKEN, Wako, Japan.

54. T. Uesaka: “Polarized ^{3}He Target for the Polarization Correlation Experiment at NUCLOTRON”, 10th International Workshop on Polarized Sources and Targets, Sep. 22–26, 2003, Novosibirsk, Russia.

55. T. Uesaka, M. Hatano, T. Wakui, H. Sakai, A. Tamii: “The CNS Polarized Proton Solid Target for Radioactive Isotope Beam Experiment”, 9th International Workshop on Polarized Solid Targets and Techniques, Oct. 27–29, 2003, Bad Honnef, Germany.

56. M. Watanabe, Y. Chiba, K. Ohtomo, H. Tsutsui, T. Koseki, T. Katayama, S. Watanabe, and Y. Ohshiro: "A broad-band rf cavity using Finemet cut-cores as a buncher of heavy ion beams", The third Asian Particle Accelerator Conference, Mar. 22–26, 2004, Pohang Accelerator Laboratory and Pohang University of Science and Technology, Gyeongju, Korea.

57. S. Watanabe, Y. Ohshiro, T. Katayama, T. Watanabe, and T. Ikeda: "The possibility of the ion beam machining of the high temperature superconductor Bi2223", 14th Symp. on Accel. Sci. and Technology, Nov. 11–13, 2003, KEK, Tsukuba, Japan.

58. T. Watanabe, S. Watanabe, T. Ikeda, T. Katayama, M. Kase, T. Kawaguchi, and Y. Sasaki: "Development of Highly Sensitive HTS-SQUID Monitor for Nondestructive Beam Current Measurement", 14th Symp. on Accel. Sci. and Technology, Nov. 11–13, 2003, KEK, Tsukuba, Japan.

59. T. Wakui, M. Hatano, H. Sakai, A. Tamii and T .Uesaka: "Proton Polarization in Naphthalene Crystal with a CW Ar-ion Laser", 9th International Workshop on Polarized Solid Targets and Techniques (Polarized Solid Targets), Oct. 27–29, 2003, Bad Honnef, Germany.

60. T. Wakui, M. Hatano, H. Sakai, A. Tamii and T .Uesaka: "CNS Polarized Proton Solid Target", Workshop on Perspectives of Polarization in RI Beam Induced Reactions, Mar. 2–4, 2004, CNS, University of Tokyo, Wako, Japan.

61. Y. Yamaguchi, C. Wu, D. Q. Fang, M. Fukuda, N. Iwasa, T. Izumikawa, H. Jeppesen R. Kanungo, R. Koyama, T. Ohnishi, T. Ohtsubo, A. Ozawa, W. Shinozaki, T. Suda, T. Suzuki, M. Takahashi, I. Tanihata, S. Watanabe: "Halo structure of ^{17}B studied via its reaction cross section", International Symposium 'A New Era of Nuclear Structure Physics'(NENS03), Nov. 19–23, 2003, Kurokawa Village, Japan.

B. JPS Meetings

1. H. Arai. M. Imanaka, T. Tsukada, T. Nakagawa, I. Arai and S.M. Lee: "Effect of Negatively Biased Disc to Electron Cyclotron Resonance Plasma", at the JPS Spring meeting, Mar. 27–30, 2003, Kyushu University, Fukuoka, Japan.

2. H. Baba, S. Shimoura, T. Minemura, Y.U. Matsuyama, A. Saito, H. Akiyoshi, N. Aoi, T. Gomi, Y. Higurashi, K. Ieki, N. Imai, N. Iwasa, H. Iwasaki, S. Kanno, S. Kubono, M. Kunibu, S. Michimasa, T. Motobayashi, T. Nakamura, H. Sakurai, M. Serata, E. Takeshita, S. Takeuchi, T. Teranishi, K. Ue, K. Yamada, Y. Yanagisawa: "Study of Excited States in Unstable Nucleus ^{14}O via α Inelastic Scatterings", at the JPS Spring meeting, Mar. 27–30, 2004, Kyushu University, Fukuoka, Japan.

3. T. Fukuchi, S. Shimoura, M. Kurokawa: "Performance of CNS Ge array", at the JPS Fall meeting, Sep. 9–12, 2003, Miyazaki World Convention Center "Summit", Miyazaki, Japan.

4. T. Fukuchi, S. Shimoura, E. Ideguchi: "Development of Position Sensitive Ge Detector using the Neural Network", at the JPS Spring meeting, Mar. 27–30, 2004, Kyushu University, Fukuoka, Japan.

5. T. Gunji, H. Hamagaki, M. Inuzuka, K. Ozawa, A. Andronic, O. Busch, C. Garabatos, H. Appelshauser, T. Mahmoud, D. Emschermann, B. Vulpescu: " Electron identification of the ALICE TRD by a Neural Network", at the JPS Fall meeting, Sep. 9–12, 2003, Miyazaki World Convention Center "Summit", Miyazaki, Japan.

6. T. Gunji for the PHENIX Collaboration: "$J/\psi \rightarrow e^+e^-$ Measurements in Au+Au Collisions at $\sqrt{s_{NN}}$= 200 GeV at RHIC-PHENIX", at the JPS Spring meeting, Mar. 27–30, 2004, Kyushu University, Fukuoka, Japan.

7. H. Hamagaki: "Future prospects on the studies of QCD matter at ultra-high temperature", presented in the Nuclear Theory and Experiment Joint Symposium on 'Recent Progress of QGP Search' at the JPS Fall meeting, Sep. 9, 2003, Miyazaki World Convention Center "Summit", Miyazaki, Japan.

8. M. Hatano: "Measurement of Vector Analyzing Power in the $\vec{p}+^6$He Elastic Scattering", at the JPS Spring meeting, Mar. 27–30, 2004, Kyushu University, Fukuoka, Japan.

9. J.J. He, S. Kubono, T. Teranishi, M. Notani, H. Baba, S. Nishimura, J.Y. Moon, M. Nishimura, S. Michimasa, H. Iwasaki, Y. Yanagisawa, N. Hokoiwa, M. Kibe, J.H. Lee, S. Kato, Y. Gono and C.S. Lee: "Measurement of ^{22}Mg+p and ^{21}Na+p elastic scattering with CRIB" at the JPS Fall meeting, Sep. 9–12, 2003, Miyazaki World Convention Center "Summit", Miyazaki, Japan.

10. E. Ideguchi: “Study of High-Spin States via Low-Energy Unstable Nuclear Beams”, at the JPS Fall meeting, Sep. 9–12, 2003, Miyazaki World Convention Center “Summit”, Miyazaki, Japan.

11. E. Ideguchi, H. Baba, T. Fukuchi, N. Hokoiwa, C. Ishida, H. Iwasaki, T. Koike, T. Komatsubara, T. Kubo, M. Kurokawa, S. Michimasa, K. Miyagawa, K. Morimoto, M. Niikura, T. Ohnishi, S. Ota, A. Ozawa, S. Shimoura, T. Suda, M. Tamaki, I. Tanihata, N. Umezawa, Y. Wakabayashi, K. Yoshida, “Study of High-Spin States in a ^{48}Ca Region via Low-Energy Secondary Beams”, at the JPS Spring meeting, Mar. 27–30, 2004, Kyushu University, Fukuoka, Japan.

12. T. Ikeda, T. Uesaka, T. Kawabata, T. Saita, K. Yako, H., Sakai: “Development of Cryogenic Targets for Nuclear Physics Experiments”, at the JPS Fall meeting, Sep. 9–12, 2004, Miyazaki World Convention Center “Summit”, Miyazaki, Japan.

13. M. Imanaka, H. Arai, T. Nakagawa, Y. Ohshiro, S. Watanabe and T. Katayama: “Nano-Cluster Ion Source by Plasma-Gas-Aggregation”, at the JPS Spring meeting, Mar. 27–30, 2003, Kyushu University, Fukuoka, Japan.

14. M. Inuzuka, H. Hamagaki, K. Ozawa, T. Sakaguchi, T. Tamagawa, F. Kajihara, T. Isobe, T. Gunji, S. Oda, Y. Yamaguchi, S. Sawada, S. Yokkaichi: “Development of Gas Electron Multiplier (GEM)”, at the JPS Fall meeting, Sep. 9–12, 2003, Miyazaki Word Convention Center “Summit”, Miyazaki, Japan.

15. M. Inuzuka, H. Hamagaki, K. Ozawa, T. Tamagawa, S. Oda, Y. Yamaguchi: “Development and Application of Gas Electron Multiplier (GEM)”, at the JPS Spring meeting, Mar 27–30, 2004, Kyushu University, Fukuoka, Japan.

16. T. Isobe, H. Hamagaki, K. Ozawa, M. Inuzuka, T. Sakaguchi, T. Gunji, S.X. Oda, Y.L. Yamaguchi, S. Yokkaichi, and S. Sawada: “Development of prototype Time Projection Chamber with CF_4 for relativistic heavy ion experiments”, at the JPS Spring meeting, Mar. 27–30, 2004, Kyusyu University, Fukuoka, Japan.

17. T. Kawabata, H. Akimune, H. Fujimura, H. Fujita, Y. Fujita, M. Fujiwara, K. Hara, K. Y. Hara, K. Hatanaka, T. Ishikawa, M. Itoh, J. Kamiya, M. Nakamura, H. Sakaguchi, Y. Shimbara, H. Takeda, A. Tamii, T. Noro, H. Toyokawa, M. Uchida, T. Wakasa, Y. Yasuda, H. P. Yoshida, M. Yosoi: “Isoscalar $M1$ strength in ^{11}B”, at the JPS Fall meeting, Sep. 9–12, 2003, Miyazaki World Convention Center “Summit”, Miyazaki, Japan.

18. S. Michimasa, S. Shimoura, H. Iwasaki, M. Tamaki, N. Aoi, H. Baba, N. Iwasa, S. Kanno, S. Kubono, K. Kurita, M. Kurokawa, T. Minemura, T. Motobayashi, M. Notani, H.J. Ong, S. Ota, A. Saito, H. Sakurai, S. Takeuchi, E. Takashita, Y.Yanagisawa A. Yoshida: “Excited States in ^{23}F by One-Proton Transfer Reaction”, at the JPS Fall meeting, Sep. 9–12, 2003, Miyazaki World Convention Center “Summit”, Miyazaki, Japan.

19. M. Niikura, S. Shimoura, H. Iwasaki, S. Michimasa, M. Tamaki, S. Ota and H. Baba: “Development of NaI(Tl) Calorimeter for Charged Particles”, at the JPS Fall meeting, Sep. 9–12, 2003, Miyazaki World Convention Center “Summit”, Miyazaki, Japan.

20. M. Notani, S. Kubono, T. Teranishi, T. Minemura, Y. Yanagisawa,S. Michimasa, K. Ue, Zs. Fülöp, J.J. He, H. Iwasaki, H. Baba, M. Tamaki, S. Shimoura, A. Odahara, N. Hokoiwa, Y. Wakabayashi, T. Sasaki, T. Fukuchi, Y. Gono, E.K. Lee, K.I. Hahn, J.Y. Moon, C.C. Yun, J.H. Lee, C.S. Lee and S. Kato: “Direct measurement of the astrophysical reaction ^{14}O$(\alpha, p)^{17}$F using a low-energy radioactive ^{14}O beam”, at the JPS Fall meeting, Sep. 9–12, 2003, Miyazaki World Convention Center “Summit”, Miyazaki, Japan.

21. S.X. Oda, H. Hamagaki, K. Ozawa, M. Inuzuka, T. Isobe, Y.L. Yamaguchi: “Development of a time projection chamber using gas electron multipliers as readout (GEM-TPC)”, at the JPS Spring meeting, Mar. 27, 2004, Kyushu University, Fukuoka, Japan.

22. A. Odahara, Y. Gono, Y. Isozumi, T. Kikegawa, Y. Mochizuki: “Change of decay constant of ^{40}K under ultra high-pressure”, at the JPS Kyushu branch meeting, Nov. 29, 2003, Fukuoka University of Education, Fukuoka, Japan.

23. A. Odahara, Y. Gono, T. Fukuchi, Y. Wakabayashi, N. Hokoiwa, M. Kibe, T. Teranishi, S. Kubono, M. Notani, S. Michimasa, J. J. He, Y. Yanagisawa, H. Iwasaki, S. Shimoura, H. Watanabe and T. Kishida: “Development of Unstable Nuclear Beam ^{17}N to Search for High-Spin Isomers in $N = 51$ Isotones”, at the JPS Fall meeting, Sep. 9–12, 2003, Miyazaki World Convention Center “Summit”, Miyazaki, Japan.

24. S. Ota, S. Shimoura, H. Iwasaki, M. Kurokawa, S. Michimasa, S. Kubono, T. Teranishi, M. Notani, M. Tamaki, T. Murakami, N. Iwasa, T. Motobayashi, Y. Yanagisawa, T. Minemura, S. Takeuchi, T. Gomi, K. Yamada, A. Saito, H. Baba, Y.U. Matsuyama, S. Kanno, E. Takeshita, K. Demichi, K. Hasegawa, K. Kurita, H. Sakurai, N. Aoi, E. Ideguchi, A. Odahara, T. Fukuchi, K. Miller, Z. Elekes, M. Ishihara: "Spectroscopy of ^{13}B via ^{4}He(^{12}Be,^{13}Bγ) Reaction", at the JPS Fall meeting, Sep. 9–12, 2003, Miyazaki World Convention Center "Summit", Miyazaki, Japan.

25. S. Ota: "Proton Transfer Reaction on Neutron-Rich Nucleus ^{12}Be", at the JPS Spring meeting, Mar. 27–30, 2004, Kyushu University, Fukuoka, Japan.

26. K. Ozawa (invited): "Observation of the QCD world through the measurements of vector mesons", at the JPS Fall meeting, Sep. 9, 2003, Miyazaki World Convention Center "Summit", Miyazaki, Japan.

27. T. Sakaguchi for the PHENIX Collaboration: "π^0 Measurement in d-Au collisions at $\sqrt{s_{NN}} = 200$ GeV at RHIC-PHENIX", at the JPS Fall meeting, Sep. 11, 2003, Miyazaki World Convention Center "Summit", Miyazaki, Japan.

28. T. Sakaguchi for the PHENIX Collaboration: "Direct Photon Search in Au-Au Collisions at RHIC-PHENIX", at the JPS Spring meeting, Mar. 30, 2003, Kyusyu University, Fukuoka, Japan.

29. S. Shimoura: "Spectroscopy of Exotic Nuclei via Intermediate-Energy Direct Reactions with light probes", at the JPS Fall meeting, September 9–12, 2003, Miyazaki World Convention Center "Summit", Miyazaki, Japan.

30. K. Suda, H. Okamura, T. Uesaka, H. Kumasaka, R. Suzuki, T. Ikeda, K. Itoh, H. Sakai, A. Tamii, K. Sekiguchi, K. Yako, Y. Maeda, M. Hatano, T. Saito, H. Kuboki, N. Sakamoto and Y. Satou: "Study of Spin-Isospin Responses in Doubly Magic Nucleus ^{16}O", at the JPS Fall meeting, Sep. 9–12, 2004, Miyazaki World Convention Center "Summit", Miyazaki, Japan.

31. M. Tamaki, S. Shimoura, H. Iwasaki, S. Michimasa, N. Aoi, N. Iwasa, H.J. Ong, S. Ota, S. Kanno, S. Kubono, K. Kurita, M. Kurokawa, A. Saito, H. Sakurai, S. Takeuchi, E. Takeshita, M. Notani, H. Baba, T. Minemura, T. Motobayashi, Y. Yanagisawa, A. Yoshida: "Alpha Inelastic Scattering of the Neutron-Rich Nucleus ^{22}O", at the JPS Fall meeting, Sep. 9–12, 2003, Miyazaki World Convention Center "Summit", Miyazaki, Japan.

32. T. Uesaka: "Nuclear Study with High Density Polarized Targets under High Temperature and Low Field", at the JPS Fall meeting, Sep. 9–12, 2004, Miyazaki World Convention Center "Summit", Miyazaki, Japan.

33. Y. Wakabayashi, A. Odahara, N. Hokoiwa, M. Kibe, Y. Gono, T. Fukuchi, T. Teranishi, S. Kubono, M. Notani, S. Michimasa, J.J. He, Y. Yanagisawa, S. Shimoura, H. Watanabe and T. Kishida: "Development of Secondary Beam ^{17}N by CNS, University of Tokyo", at the JPS Kyushu branch meeting, Nov. 29, 2003, Fukuoka University of Education, Fukuoka, Japan.

34. Y. Wakabayashi, A. Odahara, Y. Gono, T. Fukuchi, N. Hokoiwa, M. Kibe, T. Teranishi, S. Kubono, M. Notani, Y. Yanagisawa, S. Michimasa, J.J. He, H. Iwasaki, S. Shimoura, H. Watanabe, T. Kishida, E. Ideguchi, H. Baba, S. Nishimura, M. Nishimura, J. Y. Moon, S. Kato and H. Sagawa: "Gamma-Ray Spectroscopy by Secondary Fusion Reactions using CRIB", at the JPS Meeting, Mar. 27–30, 2004, Kyushu University, Fukuoka, Japan.

35. Y. Wakabayashi, A. Odahara, N. Hokoiwa, M. Kibe, Y. Gono, T. Fukuchi, T. Teranishi, S. Kubono, M. Notani, S. Michimasa, J.J. He, Y. Yanagisawa, S. Shimoura, H. Watanabe and T. Kishida: "Search for high-spin isomers using unstable nuclear beam ^{17}N", at the JPS Spring meeting, Mar. 27–30, 2004, Kyushu University, Fukuoka, Japan.

36. T. Wakui: "Proton Polarization in Crystals of Aromatic Molecules", at the JPS Fall meeting, Sep. 10, 2003, Miyazaki World Convention Center "Summit", Miyazaki, Japan.

C. Lectures

1. S. Kubono: Lecture on Nucleosynthesis and the Universe, Public Lecture of Basic Sciences, Nov. 21, 2003, Hosei University, Tokyo, Japan.

2. S. Kubono: Lecture on Study of Stellar Reactions with Low-Energy RI Beams, The 2nd CNS International Summer School (CISS03), Sep. 16–20, 2003, CNS, Wako, Japan.

3. S. Shimoura: “Special Lectures on Exotic Nuclei”, Jul. 16–18, 2003, Kyushu University, Fukuoka, Japan.

D. Seminars

1. M. Notani: “Search for New Isotopes and Study of Unstable Nuclei Reactions”, Dec. 4, 2003, Colloquium of Nuclear Physics group at Oak Ridge National Laboratory (ORNL), Tennessee, USA.

Personnel

Director

SAKAI, Hideyuki	*Professor, Department of Physics, Graduate School of Science*

Scientific Staff

1. Accelerator Research

KATAYAMA, Takeshi	*Professor*
WATANABE, Shin-ichi	*Research Associate*

2. Heavy-Ion Collisions

SHIMOURA, Susumu	*Professor*
UESAKA, Tomohiro	*Lecturer*
IDEGUCHI, Eiji	*Lecturer* (Aug. 2003–)
IWASAKI, Hironori	*Research Associate*
KAWABATA, Takahiro	*Research Associate*
WAKUI, Takashi	*Research Associate*

3. Nuclear Structure in Extreme States

KUBONO, Shigeru	*Professor*
HAMAGAKI, Hideki	*Associate Professor*
TERANISHI, Takashi	*Research Associate*
OZAWA, Kyoichiro	*Research Associate*

Guest Professors

KOIKE, Yasuro	*Hosei University*
FUKUDA, Mitsuhiro	*Japan Atomic Energy Research Institute*
OTSUKA, Takaharu	*University of Tokyo*

Technical Staff

OHSHIRO, Yukimitsu YAMAZAKI, Norio

Technical Assistants

SHIMAZAKI, Takaichi
YAMAKA, Shoichi
KAMETANI, Soichiro (Nov.1–30, 2003)
SUZUKI, Masaharu
ISOBE, Tadaaki (–Oct. 2003)

Post Doctoral Associates

SAKAGUCHI, Takao
HE, Jianjun
YAKO, Kentaro (–May 2003)
IMANAKA, Masashi
KAJI, Daiya
KIM, Ka-hae
SUZUKI, Ken (Apr. 1–22, 2003)
NOTANI, Masahiro
INUZUKA, Masahide
TERASAWA, Mariko
FUKUCHI, Tomonori
MATSUMOTO, Takashi (–Aug. 2003)
KIKUCHI, Takashi

Research Assistants

SAITO, Takaaki (May–Oct. 2003)
OTA, Shinsuke (Nov. 2003–)

Graduate Students

KAMETANI, Soichiro
KAJIHARA, Fukutaro
ISOBE, Tadaaki
TAMAKI, Mitsuru
ODA, Susumu
MICHIMASA, Shin'ichiro
GUNJI, Taku
KURIHARA, Narumi
NIIKURA, Megumi

Administration Staff

HIRANO, Midori
YAMAMOTO, Ikuko
SUZUKI, Naho
TAKEUCHI, Kazuko
ITAGAKI, Toshiko
ENDO, Takako

Committees

Council

OKAMURA, Sadanori (Chair)	*Dean, Graduate School of Science*
WADATI, Miki	*Department of Physics, Graduate School of Science*
IWASAWA, Yasuhiro	*Department of Chemistry, Graduate School of Science*
SAKAI, Hideyuki	*Department of Physics, Graduate School of Science*
OTSUKA, Takaharu	*Department of Physics, Graduate School of Science*
KATAYAMA, Takeshi	*Center for Nuclear Study, Graduate School of Science*
SHIMOURA, Susumu	*Center for Nuclear Study, Graduate School of Science*
NAGAMINE, Kanetada	*Institute of Materials Structure Science, High Energy Accelerator Research Organization*
TSUKADA, Masaru	*Department of Physics, Graduate School of Science*

Steering Committee

SAKAI, Hideyuki	*Department of Physics, Graduate School of Science*
KATAYAMA, Takeshi	*Center for Nuclear Study, Graduate School of Science*
SHIMOURA, Susumu	*Center for Nuclear Study, Graduate School of Science*
KUBONO, Shigeru	*Center for Nuclear Study, Graduate School of Science*
HAMAGAKI, Hideki	*Center for Nuclear Study, Graduate School of Science*
TSUKADA, Masaru	*Department of Physics, Graduate School of Science*
AIHARA, Hiroaki	*Department of Physics, Graduate School of Science*
OTSUKA, Takaharu (Chair)	*Department of Physics, Graduate School of Science*
HAYANO, Ryugo	*Department of Physics, Graduate School of Science*
SAKURAI, Hiroyoshi	*Department of Physics, Graduate School of Science*
OHTA, Toshiaki	*Department of Chemistry, Graduate School of Science*
KOBAYASHI, Tomio	*International Center for Elementary Particle Physics*
KOMAKI, Ken'ichiro	*Institute of Physics, Graduate School of Arts and Sciences*
NAKAZAWA, Masaharu	*Department of Quantum Engineering and Systems Science, Graduate School of Engineering*

Program Advisory Committee

GONO, Yasuyuki	*Kyushu University*
HAMAMOTO, Ikuko	*University of Lund, Sweden*
HATANAKA, Kichiji	*RCNP, Osaka University*
MAEDA, Kazushige	*Tohoku University*
NAKAMURA, Takashi (Chair)	*Tokyo Institute of Technology*